Dopage et mise en forme de biocéramiques apatitiques pour applications en ingénierie tissulaire osseuse

Aurélie Jacobs

UNIVERSITE CLERMONT AUVERGNE

Ecole doctorale des Sciences de la Vie, Santé, Agronomie et Environnement

THESE DE DOCTORAT

Présentée à l'Université Clermont Auvergne par

Aurélie JACOBS

En vue de l'obtention du grade de Docteur d'Université

Spécialité : **Ingénierie de la Santé**

Soutenue publiquement le 09 décembre 2020

Dopage et mise en forme de biocéramiques apatitiques pour applications en ingénierie tissulaire osseuse

Directeur de thèse : M. Guillaume RENAUDIN (ICCF UMR 6296, SIGMA Clermont)

Co-directeur de thèse : M. Stéphane DESCAMPS (ICCF UMR 6296, Université Clermont Auvergne)

JURY

Rapporteurs

M. Marc BOHNER	Fondation RMS, Bettlach, Suisse
M. Pierre LAYROLLE	Université de Nantes

Examinatrices

Mme Joëlle AMEDEE VILAMITJANA	Université de Bordeaux
Mme Karine ANSELME	Université de Haute-Alsace
Mme Nathalie DOUARD	Mines Saint-Etienne
Mme Christiane FORESTIER	Université Clermont Auvergne

Institut de Chimie de Clermont-Ferrand, UMR 6296, Université Clermont Auvergne

REMERCIEMENTS

Les travaux de recherche présentés dans ce manuscrit ont été réalisés au sein de l'équipe Matériaux Pour la Santé de l'Institut de Chimie de Clermont-Ferrand de l'Université Clermont Auvergne, sous la direction de Guillaume Renaudin et Stéphane Descamps.

Je remercie Fabrice Leroux, directeur de l'ICCF et Jean-Marie Nedelec directeur de l'équipe MPS, de m'avoir permis d'effectuer cette thèse. Merci également à Christiane Forestier de m'avoir accueillie au sein de son laboratoire afin de réaliser une partie de mes travaux.

Je souhaite remercier grandement mes directeurs de thèse, Guillaume et Stéphane pour m'avoir confié ce travail de recherche. Merci pour votre confiance, votre encadrement et tous vos conseils durant ces trois années de thèse. J'ai beaucoup appris à vos côtés grâce au partage de vos connaissances scientifiques.

Je tiens à remercier l'ensemble des membres de mon jury de thèse : Marc Bohner et Pierre Layrolle qui ont accepté d'être rapporteurs de ce travail ainsi que Joëlle Amédée Vilamitjana, Karine Anselme, Nathalie Douard et Christiane Forestier qui ont examiné mon travail.

Plus généralement je remercie tous les membres de l'équipe MPS avec qui j'ai pu travailler ou plus simplement discuter pendant ces trois années. Un merci particulier à Charlotte Vichery pour son aide sur certains appareils, ses conseils scientifiques et plus généralement pour toutes nos discussions professionnelles et personnelles. Merci également à mes collègues doctorants et anciens doctorants au sein de l'équipe. Plus particulièrement, Florestan je te souhaite bon courage pour la suite de ta thèse et Xavier j'ai été ravie de partager mon bureau avec toi pendant 2 ans et d'avoir assisté à ta soutenance de thèse. Je remercie aussi les doctorants de l'ICCF pour les bons moments passés ensemble et plus particulièrement Olympe. Je souhaite remercier aussi les doctorants du LMGE, avec qui j'ai travaillé plusieurs mois, pour leur bonne humeur et merci de m'avoir prêté une paillasse !

J'aimerais remercier aussi les personnes qui ont participé de près ou de loin à la réalisation des travaux présentés dans ce manuscrit : David Marchat du CIS de l'Ecole des Mines de Saint-Etienne, Frédéric Velard de l'unité BIOS de Reims et Christelle Blavignac du CICS de l'UCA.

Un énorme merci à mes amis de très longue date « Les Lardons » : Cindy, Emeline, Quentin et Aurélie (je ne divulgue pas vos surnoms !). Merci pour les visios sport et apéros pendant le confinement, pour toutes nos soirées d'anniversaires et de réveillons et pour tout le reste depuis des dizaines d'années maintenant.

Merci à Mélodie, ma meilleure amie rencontrée sur les bancs de la fac, pour tous nos nombreux moments partagés ensemble, toutes nos discussions et pour ton soutien dans toutes les épreuves. Je nous souhaite de conserver cette relation encore très longtemps !

Nastasia, je te souhaite le meilleur pour la suite à toi et toute ta petite famille.

Merci à mes parents pour leur soutien, malgré qu'ils ne comprennent pas toujours tout ce que je fais. Bon courage à ma sœur jumelle Amélie pour sa (peut-être) future thèse de pharmacie !

Un merci également à ma belle-famille pour tous les bons moments partagés et ceux à venir.

Une mention spéciale pour « Professeur Bobby ».

Pour finir, j'adresse le plus grand des mercis à Nathan, qui m'accompagne dans cette aventure, merci pour ton soutien, ta patience et je nous souhaite tout le meilleur pour la suite.

TABLE DES MATIERES

LISTE DES FIGURES ET TABLEAUX

Tableau 2.3 : caractéristiques des pastilles Cu0-1050 frittées et polies, moyennes obtenues sur des lots d'environ 35 échantillons.

Tableau 2.4 : Composition minéralogique des pastilles Cu0-1050 et Cu10-1050.

Tableau 2.5 : Evolutions des paramètres de mailles des phases HAp et β-TCP des matériaux non dopés Cu0-1050 et dopés Cu10-1050 synthétisés par voie aqueuse.

Tableau 2.6 : Evolutions des paramètres de mailles des phases HAp et β-TCP des matériaux non dopés et dopés synthétisés par voie sol-gel ([4]).

LISTE DES ABREVIATIONS

α-TCP : alpha-Tricalcium Phosphate

ALP : Alkaline Phosphatase

ATCC : American Type Culture Collection

β-TCP : beta-Tricalcium Phosphate

BCP : Biphasic Calcium Phosphate

BMP : Bone Morphogenetic Protein

BMU : Basic Multicellular Unit

BSP : sialoprotéine osseuse

CFU : Colony Forming Unit

Col I : Collagène de type I

CSM : Cellules Souches Mésenchymateuses

DMSO : Diméthylsulfoxyde

DRX : Diffraction des Rayons X

EARSS: European Antimicrobial Resistance Surveillance System

HAp : Hydroxyapatite

HDF : Human Dermal Fibroblasts

HMDS : Hexamethyldisilazane

h-MSCs : human Mesenchymal Stem Cells

HUVEC : Human Umbilical Vein Endothelial Cells

IAS : Infection Associée aux Soins

ISO : Infection du Site Opératoire

JIS : Japanese Industrial Standard

MAPK : Mitogen-Activated Protein Kinase

MEB : Microscopie Electronique à Balayage

MEM : Minimum Essential Media

MP-AES : Microwave Plasma – Atomic Emission Spectroscopy

MRSA : methicillin-resistant *Staphylococcus aureus*

MSSA : methicillin-sensitive *Staphylococcus aureus*

OCN : Ostéocalcine

OD : Optical Density

OPG : Ostéoprotégérine

OPN : Ostéopontine

PBS : Phosphate Buffer Saline

PGA : acide polyglycolique

PLA : acide polylactique

ppm : partie par million

PSO : Perte de Substance Osseuse

RANK-L : Receptor Activator of Nuclear factor-κB Ligand

ROS : Reactive Oxygen Species

rpm : rotation par minute

SARM : *Staphylococcus aureus* résistant à la méticilline

SEM : Scanning Electronic Microscopy

SVF : Sérum de Veau Fétal

TCP : Phosphate Tricalcique

TS : Tryptic Soy broth without dextrose

VEGF : Vascular Endothelial Growth Factor

XRPD : X-ray Powder Diffraction

INTRODUCTION GENERALE

Le tissu osseux est un matériau composite naturel constitué d'une phase minérale apatitique assurant une fonction de support mécanique et d'une phase organique impliquée dans l'homéostasie ionique et l'hématopoïèse. L'os est un tissu vivant en perpétuel renouvellement grâce à un mécanisme de résorption osseuse effectué par les ostéoclastes et de formation osseuse réalisé par les ostéoblastes. Cependant ce remodelage osseux peut s'avérer insuffisant pour réparer un défaut osseux critique lors d'atteintes traumatiques ou pathologiques. Il est alors nécessaire d'avoir recours à des substituts osseux naturels (autogreffes, allogreffes, xénogreffes) ou synthétiques. Néanmoins, l'utilisation de substituts osseux naturels est restreinte notamment par des problèmes de quantité disponible limitée, d'augmentation des risques de complication, de risques de rejet immunitaire et de transmission d'infection.

Une première problématique réside dans le fait de développer des substituts osseux de synthèse et parmi eux les phosphates de calcium apparaissent comme des biomatériaux de choix du fait de leur forte similarité avec la partie minérale de l'os et de leur biocompatibilité. Plus précisément, l'hydroxyapatite (HAp, $Ca_5(PO_4)_3OH$) et le phosphate tricalcique (β-TCP, $Ca_3(PO_4)_2$) peuvent être combinés dans des biocéramiques de phosphates de calcium biphasiques, nommées BCP, afin de conjuguer leurs propriétés : bioactivité, ostéoconduction, biorésorbabilité. Ces biomatériaux peuvent être utilisés sous différentes formes selon les besoins cliniques : granules, blocs, poudres, revêtements de prothèse.

Une seconde problématique réside dans la maîtrise du risque infectieux lors de l'implantation d'un biomatériau. En 2015, la chirurgie orthopédique représente 27,4% de l'ensemble des chirurgies pratiquées en France avec un taux d'incidence des infections du site opératoire de 1,15%. Les infections en sites osseux sont complexes à traiter du fait de leur localisation en profondeur dans le tissu et les conséquences pour le patient sont généralement sévères puisqu'en 2015 pour 312 ISO 86% ont nécessité une reprise chirurgicale. A cela s'ajoute également le développement de l'antibiorésistance qui représente aujourd'hui un problème grave de santé publique. C'est pourquoi la recherche porte sur la mise au point d'implants apportant une solution préventive au développement d'une infection.

Outre les antibiotiques il existe une grande variété de composés possédant des propriétés antibactériennes dont certains ions métalliques comme le cuivre, l'argent et l'or. Le cuivre est un métal nécessaire pour le métabolisme des organismes vivants, il est impliqué dans de nombreux processus biologiques. Il est, par ailleurs, connu et utilisé depuis des siècles pour la préservation et la distribution de l'eau par exemple. Les BCP ont la capacité d'accepter

facilement des substitutions ou insertions ioniques dans leur composition chimique (notion de dopage) et donc le dopage de ces céramiques par des ions cuivre Cu^{2+} apparaît être une alternative prometteuse pour le développement substituts osseux synthétiques antibactériens. L'intérêt primordial étant d'apporter la propriété antibactérienne sur le site même de l'éventuelle infection, avant même que celle-ci ne s'implante.

Les travaux développés dans ce manuscrit ont porté sur le dopage ionique de biocéramiques de phosphates de calcium sous forme de poudres et de pastilles, suivi de leurs caractérisations chimiques et de leurs évaluations biologiques. Les travaux de synthèse et de caractérisation des matériaux ont été réalisés sur les 3 cations d'intérêt énoncés précédemment : cuivre, argent et or. Ces travaux font suite aux études et compétences préalablement développées au sein de l'équipe Matériaux Pour la Santé (MPS) de l'ICCF. La partie relative aux évaluations biologiques, cytotoxicité et propriétés antibactériennes, a été exclusivement réalisé sur les matériaux dopés au cuivre. Ces études biologiques n'étaient pas développées dans l'équipe avant ces travaux de thèse et ont nécessité la mise au point de différents protocoles adaptés aux besoins de l'étude. C'est notamment le cas pour le test de viabilité MTT qui a été développé et mis en place avec des cellules souches mésenchymateuses humaines et l'élaboration des protocoles d'évaluations bactériennes qui font intervenir, en partie, des souches cliniques isolées directement à partir de cas d'infections ostéo-articulaires. Au cours de ces études, une attention particulière a été portée sur les effets du taux de dopage, et plus encore des taux de cuivre relargué en milieux biologiques, afin de mieux comprendre les effets intrinsèques à l'élément dopant. De façon générale le potentiel du cuivre pour ses propriétés antibactériennes est établi dans la littérature, mais les données quantitatives en terme de composition chimique et minéralogique, nécessaires avant tout espoir de développement d'un produit d'application clinique, sont manquantes.

Ce manuscrit est structuré comme suit :

Le chapitre 1 est consacré à l'étude bibliographique du tissu osseux, des biomatériaux de substitution et plus précisément des BCP. La problématique des infections en site osseux est ensuite abordée, ainsi que le dopage des biocéramiques avec des ions cuivre, argent et or qui sont connus notamment pour leurs propriétés antibactériennes.

Le chapitre 2 traite des synthèses, mises en forme et caractérisations de BCP dopées au cuivre, à l'argent et à l'or. Les mécanismes de dopage mis en jeu lors des synthèses de ces matériaux sont mis en évidence.

Le chapitre 3 est dédié aux évaluations biologiques de différentes poudres de BCP dopées au cuivre. Des cellules souches mésenchymateuses humaines (CSM), extraites à partir de moelle osseuse, sont utilisées pour évaluer la cytotoxicité des matériaux et l'activité antibactérienne est étudiée avec des souches bactériennes d'intérêt clinique.

Le chapitre 4 présente ensuite les évaluations de la cytotoxicité et des propriétés antibactériennes de pastilles de BCP dopées au cuivre, sur un modèle d'étude similaire au chapitre 3.

Concernant la rédaction de ce manuscrit de thèse, le choix a été fait d'inclure, au fil du texte, l'ensemble des publications liées à cette étude ; que ce soit les articles parus et acceptés, mais également les articles soumis (en cours d'évaluation).

CHAPITRE 1 : SYNTHÈSE BIBLIOGRAPHIQUE

1. Le tissu osseux

1.1. Architecture et fonctions des os

Le tissu osseux est un tissu conjonctif dur spécialisé, qui est composé de cellules osseuses (ostéoblastes, ostéocytes et ostéoclastes) et d'une matrice extracellulaire minéralisée qui lui confère sa dureté. Cette matrice extracellulaire est composée de 2 parties : une phase organique et une phase minérale [5].

Les os ont une première fonction qui est structurelle, c'est-à-dire qu'ils permettent la locomotion, le soutien corporel en servant de support aux muscles et la protection des organes internes.

Leur deuxième fonction est métabolique [6]. En effet, les os stockent 99% du calcium et 85% du phosphore du corps humain. Le tissu osseux sert donc de réservoir et intervient dans l'homéostasie en régulant les concentrations ioniques [7].

Enfin, ils ont aussi un troisième rôle dans l'hématopoïèse puisque la moelle osseuse est le lieu de création et de renouvellement des cellules sanguines [8].

1.2. Morphologie et composition des os

Le squelette est constitué de 3 principaux types d'os : les os longs (fémur, tibia), les os courts (os du poignet) et les os plats (omoplates, os crâniens). L'épiphyse constitue l'extrémité des os longs et est recouverte de cartilage. La diaphyse représente la partie allongée centrale de l'os long, là où se trouve la moelle osseuse. La métaphyse représente la jonction entre la diaphyse et l'épiphyse [9]. D'un point de vue structurel, l'os est composé de deux parties distinctes : (i) une partie périphérique compacte (os cortical) et (ii) une partie centrale spongieuse (os trabéculaire).

L'os cortical se situe sur la face externe de tous les os et représente 80% de la masse osseuse totale. Il est dense et épais, ce qui confère leur rigidité aux os. Il compose en grande partie la diaphyse des os longs. Il est composé d'ostéons qui contiennent les canaux de Havers, à l'intérieur desquels se trouvent des vaisseaux sanguins et des nerfs (**Figure 1.1**) [5].

L'os trabéculaire (ou spongieux) est constitué de cavités qui contiennent la moelle osseuse, il a une très grande porosité et sa résistance mécanique est faible. Il se retrouve aux extrémités des os longs dans l'épiphyse et la métaphyse, ainsi que dans la partie centrale des os courts.

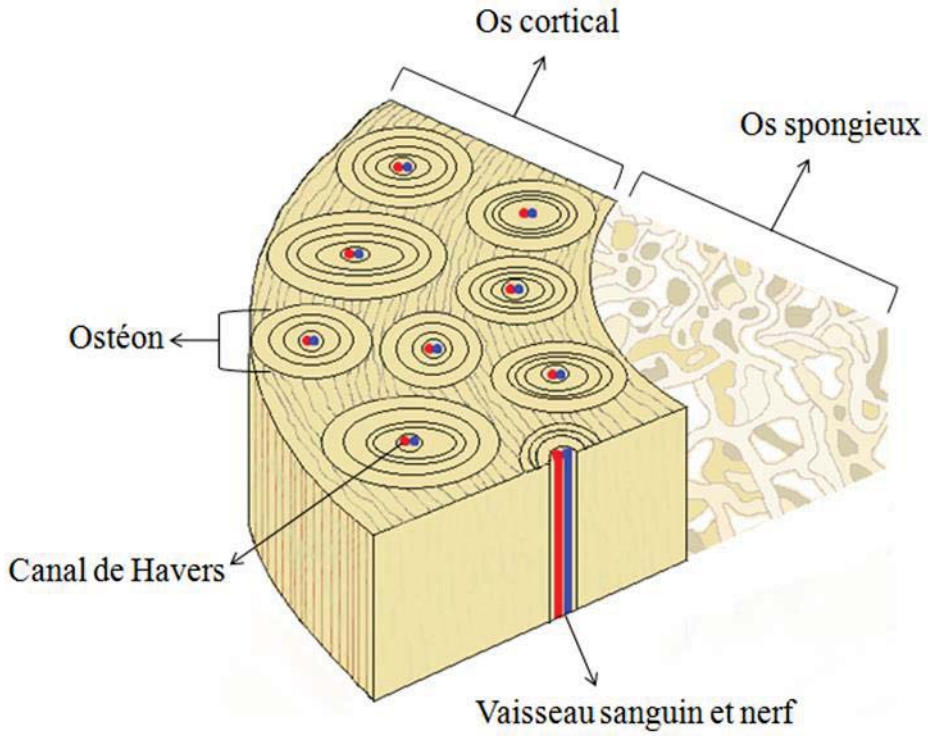

Figure 1.1 : Représentation schématique de la composition du tissu osseux.

De manière générale, la matrice osseuse est constituée à 65% en volume d'une phase minérale et à 35% d'une phase organique [10].

La phase minérale est composée en majorité de phosphates de calcium apatitiques. Il s'agit d'une hydroxyapatite nanométrique carbonatée, déficitaire en calcium et multisubstituée dont la formule chimique moyenne est :

$Ca_{8,3}\square_{1,7}\ (PO_4)_{4,3}\ (CO_3, HPO_4)_{1,7}\ (OH)_{0.3}\square_{1,7}$ avec □= lacune [11].

Différents ions en substitutions sont retrouvés dans cette phase minérale et la composition chimique de l'os est présentée dans le **Tableau 1.1**. Cette composition peut varier selon le type d'os et l'âge [12].

Tableau 1.1 : Composition chimique de l'os [3].

Eléments	% massique
Ca	36,6
P	17,1
CO_2	4,8
Na	1,0
Mg	0,6
Cl	0,1
F	0,1
K	0,07
Sr	0,05

La phase organique est composée essentiellement de collagène de type I (Col I) organisé sous forme de fibres qui assurent la flexibilité de l'os. Elle contient également des protéines non collagéniques (ostéocalcine (OCN), ostéopontine (OPN), ostéonectine) et des facteurs de croissance sécrétés par les cellules ostéoblastiques [5]. Ce sont des molécules qui jouent un rôle majeur dans l'étape de remodelage osseux [13].

1.3. Les cellules osseuses

Les cellules du tissu osseux sont responsables de la formation et du remodelage osseux. Elles ont deux origines distinctes : les ostéoblastes responsables de la formation osseuse proviennent de progéniteurs mésenchymateux et les ostéoclastes impliqués dans la dégradation osseuse, sont issus de la lignée hématopoïétique [7].

1.3.1. Les cellules souches mésenchymateuses

Les cellules souches mésenchymateuses (CSM) sont des cellules indifférenciées capables de se multiplier à l'identique afin de donner des cellules filles. Elles font partie des cellules souches d'origine mésodermique et sont multipotentes ; c'est-à-dire qu'elles peuvent produire différents types cellulaires appartenant aux tissus squelettiques [14]. Elles ont une distribution large puisqu'elles sont retrouvées par exemple dans : l'os, le cartilage, le sang, le tissu

adipeux, les muscles, les ligaments [15]. Les deux sources les plus communes de CSM sont la moelle osseuse et les tissus adipeux. Ce sont des cellules qui présentent un intérêt thérapeutique puisqu'elles sont cultivables, elles ont des propriétés de différenciation, d'adressage aux tissus lésés et de modulation de l'intensité et de l'orientation d'une réponse immunitaire [16].

1.3.2. Les ostéoblastes

Les ostéoblastes sont des cellules mononucléées de 20 à 50 µm. Ce sont les cellules formatrices du tissu osseux et elles contrôlent sa minéralisation. Pour cela elles produisent du collagène qui est à l'origine de la matrice organique et des protéines incluses dans la matrice osseuse telles que : l'OCN, l'OPN, des protéoglycanes et des facteurs de croissance. Les ostéoblastes contrôlent ensuite la minéralisation de la matrice par dépôts de cristaux d'hydroxyapatite [5,17].

Les ostéoblastes sont issus des CSM et leur différenciation ostéoblastique implique l'expression des facteurs de transcription Cbfa1 et Runx2 [18]. Au cours de leur différenciation les cellules ostéoblastiques suivent 3 stades successifs : le progéniteur ostéoblastique, le pré-ostéoblaste et l'ostéocyte. Lors de la différenciation ostéoblastique différents marqueurs sont exprimés. L'ALP (Alkaline Phosphatase) est une glycoprotéine exprimée lors du développement osseux et des étapes de minéralisation. Elle est fortement activée dès le début de la différenciation et ensuite également pendant tous les stades suivants. Pendant la phase suivante de maturation cellulaire les gènes associés à la production de matrice extracellulaire sont exprimés : ALP, Col I, OPN, et fibronectine [19]. Enfin lors de la dernière étape qui correspond à la minéralisation de la matrice osseuse nouvellement formée les marqueurs BSP (sialoprotéine osseuse) et OCN sont exprimés [20].

1.3.3. Les ostéoclastes

Les ostéoclastes sont des cellules plurinucléées et de grande taille (100 µm). Les précurseurs des ostéoclastes sont des cellules souches hématopoïétiques de la lignée monocyte/macrophage. Les ostéoclastes sont de grosses cellules mobiles caractérisées par une bordure en brosse formée par des extensions de la membrane cytoplasmique. La fonction de cette bordure en brosse est de détruire l'os ancien lors du renouvellement osseux [5,21].

1.3.4. Les ostéocytes

Ce sont les cellules les plus abondantes de l'os, de forme étoilée, elles sont espacées dans la matrice en formant un réseau. Ce sont les cellules du tissu osseux mature puisqu'elles dérivent d'ostéoblastes qui ne sont pas morts par apoptose. Elles présentent un grand nombre d'extensions cytoplasmiques ce qui leur permet de communiquer entre elles et avec les ostéoblastes environnants. Grâce à cette communication elles interviennent dans le processus d'adaptation fonctionnelle. En effet, elles sont sensibles aux stimuli mécaniques qui détectent les besoins d'augmentation ou de diminution de la formation osseuse [22,23].

1.4. Le remodelage osseux

Le tissu osseux est une structure vivante qui suit un cycle permanent de formation et de destruction, c'est un phénomène appelé « remodelage osseux ». Il permet de remplacer l'os ancien et fragilisé par un nouveau [5].

Il y a en permanence entre 3 et 5 % du squelette humain qui est en remodelage [24]. Il a lieu dans des unités appelées « unité multicellulaire basique » ou BMU (pour *basic multicellular unit*) qui sont mobiles et progressent dans le tissu osseux [25]. Dans le corps humain il y a en tout temps environ 1 millions de BMU actives qui participent au renouvellement osseux [22]. L'activité de résorption qui a lieu dans une BMU dure environ 3 semaines et la phase de formation osseuse dure 3 à 4 mois. Ce processus est très important puisqu'environ 5 à 10 % du squelette est renouvelé par an et en 10 ans le squelette humain en entier est remplacé [26].

Ce remodelage comprend 4 étapes : (i) la phase d'activation où les ostéoclastes sont recrutés, (ii) la phase de résorption où les ostéoclastes résorbent l'os, (iii) la phase d'inversion où les ostéoclastes meurent par apoptose et les ostéoblastes sont recrutés et (iv) la phase de formation où les ostéoblastes forment une nouvelle matrice qui est ensuite minéralisée [27] (**Figure 1.2**).

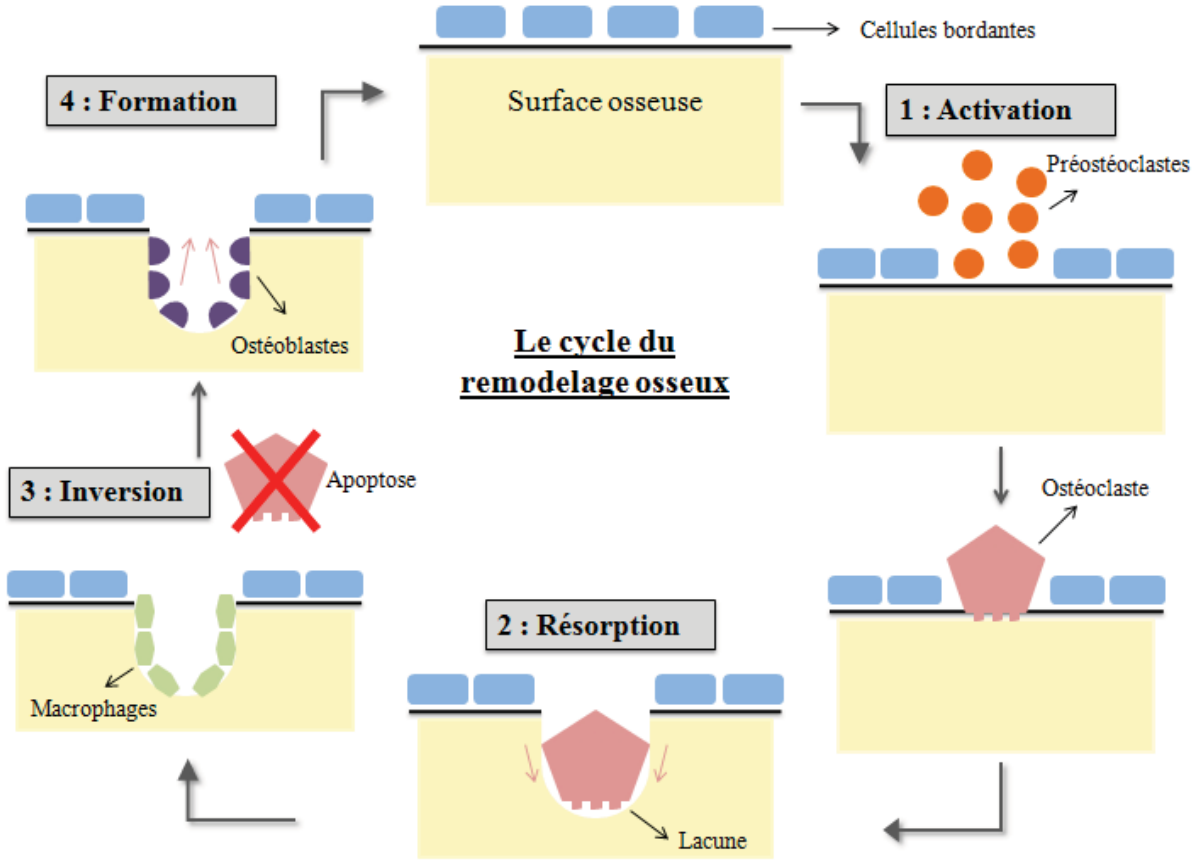

Figure 1.2 : Représentation schématique des étapes du remodelage osseux.

1.4.1. La phase d'activation

La phase d'activation est sous l'influence de signaux hormonaux. Les pré-ostéoclastes fusionnent pour former des ostéoclastes et les cellules bordantes qui recouvrent normalement la surface de la matrice osseuse se rétractent. Les ostéoclastes peuvent alors s'attacher à la matrice osseuse. Plus précisément, les ostéoblastes expriment la protéine RANK-L (Receptor Activator of Nuclear factor-κB Ligand) qui se lie à son récepteur RANK exprimé par les ostéoclastes et leurs précurseurs. Cette liaison stimule l'ostéoclastogénèse. A l'inverse, l'ostéoprotégérine (OPG) produite par les cellules stromales et les ostéoblastes, est un antagoniste de RANK-L qui inhibe la différenciation, l'activité et la survie des ostéoclastes. Les ostéoblastes contrôlent l'ostéoclastogénèse et donc la phase d'activation du remodelage osseux en modulant l'équilibre OPG/RANK-L [28,29].

1.4.2. La phase de résorption

Les ostéoclastes activés lors de la phase précédente s'attachent à la matrice osseuse via des intégrines. Plus précisément ils s'attachent aux protéines de la matrice : OPN, fibronectine, Col I, sialoprotéine. Lors de la phase de résorption la partie minérale de l'os est dissoute par un phénomène d'acidification créé par des ions H^+ sécrétés par des pompes à protons situées au niveau de la bordure en brosse des ostéoclastes. L'acidité créée permet la dissolution de la matrice minérale et entraine la libération de calcium et phosphore. La matrice organique, qui est alors exposée, va être digérée par des enzymes libérées également au niveau de la bordure en brosse des ostéoclastes [30].

1.4.3. La phase d'inversion

La phase d'inversion a lieu lorsque les ostéoclastes, qui ont achevé la formation d'une lacune de résorption, meurent par apoptose. Ils sont ensuite remplacés par des macrophages qui lissent le fond de la lacune qui est appelée lacune de Howship [31]. Cette surface est riche en facteurs de croissances qui recrutent des cellules ostéoprogénitrices de la moelle osseuse [32].

1.4.4. La phase de formation

Enfin, lors de la phase de formation, des cellules ostéoprogénitrices viennent tapisser le fond de la lacune et se différencient en ostéoblastes. Ces ostéoblastes prolifèrent et sécrètent dans un premier temps une nouvelle matrice collagénique non minéralisée. Dans un second temps, ils minéralisent cette nouvelle matrice par dépôt de cristaux d'apatite phosphocalcique [32]. Pour cela le calcium et le phosphore du milieu extracellulaire sont captés par les ostéoblastes puis transférés sur le site de minéralisation entre les fibres de collagène.

Après cette dernière étape, une partie des ostéoblastes meurt par apoptose et les autres deviennent des ostéocytes et des cellules bordantes [20].

Ce remodelage est en équilibre chez le sujet adulte, toutefois, la réduction de la masse osseuse est un phénomène inévitable qui débute à partir de 40 ans environ et croît avec l'âge. Le pourcentage de perte osseuse est de l'ordre de 0,3 à 0,5 % par an [33]. Aussi, ce phénomène est plus important encore chez la femme après la ménopause [34]. À la suite d'un traumatisme, d'une tumeur, d'une infection ou d'une chirurgie, des lacunes appelées « pertes de substances osseuses » (PSO) peuvent apparaître dans le tissu osseux, indiquant un mauvais comblement osseux de la région endommagée.

Il devient parfois nécessaire d'apporter une source extérieure de tissu osseux afin de permettre de combler efficacement le déficit osseux et d'assurer l'invasion cellulaire et vasculaire pour stimuler et accélérer la guérison. Pour cela, il est possible d'utiliser des substituts osseux.

2. Les biomatériaux

2.1. Caractéristiques d'un substitut osseux

Les substituts osseux sont des biomatériaux dont le rôle est de reconstituer un stock osseux déficient. Pour cela, ils peuvent agir en renforçant une structure osseuse ou en comblant une perte osseuse. Ils doivent pouvoir se substituer à l'os et s'intégrer dans le tissu receveur en toute innocuité [35]. Il est donc nécessaire que certaines de leurs caractéristiques physico-chimiques soient contrôlées.

2.1.1. Non toxicité et biocompatibilité

Un matériau implanté dans le tissu osseux doit présenter une sécurité biologique sur le court et le long terme puisque les processus de réparation osseuse peuvent durer plusieurs mois/années. Les substituts se résorbent progressivement pour laisser place aux nouveaux tissus osseux donc il faut également s'assurer de la non-toxicité de leurs sous-produits de dégradation [36].

La biocompatibilité est la capacité d'un matériau étranger à être accepté et/ou toléré par le corps et le système immunitaire. Un matériau non biocompatible induira une réaction inflammatoire et un rejet du matériau qui ne pourra pas s'intégrer dans le corps. La biocompatibilité est une des premières caractéristiques que doit avoir un biomatériau [37].

2.1.2. Bioactivité et ostéointégration

Les substituts doivent être bioactifs, c'est-à-dire qu'ils sont capables d'interagir directement avec les tissus biologiques afin d'aboutir à une réelle liaison chimique avec l'os [35]. La bioactivité est directement liée à l'ostéointégration qui représente la liaison structurelle et fonctionnelle directe qui se met en place entre les tissus et la surface de l'implant. Lors de la 1ère étape de l'ostéointégration les protéines présentes dans les fluides biologiques environnants s'adsorbent à la surface du matériau comme la fibronectine, l'ostéopontine et le collagène. Ensuite les cellules osseuses se lient à ces molécules via des intégrines et adhèrent à la surface de l'implant. Enfin ces cellules communiquent entre elles et synthétisent leurs

propres protéines de la matrice extracellulaire afin de créer un environnement favorable à leur prolifération et leur différenciation [38]. Si les liaisons entre l'implant et les tissus sont faibles ou peu stables le matériau sera recouvert d'une couche de tissu collagénique, il s'agit d'une capsule fibreuse [39].

2.1.3. Ostéoconduction, ostéoinduction et ostéogénèse

L'ostéoconduction est la propriété passive du biomatériau à recevoir la repousse osseuse, donc ce dernier doit servir de support pour l'invasion vasculaire et cellulaire à partir du tissu osseux receveur [40].

Le substitut doit aussi permettre l'induction d'une cascade de réactions biologiques nécessaires à la genèse osseuse : recrutement, différenciation et prolifération cellulaires et libération de facteurs de croissance ; il s'agit de l'ostéoinduction [41].

Une autre propriété importante est sa capacité à permettre l'ostéogenèse c'est-à-dire la synthèse d'un nouveau tissu osseux. Ce potentiel est possible grâce au recrutement d'ostéoblastes qui sont des cellules ostéoformatrices [42].

2.1.4. Porosité

La porosité est une caractéristique très importante à maîtriser puisque la surface spécifique du matériau et le volume des pores ont des conséquences directes sur la capacité de vascularisation et de résorption du substitut [43]. Une macroporosité comprise entre 150 et 500 µm est optimale pour une croissance osseuse [42]. Une microporosité inférieure à 10 µm est également intéressante car elle entraîne une augmentation de la surface spécifique et donc une plus grande adsorption de protéines nécessaires à la réparation osseuse [44].

2.1.5. Résorbabilité

En plus des notions citées précédemment, la résorption du biomatériau est une étape importante qui doit avoir lieu au fur et à mesure de la formation osseuse [45]. Si elle a lieu trop rapidement il ne peut pas servir de support efficace et à l'inverse s'il se dégrade trop lentement il peut gêner la formation osseuse par manque de place.

2.2. Classifications des biomatériaux

2.2.1. Substituts osseux d'origine naturelle

La greffe osseuse est une procédure très fréquente avec près de 2,2 millions de greffes réalisées chaque année dans le monde [46].

2.2.1.1 L'autogreffe

L'autogreffe ou greffe autologue consiste à prélever un greffon osseux et à l'implanter chez le même individu. C'est une procédure considérée comme « gold standard » car théoriquement l'autogreffe possède 3 propriétés idéales pour un substitut : l'ostéoconduction, l'ostéoinduction et l'ostéogénèse. Néanmoins, ces procédures ne sont pas facilement généralisables puisqu'elles nécessitent un second site opératoire, elles sont limitées en terme de quantité d'os disponible et entraîne des facteurs de morbidité [47].

2.2.1.2. L'allogreffe

L'allogreffe ou greffe allogène consiste à prélever un greffon sur un individu et à l'implanter sur un individu différent de la même espèce. C'est une bonne alternative à l'autogreffe en évitant un second site opératoire chez l'individu receveur. Cependant cette procédure présente des risques infectieux et immunologiques de rejet notamment si le greffon est reconnu comme corps étranger. De plus les conditions de préparation peuvent diminuer les propriétés d'ostéoinduction [47].

2.2.2. Substituts osseux d'origine synthétique

Les limites évoquées précédemment concernant les substituts osseux d'origine naturelle ont fait apparaître un intérêt pour l'utilisation de substituts osseux de synthèse. Il existe différentes formes et compositions de biomatériaux synthétiques : les biocéramiques de phosphates de calcium, les verres bioactifs, les polymères, les ciments, les matériaux composites et les alliages métalliques.

2.2.2.1. Les biocéramiques de phosphates de calcium

Pour la majorité, ces céramiques cristallines résultent de la neutralisation des différentes acidités de l'acide phosphorique (H_3PO_4, $H_2PO_4^-$, HPO_4^{2-}) par l'oxyde de calcium (CaO). Aujourd'hui, elles sont très utilisées dans le domaine biomédical du fait de leur biocompatibilité et de leur similarité chimique avec la partie minérale de l'os [48]. Ce sont des céramiques biodégradables et bioactives qui peuvent être composées d'hydroxyapatite (HAp de formule générale $Ca_5(PO_4)_3OH$), de phosphates tricalciques (TCP de formule $Ca_3(PO_4)_2$)) ou d'une combinaison des 2, on parle alors de biocéramiques de phosphate de calcium biphasiques (BCP) [49].

2.2.2.2. Les verres bioactifs

Les verres bioactifs sont des matériaux amorphes composés principalement des oxydes SiO_2, Na_2O, CaO et P_2O_5, en différentes proportions. Ils sont ostéoconducteurs et leur résorption dépend de leur composition. Ils sont caractérisés par une grande bioactivité car ils se lient chimiquement à l'os et de l'HAp se forme à l'interface entre le matériau et l'os, favorisant la régénération osseuse [50].

2.2.2.3. Les polymères

Il existe des polymères naturels issus de protéines de la partie organique de l'os ou de polysaccharides. Ils sont donc biocompatibles, cependant leur origine biologique entraîne les mêmes inconvénients que les allogreffes.

Des polymères synthétiques biodégradables sont utilisés en reconstruction osseuse. Ils sont biodégradables, avec une vitesse de dégradation ajustable, et possèdent aussi des propriétés mécaniques modulables. Ils servent de fixation mécanique (vis, plaques, …) grâce à leurs propriétés mécaniques et un faible taux de dégradation. Lorsque le support mécanique n'est pas nécessaire les polymères peuvent servir de support pour des cellules osseuses, avec un taux de dégradation plus élevé. Cependant, leur utilisation peut induire des réactions inflammatoires avec la libération de sous-produits de dégradation acides [51].

2.2.2.4. Les ciments phosphocalciques

Les ciments phosphocalciques sont des mélanges auto-durcissables composés d'une phase solide et d'une phase liquide qui est généralement un agent de durcissement aqueux. Ce sont des matériaux biocompatibles et injectables qui servent à combler des défauts osseux de différentes tailles [52]. Aujourd'hui les recherches se focalisent principalement sur l'amélioration de leurs propriétés biologiques, notamment l'utilisation de ciments comme supports de principes actifs dans le cas d'infections par exemple [53].

2.2.2.5. Les biomatériaux composites

Les biomatériaux composites sont constitués de 2 phases : une matrice et une phase dispersée dans cette matrice. Généralement la matrice sert de support mécanique à la phase dispersée qui elle apporte des propriétés biologiques. En chirurgie osseuse la matrice est très souvent composée de polymères, synthétiques comme l'acide polyglycolique (PGA) ou l'acide polylactique (PLA) ou naturels comme le collagène, la cellulose et le chitosan. Les phosphates de calcium sont souvent utilisés dans la phase dispersée du fait de leur similarité chimique avec la partie minérale de l'os et de leur biocompatibilité, bioactivité et ostéoconductivité ; même si leurs propriétés mécaniques peuvent être insuffisantes [54].

2.2.2.6. Les alliages métalliques

L'utilisation de métaux en orthopédie est très courante notamment grâce à leurs excellentes propriétés mécaniques et leur haute résistance à la corrosion en milieu biologique. Ils servent par exemple à fixer des fractures et sont utilisés comme support physique en zone porteuse (prothèse de hanche ou de genou par exemple). Les biomatériaux métalliques sont composés généralement d'acier inoxydable, de titane, d'alliages de titane ou d'alliages cobalt-chrome. Ces métaux sont utilisés car ils sont biocompatibles. Ce sont des substituts permanents, qui ne se résorbent pas et qui ne sont pas bioactifs. Leur inactivité chimique entraîne une faible interaction biologique avec l'os et donc limite leur pérennité dans le site d'implantation. Aujourd'hui des procédés de modification de surface sont en développement pour améliorer les propriétés biologiques de ces matériaux [55].

Le **Tableau 1.2** regroupe les différents biomatériaux et les avantages et inconvénients liés à leur utilisation.

Tableau 1.2 : Avantages et inconvénients liés à l'utilisation des principaux biomatériaux.

BIOMATERIAUX	AVANTAGES	INCONVENIENTS
Autogreffes	Faible coût, ostéoconducteurs, ostéoinducteurs, ostéogéniques, résorbables, non toxique, bioactifs	Limitation en quantité, facteurs de morbidité
Allogreffes	Faible coût, ostéoconducteurs, ostéoinducteurs selon les conditions de préparation du greffon, résorbables, bioactifs	Risques infectieux et immunologiques
Biocéramiques de phosphates de calcium	Biocompatibles, ostéoconducteurs, ostéoinducteurs, vitesse de résorption contrôlable, dopage par substitutions ioniques, bioactifs	Faibles propriétés mécaniques
Verres bioactifs	Bioactifs, ostéoconducteurs, résorbables	Faibles propriétés mécaniques
Polymères	Biocompatibles, biodégradables, vitesse de résorption contrôlable	Toxicité des sous-produits de dégradation Faibles propriétés mécaniques
Ciments phosphocalciques	Biocompatibles et injectables Ajustables à la taille du défaut osseux	Peu de propriétés biologiques Peu résorbables Faibles propriétés mécaniques
Matériaux composites	Dépendant des 2 phases utilisées	Dépendant des 2 phases utilisées
Alliages métalliques	Fortes propriétés mécaniques, résistance à l'usure et à la corrosion	Peu de propriétés biologiques Non bioactifs, Non résorbables

2.3. Les biocéramiques de phosphates de calcium biphasiques (BCP)

2.3.1. Composition chimique des BCP

L'hydroxyapatite phosphocalcique fait partie de la famille chimique des apatites. Ce sont des composés dont la formule chimique est : $M_{10}(XO_4)_6(Y)_2$, où *M* est un cation divalent, XO_4 est un anion trivalent et *Y* est un anion monovalent. Dans le cas de l'HAp, Ca^{2+}, PO_4^{3-} et OH^- sont respectivement retrouvés dans la formulation chimique [56].

Le β-TCP fait partie des phosphates de calcium tricalciques et sa formule chimique est : $Ca_3(PO_4)_2$ [57].

Les céramiques de phosphates de calcium biphasées (BCP) sont constituées d'un mélange en proportion variable d'hydroxyapatite (HAp) : $Ca_{10}(PO_4)_6(OH)_2$ (constituant la phase majoritaire) et de phosphates tricalciques bêta (β-TCP, pouvant atteindre jusqu'à 40% massique) [58].

2.3.2. Caractéristiques biologiques des BCP

L'HAp et le β-TCP sont des matériaux biocompatibles, ils ne provoquent pas d'effet indésirable, de réaction immunologique ou de toxicité dans leur site d'implantation.

L'HAp est un matériau bioactif puisqu'à l'interface tissu/implant, des réactions biochimiques ont lieu et permettent la formation d'une liaison biologique entre le substitut et les tissus [59]. Il est également ostéoconducteur en servant de support pour recevoir la repousse osseuse par invasion cellulaire et vasculaire à partir du tissu receveur [49].

Le β-TCP est lui aussi bioactif et ostéoconducteur, mais une autre de ses caractéristiques est qu'il est biorésorbable [49]. En effet, les ions calcium et phosphate se solubilisent et sont utilisés pour la néoformation osseuse [60].

La solubilité des BCP dépend du rapport molaire calcium/phosphate. Elle augmente lorsque ce rapport diminue. Le β-TCP est caractérisé par un rapport molaire Ca/P de 1,5 et l'HAp de 1,67 [61]. De ce fait, la phase HAp est peu biodégradable alors que la phase β-TCP est plus résorbable [62].

La dégradation du biomatériau après son implantation est une étape essentielle pour permettre son remplacement par de l'os néoformé. Mais, comme vu précédemment, c'est un phénomène qui doit être contrôlé afin d'assurer un équilibre entre dégradation et reconstruction osseuse.

Cette composition biphasée permet de conjuguer les propriétés de chacune des deux phases : l'HAp sert de support à l'adhésion cellulaire pendant la phase initiale de l'implantation et ensuite le β-TCP permet une biodégradation progressive [49].

2.3.3. Les substitutions ioniques dans les BCP

Une caractéristique importante de ces substituts osseux est de pouvoir accepter des substitutions ioniques [63]. L'apport d'ions peut jouer un rôle important sur l'amélioration des propriétés des biocéramiques. C'est le cas, par exemple, pour les ions strontium Sr^{2+} qui permettent une meilleure ostéointégration des biomatériaux [64]. Les ions zinc Zn^{2+} incorporés dans des biocéramiques ont un effet sur la formation et la minéralisation osseuse [65]. Les ions cuivre Cu^{2+} peuvent apporter des propriétés antibactériennes et angiogéniques [66,67]. Les ions magnésium Mg^{2+} sont connus pour leur effet sur la minéralisation osseuse et permettent également de stabiliser la phase β–TCP pendant les calcinations à haute température [68].

2.3.4. Les modes des synthèses des BCP

Différentes méthodes de synthèse sont employées pour obtenir ces poudres biphasiques, par exemple : le mélange de poudres de phosphates de calcium [69], la précipitation [70], la voie hydrothermale [71], la réaction à l'état solide [72], la méthode sol-gel [73], la technique de spray-pyrolyse [74].

2.3.5. Interactions en milieu biologique et utilisations cliniques des BCP

Après l'implantation d'une biocéramique il se met en place une cascade de réactions pour finir par l'intégration de l'implant. Tout d'abord, au contact du milieu biologique, la surface du biomatériau se dissout pour atteindre un équilibre chimique avec les fluides environnants et une couche d'apatite carbonatée précipite à la surface de l'implant [75]. Des protéines d'adhésion cellulaire (ostéopontine, sialoprotéine) s'adsorbent sur cette couche carbonatée et favorisent l'attachement des ostéoblastes. Ensuite le cycle du remodelage osseux classique se met en place et la biocéramique est très progressivement résorbée au fur et à mesure de la formation du nouveau tissu osseux [38].

Au niveau clinique l'HAp est utilisée pour le comblement osseux sous forme de granules ou de revêtement de prothèses métalliques mais il n'est pas utilisé dans le cas où une régénération osseuse est souhaitée du fait de sa très faible résorption. Le β-TCP est

également utilisé sous formes de granules ou de blocs mais est contre indiqué comme matériau d'implant durable du fait de sa résorption rapide. C'est pourquoi ces matériaux sont souvent utilisés en association en proportions adaptées aux besoins cliniques [76].

3. Chirurgie osseuse et risques associes

3.1. La chirurgie osseuse

Les interventions chirurgicales portant sur le système osseux sont de plus en plus fréquentes en raison notamment de l'allongement de l'espérance de vie. En 2013 les interventions en chirurgie orthopédique représentaient 24,3% du total des interventions chirurgicales pratiquées en France selon l'Institut de Veille Sanitaire (INVS) [77]. En 2015, la chirurgie orthopédique représentait 27,4 % du total des opérations chirurgicales pratiquées en France. La pose de prothèse de hanche de première intention représente 54,2% et celle de prothèse de genou 38,5%. Les reprises de prothèses sont de 5,5% pour les hanches et 1,8% pour les genoux [1].

3.2. Les infections associées

3.2.1. Définitions

Le terme d'infection nosocomiale est employé lorsque l'infection est contractée dans un établissement de santé. Cependant cette notion a été redéfinie à la suite de la diminution du temps de séjour hospitalier et à l'augmentation des soins à domicile. Aujourd'hui il est plus adapté de parler d'Infections Associées aux Soins (IAS) et qui concerne une infection qui survient au cours ou après une prise en charge et qui n'était ni présente, ni en incubation, au début de la prise en charge. Parmi les IAS se trouvent les Infections du Site Opératoire (ISO) qui comprennent 3 niveaux : superficiel, profond et organe ou espace en fonction de leur localisation et de leur importance.

3.2.2. Les ISO : incidence et microorganismes impliqués

En 2015 sur 29 293 interventions de chirurgie orthopédique, le taux d'incidence des ISO était de 1,15% (soit n = 336). Plus précisément, 1,21 % lors de pose de prothèse de hanche totale de première intention et 0,86 % pour les prothèses de genou primaires. Concernant la localisation des infections, en moyenne 22 % sont des ISO superficielles, 54% sont des ISO profondes et 23 % sont des ISO de l'organe ou de l'espace. L'impact pour le patient, le

chirurgien et l'établissement est considérable. En effet, cela implique un retard et une diminution des probabilités de guérison du patient ainsi qu'un retour à la fonctionnalité initiale difficile. Les temps d'hospitalisation sont prolongés et donc les coûts de séjour également puisque très souvent une reprise chirurgicale est nécessaire. En effet, en 2015 pour 312 ISO 86 % ont eu besoin d'une reprise chirurgicale. La répartition des principaux germes impliqués dans les ISO est donnée dans la **Figure 1.3**. Dans 40,1 % des cas *S. aureus* est responsable des ISO, dont 17,3 % correspondent à des *S. aureus* résistant à la méticilline (SARM), suivi par *S. epidermidis* (13,1 %) et *E. coli* (8,2 %) [1].

Le risque d'ISO est dépendant de 3 facteurs : l'importance de la contamination, la virulence bactérienne et la résistance de l'hôte. Elle peut être exprimée par la formule suivante :

$$\text{Risque d'ISO} = \frac{Importance\ de\ la\ contamination * Virulence\ bactérienne}{Résistance\ de\ l'hôte}$$

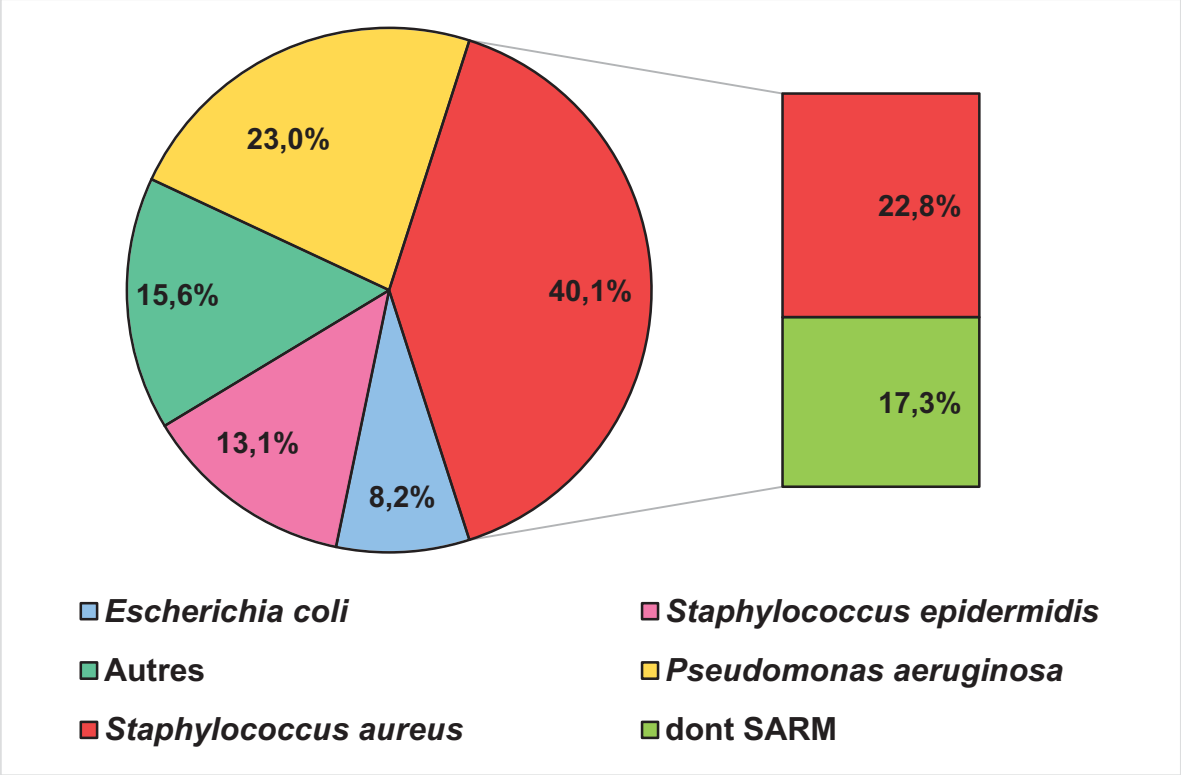

Figure 1.3 : Répartition des principaux microorganismes impliqués dans les ISO en chirurgie orthopédique en 2015 [1].

3.3. Les microorganismes impliqués dans les infections d'implants osseux

3.3.1. La course à la surface

Lors de l'implantation d'un biomatériau se met en place une « course » pour la colonisation des surfaces entre les cellules de l'hôte et les bactéries potentiellement présentes [78]. Il s'agit d'une compétition entre l'intégration de l'implant par les cellules osseuses et l'adhésion de bactéries.

Si les cellules osseuses parviennent à coloniser rapidement la surface de l'implant, les bactéries n'auront plus de surface à leur disposition. En revanche, si les bactéries colonisent la surface en premier, elles vont y adhérer pour former un biofilm. Ce biofilm pourra par la suite servir de base pour leur multiplication et/ou le développement d'autres bactéries [79].

3.3.2. La formation d'un biofilm

La formation d'un biofilm est un processus en 4 étapes : attachement, adhésion, formation du biofilm et détachement (**Figure 1.4**). L'attachement correspond aux premiers moments de la colonisation (1 à 2 heures) où les bactéries établissent des liaisons non spécifiques avec la surface en fonction des caractéristiques physico-chimiques du matériau et des conditions environnantes (1). Ensuite pendant la phase d'adhésion des liaisons spécifiques et irréversibles sont mises en place grâce à des interactions entre protéines de la surface et protéines bactériennes (adhésines et fimbriae) (2). La formation du biofilm peut alors commencer, les bactéries prolifèrent et forment des couches denses. Quand une concentration suffisante est atteinte une matrice de polysaccharides est sécrétée dans laquelle les bactéries s'enferment, ce qui forme le biofilm (3). Finalement, lorsque le biofilm est assez important des bactéries situées à la périphérie se détachent et se dispersent dans les fluides environnants pour aller coloniser de nouveaux sites (4) [80].

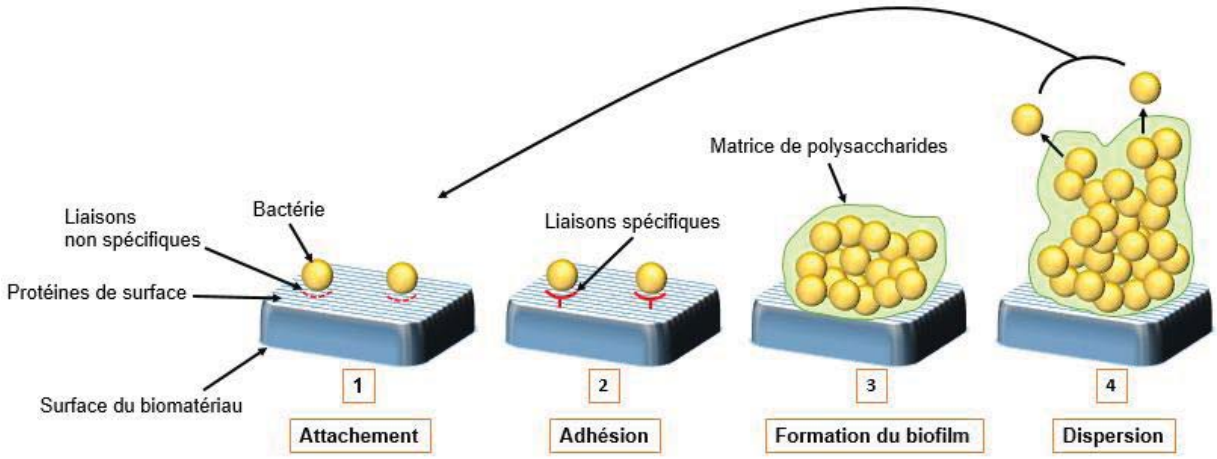

Figure 1.4 : Etapes de la formation d'un biofilm sur une surface.

3.3.3. Implant et biofilm bactérien

L'adhésion bactérienne est un phénomène complexe et multifactoriel qu'il est nécessaire de considérer dans le cas de l'implantation d'un biomatériau. Trois facteurs principaux interfèrent avec ce processus : les propriétés de surface du biomatériau et de la bactérie, et l'environnement dans lequel a lieu l'adhésion [81].

Lors d'une infection, la présence d'un biofilm rend le traitement encore plus difficile, car il a une meilleure résistance aux antibiotiques et au système immunitaire en limitant la pénétration des molécules. En effet, Olson *et al.* ont montré que des biofilms de *S. aureus* étaient résistants à des antibiotiques classiquement utilisés alors que ses formes planctoniques y étaient sensibles [82]. De plus, les biofilms seraient impliqués dans 65 % des infections nosocomiales [83].

En 2002, Karlov *et al.* ont démontré que la présence d'un implant participait vivement à l'adsorption de *S. aureus* sur des disques de titane métallique recouverts de phosphate de calcium [84]. Le risque infectieux serait alors augmenté lorsqu'il s'agit de la mise en place d'un implant au sein des tissus. Il est donc essentiel de rechercher des solutions contre le phénomène de formation de biofilm.

3.3.4. Les principaux microorganismes impliqués

Les bactéries ont généralement une taille comprise entre 1 et 10 µm et des familles de bactéries peuvent se différencier selon leurs formes. Deux formes sont principalement retrouvées : les coques et les bacilles. Ensuite différents arrangements sont retrouvés au sein de chaque famille, par exemple : bactérie isolée, en amas, diplocoques ou diplobacilles (**Figure 1.5**).

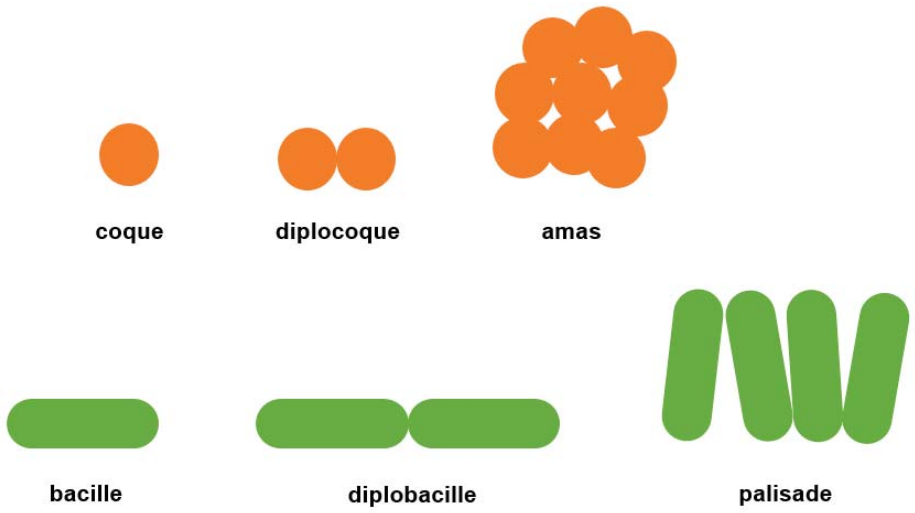

Figure 1.5 : Différentes formes de bactéries selon les familles.

Il existe 2 types de bactéries, appelées Gram + et Gram -. Cette classification est basée sur la composition de la paroi cellulaire des bactéries qui contient un mélange de polysaccharides, de lipides et de peptides ; l'ensemble étant appelé peptidoglycane. Les Gram + ont une paroi cellulaire très épaisse composée de nombreuses couches de peptidoglycane alors que les Gram – ont seulement 1 ou 2 couches de peptidoglycane et une membrane externe (**Figure 1.6**).

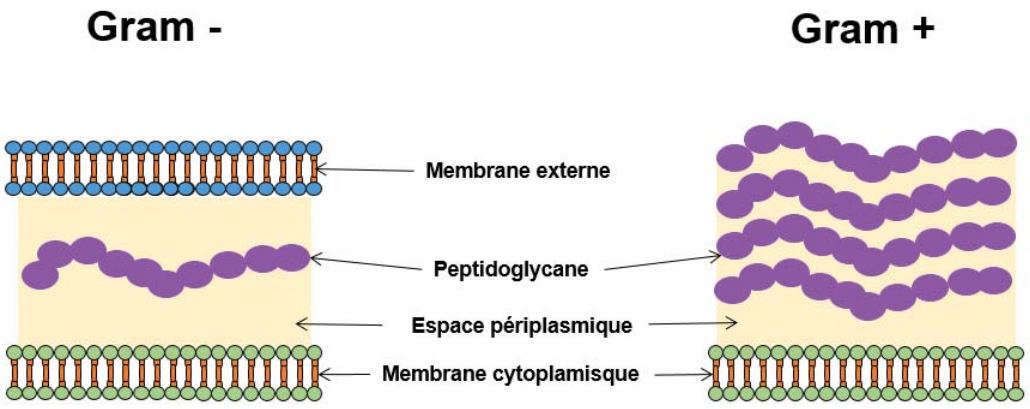

Figure 1.6 : Paroi des bactéries Gram – et Gram +.

Parmi les microorganismes retrouvés lors d'ISO, *S. aureus* est le plus fréquent. C'est une coque Gram + d'environ 1 µm qui est présente naturellement chez l'homme, qui peut se multiplier et produire des toxines. C'est une bactérie responsable de près de 90% des infections de l'os (ostéomyélites) [84]. La méticilline est un antibiotique couramment utilisé pour lutter contre *S. aureus*. Cependant, des SARM se sont développés. Cette résistance est déterminée par la présence du gène *mecA* qui code pour une protéine impliquée dans la synthèse membranaire PLP2a qui a moins d'affinité pour les β-lactamines qui sont une classe d'antibiotique dont fait partie la méticilline [85].

E. coli est un microorganisme Gram – sous forme de bacille de 2 à 6 µm de longueur. C'est une bactérie généralement non pathogène présente dans la flore intestinale mais des mutations ont conduit à des formes pathogènes responsables d'infections [86].

P. aeruginosa est un bacille Gram – d'environ 1,5 µm de longueur. C'est une bactérie rencontrée fréquemment dans l'eau et les milieux humides comme les sols. Elle est aussi retrouvée dans la flore intestinale et peut devenir pathogène chez des patients immunodéprimés ou en cas de plaies. C'est un microorganisme naturellement résistant à de nombreux antibiotiques et qui développent rapidement des résistances [87].

3.3.5. Les antibiotiques et les résistances bactériennes

Malgré les procédés d'asepsie rigoureux mis en place lors des interventions chirurgicales, le risque d'infection n'est pas nul. Des antibiotiques peuvent alors être utilisés pour tuer (action bactéricide) ou stopper la croissance (action bactériostatique) des bactéries responsables de l'infection. Il s'agit notamment de procédures de traitements antibiotiques prophylactiques.

Les antibiotiques sont des molécules qui agissent spécifiquement en inhibant une étape essentielle au développement de la bactérie (synthèse de la paroi, de l'ADN, de protéines, production d'énergie). Mais, la généralisation et l'utilisation massive des antibiotiques ont conduit au développement de souches bactériennes résistantes [88]. Du fait que ces molécules n'agissent que sur un seul des processus vitaux, leur mécanisme d'action est aisément contournable par la bactérie. De plus, l'interface entre l'implant et le tissu osseux étant peu vascularisée, la diffusion des antibiotiques est très limitée.

En 1999, l'Europe a mis en place un système de surveillance (EARSS: European Antimicrobial Resistance Surveillance System). Il permet de suivre l'évolution de la résistance aux antibiotiques de 7 bactéries pathogènes, dont la résistance est en augmentation [89]. Parmi ces résistances, les souches SARM sont les plus fréquentes [1].

3.4. Les biomatériaux antibactériens

Malgré toutes les précautions prises lors des interventions chirurgicales le risque d'infection reste présent. Les recherches se portent aujourd'hui sur des alternatives antibactériennes à large spectre d'action pouvant être utilisées avec des biomatériaux. La modification de surface est une technique visant à empêcher l'adhésion des bactéries et donc la formation de biofilm [81]. Le greffage polymérique est employé mais il modifie aussi les propriétés du biomatériau et donc peut limiter sa biocompatibilité, sa bioactivité et son intégration au tissu osseux. L'imprégnation d'antibiotiques est aussi possible [90], mais avec l'augmentation des résistances bactérienne citée précédemment il est nécessaire de développer de nouvelles approches. C'est pour cela qu'aujourd'hui l'utilisation d'ions métalliques, en dopage du biomatériau, est favorisée car ils peuvent agir – localement – sur plusieurs mécanismes bactériens contrairement aux antibiotiques. De nombreux métaux sont reconnus pour avoir des propriétés antibactériennes, parmi lesquels sont retrouvés par exemple : l'argent [91], le cuivre [92], le zinc [93] et le fer [94].

4. Les substitutions ioniques dans les biocéramiques de phosphates de calcium

4.1. Les substitutions ioniques et le dopage

La famille des apatites présente la formulation suivante : $M_{10}(XO_4)_6(Y)_2$, où *M* est un cation divalent, XO_4 est un anion trivalent et *Y* est un anion monovalent [56]. Une des caractéristiques de l'HAp ($Ca_{10}(PO_4)_6(OH)_2$) est que chacun de ses groupements ioniques peut être substitué par un autre de même valence ou de valence différente. Dans la composition de l'HAp l'ion Ca^{2+} peut être remplacé totalement ou partiellement par des cations bivalents mais aussi monovalents et trivalents comme K^+ [95], Na^+ [96], Ag^+ [97], Sr^{2+} [64], Cd^{2+} [98], Cu^{2+} [4], Zn^{2+} [99], Fe^{3+} [63]. Les sites PO_4^{3-} peuvent être substitués par des groupements divalents comme SO_4^{2-} et CO_3^{2-} [100], ou tétravalents comme SiO_4^{4-} [56]. Enfin le groupement OH^- peut être substitué par des halogénures comme F^- [101], Br^- [102] et Cl^- [103]. L'incorporation d'éléments chimiques étrangers désirés lors de la synthèse du biomatériau est appelé dopage. Des études récentes ont montré la possibilité d'incorporation de dopants métalliques par un mécanisme d'insertion, et non de substitution comme il était généralement admis [63,65,99].

Le β-TCP peut aussi présenter des substitutions de l'ion Ca^{2+} notamment par Mg^{2+} [104], Sr^{2+} [64], Cu^{2+} [4] et Ag^+ [97]. Des cas de co-dopages ont aussi été étudiés avec Ag^+/Zn^{2+} et $Ag+/Cu^{2+}$ [105] et Zn^{2+}/Mg^{2+} [106].

4.2. Le cuivre

Les propriétés des ions cuivre et de leurs utilisations dans les biomatériaux sont développées dans la revue suivante :

Aurélie Jacobs, Guillaume Renaudin, Christiane Forestier, Jean-Marie Nedelec, Stéphane Descamps, **Biological properties of copper-doped biomaterials for orthopedic applications: a review of antibacterial, angiogenic and osteogenic aspects**, *Acta Biomaterialia*, 2020. https://doi.org/10.1016/j.actbio.2020.09.044

Acta Biomaterialia xxx (xxxx) xxx

Contents lists available at ScienceDirect

Acta Biomaterialia

journal homepage: www.elsevier.com/locate/actbio

Review article

Biological properties of copper-doped biomaterials for orthopedic applications: A review of antibacterial, angiogenic and osteogenic aspects

Aurélie Jacobs[a], Guillaume Renaudin[a,*], Christiane Forestier[b], Jean-Marie Nedelec[a], Stéphane Descamps[a]

[a] Université Clermont Auvergne, CNRS, SIGMA Clermont, ICCF, F-63000 Clermont-Ferrand, France
[b] Université Clermont Auvergne, CNRS, LMGE, F-63000 Clermont-Ferrand, France

ARTICLE INFO

Article history:
Received 29 June 2020
Revised 17 September 2020
Accepted 21 September 2020
Available online xxx

Keywords:
Copper
Biomaterials
Antibacterial
Angiogenic
Osteogenic

ABSTRACT

Copper is an essential trace element required for human life, and is involved in several physiological mechanisms. Today researchers have found and confirmed that Cu has biological properties which are particularly useful for orthopedic biomaterials applications such as implant coatings or biodegradable filler bone substitutes. Indeed, Cu exhibits antibacterial functions, provides angiogenic ability and favors osteogenesis; these represent major key points for ideal biomaterial integration and the healing process that follows. The antibacterial performances of copper-doped biomaterials present an interesting alternative to the massive use of prophylactic antibiotics and help to limit the development of antibiotic resistance. By stimulating blood vessel growth and new bone formation, copper contributes to the improved bio-integration of biomaterials. This review describes the bio-functional advantages offered by Cu and focuses on the antibacterial, angiogenic and osteogenic properties of Cu-doped biomaterials with potential for orthopedic applications.

1. Introduction

Several situations can lead to the use of bone substitutes. It is the case, for example, after a trauma, a bone infection, or more generally after a local bone disease requiring bone tissue removal. In these situations, bone defects may occur, corresponding to a poor filling of the damaged area. With the increase in life expectancy, problems of bone fragility and fractures are also becoming more frequent, resulting in a multiplication of the number of orthopedic surgery procedures. Every year 2.2 million bone graft procedures are carried out worldwide [1].

Conventional solutions present limits in terms of both quality and quantity. Indeed, the autograft remains the ideal transplant, since it has all the desired characteristics: perfect biocompatibility, enabling osteoinduction and osteoconduction with no toxicity. However, it is limited in terms of quantity and usually requires a second sampling site, which increases the risks associated with the surgical procedure. Allografts are possible, but present risks of immune intolerance in the recipient patient, and the osteogenic properties are not always retained, depending on the conservation methods used. This is why the use of synthetic bone substitutes is necessary [2]. These are orthopedic biomaterials whose purpose is to rebuild a deficient bone stock; they must be able to replace the bone and integrate the recipient tissue in a completely safe way. As a basic minimum, the use of synthetic material must have no harmful effect on the biological environment, and ideally the biomaterial must be bioactive and osteoconductive, and present long-term stability or bioresorbability [3]. In this paper, we focus exclusively on biomaterials used for orthopedic applications. These must be bioactive and designed for more interactive purposes than others with benign functions [4].

The risk of infection is an important factor that needs to be controlled during the implantation of a bone substitute. For elective surgeries infection rates vary from 0.7% to 4.2%, and up to 30% in the case of third-degree open fractures [5]. Infections in bone sites are difficult to treat because of their deep localization in the tissue, and depend on the microorganism involved. Bone can be poorly vascularized tissue, and infections or trauma can lead to tissue necrosis. The implant is then recognized as a foreign body; bone sequestration occurs and promotes the persistence and relapse of infection [6]. Consequences for the patient are generally severe: delayed healing, often necessary iterative surgery, longer hospitalization times and therefore increased costs. This is why an-

* Corresponding author.
E-mail address: guillaume.renaudin@sigma-clermont.fr (G. Renaudin).

https://doi.org/10.1016/j.actbio.2020.09.044
1742-7061/

tibiotics are used in prophylaxis, to avoid the development of infections [7]. However, the massive use of antibiotics has led to the development of resistant bacterial strains [8]. In 1999, Europe set up a supervision system that tracks the increase in antibiotic resistance of 7 pathogenic bacteria [9]. This is especially the case for Methicillin-Resistant *Staphylococcus aureus* (MRSA). During the implantation of a biomaterial, a "race for surface colonization" takes place between host cells and potentially present bacteria [10]. Indeed, initial colonization by bone cells prevents bacteria adhesion. On the other hand, if the bacteria colonize the surface first, they can form a biofilm; a bacterial environment allowing multiplication and resistance to treatments [11]. In 2002, Karlov et al. demonstrated the strong adsorption of *S. aureus* at the surface of titanium discs coated with calcium phosphate, compared to uncoated discs [12]. Therefore, in recent years, research has focused on the development of synthetic bone substitutes providing a preventive solution to the development of infection. To meet the biological needs, an alternative is to chemically modify these biomaterials during their synthesis. This process is named chemical doping, especially with metals ions (such as Ag^{+} [13], Cu^{2+} [14], Fe^{2+} [15,16], Zn^{2+} [17] and Mn^{2+} [18] among many others). Co-doped materials have also been detailed in recent reviews [19,20]. It is an effective system because ions have an activity directly at the site of implantation, unlike antibiotics, and they have no toxicity at low concentration [21].

Copper (Cu) is an essential trace element, necessary for human development by catalyzing metabolic processes, and is involved in bone formation [22,23]. It also has antibacterial properties and promotes angiogenesis [24,25]. Thus, the Cu^{2+} copper cation appears to be a promising dopant considering its high antibacterial properties and its limited cytotoxicity [26]. This review focuses on the interest of using Cu for its antibacterial properties, mainly when combined with biomaterials. In addition, its angiogenic and osteogenic capacities are discussed. Both metallic (Cu^{0}) and cationic (Cu^{2+}, and also Cu^{+}) forms are concerned here, introduced either in ceramic (bone substitutes, prosthesis coatings), composite or metallic (prostheses) biomaterials.

A bibliographic search via Web of Science ®, using the search string "(copper OR Cu) AND biomaterial*" dates the first paper back in 1965 but shows a real takeoff in the 2000s. Since then, an exponential increase in the literature devoted to the topic can be observed (Fig. 1). If we focus more on the biological aspects covered by this review using the search string "(copper OR Cu) AND biomaterial* AND (antibacter* OR osteogen* OR angiogen*), the first search result dates from 1998 and a similar increase is observed, with more than 400 papers published in the last 3 years (Fig. 2). This review – involving more than a hundred studies – complements the previous review from Jin et al. on a closely-related topic [27]. This update was motivated by the numerous recently-published related studies based on the biological interest of copper in orthopedic biomaterials; nearly a quarter of the studies described in this work date from the past two years and almost one half are papers published after 2016. These include the effects of Cu ions alone and mainly of Cu-doped biomaterials in antibacterial, angiogenic and osteogenic properties. First, we will detail the different types of biomaterials that can insert copper atoms. On this basis, the variations in their biological properties, when associated with Cu, will be described. This review also provides a critical analysis of the experimental conditions used to evaluate these biological effects.

Despite the promising characteristics for orthopedic applications engendered by doping with copper, the results in the literature show that researchers are still far from commercial success. This is not simply due to the regulatory burden linked to the launch of such metal-doped materials on the health market, but also to the difficulty of proving experimentally the intrinsic effect of the doping element itself. The challenge today in finalizing such a project is to combine in the same study the mastery of all the involved characteristics, namely the material (chemical composition, phase composition, forming and handling), biomechanical aspects (brittleness, mechanical resistance and oxidation resistance) and biological aspects (cytotoxicity, bactericidal, osteogenic and angiogenic properties). The difficulty, or even the impossibility, of extracting all this information from the literature comes from the fact that the materials studied and the experimental protocols used are never, or only rarely, the same.

2. State of the art on the biological interest of copper

2.1. Copper involved in biological processes

Cu is an essential trace element which must be provided by external food sources and water [28]. This metal is required by all living organisms because it is involved in numerous physiological functions like respiration, production of energy, formation of tissues, angiogenesis, neuromodulation and several metabolic processes, where it acts as enzyme cofactors [22]. It is also well established that Cu is involved in the maturation and growth of numerous tissue collagens, and especially in bone collagen [29]. Cu appears essential for bone mineralization and osteoblast functions [23].

According to the U.S. Institute of Medicine (IOM), the suitable dosage of Cu for adults is 0.9 mg/day, and the European Food Safety Authority (EFSA) recommends 1.6 mg/day for men and 1.3 mg/day for women [30,31]. For adults, the tolerable upper intake level is 10 mg/day; above this value, damage can appear [30]. Cu is the third most prevalent mineral present in the body. 100 mg of Cu is present in a 70 kg healthy body, with ⅔ located in the skeleton and muscles and the highest concentrations are found in the liver, brain, kidneys and heart [32].

Cu deficiency leads to several disorders such as anemia, leucopenia, myeloneuropathy and Menke's disease, which causes neuronal degeneration, connective tissue and hair abnormalities and bone fragility [33,34]. Menke's disease is due to mutations of the Cu-ATPase ATP7A that normally facilitates Cu export from enterocytes to the blood, resulting in an intestinal accumulation of Cu [35]. On the contrary, an excess of Cu concentration in the body is toxic and results in Wilson's disease, which is a genetic disease linked to an accumulation of Cu in the body and causing damage to the liver and nervous system [36]. Another clinical manifestation is the formation of the Kayser Fleischer ring, corresponding to a hallmark brown discoloration of the cornea. This ophthalmologic manifestation appears in nearly 100% of patients with neurological Wilson's disease and about 50% of those with hepatic symptoms [37]. Alzheimer's disease, diabetes and cancers are diseases that can be impacted by excess amounts of Cu due to a failure in Cu regulation and homeostasis mechanisms [32].

2.2. The use of copper as an antimicrobial in water, air and hospital environments

Cu has been used for its anti-microbial properties for centuries; the Egyptians used it for the preservation of water [38]. Nowadays it is still widely used for drinking water distribution, because it resists corrosion and limits bacterial growth, more particularly that of enteric bacteria [39,40]. Other studies have shown that Cu is also effective in aquatic environments and ventilation systems. Swain et al. in 2014, synthesized CuO-NPs (copper oxide nanopowders) and demonstrated their antibacterial properties against 8 bacterial strains and 4 fungal organisms frequently responsible for contamination in aquaculture [41]. In 2012, Schmidt et al. compared the formation of biofilms after 30 weeks on Cu

Please cite this article as: A. Jacobs, G. Renaudin, C. Forestier et al., Biological properties of copper-doped biomaterials for orthopedic applications: A review of antibacterial, angiogenic and osteogenic aspects, Acta Biomaterialia, https://doi.org/10.1016/j.actbio.2020.09.044

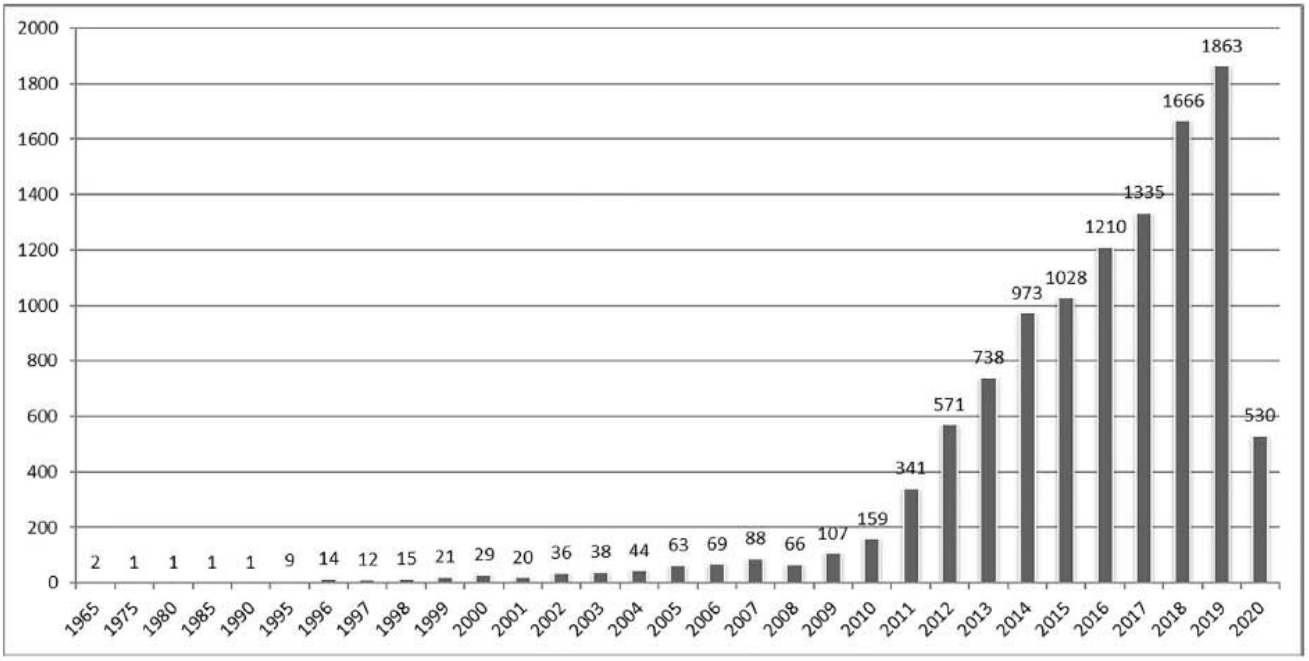

Fig. 1. Number of articles on copper-doped biomaterials as a function of published year (for the search "(copper OR Cu) AND biomaterial*" from Web of Science ®).

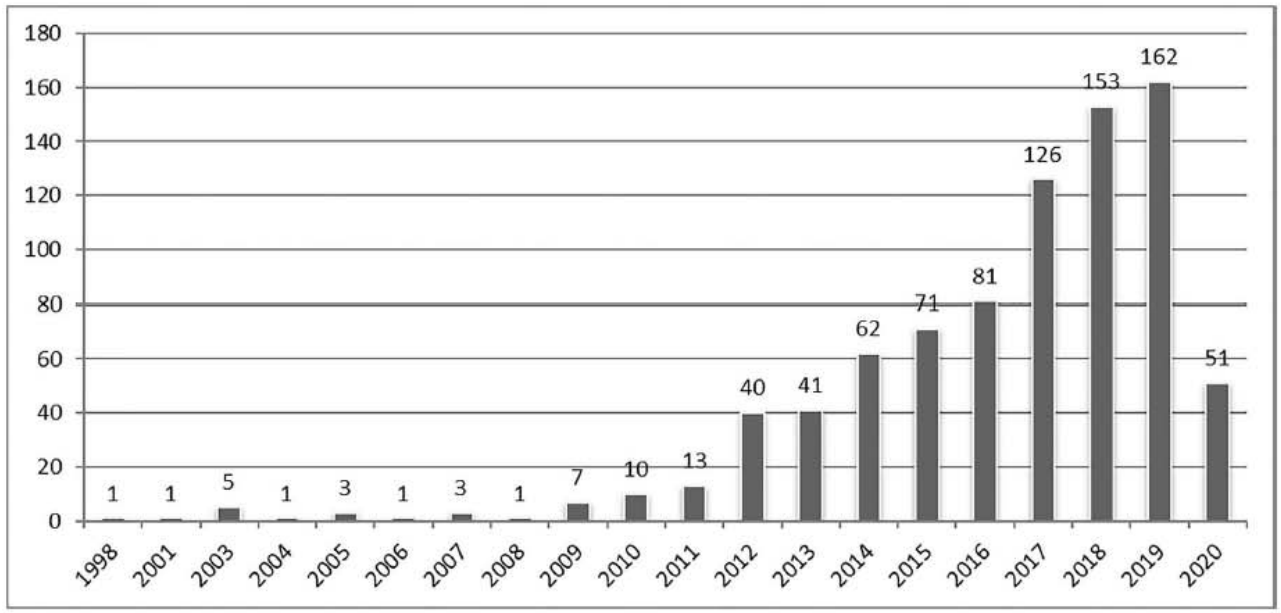

Fig. 2. Number of articles on the biological aspects of copper-doped biomaterials as a function of published year (for the search "(copper OR Cu) AND biomaterial* AND (antibacter* OR osteogen* OR angiogen*)" from Web of Science ®).

and Al heat exchangers. The results showed that bacterial concentrations in biofilms on Cu were at a much lower level than on the aluminum heat exchangers [42].

Using Cu is especially interesting in hospital environments where there is a significant risk of nosocomial infections. Indeed, the World Health Organization (WHO) has announced that at any time, 1.4 million people in the world are concerned by nosocomial infections [43]. Considering furthermore the increase in antibiotic resistance, several studies have focused on using Cu on surfaces/items present in hospitals. Prado et al. showed that after 48h, MRSA, *Klebsiella pneumoniae* and *Acinetobacter baumannii* did not adhere to Cu samples, contrary to stainless steel. However, *Pseudomonas aeruginosa* was still able to adhere [44]. In another study, the nosocomial infection rate was studied for one year in an intensive care unit. Some patients were placed in rooms containing Cu alloy surfaces and others in traditional rooms. Then the proportion of patients who developed a nosocomial infection with MRSA or VRE (Vancomycin-Resistant *Enterococcus*) was compared between the two types of rooms. In rooms containing Cu, 7.1 % of the patients developed a nosocomial infection, compared with 12.3% in

Please cite this article as: A. Jacobs, G. Renaudin, C. Forestier et al., Biological properties of copper-doped biomaterials for orthopedic applications: A review of antibacterial, angiogenic and osteogenic aspects, Acta Biomaterialia, https://doi.org/10.1016/j.actbio.2020.09.044

standard rooms, demonstrating a significant reduction in the number of nosocomial infections thanks to Cu alloy surfaces [45].

It therefore appears that copper is potentially of interest for its antibacterial properties, either in its metallic or cationic form. The following section details the main results of relevant studies carried out during the past decade. The angiogenic and osteogenic properties are then presented. Before studying the three biological functions mentioned above, it is pertinent to approach the subject of cytotoxicity. Indeed, these copper-doped biomaterials should cause no toxicity when implanted; therefore, cytotoxicity is the first aspect to study before evaluating other properties. As with all biological products whose purpose is to be used in the body, the effect is dose-dependent and may vary depending on the living cells/tissues/organisms. In the case of bone biomaterials, the cytotoxic effects can be evaluated using bone cells like Bone Marrow Stem Cells (BMSC), pre-osteoblasts, osteoblasts or osteoclasts. Cells involved in the wound-healing process, like fibroblasts and endothelial cells, may also be considered. In 2016, Wang et al. described the dose-dependent cytotoxicity of Cu^{2+} using fibroblasts with a critical level of 10 mg/mL [46]. In 2019, Li et al. found dose-response relationships between Cu and 3 cell types. The half-maximum inhibitory concentration IC_{50} was 327.9 µM for human endothelial cells, 134.6 µM for mouse osteoblastic cells and 0.7 µM for rat BMSC [47]. This review focused on the main results concerning the intrinsic biological response provided by copper doping. Cytotoxicity is an experimental step that needs to be evaluated first but is not an intrinsic property of the doping; this feature is therefore not developed further here.

3. Copper as an antibacterial agent in biomaterials and the mechanisms involved

In 2008 Cu was officially recognized as a metallic antimicrobial agent by the Environmental Protection Agency (EPA) [48]. The medical field is highly concerned by infections; in consequence, Cu appears to offer promising perspectives and represents an important research topic. This is even more challenging in the orthopedic field with the development of bacterial resistance to antibiotics.

Studies on different Cu-doped orthopedic biomaterials and the antibacterial experiments performed are listed in Table 1. Cu is added to the composition of different types of materials such as calcium phosphate bioceramics, bioactive glasses, biomedical cements, biocomposites and coated/alloyed metals (titanium-based, stainless steel and Co-based alloys). Clinical applications of the different types of biomaterial can be found in the proceeding of Deb and coworkers [49].

3.1. Doped-bioceramics

3.1.1. Calcium phosphate bioceramics

Calcium phosphates are the most widely-used bioceramics due to their chemical and structural similarities with the mineral part of bones [50]. Among them, hydroxyapatite (HAp, $Ca_{10}(PO_4)_6(OH)_2$) and tricalcium phosphate (TCP, $Ca_3(PO_4)_2$) are often studied, alone or mixed together to form Biphasic Calcium Phosphates (BCP) [51–54]. BCP are interesting materials because of the difference in solubility of the two compounds, which enables the regulation of bioresorbability and the kinetic release of the ionic components [55].

Among bioceramics, in 2010 Stanic et al. used Cu-doped hydroxyapatite nanopowders against *Escherichi coli, S. aureus* and *Candida albicans* with approximately 95% of microorganism reduction (R%) for the 3 strains. In this study, undoped HAp also showed some bacterial reduction: approximately 60% reduction for *E. coli* and 70% for *S. aureus* and *C. albicans* [56]. Also in 2010, Li et al. evaluated Cu-doped HAp powders against *E. coli* and for all samples the survival rate was less than 1% after 24h. Pure HAp also has an antimicrobial effect with, 26.9% of bacteria surviving [57]. In 2014, Radovanovic et al., used Cu-doped BCP powders (HAp/α-TCP) and obtained a significant R% after 24h of incubation for the 4 tested microorganisms: *S. aureus, E. coli, P. aeruginosa* and *C. albicans* compared to pure HAp [58]. Shanmugan and Gopal tested fluorapatite (FAp) and HAp doped with Cu against *S. aureus, E. coli* and *C. albicans*. For doped HAp, antimicrobial activity was higher against *C. albicans* and *S. aureus* than for *E. coli*. For the doped FAp the antibacterial activity was better against *S. aureus* and *E. coli* than the antifungal activity against *C. albicans*. In this study, pure HAp and FAp also showed some antimicrobial activity [59]. In 2019 Bhattacharjee et al. synthesized Cu-doped hydroxyapatite. All samples tested were effective against *E. coli* and *S. aureus*, with a significant decrease in bacterial viability [60]. It is also important to mention the existence of contradictory data in the literature. In 2017, Marques et al., evaluated Cu-doped BCP (HAp/β-TCP) compacted pellets against *E. coli* and *S. aureus*, and no antimicrobial activity was demonstrated [61]. In this study several cations, including copper, showed no cytotoxicity issues, but only silver exhibited antimicrobial activity against Gram-positive *S. aureus*. Although the biological part of this study was not very detailed, it highlights the importance of the protocol used for the interpretation of bactericidal results, including the ceramic synthesis method, the final shaping of the materials (pellets vs. powders) and the reference used.

3.1.2. Bioactive glasses

Bioactive glasses are amorphous silica-based materials, initially developed by L.L. Hench and coworkers [62], and are generally composed of SiO_2, Na_2O, CaO and P_2O_5. These biomaterials are known to exhibit high bioactivity; these glasses react with body fluids and form HAp at the interface between the material and the bone, which promotes new bone formation [63].

In the field of bioactive glasses, Wu et al. in 2013 worked with Cu-loaded mesoporous-bioactive glass with molar ratio Cu/Ca/P/Si = 5/10/5/80 and evaluated their materials against *E. coli* over 1, 3 and 7 days. Already from day 1 there was a significant decrease in the number of survival bacteria with the doped bioactive glass. Even with the undoped material, from day 3 there was a significant reduction in bacteria survival [64]. In this study, Cu enabled a faster antibacterial effect (day 1 compared to day 3) and, as mentioned previously, it is important to have a short-term effect to prevent bacterial adhesion to the surface of biomaterials, leading to nosocomial infections [10]. The same year, Palza et al. synthesized bioactive glass with Cu ions. The copper content of their samples (in weight percent) was 3.7 wt% and 8.4 wt%. The authors demonstrated antimicrobial properties and found that the bactericidal effect was lower toward ampicillin-resistant *E. coli* DH5α than *Streptococcus mutans*. In this study, they also demonstrated that antimicrobial activity is enhanced when bioactive glass samples are immersed for 24h before the addition of bacteria, in other words when there are more metal ions in the culture media [65]. In 2005 Abou Neel et al. developed phosphate-based glass fibers containing Cu. The tested strain was *Staphylococcus epidermidis* and the results indicated a significant reduction in the number of CFU (Colony Forming Units) with the doped material compared to the control [66]. In 2017, bioactive glass-ceramics containing Cu were evaluated against *S. aureus* and *P. aeruginosa*. The authors found that the inhibitory and bactericidal effects were more significant on *P. aeruginosa* than on *S. aureus*. Furthermore, for *P. aeruginosa* the doped materials showed greater efficiency compared to gentamicin (an antibiotic used in the medical field to treat severe infections) [67]. In another study, Pouroutzidou et al. synthesized Cu-doped bioactive glass nanopowders and tested their materials

Please cite this article as: A. Jacobs, G. Renaudin, C. Forestier et al., Biological properties of copper-doped biomaterials for orthopedic applications: A review of antibacterial, angiogenic and osteogenic aspects, Acta Biomaterialia, https://doi.org/10.1016/j.actbio.2020.09.044

Table 1
Studies that evaluated the antibacterial effect of copper-doped biomaterials.

Biomaterial	Chemical composition	Copper concentration released	Bacterial strains tested	References
Calcium phosphates bioceramics	FAp ($Ca_{10-x}Cu_x(PO_4)_6F_2$) and HAp ($Ca_{10-x}Cu_x(PO_4)_6(OH)_2$ powders with $x = 0.05$ to $x = 0.5$	n.s.	*E. coli* *S. aureus* *C. albicans*	[59]
	Biphasic HAp($Ca_{10-x}Cu_x(PO_4)_6(OH)_2$)/α-TCP powders with $x = 0.02$ or 0.04	n.s.	*E. coli* *S. aureus* *C. albicans* *P. aeruginosa*	[58]
	HAp nanopowders (CuHAP1 and CuHAP2 with Cu/(Ca+Cu) = 0.0004 and 0.004 respectively	n.s.	*E. coli* *S. aureus* *C. albicans*	[56]
	HAp pellets and powders (Cu/Ca = 0.001, 0.05, 0.1, 0.15)	n.s.	*E. coli*	[57]
	BCP (HAp 50% and β-TCP 50%) powders compacted into pellets with Cu = 2.6mol%	n.s.	*E. coli* *S. aureus*	[61]
	Cu-doped $HApCa_{10}(PO_4)_6[Cu_x(OH)_{2-2x}O_x]$ with $x = 0.2$, 0.4, 0.6 and 0.8, synthesized by Wet Chemical Method and Solid State Method	n.m.	*E. coli* *S. aureus*	[60]
Bioactive glasses	Cu-loaded mesoporous-bioactive glasses (CU-MBG): 0Cu-MBG (molar ratio Cu/Ca/P/Si = 0/15/5/80) and 5Cu-MBG (molar ratio Cu/Ca/P/Si = 5/10/5/80)	n.s.	*E. coli*	[64]
	Bioactive glass (BG) and BG with copper ions (CuBG1 and CuBG2 with CuO = 3.7 wt.% and 8.4 wt.% respectively)	n.s.	*E. coli* (ampicillin-resistant) *S. mutans*	[65]
	Bioactive glass-ceramics: $60SiO_2$•(32-x)CaO•$8P_2O_5$•xCuO with $x = 0$; 0.5; 1.5; 2.5 and 4(mol%)	n.s.	*S. aureus* *P. aeruginosa*	[67]
	Bioactive glass nanopowders with composition in mol%: 60 SiO_2, 30 CaO, 7.5 MgO and 2.5 CuO	n.m.	*L. monocytogenes* *B. cereus* *S. aureus* *E. coli S.* Typhimurium *S.* Enteriditis *P. aeruginosa*	[68]
	Copper doped bioactive glass (Cu = 2wt%)	n.m.	*E. coli* *S. aureus*	[69]
	Copper-containingmesoporous bioactive glass nanoparticles: Cu-MBG 2% (molar ratio Cu/Ca/Si = 2/13/85)	n.s.	*E. coli* *S. aureus* *S. epidermidis*	[70]
	Phosphate-based glass fibers (PGF) containing CuO with CuO mol% = 0, 1, 5 and 10	n.s.	*S. epidermidis*	[66]
	Cu-doped calcium phosphate glasses (CPG, CPG-Cu2, CPG-Cu4 and CPG-Cu6 with 0, 2.2, 4.5 and 6.3 mol % of Cu respectively	n.s.	*S. aureus*	[71]
Bone cements	Cu-TCP cement: Cu-substituted TCP (Cu = 0.30 wt %) powder with Monocalcium Phosphate Monohydrate (MCPM) and Carbonated Hydroxyapatite (CHA) (mass proportion 1/0.764/0.091) mixed with citric acid (0.45M) to form Dicalcium Phosphate Dihydrate (DCPD, brushite)	n.s.	*E. coli* *S. aureus S.* Enteriditis *P. aeruginosa*	[73]
	Cu-substituted dicalcium silicate cement: - C2S-5Cu = 0.06 Cu^{2+} (molar ratio) - C2S-10Cu = 0.11 Cu^{2+} (molar ratio)	n.s.	*P. aeruginosa* *S. aureus* *E. faecalis* *E. coli*	[74]
Biocomposites	PDLLA (poly(D, L-lactide)) scaffolds with Copper doped BG particles (CuBG = $60SiO_2$-25CaO-$1Na_2O$-$4P_2O_5$-1CuO in mol %): composite with 10 wt % of glass particles	n.s.	*Methicillin-resistant S. aureus*	[76]
	Biocomposite aerogel composed of Cu-doped mesoporous BG (Cu-MBGs with molar ratio Si/Cu/Ca/P=75/5/15/5)) and nanofibrillatedcelluloseNFC: MBGSi75Cu5 (5:2) and NFC:MBGSi75Cu5 (10:1)	n.s.	*E. coli*	[46]
	Water-soluble Cu/polyacrylicacid (Cu/PAA) composites	n.m.	*S. aureus* *B. subtilis* *E. coli* *P. aeruginosa*	[78]
	Nano HAp powders soaked with copper (nHAp-Cu), and combined with PEG 400 (nHAP-Cu/PEG 400)	n.m.	*E. coli* *S. aureus*	[77]
	Tri-component composite: Chitosan/Polyvinyl pyrrolidone (CS/PVP) with Cu-HAp weight ratios (0, 20, 40, 60, and 80 wt%)	n.m	*S. aureus* *B. subtilis* *E. coli* *C. albicans* *P. notatum* *R. stolonifer*	[79]

(continued on next page)

Please cite this article as: A. Jacobs, G. Renaudin, C. Forestier et al., Biological properties of copper-doped biomaterials for orthopedic applications: A review of antibacterial, angiogenic and osteogenic aspects, Acta Biomaterialia, https://doi.org/10.1016/j.actbio.2020.09.044

Table 1 (*continued*)

Biomaterial	Chemical composition	Copper concentration released	Bacterial strains tested	References
Coated/alloyed metals (Titanium, stainless steel and Co-based alloys)	CuHAP coating on titanium ($Ca_{10-x}Cu_x(PO_4)_6(OH)_2$ with $x = 0.025$)	n.m.	*E. coli*	[82]
	Copper doped $CaSiO_3$ coated on Ti: 1x-CS, 2x-CS, 3x-CS, 4x-CS and 5x-CS with Cu (wt%) = 1.654, 2.939, 4.399, 5.768, 7.268 respectively	n.s.	*E. coli* *S. aureus*	[83]
	Micro-Ti surface: TiO_2 matrix with amorphous CaO, $CaSiO_3$ and SiO_2. Cu-Hier-Ti surface: $CaO{\cdot}3CuO{\cdot}4TiO_2$ and $CaO{\cdot}TiO_2{\cdot}SiO_2$	n.m.	*S. aureus*	[84]
	Cu-HAp coated titanium (Cu-HA-coated Ti) with Cu content (atom %) HA=0, B1 = 2.4, B2 = 2.7, B3 = 4.2, B4 = 6.6	HA = 0.5 ppm* B1 = 31 ppm* B4 = 68 ppm*	*E. coli* *S. aureus*	[85]
	Titanium plates Ti6Al4V with Cu layer at 1µg/mm^2	n.s.	*S. aureus*	[86]
	Cu-doped calcium phosphate based coating on titanium implants with Cu01 = 4.1 µg of coating and Cu03 = 25.1 µg	n.s.	*E. coli*	[87]
	Cu-chitosan complexes coated on stainless steel 316L with Cu (%) = 2.93, 5.82, 11.45 and 16.50	n.m	*E. coli* *S. aureus*	[88]
	317L-Cu stainless steel (317L-Cu SS) with (wt.%): Cr 19, Ni 13, Mo 3.5, Cu 4.5 and Fe in balance	n.m.	*E. coli* *S. aureus*	[89]
	Ti-6Al-4V-*x*Cu (x = 1, 3, 5 wt%)	n.m.	*E. coli* *S. aureus*	[90]
	317L = 00Cr19Ni13Mo3 and 317L-Cu = 00Cr19Ni13Mo3-4.5 with Cu wt% = 4.5	n.s.	*E. coli* *S. aureus*	[91]
	304 Cu-bearing stainless steel with (wt.%): C 0.016, Cr 18.52, Ni 8.36, Mn 0.43, Si 0.61, Cu 3.90, and Fe in balance	n.m.	*P. gingivalis*	[92]
	Ti-Cu alloys	n.s.	*E. coli* *S. aureus*	[93]
	Cu-bearing titanium alloy Ti-6Al-4V-5Cu with (wt%) Al/V/Cu/Fe/C/N/O/H/Ti = 6.06/3.75/4.85/0.06/0.01/0.002/0.05/0.001/Balance	n.s.	*S. aureus*	[94]
	Commercial stainless steels type 200 (200-C) with 1.45 wt % of Cu and stainless steels enriched with 2.77 wt % of Cu	n.m.	*E. coli* *S. aureus*	[95]
	Austenitic stainless steel (0Cr18Ni9) and Cu bearing austenitic antibacterial stainless steel (0Cr18Ni9- 3.8 wt % Cu)	0.35 ppm, 1h** 0.55 ppm, 3h** 1.1 ppm, 5h** 1.4 ppm, 7h**	*E. coli*	[96]
	Co-Cr-Mo-Cu alloys (Co-*x*Cu) with 1 wt % Cu, 2 wt % and 4 wt %.	n.s.	*S. aureus*	[97]

n.s.: not significative (measured but not related to antimicrobial activity)
n.m.: not measured
* Measured by ICP-MS after 8h with the same conditions used for bacteria growth
** Measured by ICP-MS

against 7 bacterial strains: *Listeria monocytogenes, Bacillus cereus, S. aureus, E. coli, Salmonella* Typhimurium, *Salmonella* Enteriditis and *P. aeruginosa*. The authors found a significant reduction in the bacterial growth rate for 3 strains: *B. cereus, S. aureus* and *P. aeruginosa* [68]. Gupta et al. tested Cu-doped bioactive glasses against *E. coli* and *S. aureus*. A growth inhibition zone (about 2 cm) was observed for both bacterial strains, and this inhibition zone was larger than the inhibition zone observed with the other dopants studied (silver and iron) and similar to the effect obtained with the positive control carried out with the antibiotic gentamicin [69]. Bari et al. studied firstly the antibacterial activity of Cu-containing mesoporous bioactive glass nanoparticles and secondly the effect of their ionic dissolution extracts. For all tested bacteria, growth inhibition was observed with all tested samples and the study demonstrated a positive correlation between the extract concentrations and bacterial growth inhibition [70]. Still in the same year, Foroutan et al. worked with Cu-doped calcium phosphate glasses. All tested samples showed antibacterial activity against *S. aureus*, and this effect intensifies when the Cu content increases [71].

These five studies published in 2017 [68–71] showed the importance of the ionic dissolution products of bioactive glasses, including dopant dissolution (concentration and kinetic) in the context of bone tissue engineering, which was already reviewed about ten years ago by Hoppe et al. [72] but which remains rarely studied in the literature (Table 1).

3.2. Bone cements

Biomedical cements consist of self-hardening mixtures of a solid and a liquid phase. In 2017 Rau et al. synthesized calcium phosphate cement composed of Tricalcium Phosphate doped with Cu (Cu-TCP). The self-hardening process involves the addition of monocalcium phosphate monohydrate ($Ca(H_2PO_4)_2{\cdot}H_2O$) with a solution of citric acid and leads to the precipitation of a brushite phase (Cu-doped $CaHPO_4{\cdot}2H_2O$). The hardened cement showed antibacterial activity exclusively against the Gram-negative strains (*E. coli, P. aeruginosa* and *S.* Enteriditis), whereas the growth of the Gram-positive *S. aureus* was not impaired [73]. The antibacterial activity of the copper-containing cement was significantly higher than that of its Cu-doped TCP precursor powder. Recently, Zhang et al. used a Cu-substituted Ca-silicate self-curing cement (composed of Ca_2SiO_4) against 4 strains: *P. aeruginosa, S. aureus, E. faecalis* and *E. coli*. The authors found that pure cement showed a significant decrease in viable bacteria compared to the control within a few hours. Adding Cu enabled them to prolong the antibacterial effect for several more hours [74].

Please cite this article as: A. Jacobs, G. Renaudin, C. Forestier et al., Biological properties of copper-doped biomaterials for orthopedic applications: A review of antibacterial, angiogenic and osteogenic aspects, Acta Biomaterialia, https://doi.org/10.1016/j.actbio.2020.09.044

3.3. Biocomposites

Biocomposite materials consist of an assembly of at least 2 components: an inorganic filler dispersed in a polymer matrix. Boccaccini and coworkers' review of polymer/bioglass nanocomposites exposed the different preparation methods for biocompatible composites [75]. In 2016 Bejarano et al. worked with a biodegradable poly (D, L-lactide) (PDLLA) mixed with a sol-gel bioactive glass doped with 1 mol % of CuO; the final composition of the material was PLA/10-CuBG (10wt % of Cu-doped glass particles). The authors tested their composite against a MRSA. After 1 day and 3 days, antibacterial activity was around 40%, and after 7 days reached 98% compared to the PDLLA scaffold. In this study, samples without Cu, PLA/10-BG also exhibited an antibacterial effect. In fact the bacterial viability rate was 80% after 3 days, and 40% after 7 days [76]. The same year Wang et al., used a biocomposite aerogel composed of Cu-containing mesoporous bioactive glasses and nanofibrillated cellulose (potentially used as wound dressing materials). Their results indicated that the composite aerogels containing Cu significantly inhibit the growth of Gram-negative *E. coli*. Samples composed of composite aerogel without Cu and nanofibrillated cellulose alone did not show any antibacterial effect [46]. In 2010 Sahithi et al. developed a composite based on nano-hydroxyapatite powders soaked with Cu and combined with polyethylene glycol (PEG 400). The combination of these 2 compounds exhibited significant antimicrobial activity against *S. aureus* and *E. coli*, and a greater effect on Gram-positive *S. aureus* [77]. In 2014 in the study of Li et al., a water-soluble Cu°/polyacrylic acid (Cu/PAA) composite was used against 4 bacterial species: *S. aureus, B. subtilis, E. coli* and *P. aeruginosa*. Results indicated that Cu°/PAA could inhibit bacterial growth of the 4 strains and showed bactericidal activity against three of the tested strains, except for *B. subtilis* [78]. This composite illustrates the fact that copper presents effective bactericidal activity in both its cationic and metallic forms. Finally, in 2020, Narayanan et al. synthesized a tri-component composite containing Chitosan/Polyvinyl pyrrolidone with Cu-Hap, and evaluated the antibacterial properties of these composites against 3 bacterial strains (*S. aureus, B. subtilis* and *E. coli*) and 3 fungi (*C. albicans, Penicillium notatum* and *Rhizopus stolonifer*). The results indicated that the addition of Cu-HAp increases growth inhibition for all the microorganisms tested [79].

3.4. Coating/alloying of metallic biomaterials

Metallic biomaterials are widely used in orthopedics thanks to their mechanical properties and their corrosion and wear resistance. They are usually composed of stainless steel, or titanium, cobalt and tantalum alloys. However, these materials have no biological interactions with tissues. Coating/alloying is an interesting approach with a view to establishing and enhancing biological properties at the implant-tissue interface [80].

3.4.1. Coatings on Titanium alloys

The interest of choosing titanium alloys for orthopedic implants was detailed in the review of Geehta and coworkers [81]. Concerning coatings on titanium, in 2015 Huang et al. coated titanium with Cu-doped HAp and obtained an antimicrobial ratio >75% against *E. coli* [82]. Kalaivani et al. worked with a Cu-doped $CaSiO_3$ coating and evaluated its antibacterial properties on *E. coli* and *S. aureus*. Results indicated that pure powder did not exhibit antibacterial properties, whereas there was a gradual increase of the antibacterial activity with the amount of Cu present in the doped coatings [83]. Recently, in 2019, Huang et al. coated titanium with a Cu-containing ceramic. The authors did not observe antibacterial activity against *S. aureus* but demonstrated that their Cu-doped material promoted the bactericidal effect of macrophages [84]. The same year, Ghosh et al. coated Cu-doped hydroxyapatite onto titanium with varying Cu contents and tested these samples against *E. coli* and *S. aureus*. Their results indicated that the number of viable bacteria decreased as the Cu content in the coatings increased, whereas hydroxyapatite without Cu gave results similar to those observed with the control. The antibacterial rate was 78% after 8h of culture for *E. coli*, and 83% for *S. aureus*. In parallel with this experiment, the Cu ions release during antibacterial tests were analyzed by ICP-MS. After 8h, for the control (hydroxyapatite without Cu) the concentration of Cu ions was 0.5 ppm, compared to 31 ppm for the sample with the lowest Cu content and 68 ppm for the sample having the highest Cu content [85]. It is important to mention that this is the only study referenced in which the quantities of copper released were measured during biological tests (Table 1). Burghardt et al. prepared titanium plates coated with galvanically deposited copper. The results indicated that after 6h no viable *S. aureus* bacteria was found in a medium containing Cu ions released by the coated material. After 24 h of growth on the surface of the materials, a complete removal of adherent bacteria was observed with Cu-coated titanium plates [86]. In 2019, Wolf-Brandstetter et al. coated titanium implants with Cu-doped calcium phosphate. After 2 h of culture with *E. coli*, coatings containing the highest amount of Cu showed a significantly lower number of viable bacteria, and this effect was prolonged to 12 h. Results also indicated a reduction in adherent bacteria after 12 h on the surfaces of implants [87].

3.4.2. Coating on stainless steel

In 2020 Akhtar et al. coated stainless steel 316L with Cu-chitosan complexes and evaluated their antibacterial effect against *E. coli* and *S. aureus*. Results indicated a strong effect against both strains after 3 h with Cu-chitosan complexes, with no bacterial growth, and this effect was still observed after 24 h. Coating with chitosan alone did not evince antibacterial activity [88].

3.4.3. Copper-bearing metals

Cu can also be added to the composition of stainless steel, titanium and cobalt alloys; i.e. Cu-alloying. In 2012 Ren et al. used 317L-Cu stainless steel against *E. coli* and *S. aureus*, their material shows some antibacterial effect after 2 h: 20% growth inhibition for *S. aureus* and 40% for *E. coli* and after 12 h this rate increased to 80% and 90%, respectively. Finally, after 24 h the material killed 99% of the bacteria. In this study, the bactericidal effect observed with *S. aureus* was lower than that observed with *E. coli* in the first hours of the test, but finally after 24 h the antibacterial activity was the same for the 2 strains [89]. Two years later, the same authors tested a Cu-bearing titanium alloy on the same 2 strains. After 24 h of co-culturing, they observed a significant reduction in the number of viable bacteria, and this effect was accentuated when the Cu content was increased [90]. In 2011 Chai et al. used austenitic stainless steel 317L containing Cu. Quantitative bacterial analyses continuously showed (6, 12, 24 and 48 h) that the Cu-doped material inhibited bacterial growth compared to undoped 317L for both *S. aureus* and *E. coli*. After 48 h of incubation, almost no viable bacteria were found [91]. 304 Cu-bearing stainless steel was tested against the anaerobe *Porphyromonas gingivalis* in 2013 by Zhang et al. The authors observed the morphologies of the bacteria at the surface of doped and undoped stainless steel. Irregular shapes and sizes were found after 2 h, 4 h and 6 h for the doped material. After 8 h the bacterial cells appeared fragmented. The number of viable bacteria slowly decreased after 2 h, almost no viable bacteria were found after 8 h and an antibacterial rate of 100% was achieved after 10 h [92]. The same year, Zhang et al. evaluated an antibacterial titanium-Cu alloy with *E. coli* and *S. aureus* using agar diffusion assay and plate-count method. With

Please cite this article as: A. Jacobs, G. Renaudin, C. Forestier et al., Biological properties of copper-doped biomaterials for orthopedic applications: A review of antibacterial, angiogenic and osteogenic aspects, Acta Biomaterialia, https://doi.org/10.1016/j.actbio.2020.09.044

agar diffusion assay, no inhibition zone was observed with the Cu-doped material compared to the positive control sample, consisting of antibiotic tablets with erythromycin, penicillin, kanamycin and gentamicin. Then authors evaluated the colonization on the material surfaces by the 2 bacterial strains with plate-count method and after polishing the samples to investigate the corrosion properties. Results indicated that no viable bacteria were found even after polishing, attesting a strong antibacterial effect on the surface and also inside the material [93]. This study shows that the bactericidal activity can come either from direct contact with the biomaterial or from the release into the biological medium of the doping element. In 2015 Ma et al. synthesized Cu-bearing titanium alloy and studied the adhesive capacity of *S. aureus* on this material. All samples showed significant bacterial adhesion reduction (between 62.5% and 98.6%) compared to the control. Moreover, there were only a few randomly-distributed bacteria on the Cu-doped alloy and no formation of a complete biofilm like that observed on the control [94]. In 2012, Nan et al. compared the antibacterial rate of 3 stainless steels: a commercial type 200 steel (Cu wt% = 1.45), a custom-designed one (Cu wt%= 2.77) and a control without Cu. For *E. coli*, antibacterial rates were 0%, 76.70% and 99.99% for the control, the commercial type and the custom type, respectively. For *S. aureus*, the results were 0%, 99.99% and 99.99%. These results confirm the antibacterial efficiency of Cu [95]. Cu-bearing austenitic antibacterial stainless steel was already used against *E. coli* by the same authors in 2008. After 9 h of culture on the surface of the doped material the outer membrane collapsed, and after 24 h all the bacteria were thin and shriveled. In this study the authors measured the amount of Cu released in the supernatant during bacterial tests, and results showed approximately 0.35 ppm at 1 h, 0.55 ppm at 3 h, 1.1 ppm at 5 h and 1.4 ppm at 7 h. They concluded that more cell damage is caused when the quantity of Cu released is increased [96].

Co-Cr-Mo alloys have been also widely used in total hip or knee replacements due to their corrosion resistance and mechanical properties. In 2016 Zhang et al. used Co-Cr-Mo and Co-Cr-Mo-Cu alloys against *S. aureus* over a period of 24 h. The alloy without Cu did not demonstrate any antibacterial activity, whereas Cu-added alloys exhibited antibacterial rates >94% [97].

3.5. Assessment of the effect of copper introduced into biomaterials

3.5.1. Comparison of bacteriological results

All these studies clearly demonstrated that the Cu used in these biomaterials has antibacterial activity. However, it is essential to take into account many parameters that can influence the results. Among these factors: the type of bacteria (Gram positive or negative), the type of tests used to evaluate the antibacterial effect, the experimental conditions and the variation in Cu content between studies. Another key factor to consider is the release rate of Cu ions (kinetic and amount) in the biological media.

Bacterial strains, experimental tests and results are presented in Table 2 (bacterial activity is simply noted as positive (+) or ineffective (-) because it was not possible to classify quantitatively the bactericidal action between studies due to different protocols used). Regarding the strains used in the experiments, results differ according to the Gram of the bacteria. Gram-positive bacteria have negatively charged cell surface and a very thick peptidoglycan membrane (20–80 nm). Cu ions are positively charged, and thus attracted to the negatively-charged surface, resulting in cell damage and the apoptosis of Gram-positive. By contrast, Gram-negative bacteria have a very thin layer of peptidoglycan (6–15 nm) and an outer membrane which can represent a barrier and prevent the diffusion of Cu [70]. It was clearly demonstrated that Cu has an effect on bacterial membranes in the studies of Li et al. and Nan et al., in which morphological modifications of bacterial cells were observed [78,96].

Another key point regarding bacterial strains is their origin. American Type Culture Collection (ATCC) strains were used in all the studies previously cited; enabling comparison of the results between studies [58]. It is apparent that the use of clinical strains recently isolated from patients with bone infections would provide a better overview of situations encountered in current medical practice.

A significant factor which needs to be considered for the interpretation of the results is the nature of the test used and all its parameters. Among the different experiments used to evaluate antibacterial properties, quantitative determination of the colony forming units (*i.e.* viable bacteria) by plating on agar plates is the method most often applied in the studies. An agar diffusion test and the measurement of optical density are also implemented. Some other methods are also cited, such as MTT assay and the use of resazurin. Thus, it is difficult to correctly compare and interpret results from different experiments. Experiment settings also vary. This is particularly the case for the length of incubation (ranging from a few hours to a few days), for the definition of the reference (as well as positive and negative controls) and for the quantity of materials tested (concentrations vary from µg/mL to g/mL). In some studies, the undoped material has an antibacterial property but the reasons for this effect are not investigated.

Finally, another aspect which is important to underline concerns the measurement of the amount of Cu released during experiments, and therefore the concentration of Cu involved in the antibacterial process. The Cu doping rates of materials are different depending on the studies; thus, it appears essential to know the amount of Cu responsible for the effects observed during bacterial tests. However, among the 37 studies cited in Table 1, only 2 measured the Cu released during antibacterial assays. Nan et al. used Cu-bearing austenitic antibacterial stainless steel with 3.8 wt% of Cu. They measured, using ICP-MS, the concentration of Cu released; results indicate approximately 0.35 ppm at 1 h, 0.55 ppm at 3 h, 1.1 ppm at 5 h and 1.4 ppm at 7h [96]. Ghosh et al. coated titanium with Cu-doped hydroxyapatite with a Cu content (atom %) of HA=0, B1= 2.4 et B4 = 6.6. They also measured Cu by ICP-MS after 8h with the same conditions used for the bacterial tests. The results show 0.5 ppm, 31 ppm and 68 ppm for HA, B1 and B4, respectively [85]. It is surprising to find Cu in the undoped sample (HA, perhaps corresponding to the detection limit) and in this study Cu concentrations are much higher than those cited previously (ceramic versus metal doping). These values confirm that it is necessary to measure Cu concentrations, since they can vary considerably between materials and therefore strongly influence the antibacterial results observed. As reported in Table 1, 22 studies did measure the Cu released but not in the exact same conditions as those used for antimicrobial tests (i.e. same culture medium, same concentration of material in the culture medium), so it is impossible to know the amount of Cu responsible for the results observed; and 13 did not measure Cu concentrations at all, notwithstanding the fact that a significant copper release rate could cause cytotoxicity problems.

To conclude, it appears very important to consider all the parameters mentioned above to correctly interpret and compare results obtained from different studies. It is, however, almost impossible to achieve this via the literature with the aim of deducing simple guidelines concerning the chemical compositions to be favored.

3.5.2. Mechanisms involved in the antibacterial activity of copper

Concerning the modes of action of Cu, several mechanisms have been described in the literature. The most important process is based on the redox properties of Cu; in fact, it can produce re-

Please cite this article as: A. Jacobs, G. Renaudin, C. Forestier et al., Biological properties of copper-doped biomaterials for orthopedic applications: A review of antibacterial, angiogenic and osteogenic aspects, Acta Biomaterialia, https://doi.org/10.1016/j.actbio.2020.09.044

Table 2
Antibacterial test parameters in studies with Cu-doped biomaterials.

Bacterial type	Bacterial strain	Biomaterial	Type of experiment	Antibacterial effect*	References
Gram -	*E. coli*	Calcium phosphates bioceramics	Quantitative method and Agar diffusion test	+	[56]
			Quantitative method and Agar diffusion test	+	[57]
			Quantitative method	-	[59]
			Quantitative method	+	[58]
			Agar diffusion test	-	[61]
			Quantitative method, MTT assay and Optical density	+	[60]
		Bioglasses	Quantitative method	+	[64]
			MTT assay	+	[70]
			Agar diffusion test	+	[69]
			Quantitative method and Optical density	-	[68]
		Biomedical cements	Quantitative method and Agar diffusion test	+	[73]
			Quantitative method	+	[74]
		Biocomposites	Optical density	+	[77]
			Optical density	+	[78]
			Optical density	+	[46]
			Agar diffusion test	+	[79]
		Coated/alloyed metals	AFM analysis	+	[96]
			Quantitative method	+	[91]
			Quantitative method	+	[95]
			Quantitative method	+	[89]
			Quantitative method and Agar diffusion test	+	[93]
			Quantitative method	+	[90]
			Quantitative method	+	[83]
			Quantitative method	+	[82]
			Quantitative method and Optical density	+	[85]
			Optical density and LIVE/DEAD staining	+	[87]
			Quantitative method	+	[88]
	P. aeruginosa	Calcium phosphates bioceramics	Quantitative method	+	[58]
		Bioglasses	Resazurin test	+	[67]
			Quantitative method and Optical density	+	[68]
		Biomedical cements	Quantitative method and Agar diffusion test	+	[73]
			Quantitative method	+	[74]
		Biocomposites	Optical density	+	[78]
	S. Typhimurium	Bioglasses	Quantitative method and Optical density	-	[68]
	S. Enteriditis	Bioglasses	Quantitative method and Optical density	-	[68]
		Biomedical cements	Quantitative method and Agar diffusion test	+	[73]
	P. gingivalis	Coated/alloyed metals	Quantitative method and SEM	+	[92]
Gram +	*S. aureus*	Calcium phosphates bioceramics	Quantitative method and Agar diffusion test	+	[56]
			Quantitative method	+	[58]
			Quantitative method	+	[59]
			Agar diffusion test	-	[61]
			Quantitative method, MTT assay and Optical density	+	[60]
		Bioglasses	Resazurin test	+	[67]
			MTT assay	+	[70]
			Agar diffusion test	+	[69]
			Quantitative method and Optical density	+	[68]
			Quantitative method	+	[71]
		Biomedical cements	Quantitative method and Agar diffusion test	-	[73]
			Quantitative method	+	[74]
		Biocomposites	Optical density	+	[77]
			Optical density	+	[78]
			Agar diffusion test	+	[79]
		Coated/alloyed metals	Quantitative method	+	[91]
			Quantitative method	+	[89]
			Quantitative method	+	[95]
			Quantitative method and Agar diffusion test	+	[93]
			Quantitative method	+	[90]
			Quantitative method	+	[83]
			Quantitative method	+	[86]
			Quantitative method and SEM	+	[94]
			Quantitative method	+	[97]
			Quantitative method	-	[84]
			Quantitative method and Optical density	+	[85]
			Quantitative method	+	[88]
	L. monocytogenes	Bioglasses	Quantitative method and Optical density	-	[68]
	S. mutans	Bioglasses	Quantitative method	+	[65]
	B. subtilis	Biocomposites	Optical density	+	[78]
			Agar diffusion test	+	[79]
	B. cereus	Bioglasses	Quantitative method and Optical density	+	[68]
	S. epidermidis	Bioglasses	Quantitative method	+	[66]
			MTT assay	+	[70]
	E. faecalis	Biomedical cements	Quantitative method	+	[74]

(continued on next page)

Please cite this article as: A. Jacobs, G. Renaudin, C. Forestier et al., Biological properties of copper-doped biomaterials for orthopedic applications: A review of antibacterial, angiogenic and osteogenic aspects, Acta Biomaterialia, https://doi.org/10.1016/j.actbio.2020.09.044

Table 2 (*continued*)

Bacterial type	Bacterial strain	Biomaterial	Type of experiment	Antibacterial effect*	References
Yeast	*C. albicans*	Calcium phosphates bioceramics	Quantitative method and Agar diffusion test	+	[56]
			Quantitative method	+	[58]
			Quantitative method	+	[59]
		Biocomposites	Agar diffusion test	+	[79]
	P. notatum	Biocomposites	Agar diffusion test	+	[79]
	R. stolonifer	Biocomposites	Agar diffusion test	+	[79]
Antibiotic resistance	*E. coli* (ampicillin resistant)	Bioglasses	Quantitative method	+	[65]
	S. aureus (methicillin-resistant)	Biocomposites	Quantitative method	+	[76]

* "+" = antibacterial effect and "-" = no antibacterial effect

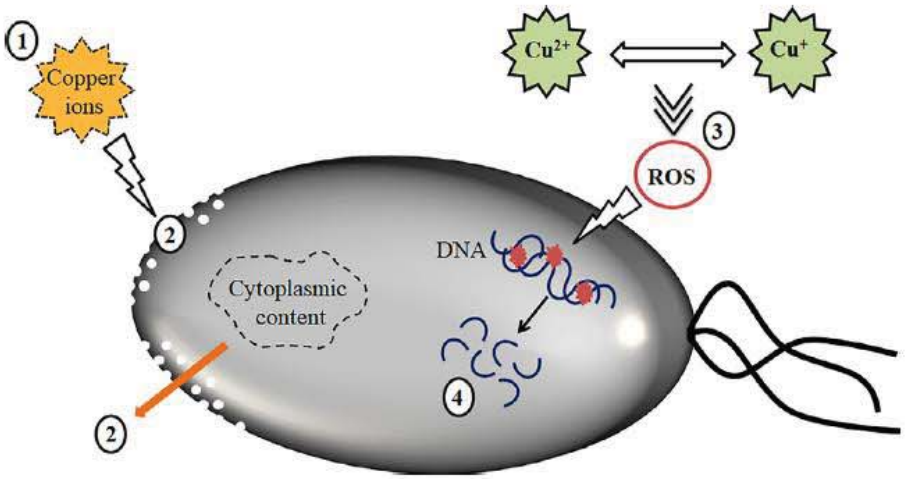

Fig. 3. The killing process involved in the antibacterial properties of copper. Copper ions are released from the doped biomaterial (1) and cause membrane damage leading to a loss of cytoplasmic content (2). Then the production of ROS (3) causes DNA fragmentation (4) and cell death.

active oxygen species (ROS) in a Fenton-type reaction and ROS cause damage to lipids, proteins, membrane and DNA. Significant oxidative stress is caused by an increase in the intrinsic amount of Cu and leads to redox cycling between the different forms of Cu: Cu°, Cu^{+} and Cu^{2+} [98,99]. The DNA double helix contains binding sites for copper, which leads, after Cu^{2+} bonding, to disorders in helical structures and the denaturation of DNA [100]. Damage to the membrane is related to the fact that Cu^{2+} can interact with SH-groups and lead to their inactivation [100]. The interaction of copper with proteins was clearly demonstrated by Nandakumar et al. by quantitative proteomic profiling on *E. coli* after exposure to metallic copper surfaces. Results indicated that of 509 proteins identified, 209 were differently expressed after contact with copper. Proteins involved in efflux pumps were up-regulated and proteins related to biogenesis functions were down-regulated [101]. The bacterial killing process can be separated into 4 steps (Fig. 3). First, the Cu is released from the Cu-doped surface/material. Secondly, cell damage begins with membrane ruptures leading to a loss of cytoplasmic content. Next, the production of ROS causes further cell damage by interacting with proteins and lipids, and finally DNA is fragmented, leading to cell death [38].

Some mechanisms can protect bacteria from the toxic effects of Cu ions: (i) active export of Cu from the cell with Cu-transporting ATPase pumps, (ii) sequestration of Cu by Cu-binding metal chaperones or metallothionein, (iii) relative impermeability of bacterial membranes and (iv) transformation of Cu^{+} into the less toxic Cu^{2+} form by multi-Cu oxidases [24,100]. These mechanisms only enable tolerance to Cu ions, delaying the deadly effects, and they are not considered as real resistance processes [102].

4. Angiogenic properties of copper-doped biomaterials

4.1. Effects of copper on angiogenesis

After surgery or injury, the wound healing process takes place in order to repair damaged tissues [103]. In this mechanism, five phases occur: coagulation and hemostasis, inflammation, detersion and proliferation, which encompasses the major healing process and remodeling. It is a complex process in which various cell types and chemical mediators need to be activated and coordinated to enhance healing quality. Angiogenesis is the process of formation and growth of new blood vessels from pre-existing vessels. This physiological mechanism is critical during the complete wound-healing process and plays a vital role during the proliferative phase [104].

Recently it was shown that Cu ions bind to and interact with several growth factors involved in blood vessel formation [105]. Vascular Endothelial Growth Factor (VEGF) is a crucial mediator in the angiogenic process during the proliferative phase. Sen et al. showed that Cu sulfate significantly increased VEGF expression. It accelerated and improved the closure of excisional murine dermal wounds [106]. Angiogenin (ANG) is a ribonuclease and a strong stimulator of angiogenesis that interacts with endothelial cells [107]. Cu can modulate angiogenin transcription and affect the localization of ANG to enhance its function; moreover, it can

Please cite this article as: A. Jacobs, G. Renaudin, C. Forestier et al., Biological properties of copper-doped biomaterials for orthopedic applications: A review of antibacterial, angiogenic and osteogenic aspects, Acta Biomaterialia, https://doi.org/10.1016/j.actbio.2020.09.044

negatively affect endothelial cell migration [108]. Matrix metalloproteinases (MMPs) are involved in the wound-healing process, in particular by regulating the activity of growth factors such as VEGF and promoting cell proliferation in angiogenesis. It has been found that Cu in low concentrations stimulates the activity of MMPs, and high concentrations increase the expression of MMPs in fibroblasts [109].

In 2012, Pickart et al. showed that tripeptide glycyl-L-histidyl-L-lysine (GHK) has a strong affinity for Cu. The authors demonstrated that the complex of GHK with Cu ions (GHK-Cu) increases the expression of proteins such as MMPs, VEGF, collagen, elastin, fibroblast growth factor and nerve growth factor. In addition, this complex has an anti-inflammatory action with the suppression of free radicals in order to prevent oxidative stress [110]. Recently, the angiogenic effects of Cu nanoparticles were investigated with human fibroblast, endothelial and keratinocyte cells. The authors observed that Cu nanoparticles can increase cell migration in the 3 cell types, stimulate the proliferation of endothelial and fibroblast cells, enhance collagen deposition and promote skin wound healing *in vivo*, and do not accumulate in the liver [111]. Cu has beneficial effects on healing mechanisms and particularly on angiogenesis. When a biomaterial is implanted, the wound-healing process takes place; it is therefore rational to investigate if these biological properties are enhanced with Cu-doped biomaterials.

4.2. Effects of copper-doped biomaterials on angiogenesis

Studies on Cu-doped biomaterials and their angiogenic properties are listed in Table 3. Barralet et al. worked with a degradable osteoconductive copper-adsorbed macroporous scaffold. Results indicate that low doses of Cu enable the formation of micro-vessels and improve the wound-healing process in mice [112]. Wu et al. synthesized Cu-containing mesoporous bioactive glass and found a significant increase in VEGF secreted by human Bone Marrow Stromal Cells (hBMSC) and in alkaline phosphatase (ALP) activity – with copper concentrations between 14.2 and 152.7 ppm – indicating an improvement of the angiogenesis capacity compared to undoped materials [64]. Kong et al. worked with a Cu-doped calcium silicate bioceramic. The authors found that the Cu ions extracted from their material exhibited a significant angiogenic effect, with an increase in the vascularization of Human Umbilical Vein Endothelial Cells (HUVEC) and Human Dermal Fibroblasts (HDF) in co-culture and VEGF expression – with an optimal Cu^{2+} concentration of 0.7 ppm only [113]. A borate-based bioactive glass scaffold doped with Cu was fabricated by Wang et al. in 2014. Their results indicated enhanced blood vessel formation and an increase in new bone formed; in other words better bone regeneration in rat calvarial defects when compared to undoped material [114]. In 2016 the same authors evaluated the angiogenesis potential of their Cu-doped borosilicate bioactive glass in a rat calvarial defect model after 8 weeks of implantation. Results showed a much higher number of blood vessels with Cu-doped material than with undoped bioactive glass [115]. The same year, a biocomposite aerogel of mesoporous bioactive glass containing Cu and nanofibrillated cellulose was evaluated on HUVECs and 3T3 fibroblasts. The authors demonstrated a major increase in newly-formed vessels and a significantly higher gene expression of angiogenic genes in 3T3 fibroblasts [46]. In 2016, Bejarano et al. synthesized a composite material with PDLLA polymer mixed with Cu-doped bioactive glass. Results indicated that the doped composite promoted the angiogenesis marker VEGF expression of ST-2 mice bone marrow stromal cells [76]. Recently, Romero-Sanchez et al. evaluated the biological effects of ionic products of Cu-containing mesoporous bioactive glass on bovine aorta endothelial cells (BAEC) and *in vivo* with *zebrafish* embryos. The results showed higher endothelial cell migration and an increase of sub-intestinal venous plexus, indicating that those materials promote angiogenesis [116]. In 2016, Lin et al., synthesized Cu-doped silicate bioactive glass scaffolds. An *in vitro* study was performed with mouse pre-osteoblastic cells to evaluate the ability of the scaffolds to support the growth and differentiation of an osteogenic cell line. *In vivo* experiments were carried out in rat calvarial defects with an implantation time of 6 weeks. Samples showed good cell viability, proliferation and attachment to the surface, comparable to the control except for the sample with the highest Cu content (2 wt% CuO). *In vivo* results showed an increase in blood vessel area with increasing Cu content. A significant result was obtained with the scaffolds containing the highest Cu amount compared to undoped material [117]. Rath et al. fabricated scaffolds of bioactive Cu-doped glass and evaluated their angiogenic potential with BMSC and human dermal microvascular endothelial cells (HDMEC). Results indicated that scaffolds in combination with BMSC enhanced angiogenic potential with an increase in VEGF secretion and allow the formation of endothelial tubes with HDMEC [118]. In 2018, Elrayah et al. worked with Cu-substituted hydroxyapatite scaffolds with several micro- and nano-topographic structures. Their results showed that human Endothelial Cell (EC) viability is dependent on the surface morphology of the scaffold and the culture time. A flower-like shape was the most favorable structure for angiogenic proliferation in EC, and Cu-doped scaffolds enabled an increase in blood vessel formation after 8 weeks in a rabbit model [119]. Recently, Mou et al. fabricated a Cu-doped composite with a nano-calcium-deficient hydroxyapatite and a multi (amino acid) copolymer. Results showed that the sample doped with 1% Cu exhibited better cell adhesion with pseudopods with rat BMSC and superior proliferation compared to an undoped composite. *In vivo* studies indicated greater blood vessel formation and bone regeneration with 1% doped material [120]. Finally, Zhang et al. used calcium phosphate cement doped with Cu and evaluated its angiogenic properties with rat BMSC and HUVEC in co-culture. The results showed good activity and proliferation of both cell types, and an increase in VEGF expression [121].

These studies clearly demonstrate that Cu ions added to biomaterial compositions have beneficial effects on healing mechanisms, and particularly on angiogenesis. Effective concentrations of copper for angiogenesis are heterogeneous; Wu *et al.* indicated efficient Cu^{2+} concentrations ranging from 14.2 to 152.7 ppm [64] and Kong *et al.* demonstrated beneficial results with 0.7 ppm [113]. However, as previously explained, it is essential to take into account several parameters that can influence the results: the type of endothelial cells used, the *in vivo* models, the type of tests used to evaluate the pro-angiogenic effect and the different Cu contents between the biomaterials.

Various endothelial cells were used to investigate angiogenic properties: HUVECS, BAEC, mouse pre-osteoblastic cells, HDMEC. The *in vivo* models used differ between studies: rat, mouse, *zebrafish*. To evaluate the angiogenic effects several parameters were investigated: blood vessel formation, endothelial cell proliferation, level of expression of angiogenic factors like VEGF and of genes characteristic of angiogenesis. As explained before, the wound-healing process and therefore angiogenesis is a complex process involving various cell types and chemical mediators that need to be activated and coordinated to be efficient. Wolf-Brandstetter et al. explained that it appears difficult to evaluate the pro-angiogenic effect of Cu ions using only *in vitro* endothelial cell monoculture models. The authors suggest more complex *in vitro* models like co-cultures with fibroblasts or human mesenchymal stem cells and *ex vivo* models like *zebrafish* embryos, or chick embryo chorioallantoic membranes, in order to show more clearly the impact of Cu ions on angiogenesis [87].

Finally, as previously described, the amount of Cu added to materials varied depending on the studies; thus, it is apparent that this parameter clearly modifies the concentration of Cu release and

Please cite this article as: A. Jacobs, G. Renaudin, C. Forestier et al., Biological properties of copper-doped biomaterials for orthopedic applications: A review of antibacterial, angiogenic and osteogenic aspects, Acta Biomaterialia, https://doi.org/10.1016/j.actbio.2020.09.044

Table 3
Studies of angiogenic and osteogenic properties of Cu-doped biomaterials

Biomaterial		Angiogenic properties		Osteogenic properties		Ref.
Family	Description	Experimental method	Results*	Experimental method	Results*	
Bioceramics	Macroporous bioceramics scaffolds loaded with Cu	Intraperitoneal implantation during 15 days in mice	↗ micro-vessels formation			[112]
	Cu addition to calcium phosphate films			MC3T3-E1 culture (mouse pre-osteoblastic cells) Primary osteoclasts isolated from rabbit long bones	↘ MC3T3-E1 proliferation → MC3T3-E1 differentiation ↘ Primary osteoclasts resorptive activity	[131]
	Brushite scaffolds loaded with Cu			MG 63 osteoblastic cell culture	A↗ activity and proliferation of osteoblastic cells ↗ expression of bone specific proteins (OPN, integrine β-1)	[128]
	Cu-doped calcium silicate bioceramics	HUVEC- HDF co-culture	↗ angiogenic patterns (nodes, circles and tubes) ↗ VEGF secretion			[113]
	Cu-substituted hydroxyapatite coating on titanium			MC3T3-E1 culture (mouse pre-osteoblastic cells)	→cells proliferation	[82]
	Cu-substituted hydroxyapatite scaffold	Subcutaneously implantation in rabbit models for 8 weeks	↗ blood vessel formation			[119]
Bioglasses	Cu-doped bioactive borate glass			Implantation in rat calvarial defects for 12 weeks	↗ bone regeneration	[127]

(continued on next page)

Please cite this article as: A. Jacobs, G. Renaudin, C. Forestier et al., Biological properties of copper-doped biomaterials for orthopedic applications: A review of antibacterial, angiogenic and osteogenic aspects, Acta Biomaterialia, https://doi.org/10.1016/j.actbio.2020.09.044

Table 3 (*continued*)

	Cu-doped mesoporous bioactive glass scaffolds	hBMSC culture	↗ VEGF expression	hBMSC culture	↗ALP activity from hBMSCs ↗ gene expression of ALP, OPN and OCN	[64]
	Bioactive Cu-doped glass scaffold	hBMSC culture hDMEC culture	↗ VEGF secretion from hBMSCs ↗formation of endothelial tube from HDMEC			[118]
	Borate-based bioactive glass scaffold doped with Cu	hBMSC culture Implantation in rate calvarial defect for 8 weeks	↗ ALP activity ↗ blood vessels formation	Implantation in rat calvarial defects for 8 weeks	↗ bone mineral density	[114]
	Cu-doped silicate bioactive glass scaffolds	MC3T3-E1 culture (mouse pre-osteoblastic cells) Implantation in rat calvarial defects for 6 weeks	→ cell viability, proliferation and attachment to the surface ↗ blood vessel formation	Implantation in rat calvarial defects for 6 weeks	→ bone formation	[117]
	Cu-doped borosilicate bioactive glass scaffold	Implantation in rat calvarial defects for 8 weeks	↗ blood vessels formation			[115]
	Cu-containing mesoporous bioactive glass	BAEC culture *Zebrafish* (Danio rerio) embryo assay	↗ cells migration ↗ number and thickness of subintestinal venous plexus			[116]
Biocomposite	Cu incorporation into chitosan scaffolds			Implantation in rat calvarial defects for 4 weeks	↗ bone formation	[132]
	Composite material with PDLLA polymer mixed with Cu doped bioactive glass	ST-2 mice bone marrow stromal cells culture	↗ VEGF secretion			[76]

(*continued on next page*)

Please cite this article as: A. Jacobs, G. Renaudin, C. Forestier et al., Biological properties of copper-doped biomaterials for orthopedic applications: A review of antibacterial, angiogenic and osteogenic aspects, Acta Biomaterialia, https://doi.org/10.1016/j.actbio.2020.09.044

Table 3 (*continued*)

	Biocomposite aerogel of mesoporous bioactive glass containing Cu and nanofibrillated cellulose	HUVEC culture 3T3 fibroblasts culture	↗ angiogenic patterns (branching point, tube length) ↗ blood vessel formation ↗ gene expression of Vegfa, Vegfc, Pdgf and Fgf2 for 3T3 fibroblast			[46]
	Cu-doped composite with a nano calcium-deficient hydroxyapatite and a multi-(amino acid) copolymer	rBMSC culture Implantation in rabbit femoral defect for 12 weeks	↗ adhesion and proliferation ↗ ALP activity ↗ blood vessel formation	rBMSC culture Implantation in rabbit femoral defect for 12 weeks	↗ ALP activity ↗ bone formation	[120]
Bone cements	Cu-containing calcium phosphate cement	mBMSC and HUVEC co-culture	↗mBMSC and HUVEC proliferation ↗VEGF	mBMSC and HUVEC co-culture	↗ gene expression of Col I, ALP, OPN and Runx2	[121]
	Cu-substituted dicalcium silicate cement			Implantation in a mandibular bone defect of rabbit for 16 weeks	↗ bone formation	[74]
Coated/alloyed metals	317L-Cu steel			MC3T3-E1 culture (mouse pre-osteoblastic cells)	↗ ALP expression ↗ expression of osteogenic genes (Col I, OPN, Runx2)	[129]
	Galvanic Cu deposit on titanium alloy			hBMSC culture	↗ ALP expression ↗ expression of osteogenic genes (Col I, OPG, OPN) ↗ mineralization of the cells	[86]
	Cu-bearing stainless steel			MC3T3-E1 culture (mouse pre-osteoblastic cells) Implantation in the lateral epicondyle of rats for 15 days	↗ ALP expression ↗ expression of osteogenic genes (Col I, OPN, Runx2) ↗ bone mineral density	[130]
	Titanium surface coated with Cu			SaOS-2 culture Implantation in rat femoral defect for 8 weeks	↗ gene expression of OCN and Runx2	[84]

*↗ : improvement, →: constant, ↘ : decrease

Please cite this article as: A. Jacobs, G. Renaudin, C. Forestier et al., Biological properties of copper-doped biomaterials for orthopedic applications: A review of antibacterial, angiogenic and osteogenic aspects, Acta Biomaterialia, https://doi.org/10.1016/j.actbio.2020.09.044

so the effect on *in vitro* and *in vivo* tests. Even more than the doping rate, it is the dopant dissolution (concentration and kinetics) which will have an impact on angiogenesis, as established in the review of Hoppe et al. [72].

5. Osteogenic properties of copper-doped biomaterials

5.1. Effects of copper on osteogenesis

Osteogenesis is the process by which new bone tissue is formed, and ideally a bone substitute should allow this mechanism. Osteoblasts are cells derived from mesenchymal stem cells. These are bone-forming cells and act by controlling mineralization by the deposition of hydroxyapatite crystals, producing collagen which is at the origin of the organic matrix [122]. The relation between angiogenesis and osteogenesis is known. Angiogenesis brings all the necessary elements (vascular growth, oxygen, nutrients, soluble factors and several types of cells) needed for osteoblasts to form new bone [123].

Generally synthetic biomaterials have poor osteogenic properties and in practice the addition of an osteogenic growth factor is often needed to achieve correct bone reconstruction. For example, Bone Morphogenetic Proteins (BMP) have been used successfully in bone repair, although some adverse biological effects were found *in vivo* [117]. The diamond concept described by Giannoudis et al. in 2007 clearly demonstrated the complex interactions needed for bone healing. These include 4 elements: osteogenic cells, osteoconductive scaffolds, growth factors and the mechanical environment [124]. It is known that Cu plays a role in the bone metabolism and severe Cu deficiency leads to bone abnormalities [125]. It has been shown that a Cu deficiency results in a decrease in bone strength in rats [126]. Additionally it has been found that Cu significantly increases the deposition of collagen fibers [25]. Cu has beneficial effects on the healing mechanism and can enhance bone formation. Cleary this is a crucial property when a biomaterial is implanted; it is therefore rational to investigate whether Cu-doped biomaterials can help with bone regeneration.

5.2. Effects of copper-doped biomaterials on osteogenesis

Studies on Cu-doped biomaterials and their osteogenic properties are listed in Table 3. In 2016, Lin et al., synthesized Cu-doped silicate bioactive glass scaffolds. An *in vitro* study was performed with mouse pre-osteoblastic cells to evaluate the ability of the scaffolds to support the growth and differentiation of an osteogenic cell line. Samples showed good cell viability, proliferation and attachment to the surface, comparable to the control, except for the sample with the highest Cu content (2 wt% CuO). However, the Cu-doped materials had no significant effect compared to undoped samples *in vitro*. The effects were not significant either on *in vivo* bone formation with rat calvarial defects 6 weeks after implantation [117]. Bi et al., investigated the effects of a bioactive borate glass microstructure and Cu doping on bone regeneration. Their results indicated that the trabecular microstructure showed greater new bone formation than oriented or fibrous microstructures after implantation in rat calvarial defects after 12 weeks. Cu doping (0.4 wt.%) increased osteogenesis only for the fibrous microstructure [127]. In 2014 Wang et al. synthesized borate bioactive glass with 3.0 wt.% CuO. With hBMSCs, the Cu-doped biomaterials increased the ALP activity of the cells and thus had the best capacity to support their osteogenic differentiation. Furthermore, results showed an increase in bone regeneration and blood vessel formation in rat calvarial defects at 8 weeks post-implantation [114]. Ewald et al., worked with brushite scaffolds loaded with Cu ions and evaluated their effect on the growth and activity of osteoblastic cells seeded on the scaffolds. Results indicated that cell activity and proliferation were increased by Cu ions, and the expression of bone specific proteins was enhanced. The authors demonstrated that the activity of osteoblastic cells also increased on brushite alone, compared to polystyrene, indicating an effect of the material structure also [128]. In 2015 Huang et al. worked with a Cu-substituted hydroxyapatite coating on titanium. Their results showed good cell proliferation with osteoblast-like cells from mouse skulls compared to titanium alone; however there was no significant difference between pure and Cu-doped hydroxyapatite [82]. Ren et al. demonstrated that after 3 days of culture, the ALP activity of osteoblasts and the expression of osteogenic genes such as collagen type I (ColI), osteopontin (OPN) and runt-related transcription factor 2 (Runx2) significantly increased for 317L-Cu steel in comparison to undoped 317L steel [129]. In 2015, Ren et al. worked with Cu-bearing stainless steel and demonstrated *in vivo* that more new bone tissue was formed around the Cu-doped implant [130]. Recently, in 2020, Zhang et al. worked with Cu-substituted dicalcium silicate cement, and the results showed that the quantitative new bone formation was significantly higher with Cu cement than for undoped cement [74]. Burghardt et al. prepared a composite with a Cu deposit on titanium alloy. With 0.1 mM of Cu^{2+} there was a stimulation of proliferation of MSC, an increase in ALP activity, a higher expression of ColI, osteoprotegerin (OPG), OPN and mineralization of the cells [86]. In 2010 Yang et al. worked on inorganic additives to calcium phosphate films. Cu deposition showed an inhibitory effect on osteoblast proliferation and differentiation [131]. Wu et al. prepared Cu-containing mesoporous bioactive glass scaffolds and tested these materials and their extracts on hBMSC. The authors demonstrated a significant increase in the expression of bone-related gene ALP, OPN and osteocalcin (OCN) in the cells [64]. D'Mello et al. evaluated the effect of Cu incorporation into chitosan scaffolds *in vivo* in rat calvarial defects. The amount of bone tissue regenerated was twice as high with Cu compared to the scaffold alone, and eleven times higher compared to empty defects [132]. Huang et al. evaluated the effects of a titanium surface coated with Cu on the regulation of macrophages which could interact with the osteogenic properties of the biomaterial. Their results indicated that macrophages grown with Cu^{2+} or on a Cu-doped substitute surface induce a favorable inflammatory environment for osteoblast cell proliferation and differentiation. *In vivo* results with rat models showed an increase in the expression of osteogenic markers like OCN and Runx-2 with the doped material [84]. Mou et al. synthesized a Cu-doped composite with a nano calcium-deficient hydroxyapatite and a multi (amino acid) copolymer. The authors found an increase in the ALP activity of rat BMSCs and a higher mineralization level, which demonstrated a stimulation of the osteoblastic differentiation of the cells [120]. Finally, Zhang et al. found an increase in the osteogenic gene expression of Col I, ALP, OPN and Runx2 from rat BMSC cultured with cu-containing calcium phosphate cement [121].

These studies demonstrated that Cu ions added to the composition of biomaterials can have beneficial effects on the osteogenesis process. However, in some studies, no beneficial effect was found compared to undoped materials and results indicated that the positive effect comes from the topographic structuring of the biomaterial. Surface morphometry is also a strategy studied for the antibacterial improvement of biomaterials [133]. Huang et al. explained that material structuring plays an important role in the adhesion step of cells on the surface of the biomaterial, which corresponds to the first step of bone formation, whereas chemical composition contributes to the proliferation and differentiation steps [82]. The relationship between macrophage and osteogenesis is developed in the study of Huang et al. Macrophages are first recruited in response to physiological signals and create an inflammatory microenvironment. Then bone repair cells react to this in-

Please cite this article as: A. Jacobs, G. Renaudin, C. Forestier et al., Biological properties of copper-doped biomaterials for orthopedic applications: A review of antibacterial, angiogenic and osteogenic aspects, Acta Biomaterialia, https://doi.org/10.1016/j.actbio.2020.09.044

flammatory site created by the macrophages and migrate to the material surface to start their osteogenic role. This indicates that the action of macrophages is needed to promote the proliferation and differentiation of osteoblastic cells [84]. Rodriguez et al. found that Cu reduced the proliferation rate of MSC and increased their differentiation rate, indicating that Cu regulates both processes in an opposing manner [125].

Concerning the role of Cu in osteogenesis, it appears difficult to conclude concerning a specific effect on a specific target. Beneficial effects have been demonstrated, but the precise mechanisms of action are not clearly understood. As osteogenesis is a very complex mechanism, related to angiogenesis and including various factors, cell types and biological processes, it is difficult to correctly investigate, understand and describe the effects of Cu-doped biomaterials on this physiological mechanism.

In addition to the chemical composition of biomaterials, such as copper doping covered in this review, surface properties are known to directly influence cell behavior and therefore new bone formation. Feng *et al.* demonstrated that the architecture of β-TCP scaffolds influence *in vivo* defect healing performance, with higher bone formation and vascular ingrowth [134]. A review concerning the impact of the porosity of scaffolds on osteogenesis indicated that high porosity favors bone ingrowth and osteogenesis by allowing vascularization and high oxygenation. The authors also pointed out that the mechanical properties of the scaffolds can be affected, and are reduced with too high a porosity and too large a pore size [135]. A recent review of Xiao *et al.* reported the effects of surface structure parameters, including structure size, morphology and roughness, on cell behavior. The shape and size of the surface microstructure impact cell morphology, orientation, proliferation and adhesion force, depending on cell type. A combination of micro and nano-structures induce synergistic effects on the proliferation and osteogenic differentiation of bone marrow stem cells. Surface roughness is a key factor which needs to be adjusted. A rough surface can promote cell adhesion and differentiation; however, increasing roughness can lead to cell death. In this review the authors also reported that surface structure impacts osteogenesis by interacting with protein adsorption, cilia modulation and the immune response [136].

It appears clearly that the surface properties of materials strongly influence processes involved in osteogenesis and therefore the osteointegration of orthopedic biomaterials. In a more general context, the biological response depends on a complex interaction between patient-related aspects (age, gender, metabolism, ...), material properties (architecture, biodegradation, composition, porosity, ...) and induced biological responses (cell adhesion and proliferation, protein adhesion, ...) [137].

6. Conclusion

This review focuses on the biological properties provided by Cu-doped biomaterials intended to be implanted in a bone site during orthopedic surgery. Three major properties were discussed: antibacterial, angiogenic and osteogenic, as they represent key steps for ideal bone repair. Concerning antibacterial effects, the vast majority of studies have demonstrated a positive role of copper. Cu ions can produce reactive oxygen species (ROS) and cause damage to lipids, proteins and DNA, leading to the death of the bacteria. Angiogenesis and osteogenesis are related wound-healing processes. Concerning angiogenesis, Cu ions have been found to bind and interact with several growth factors involved in blood vessel formation. For osteogenesis, the specific role of Cu ions is unclear, but some studies have found beneficial effects on osteoblastic cells.

Regarding Cu-doped biomaterials, antibacterial properties are very often found, sometimes with variations in efficacy between studies, depending on various factors such as the Gram of the bacteria, the experimental conditions used and the Cu content of the material. Cu-doped biomaterials exhibited clear angiogenic abilities with the formation of new blood vessels. Osteogenic properties are found in some papers, with new bone formation, but are not described in all studies, which indicates the presence of complex mechanisms, including the undeniable role of the structure of the material, and supports the fact that more studies are necessary to understand clearly how Cu ions interact with the physiological processes of osteogenesis.

The lack of homogeneity concerning chemical and biological characterizations prevents the specification of an ideal model for orthopedic biomaterial. A harmonization between studies would strengthen the bio-adaptation of materials to biological requirements.

Although it appears difficult to concluded on definite guidelines concerning ideal characteristics for these copper-doped materials, it is apparent that copper provides beneficial effects on biological properties. The very numerous recent studies devoted to the role of copper in biomaterials show the interest of the scientific community, and demonstrate the real potential of copper doping for biological/medical applications. Today we are clearly far from past fears linked to the alleged toxicity of this element [138] but, to our knowledge, we are also far from a commercial reality for orthopedic applications.

7. Statement of significance

This review describes the bio-functional advantages offered by Cu and focuses on the antibacterial, angiogenic and osteogenic properties of Cu-doped biomaterials used in orthopedic applications. The chemical role of doping – used in all families of biomaterials (ceramics, composites and metals) – is the main concern of this article.

Our review refers to more than one hundred and twenty papers, among which a quarter date from the past two years, indicating the interest of these materials for clinical applications and the interest of the concerned scientific community.

Declaration of Competing Interest

The authors declare that they have no known competing financial interests or personal relationships that could have appeared to influence the work reported in this paper.

References

[1] J.T.B. Ratnayake, M. Mucalo, G.J. Dias, Substituted hydroxyapatites for bone regeneration: a review of current trends, J. Biomed. Mater. Res. - Part B Appl. Biomater. 105 (2017) 1285–1299, doi:10.1002/jbm.b.33651.
[2] S.V. Dorozhkin, Biocomposites and hybrid biomaterials based on calcium orthophosphates, Biomatter 1 (2011) 3–56, doi:10.4161/biom.1.1.16782.
[3] S.V Dorozhkin, Bioceramics of calcium orthophosphates, Biomaterials 31 (2010) 1465–1485, doi:10.1016/j.biomaterials.2009.11.050.
[4] A. Tathe, M. Ghodke, A.P. Nikalje, A brief review: Biomaterials and their apllication, Int. J. Pharm. Pharm. Sci. 2 (2010) 19–23.
[5] M. Clauss, A. Trampuz, O. Borens, M. Bohner, T. Ilchmann, Biofilm formation on bone grafts and bone graft substitutes: comparison of different materials by a standard in vitro test and microcalorimetry, Acta Biomater. 6 (2010) 3791–3797, doi:10.1016/j.actbio.2010.03.011.
[6] J. Calhoun, M.M. Manring, M. Shirtliff, Osteomyelitis of the Long Bones, Semin. Plast. Surg. 23 (2009) 059–072, doi:10.1055/s-0029-1214158.
[7] G.J.A. ter Boo, D.W. Grijpma, T.F. Moriarty, R.G. Richards, D. Eglin, Antimicrobial delivery systems for local infection prophylaxis in orthopedic- and trauma surgery, Biomaterials 52 (2015) 113–125, doi:10.1016/j.biomaterials.2015.02.020.
[8] F.C. Tenover, Mechanisms of antimicrobial resistance in bacteria, Am. J. Infect. Control. 34 (2006) S3–S10, doi:10.1016/j.ajic.2006.05.219.
[9] EARSS, On-going surveillance of Pneumoniae, S Aureus, S Coli, E Faecium, E Faecalis, E Pneumoniae, K Aeruginosa, P. Aeruginosa, 2008. www.rivm.nl/earss,.
[10] A. Gristina, Biomaterial-centered infection: microbial adhesion versus tissue integration, Science (80-.). 237 (1987) 1588–1595, doi:10.1126/science.3629258.

Please cite this article as: A. Jacobs, G. Renaudin, C. Forestier et al., Biological properties of copper-doped biomaterials for orthopedic applications: A review of antibacterial, angiogenic and osteogenic aspects, Acta Biomaterialia, https://doi.org/10.1016/j.actbio.2020.09.044

[11] R.M. Donlan, Biofilms and device-associated infections, Emerg. Infect. Dis. 7 (2001) 277–281, doi:10.3201/eid0702.010226.
[12] A.V. Karlov, I.A. Khlusov, V.A. Pontak, V.P. Ignatov, M.A. Ivin, S.Y. Zinatulina, Adhesion of Staphylococcus aureus to implants with different physicochemical characteristics, Bull. Exp. Biol. Med. 134 (2002) 277–280 10.1023/A:1021567804286.
[13] G. Jacobs, R. Duval, Silver doping mechanism in bioceramics—From Ag+: doped HAp to Ag°/BCP nanocomposite, Crystals 9 (2019) 326, doi:10.3390/cryst9070326.
[14] S. Gomes, C. Vichery, S. Descamps, H. Martinez, A. Kaur, A. Jacobs, J.-M. Nedelec, G. Renaudin, Cu-doping of calcium phosphate bioceramics: From mechanism to the control of cytotoxicity, Acta Biomater. (2018) 65, doi:10.1016/j.actbio.2017.10.028.
[15] S. Gomes, A. Kaur, J.M. Grenèche, J.M. Nedelec, G. Renaudin, Atomic scale modeling of iron-doped biphasic calcium phosphate bioceramics, Acta Biomater. 50 (2017) 78–88, doi:10.1016/j.actbio.2016.12.011.
[16] G. Renaudin, S. Gomes, J.M. Nedelec, First-row transition metal doping in calcium phosphate bioceramics: a detailed crystallographic study, Materials (Basel) (2017) 10, doi:10.3390/ma10010092.
[17] S. Gomes, A. Kaur, J.M. Nedelec, G. Renaudin, X-ray absorption spectroscopy shining (synchrotron) light onto the insertion of Zn2+ in calcium phosphate ceramics and its influence on their behaviour under biological conditions, J. Mater. Chem. B. 2 (2014) 536–545, doi:10.1039/c3tb21397h.
[18] F. Westhauser, S. Wilkesmann, Q. Nawaz, S.I. Schmitz, A. Moghaddam, S.C. Injury, K. Aschaffenburg-alzenau, Osteogenic properties of manganese-doped mesoporous bioactive glass nanoparticles, J. Biomed. Mater. Res. (2020) 1–10, doi:10.1002/jbm.a.36945.
[19] B. Yilmaz, A.Z. Alshemary, Z. Evis, Co-doped hydroxyapatites as potential materials for biomedical applications, Microchem. J. 144 (2019) 443–453, doi:10.1016/j.microc.2018.10.007.
[20] I. Cacciotti, Multisubstituted hydroxyapatite powders and coatings: the influence of the codoping on the hydroxyapatite performances, Int. J. Appl. Ceram. Technol. 16 (2019) 1864–1884, doi:10.1111/ijac.13229.
[21] F. Paladini, M. Pollini, A. Sannino, L. Ambrosio, Metal-based antibacterial substrates for biomedical applications, Biomacromolecules 16 (2015) 1873–1885, doi:10.1021/acs.biomac.5b00773.
[22] P. Chellan, P.J. Sadler, The elements of life and medicines, Philos. Trans. R. Soc. A Math. Phys. Eng. Sci. (2015) 373, doi:10.1098/rsta.2014.0182.
[23] N.M. Lowe, W.D. Fraser, M.J. Jackson, Is there a potential therapeutic value of copper and zinc for osteoporosis? Proc. Nutr. Soc. 61 (2002) 181–185, doi:10.1079/pns2002154.
[24] M. Vincent, R.E. Duval, P. Hartemann, M. Engels-Deutsch, Contact killing and antimicrobial properties of copper, J. Appl. Microbiol. 124 (2018) 1032–1046, doi:10.1111/jam.13681.
[25] C. Gérard, L.J. Bordeleau, J. Barralet, C.J. Doillon, The stimulation of angiogenesis and collagen deposition by copper, Biomaterials 31 (2010) 824–831, doi:10.1016/j.biomaterials.2009.10.009.
[26] F. Heidenau, W. Mittelmeier, R. Detsch, M. Haenle, F. Stenzel, G. Ziegler, H. Gollwitzer, A novel antibacterial titania coating: metal ion toxicity and in vitro surface colonization, J. Mater. Sci. Mater. Med. 16 (2005) 883–888, doi:10.1007/s10856-005-4422-3.
[27] S. Jin, L. Ren, K. Yang, Bio-functional Cu containing biomaterials: a new way to enhance bio-adaption of biomaterials, J. Mater. Sci. Technol. 32 (2016) 835–839, doi:10.1016/j.jmst.2016.06.022.
[28] C. and H.-A.M. Linder, Copper biochemistry and molecular biology, Am. J. Clin. Nutr. 63 (1996) 797S–811S, doi:10.1093/ajcn/63.5.797.
[29] W. Opsahl, H. Zeronian, M. Ellison, D. Lewis, R.B. Rucker, R.S. Riggins, Role of copper in collagen cross-linking and its influence on selected mechanical properties of chick bone and tendon, J. Nutr. 112 (1982) 708–716, doi:10.1093/jn/112.4.708.
[30] Institute of Medecine, Dietary reference intakes for vitamin A, vitamin K, arsenic, boron, chromium, copper, iodine, iron, manganese, molybdenum, nickel, silicon, vanadium, and zinc, 2001. 10.17226/10026.
[31] EFSA, Scientific opinion on dietary reference values for copper, EFSA J. 13 (2015) 1–51, doi:10.2903/j.efsa.2015.4253.
[32] A.P. Ingle, P. Paralikar, S. Shende, I. Gupta, J.K. Biswas, L.H. Da Silva Martins, M. Rai, Copper in medicine: perspectives and toxicity, Biomed. Appl. Met. (2018) 95–112, doi:10.1007/978-3-319-74814-6_4.
[33] J.Y. Uriu-Adams, C.L. Keen, Copper, oxidative stress, and human health, Mol. Aspects Med. 26 (2005) 268–298, doi:10.1016/j.mam.2005.07.015.
[34] S.M. Wazir, I. Ghobrial, Copper deficiency, a new triad: anemia, leucopenia, and myeloneuropathy, J. Community Hosp. Intern. Med. Perspect. 7 (2017) 265–268, doi:10.1080/20009666.2017.1351289.
[35] J.H. Kaplan, S. Lutsenko, Copper transport in mammalian cells: special care for a metal with special needs, J. Biol. Chem. 284 (2009) 25461–25465, doi:10.1074/jbc.R109.031286.
[36] A. Hordyjewska, Ł. Popiołek, J. Kocot, The many "faces" of copper in medicine and treatment, BioMetals 27 (2014) 611–621, doi:10.1007/s10534-014-9736-5.
[37] M.T. Lorincz, Neurologic Wilson's disease, Ann. N. Y. Acad. Sci. 1184 (2010) 173–187, doi:10.1111/j.1749-6632.2009.05109.x.
[38] G. Grass, C. Rensing, M. Solioz, Metallic copper as an antimicrobial surface, Appl. Environ. Microbiol. 77 (2011) 1541–1547, doi:10.1128/AEM.02766-10.
[39] V.B.P. Sudha, K.O. Singh, S.R. Prasad, P. Venkatasubramanian, Killing of enteric bacteria in drinking water by a copper device for use in the home: laboratory evidence, Trans. R. Soc. Trop. Med. Hyg. 103 (2009) 819–822, doi:10.1016/j.trstmh.2009.01.019.
[40] T.A. Dankovich, J.A. Smith, Incorporation of copper nanoparticles into paper for point-of-use water purification, Water Purif. (2014) 245–251, doi:10.4103/0974-8520.105261.
[41] G. Swain, N. Shinjo, Comparing biofouling control treatments for use on aquaculture nets, Int. J. Mol. Sci. 15 (2014) 22142–22154, doi:10.3390/ijms151222142.
[42] M.G. Schmidt, H.H. Attaway, P.A. Sharpe, J. John, K.A. Sepkowitz, A. Morgan, S.E. Fairey, S. Singh, L.L. Steed, J.R. Cantey, K.D. Freeman, H.T. Michels, C.D. Salgado, Sustained reduction of microbial burden on common hospital surfaces through introduction of copper, J. Clin. Microbiol. 50 (2012) 2217–2223, doi:10.1128/JCM.01032-12.
[43] WHO, Improved hand hygiene to prevent health care-associated infections, Patient Saf. Solut. (2007) 1 10.1016/s1553-7250(07)33134-6.
[44] V.J. Prado, M.M. Esparza, R.A. Vidal, C.T. Durán, Actividad bactericida de superficies de cobre frente a bacterias asociadas a infecciones nosocomiales, en un modelo in vitro de adherencia y sobrevivencia, Rev. Med. Chil. 141 (2013) 291–297, doi:10.4067/S0034-98872013000300002.
[45] C.D. Salgado, K.A. Sepkowitz, J.F. John, J.R. Cantey, H.H. Attaway, K.D. Freeman, P.A. Sharpe, H.T. Michels, M.G. Schmidt, Copper surfaces reduce the rate of healthcare-acquired infections in the intensive care unit, Infect. Control Hosp. Epidemiol. 34 (2013) 479–486, doi:10.1086/670207.
[46] X. Wang, F. Cheng, J. Liu, J.H. Smått, D. Gepperth, M. Lastusaari, C. Xu, L. Hupa, Biocomposites of copper-containing mesoporous bioactive glass and nanofibrillated cellulose: biocompatibility and angiogenic promotion in chronic wound healing application, Acta Biomater. 46 (2016) 286–298, doi:10.1016/j.actbio.2016.09.021.
[47] K. Li, C. Xia, Y. Qiao, X. Liu, Dose-response relationships between copper and its biocompatibility/antibacterial activities, J. Trace Elem. Med. Biol. 55 (2019) 127–135, doi:10.1016/j.jtemb.2019.06.015.
[48] U.S. EPA, Approves registration of antimicrobial copper alloys, Copp. Dev. Assoc. Inc. (2008) https://www.copper.org/about/pressreleases/2008/pr2008_Mar_25.html (accessed March 12, 2020).
[49] P. Deb, A.B. Deoghare, A. Borah, E. Barua, S. Das Lala, Scaffold development using biomaterials: a review, Mater. Today Proc. 5 (2018) 12909–12919, doi:10.1016/j.matpr.2018.02.276.
[50] S.V. Dorozhkin, Calcium orthophosphates, J. Mater. Sci. 42 (2007) 1061–1095, doi:10.1007/s10853-006-1467-8.
[51] G. Daculsi, R.Z. Legeros, E. Nery, K. Lynch, B. Kerebel, Transformation of biphasic calcium phosphate ceramics in vivo: ultrastructural and physicochemical characterization, J. Biomed. Mater. Res. 23 (1989) 883–894, doi:10.1002/jbm.820230806.
[52] W. Suchanek, M. Yoshimura, Processing and properties of hydroxyapatite-based biomaterials for use as hard tissue replacement implants, J. Mater. Res. 13 (1998) 94–117, doi:10.1557/JMR.1998.0015.
[53] S.V. Dorozhkin, Bioceramics of calcium orthophosphates, Biomaterials 31 (2010) 1465–1485, doi:10.1016/j.biomaterials.2009.11.050.
[54] M. Bohner, B.L.G. Santoni, N. Döbelin, β-tricalcium phosphate for bone substitution: synthesis and properties, Acta Biomater. 113 (2020) 23–41, doi:10.1016/j.actbio.2020.06.022.
[55] M. Ebrahimi, M.G. Botelho, S.V. Dorozhkin, Biphasic calcium phosphates bioceramics (HA/TCP): concept, physicochemical properties and the impact of standardization of study protocols in biomaterials research, Mater. Sci. Eng. C. 71 (2017) 1293–1312, doi:10.1016/j.msec.2016.11.039.
[56] V. Stanić, S. Dimitrijević, J. Antić-Stanković, M. Mitrić, B. Jokić, I.B. Plečaš, S. Raičević, Synthesis, characterization and antimicrobial activity of copper and zinc-doped hydroxyapatite nanopowders, Appl. Surf. Sci. 256 (2010) 6083–6089, doi:10.1016/j.apsusc.2010.03.124.
[57] Y. Li, J. Ho, C.P. Ooi, Antibacterial efficacy and cytotoxicity studies of copper (II) and titanium (IV) substituted hydroxyapatite nanoparticles, Mater. Sci. Eng. C. 30 (2010) 1137–1144, doi:10.1016/j.msec.2010.06.011.
[58] Ž. Radovanović, B. Jokić, D. Veljović, S. Dimitrijević, V. Kojić, R. Petrović, D. Janaćković, Antimicrobial activity and biocompatibility of Ag + - and Cu 2+ -doped biphasic hydroxyapatite/α-tricalcium phosphate obtained from hydrothermally synthesized Ag + - and Cu 2+ -doped hydroxyapatite, Appl. Surf. Sci. 307 (2014) 513–519, doi:10.1016/j.apsusc.2014.04.066.
[59] S. Shanmugam, B. Gopal, Copper substituted hydroxyapatite and fluorapatite: synthesis, characterization and antimicrobial properties, Ceram. Int. 40 (2014) 15655–15662, doi:10.1016/j.ceramint.2014.07.086.
[60] A. Bhattacharjee, Y. Fang, T.J.N. Hooper, N.L. Kelly, D. Gupta, K. Balani, I. Manna, T. Baikie, P.T. Bishop, T.J. White, J.V. Hanna, Crystal chemistry and antibacterial properties of cupriferous hydroxyapatite, Materials (Basel) (2019) 12, doi:10.3390/ma12111814.
[61] C.F. Marques, S. Olhero, J.C.C. Abrantes, A. Marote, S. Ferreira, S.I. Vieira, J.M.F. Ferreira, Biocompatibility and antimicrobial activity of biphasic calcium phosphate powders doped with metal ions for regenerative medicine, Ceram. Int. 43 (2017) 15719–15728, doi:10.1016/j.ceramint.2017.08.133.
[62] L.L. Hench, R.J. Splinter, W.C. Allen, T.K. Greenlee, Bonding mechanisms at the interface of ceramic prosthetic materials, J. Biomed. Mater. Res. 5 (1971) 117–141, doi:10.1002/jbm.820050611.
[63] M. Vallet-Regí, A.J. Salinas, Ceramics as bone repair materials, in: Bone Repair Biomater, Elsevier Inc., 2009, pp. 194–230, doi:10.1533/9781845696610.2.194.
[64] C. Wu, Y. Zhou, M. Xu, P. Han, L. Chen, J. Chang, Y. Xiao, Copper-containing mesoporous bioactive glass scaffolds with multifunctional properties of angiogenesis capacity, osteostimulation and antibacterial activity, Biomaterials 34 (2013) 422–433, doi:10.1016/j.biomaterials.2012.09.066.

Please cite this article as: A. Jacobs, G. Renaudin, C. Forestier et al., Biological properties of copper-doped biomaterials for orthopedic applications: A review of antibacterial, angiogenic and osteogenic aspects, Acta Biomaterialia, https://doi.org/10.1016/j.actbio.2020.09.044

[65] H. Palza, B. Escobar, J. Bejarano, D. Bravo, M. Diaz-Dosque, J. Perez, Designing antimicrobial bioactive glass materials with embedded metal ions synthesized by the sol-gel method, Mater. Sci. Eng. C. 33 (2013) 3795–3801, doi:10.1016/j.msec.2013.05.012.
[66] E.A. Abou Neel, I. Ahmed, J. Pratten, S.N. Nazhat, J.C. Knowles, Characterisation of antibacterial copper releasing degradable phosphate glass fibres, Biomaterials 26 (2005) 2247–2254, doi:10.1016/j.biomaterials.2004.07.024.
[67] R.A. Popescu, K. Magyari, A. Vulpoi, D.L. Trandafir, E. Licarete, M. Todea, R. Ştefan, C. Voica, D.C. Vodnar, S. Simon, I. Papuc, L. Baia, Bioactive and biocompatible copper containing glass-ceramics with remarkable antibacterial properties and high cell viability designed for future: in vivo trials, Biomater. Sci. 4 (2016) 1252–1265, doi:10.1039/c6bm00270f.
[68] G.K. Pouroutzidou, G.S. Theodorou, E. Kontonasaki, I. Tsamesidis, A. Pantaleo, D. Patsiaoura, L. Papadopoulou, J. Rhoades, E. Likotrafiti, C.B. Lioutas, K. Chrissafis, K.M. Paraskevopoulos, Effect of ethanol/TEOS ratios and amount of ammonia on the properties of copper-doped calcium silicate nanoceramics, J. Mater. Sci. Mater. Med. 30 (2019) 1–13, doi:10.1007/s10856-019-6297-8.
[69] N. Gupta, D. Santhiya, S. Murugavel, A. Kumar, A. Aditya, M. Ganguli, S. Gupta, Effects of transition metal ion dopants (Ag, Cu and Fe) on the structural, mechanical and antibacterial properties of bioactive glass, Colloids Surf. A Physicochem. Eng. Asp. 538 (2018) 393–403, doi:10.1016/j.colsurfa.2017.11.023.
[70] A. Bari, N. Bloise, S. Fiorilli, G. Novajra, M. Vallet-Regí, G. Bruni, A. Torres-Pardo, J.M. González-Calbet, L. Visai, C. Vitale-Brovarone, Copper-containing mesoporous bioactive glass nanoparticles as multifunctional agent for bone regeneration, Acta Biomater. 55 (2017) 493–504, doi:10.1016/j.actbio.2017.04.012.
[71] F. Foroutan, J. McGuire, P. Gupta, A. Nikolaou, B.A. Kyffin, N.L. Kelly, J.V. Hanna, J. Gutierrez-Merino, J.C. Knowles, S.Y. Baek, E. Velliou, D. Carta, Antibacterial copper-doped calcium phosphate glasses for bone tissue regeneration, ACS Biomater. Sci. Eng. 5 (2019) 6054–6062, doi:10.1021/acsbiomaterials.9b01291.
[72] A. Hoppe, N.S. Güldal, A.R. Boccaccini, A review of the biological response to ionic dissolution products from bioactive glasses and glass-ceramics, Biomaterials 32 (2011) 2757–2774, doi:10.1016/j.biomaterials.2011.01.004.
[73] J.V. Rau, V.M. Wu, V. Graziani, I.V. Fadeeva, A.S. Fomin, M. Fosca, V. Uskoković, The bone building blues: Self-hardening copper-doped calcium phosphate cement and its in vitro assessment against mammalian cells and bacteria, Mater. Sci. Eng. C. 79 (2017) 270–279, doi:10.1016/j.msec.2017.05.052.
[74] F. Zhang, M. Zhou, W. Gu, Z. Shen, X. Ma, F. Lu, X. Yang, Y. Zheng, Z. Gou, Zinc-/copper-substituted dicalcium silicate cement: advanced biomaterials with enhanced osteogenesis and long-term antibacterial properties, J. Mater. Chem. B. (2020) 1–21, doi:10.1039/c9tb02691f.
[75] A.R. Boccaccini, M. Erol, W.J. Stark, D. Mohn, Z. Hong, J.F. Mano, Polymer/bioactive glass nanocomposites for biomedical applications: a review, Compos. Sci. Technol. 70 (2010) 1764–1776, doi:10.1016/j.compscitech.2010.06.002.
[76] J. Bejarano, R. Detsch, A.R. Boccaccini, H. Palza, PDLLA scaffolds with Cu- and Zn-doped bioactive glasses having multifunctional properties for bone regeneration, J. Biomed. Mater. Res. - Part A. 105 (2016) 746–756, doi:10.1002/jbm.a.35952.
[77] K. Sahithi, M. Swetha, M. Prabaharan, A. Moorthi, N. Saranya, K. Ramasamy, N. Srinivasan, N.C. Partridge, N. Selvamurugan, Synthesis and characterization of nanoscale-hydroxyapatite-copper for antimicrobial activity towards bone tissue engineering applications, J. Biomed. Nanotechnol. 6 (2010) 333–339, doi:10.1166/jbn.2010.1138.
[78] B. Li, Y. Li, Y. Wu, Y. Zhao, Synthesis of water-soluble Cu/PAA composite flowers and their antibacterial activities, Mater. Sci. Eng. C 35 (2014) 205–211, doi:10.1016/j.msec.2013.11.006.
[79] V. Narayanan, S. Sumathi, N. Arunai Nambi Raj, Tri-component composite containing Copper-hydroxyapatite/chitosan/ polyvinyl pyrrolidone for bone tissue engineering, J. Biomed. Mater. Res. (2020), doi:10.1002/jbm.a.36950.
[80] J. Wilson, Metallic Biomaterials : State of the Art and New Challenges (2018), doi:10.1016/B978-0-08-102205-4.00001-5.
[81] M. Geetha, A.K. Singh, R. Asokamani, A.K. Gogia, Ti based biomaterials, the ultimate choice for orthopaedic implants - A review, Prog. Mater. Sci. 54 (2009) 397–425, doi:10.1016/j.pmatsci.2008.06.004.
[82] Y. Huang, X. Zhang, R. Zhao, H. Mao, Y. Yan, X. Pang, Antibacterial efficacy, corrosion resistance, and cytotoxicity studies of copper-substituted carbonated hydroxyapatite coating on titanium substrate, J. Mater. Sci. 50 (2015) 1688–1700, doi:10.1007/s10853-014-8730-1.
[83] S. Kalaivani, R.K. Singh, V. Ganesan, S. Kannan, Effect of copper (Cu2+) inclusion on the bioactivity and antibacterial behavior of calcium silicate coatings on titanium metal, J. Mater. Chem. B. 2 (2014) 846–858, doi:10.1039/c3tb21522a.
[84] Q. Huang, Z. Ouyang, Y. Tan, H. Wu, Y. Liu, Activating macrophages for enhanced osteogenic and bactericidal performance by Cu ion release from micro/nano-topographical coating on a titanium substrate, Acta Biomater 100 (2019) 415–426, doi:10.1016/j.actbio.2019.09.030.
[85] R. Ghosh, O. Swart, S. Westgate, B.L. Miller, M.Z. Yates, Antibacterial copper-hydroxyapatite composite coatings via electrochemical synthesis, Langmuir 35 (2019) 5957–5966, doi:10.1021/acs.langmuir.9b00919.
[86] I. Burghardt, F. Lüthen, C. Prinz, B. Kreikemeyer, C. Zietz, H.G. Neumann, J. Rychly, A dual function of copper in designing regenerative implants, Biomaterials (2015) 44, doi:10.1016/j.biomaterials.2014.12.022.
[87] C. Wolf-Brandstetter, R. Beutner, R. Hess, S. Bierbaum, K. Wagner, D. Scharnweber, U. Gbureck, C. Moseke, Multifunctional calcium phosphate based coatings on titanium implants with integrated trace elements, Biomed. Mater. 15 (2020) 1–18, doi:10.1088/1748-605X/ab5d7b.
[88] M.A. Akhtar, K. Ilyas, I. Dlouh, F. Siska, A.R. Boccaccini, Electrophoretic deposition of copper (II)– Chitosan complexes for antibacterial coatings, Int. J. Mol. Sci. 21 (2020) 1–19, doi:10.3390/ijms21072637.
[89] L. Ren, K. Yang, L. Guo, H.W. Chai, Preliminary study of anti-infective function of a copper-bearing stainless steel, Mater. Sci. Eng. C. 32 (2012) 1204–1209, doi:10.1016/j.msec.2012.03.009.
[90] L. Ren, Z. Ma, M. Li, Y. Zhang, W. Liu, Z. Liao, K. Yang, Antibacterial properties of Ti-6Al-4V-xCu alloys, J. Mater. Sci. Technol. 30 (2014) 699–705, doi:10.1016/j.jmst.2013.12.014.
[91] H. Chai, L. Guo, X. Wang, Y. Fu, J. Guan, L. Tan, L. Ren, K. Yang, Antibacterial effect of 317L stainless steel contained copper in prevention of implant-related infection in vitro and in vivo, J. Mater. Sci. Mater. Med. 22 (2011) 2525–2535, doi:10.1007/s10856-011-4427-z.
[92] D. Zhang, L. Ren, Y. Zhang, N. Xue, K. Yang, M. Zhong, Antibacterial activity against Porphyromonas gingivalis and biological characteristics of antibacterial stainless steel, Colloids Surfaces B Biointerfaces 105 (2013) 51–57, doi:10.1016/j.colsurfb.2012.12.025.
[93] E. Zhang, F. Li, H. Wang, J. Liu, C. Wang, M. Li, K. Yang, A new antibacterial titanium-copper sintered alloy: Preparation and antibacterial property, Mater. Sci. Eng. C. 33 (2013) 4280–4287, doi:10.1016/j.msec.2013.06.016.
[94] Z. Ma, L. Ren, R. Liu, K. Yang, Y. Zhang, Z. Liao, W. Liu, M. Qi, R.D.K. Misra, Effect of heat treatment on Cu distribution, antibacterial performance and cytotoxicity of Ti-6Al-4V-5Cu Alloy, J. Mater. Sci. Technol. 31 (2015) 723–732, doi:10.1016/j.jmst.2015.04.002.
[95] L. Nan, J. Cheng, K. Yang, Antibacterial behavior of a Cu-bearing type 200 stainless steel, J. Mater. Sci. Technol. 28 (2012) 1067–1070 10.1016/S1005-0302(12)60174-1.
[96] L. Nan, Y. Liu, M. Lü, K. Yang, Study on antibacterial mechanism of copper-bearing austenitic antibacterial stainless steel by atomic force microscopy, J. Mater. Sci. Mater. Med. 19 (2008) 3057–3062, doi:10.1007/s10856-008-3444-z.
[97] E. Zhang, C Liu, A new antibacterial Co-Cr-Mo-Cu alloy: Preparation, biocorrosion, mechanical and antibacterial property, Mater. Sci. Eng. C. 69 (2016) 134–143, doi:10.1016/j.msec.2016.05.028.
[98] C. Espírito Santo, N. German, J. Elguindi, G. Grass, C. Rensing, Biocidal mechanisms of metallic copper surfaces, Use Biocidal Surfaces Reduct. Healthc. Acquir. Infect. (2014) 103–136, doi:10.1007/978-3-319-08057-4_6.
[99] M. Hans, S. Mathews, F. Mücklich, M. Solioz, Physicochemical properties of copper important for its antibacterial activity and development of a unified model, Biointerphases 11 (2016) 018902, doi:10.1116/1.4935853.
[100] G. Borkow, J. Gabbay, Copper as a biocidal tool, Curr. Med. Chem. 12 (2005) 2163–2175, doi:10.2174/0929867054637617.
[101] R. Nandakumar, C.E. Santo, N. Madayiputhiya, G. Grass, Quantitative proteomic profiling of the Escherichia coli response to metallic copper surfaces, BioMetals 24 (2011) 429–444, doi:10.1007/s10534-011-9434-5.
[102] E. Ladomersky, M.J. Petris, Copper tolerance and virulence in bacteria, Metallomics 7 (2015) 957–964, doi:10.1039/c4mt00327f.
[103] R.S. Kirsner, W.H. Eaglstein, The wound healing process, Dermatol. Clin. 11 (1993) 629–640 10.1016/s0733-8635(18)30216-x.
[104] T. Velnar, T. Bailey, V. Smrkolj, The wound healing process: An overview of the cellular and molecular mechanisms, J. Int. Med. Res. 37 (2009) 1528–1542, doi:10.1177/147323000903700531.
[105] A.P. Kornblatt, V.G. Nicoletti, A. Travaglia, The neglected role of copper ions in wound healing, J. Inorg. Biochem. 161 (2016) 1–8, doi:10.1016/j.jinorgbio.2016.02.012.
[106] C.K. Sen, S. Khanna, M. Venojarvi, P. Trikha, E. Christopher Ellison, T.K. Hunt, S. Roy, Copper-induced vascular endothelial growth factor expression and wound healing, Am. J. Physiol. - Hear. Circ. Physiol. 282 (2002) 1821–1827, doi:10.1152/ajpheart.01015.2001.
[107] X. Gao, Z. Xu, Mechanisms of action of angiogenin, Acta Biochim. Biophys. Sin. 40 (2008) 663–669, doi:10.1111/j.1745-7270.2008.
[108] C. Giacomelli, M.L. Trincavelli, C. Satriano, Ö. Hansson, D. La Mendola, E. Rizzarelli, C. Martini, Copper (II) ions modulate Angiogenin activity in human endothelial cells, Int. J. Biochem. Cell Biol. 60 (2015) 185–196, doi:10.1016/j.biocel.2015.01.005.
[109] N. Philips, H. Hwang, S. Chauhan, D. Leonardi, S. Gonzalez, Stimulation of cell proliferation and expression of matrixmetalloproteinase-1 and interluekin-8 genes in dermal fibroblasts by copper, Connect. Tissue Res. 51 (2010) 224–229, doi:10.3109/03008200903288431.
[110] L. Pickart, J.M. Vasquez-Soltero, A. Margolina, The human tripeptide GHK-Cu in prevention of oxidative stress and degenerative conditions of aging: Implications for cognitive health, Oxid. Med. Cell. Longev. 2012 (2012) 1–8, doi:10.1155/2012/324832.
[111] S. Alizadeh, B. Seyedalipour, S. Shafieyan, A. Kheime, P. Mohammadi, N. Aghdami, Copper nanoparticles promote rapid wound healing in acute full thickness defect via acceleration of skin cell migration, proliferation, and neovascularization, Biochem. Biophys. Res. Commun. 517 (2019) 684–690, doi:10.1016/j.bbrc.2019.07.110.
[112] J. Barralet, U. Gbureck, P. Habibovic, E. Vorndran, C. Gerard, C.J. Doillon, Angiogenesis in calcium phosphate scaffolds by inorganic copper ion release, Tissue Eng. Part A. 15 (2009) 1601–1609, doi:10.1089/ten.tea.2007.0370.
[113] N. Kong, K. Lin, H. Li, J. Chang, Synergy effects of copper and silicon ions on stimulation of vascularization by copper-doped calcium silicate, J. Mater. Chem. B. 2 (2014) 1100–1110, doi:10.1039/c3tb21529f.

Please cite this article as: A. Jacobs, G. Renaudin, C. Forestier et al., Biological properties of copper-doped biomaterials for orthopedic applications: A review of antibacterial, angiogenic and osteogenic aspects, Acta Biomaterialia, https://doi.org/10.1016/j.actbio.2020.09.044

[114] H. Wang, S. Zhao, J. Zhou, Y. Shen, W. Huang, C. Zhang, M.N. Rahaman, D. Wang, Evaluation of borate bioactive glass scaffolds as a controlled delivery system for copper ions in stimulating osteogenesis and angiogenesis in bone healing, J. Mater. Chem. B. 2 (2014) 8547–8557, doi:10.1039/c4tb01355g.
[115] H. Wang, S. Zhao, W. Xiao, J. Xue, Y. Shen, J. Zhou, W. Huang, M.N. Rahaman, C. Zhang, D. Wang, Influence of Cu doping in borosilicate bioactive glass and the properties of its derived scaffolds, Mater. Sci. Eng. C. 58 (2016) 194–203.
[116] L.B. Romero-Sánchez, M. Marí-Beffa, P. Carrillo, M.Á. Medina, A. Díaz-Cuenca, Copper-containing mesoporous bioactive glass promotes angiogenesis in an in vivo zebrafish model, Acta Biomater. 68 (2018) 272–285, doi:10.1016/j.actbio.2017.12.032.
[117] Y. Lin, W. Xiao, B.S. Bal, M.N. Rahaman, Effect of copper-doped silicate 13-93 bioactive glass scaffolds on the response of MC3T3-E1 cells in vitro and on bone regeneration and angiogenesis in rat calvarial defects in vivo, Mater. Sci. Eng. C. 67 (2016) 440–452, doi:10.1016/j.msec.2016.05.073.
[118] S.N. Rath, A. Brandl, D. Hiller, A. Hoppe, U. Gbureck, R.E. Horch, A.R. Boccaccini, U. Kneser, Bioactive copper-doped glass scaffolds can stimulate endothelial cells in co-culture in combination with mesenchymal stem cells, PLoS One 9 (2014) 1–24, doi:10.1371/journal.pone.0113319.
[119] A. Elrayah, W. Zhi, S. Feng, S. Al-Ezzi, H. Lei, J. Weng, Preparation of micro/nano-structure copper-substituted hydroxyapatite scaffolds with improved angiogenesis capacity for bone regeneration, Materials (Basel) (2018) 11, doi:10.3390/ma11091516.
[120] P. Mou, H. Peng, L. Zhou, L. Li, H. Li, Q. Huang, A novel composite scaffold of Cu-doped nano calcium-deficient hydroxyapatite/multi-(Amino acid) copolymer for bone tissue regeneration, Int. J. Nanomed. 14 (2019) 3331–3343, doi:10.2147/IJN.S195316.
[121] J. Zhang, H. Wu, F. He, T. Wu, L. Zhou, J. Ye, Concentration-dependent osteogenic and angiogenic biological performances of calcium phosphate cement modified with copper ions, Mater. Sci. Eng. C. 99 (2019) 1199–1212, doi:10.1016/j.msec.2019.02.042.
[122] I. Couret, Biologie du remodelage osseux, 28 (2004) 57–65.
[123] J.M. Kanczler, R.O.C. Oreffo, Osteogenesis and angiogenesis: the potential for engineering bone, Eur. Cells Mater. 15 (2008) 100–114, doi:10.22203/eCM.v015a08.
[124] P.V. Giannoudis, T.A. Einhorn, D. Marsh, Fracture healing: the diamond concept, Inj. Int. J. Caree Inj. 38 (2007) S3–S6 10.1016/s0020-1383(08)70003-2.
[125] J. Pablo Rodriguez, S. Rios, M. Gonzalez, Modulation of the proliferation and differentiation of human mesenchymal stem cells by copper, J. Cell. Biochem. 85 (2002) 92–100, doi:10.1002/jcb.10111.
[126] J. Jonas, J. Burns, E.. Abel, M.. Cresswell, J.. Strain, C.. Paterson, Impaired mechanical strength of bone in experimental copper deficiency, Ann. Nutr. Metab. 37 (1993) 245–252, doi:10.1159/000177774.
[127] L. Bi, M.N. Rahaman, D.E. Day, Z. Brown, C. Samujh, X. Liu, A. Mohammadkhah, V. Dusevich, J.D. Eick, L.F. Bonewald, Effect of bioactive borate glass microstructure on bone regeneration, angiogenesis, and hydroxyapatite conversion in a rat calvarial defect model, Acta Biomater. 9 (2013) 8015–8026, doi:10.1016/j.actbio.2013.04.043.
[128] A. Ewald, C. Käppel, E. Vorndran, C. Moseke, M. Gelinsky, U. Gbureck, The effect of Cu(II)-loaded brushite scaffolds on growth and activity of osteoblastic cells, J. Biomed. Mater. Res. - Part A 100A (2012) 2392–2400, doi:10.1002/jbm.a.34184.
[129] L. Ren, K. Yang, Bio-functional design for metal implants, a new concept for development of metallic biomaterials, J. Mater. Sci. Technol. 29 (2013) 1005–1010, doi:10.1016/j.jmst.2013.09.008.
[130] L. Ren, H.M. Wong, C.H. Yan, K.W.K. Yeung, K. Yang, Osteogenic ability of Cu-bearing stainless steel, J. Biomed. Mater. Res. - Part B Appl. Biomater. 103 (2015) 1433–1444, doi:10.1002/jbm.b.33318.
[131] L. Yang, S. Perez-Amodio, F.Y.F. Barrère-de Groot, V. Everts, C.A. van Blitterswijk, P. Habibovic, The effects of inorganic additives to calcium phosphate on in vitro behavior of osteoblasts and osteoclasts, Biomaterials 31 (2010) 2976–2989, doi:10.1016/j.biomaterials.2010.01.002.
[132] S. D'Mello, S. Elangovan, L. Hong, R.D. Ross, D.R. Sumner, A.K. Salem, Incorporation of copper into chitosan scaffolds promotes bone regeneration in rat calvarial defects, J. Biomed. Mater. Res. - Part B Appl. Biomater. 103 (2015) 1044–1049, doi:10.1002/jbm.b.33290.
[133] D. Campoccia, L. Montanaro, C.R. Arciola, A review of the biomaterials technologies for infection-resistant surfaces, Biomaterials 34 (2013) 8533–8554, doi:10.1016/j.biomaterials.2013.07.089.
[134] Y.F. Feng, L. Wang, X. Li, Z.S. Ma, Y. Zhang, Z.Y. Zhang, W. Lei, Influence of architecture of β-tricalcium phosphate scaffolds on biological performance in repairing segmental bone defects, PLoS One 7 (2012) 1–12, doi:10.1371/journal.pone.0049955.
[135] V. Karageorgiou, D. Kaplan, Porosity of 3D biomaterial scaffolds and osteogenesis, Biomaterials 26 (2005) 5474–5491, doi:10.1016/j.biomaterials.2005.02.002.
[136] D. Xiao, J. Zhang, C. Zhang, D. Barbieri, H. Yuan, L. Moroni, G. Feng, The role of calcium phosphate surface structure in osteogenesis and the mechanisms involved, Acta Biomater 106 (2020) 22–33, doi:10.1016/j.actbio.2019.12.034.
[137] M. Bohner, Y. Loosli, G. Baroud, D. Lacroix, Deciphering the link between architecture and biological response of a bone graft substitute, Acta Biomater 7 (2011) 478–484, doi:10.1016/j.actbio.2010.08.008.
[138] M.E. Letelier, S. Sánchez-Jofré, L. Peredo-Silva, J. Cortés-Troncoso, P. Aracena-Parks, Mechanisms underlying iron and copper ions toxicity in biological systems: pro-oxidant activity and protein-binding effects, Chem. Biol. Interact. 188 (2010) 220–227, doi:10.1016/j.cbi.2010.06.013.

Please cite this article as: A. Jacobs, G. Renaudin, C. Forestier et al., Biological properties of copper-doped biomaterials for orthopedic applications: A review of antibacterial, angiogenic and osteogenic aspects, Acta Biomaterialia, https://doi.org/10.1016/j.actbio.2020.09.044

4.3. L'argent

4.3.1. Propriétés antibactériennes de l'argent et mode d'action

L'argent (Ag) est un métal classé parmi les métaux lourds et qui est connu depuis longtemps pour ses propriétés antibactériennes. En effet, l'argent était utilisé dans la fabrication de bouteilles pour stocker l'eau par le roi de Perse. Plus tard en 1869 Raudin démontra que la moisissure *Aspergillus niger* ne pouvait pas se développer dans des récipients en argent. Aujourd'hui son application se retrouve encore dans la désinfection de l'eau, la guérison de brûlures et l'élimination de tissus de granulation présents lors d'une mauvaise régulation de la cicatrisation notamment avec l'utilisation de crayon au nitrate d'argent [91,107]. Il existe également des pansements et des crèmes à l'argent utilisés sur des brûlures, des plaies traumatiques et des ulcères (**Figure 1.7**) [108]. Ce n'est pas un composé présent naturellement dans l'organisme ; contrairement au zinc ou au cuivre ; mais il est relativement bien toléré par l'organisme. Il est absorbé en petite quantité par l'intestin et en majorité excrété par le foie [109].

Depuis quelques années le domaine médical s'intéresse à l'argent pour ses propriétés antibactériennes à très faibles concentrations. En effet, Nies a démontré que seulement 0,02 mM d'Ag^{+} était nécessaire pour atteindre la concentration minimale inhibitrice sur *E. coli*, contre 20 mM par exemple pour Mn^{2+} [110]. Nishjima *et al*. ont montré que 0,25 µM d'ions Ag permettaient de tuer 99 % des bactéries *S. aureus* et *E. coli*, alors que pour le cuivre et le zinc une concentration bien supérieure est nécessaire pour obtenir ce résultat, précisément 10 µM pour le zinc pour tuer les 2 souches et pour le cuivre 25 µM pour tuer *S. aureus* et 10 µM pour tuer *E. coli* [111].

a) b)

Figure 1.7 : a) Pansement enduit à l'argent Acticoat 7 (https://www.smith-nephew.com/fr-canada/produits/traitement-avance-des-plaies/acticoat--7/), b) Bandage avec un pansement en nylon imprégné d'argent (d'après [2] avec l'accord de David J Barillo).

Concernant le mode d'action de l'argent, les mécanismes impliqués ne sont pas clairement décrits dans la littérature mais des voies d'action sont néanmoins envisagées. L'argent peut se lier aux groupements sulfures des protéines ce qui les rend inactives et bloque certaines fonctionnalités de la bactérie. Il cause aussi des perforations au niveau de la membrane bactérienne, ce qui induit une augmentation de la perméabilité et donc des fuites de métabolites. Il interagit aussi avec l'ADN bactérien ce qui perturbe sa réplication et entraîne la mort de la bactérie [112]. Il a aussi été démontré que l'argent pouvait générer des espèces réactives de l'oxygène (ROS) qui endommagent les protéines et l'ADN [113].

Dans la littérature certaines études démontrent des cas de résistance bactérienne à l'argent. Une souche de *Salmonella typhimurium* résistante à l'argent a été reportée dans un hôpital. Cette résistance est apportée par le plasmide pMG101 dont les gènes codent pour des protéines qui forment des canaux d'efflux membranaires capables d'évacuer les ions Ag^+ via une pompe à proton H^+. Ce mécanisme a aussi été observé chez des souches d'*E. coli* K-12 et 0157:H7 [114]. Ce plasmide confère également une résistance au mercure et à plusieurs antibiotiques comme l'ampicilline, le chloramphénicol, la tétracycline, la streptomycine et les sulfamides [115]. Un autre plasmide pUPI199 a aussi été isolé chez une souche environnementale de *Acinetobacter baumannii*, apportant une résistance au nitrate d'argent et ce plasmide était transférable à *E. coli* par conjugaison [116]. Cependant, les cas de résistance bactérienne à l'argent restent rares et les mécanismes d'action antibactériens des ions à plusieurs niveaux sur les bactéries, contrairement aux antibiotiques, font que le développement de ces résistances est peu probable.

4.3.2. Les biomatériaux dopés à l'argent

Aujourd'hui de nombreuses études démontrent l'efficacité antibactérienne de matériaux sous différentes formes contenant de l'argent. Deux formes sont principalement utilisées : la forme ionique Ag^+ et la forme métallique Ag° composée de nanoparticules d'argent.

En 2008 Hwang *et al*. ont préparé des nano-poudres de phosphates de calcium dopées à l'Ag avec un protocole de pyrolyse par pulvérisation électrostatique. Les particules obtenues ont une taille de 70-90 nm et les résultats des tests antibactériens ont démontré une réduction bactérienne de 99 % pour *E. coli* avec les nanopoudres contenant de l'argent [117]. En 2010 Sygnatowicz *et al.* ont synthétisé des nanopoudres d'hydroxyapatite dopées à l'argent et ont montré un effet antibactérien sur *S. aureus* [118]. De *l'hydroxyapatite* dopée à l'Ag a été déposée à la surface de substrats en titane par projection plasma et une activité antibactérienne a été démontrée sur *P. aeruginosa* avec une diminution de l'adhésion des bactéries [109]. La même année Iqbal *et al.* ont synthétisé des particules d'hydroxyapatites dopées à l'Ag par une irradiation aux micro-ondes. Ils ont démontré une zone d'inhibition de la croissance pour les 4 bactéries testées : *S. aureus*, *B. subtilis*, *P. aeruginosa* et *E. coli* [119]. Jadalannagari *et al*. ont synthétisé des nanoparticules d'HAp dopées à l'Ag par une méthode sol-gel modifiée et ont obtenu un effet antibactérien sur les 2 souches testées *S. aureus* et *E. coli* avec des zones d'inhibition de croissance bactérienne [120]. Shi *et al.* ont préparé des disques d'HAp dopés à l'Ag par voie hydrothermale et les résultats ont montré une réduction de l'adhésion de *S. aureus* et *E. coli* en présence des biocéramiques dopées [121]. Fu *et al.* ont déposé des nanoparticules d'argent sur de l'HAp préalablement déposée sur un substrat en titane qui a permis de diminuer fortement la croissance bactérienne d'*E. coli* [122]. En 2017 Gokcekaya *et al.* ont préparé des poudres d'HAp dopées à l'Ag par précipitation et déposé ces poudres sur des disques de titane et d'acier inoxydable par pulvérisation électrostatique. Les résultats ont montré une diminution significative du nombre de bactéries viables chez *E. coli* après 3h et cet effet se poursuit après 9h et 24h [123]. Récemment en 2018, Wang *et al.* ont synthétisé des particules d'HAP dopées à l'Ag et testé leur efficacité antibactérienne sur *E. coli* et *S. aureus*. A nouveau, les résultats indiquent que la croissance bactérienne des 2 souches et presque complètement inhibée par les particules dopées [124].

Il apparaît souvent dans ces études que c'est la concentration en ions Ag qui définit son efficacité. Cependant encore peu d'études mesurent les quantités d'ions relargués alors que cette information est très importante pour comprendre et interpréter les résultats observés. Parmi les études citées ici, 3 ont dosé les quantités d'argent relargué par leurs matériaux. Roy *et al.* ont mesuré les ions Ag^+ relargués dans du PBS (Phosphate Buffer Saline) à 37 °C avec

des concentrations d'environ 0,2 ppm après 6h et entre 0,6 et 3 ppm après 7 jours [109]. Shi *et al*. ont aussi mesuré les ions argent relargués dans du PBS. Après 4 jours les concentrations étaient entre 360 ppb et 1 ppb [121]. En 2012 Iqbal *et al*. ont mesuré des concentrations comprises entre 0,18 et 0,35 ppm après 12h d'immersion dans du PBS également [119]. Cependant les mesures présentées ici ne sont pas réalisées dans les mêmes milieux de culture que ceux utilisés pour évaluer les propriétés antibactériennes des matériaux. Aussi, il a été démontré que dans les milieux biologiques le taux maximal d'Ag^+ libre est d'environ 1 ppm puisqu'ensuite l'argent forme un complexe ou précipite avec des anions environnants, le rendant alors inactif [125].

Enfin, il apparaît également très important de s'assurer de la non-toxicité de ces matériaux envers les cellules eucaryotes pour assurer leur biocompatibilité. L'adhésion d'ostéoblastes humains a été évaluée sur des disques de titane et d'acier inoxydable dans l'étude de Gokcekaya *et al.* en 2017. Les résultats ont montré une très bonne adhésion des ostéoblastes dans toutes les conditions testées, avec des taux comparables au contrôle sans argent [123]. Roy *et al.* ont observé une diminution de la prolifération d'ostéoblastes humains en présence de leur matériau contenant la plus forte concentration d'argent (6 % massique) [109]. En 2016 Shi *et al.* ont également démontré une inhibition de la prolifération d'ostéoblastes murins et une diminution de leur attachement à la surface des biocéramiques pour le matériau le plus fortement dopé (197 ppm d'Ag) [121]. Il apparaît une nouvelle fois que les effets des ions argent soient fonction de leur concentration, d'où l'importance de déterminer les taux d'incorporation et d'évaluer les taux de relargage lors des tests biologiques.

4.4. L'or

4.4.1. Généralités et utilisations médicales de l'or

L'or, de symbole chimique Au, est un métal encore plus noble que Ag et Cu, ce qui signifie qu'il possède la capacité de résister à l'oxydation et à la corrosion. Un des premiers emplois médicaux de l'or a été pour la contention dentaire (**Figure 1.8**).

Figure 1.8 : Copie d'un appareil en or sur une mâchoire inférieure, destiné à immobiliser des dents. Collection Musée de l'AP-HP collection de l'ancien musée Pierre Fauchard. Source : https://www.biusante.parisdescartes.fr/histmed/image?ap-2003-6-6-8-1-4

Il est très utilisé depuis longtemps en odontologie car il est biocompatible. En effet en 2004 Turner *et al.* ont montré que des fibroblastes humains étaient capables de s'attacher et de croitre sur des surfaces recouvertes d'or [126]. Il est également malléable pour s'adapter et s'ajuster à l'anatomie des dents et il ne s'altère pas même en milieux biologiques comme la bouche [127].

L'or est très souvent utilisé sous formes de nanoparticules dans la médecine. Ces nanoparticules d'or sont principalement employées comme agents de contraste pour l'imagerie et le diagnostic médical, comme immunomarqueurs pour repérer et déterminer des structures cellulaires, comme système d'administration de médicaments et comme sources de chaleur pour traiter des cellules cancéreuses par hyperthermie [128–132].

4.4.2. Propriétés antibactériennes de l'or

En 1999 Nies a montré que les ions or, Au^{3+}, avaient une activité antibactérienne à très faible concentration sur *E. coli* avec une concentration minimale inhibitrice similaire à celle des ions Ag^{+} qui est de 0,02 mM [110]. Depuis quelques études ont également démontré les propriétés antibactériennes de composés contenant de l'or.

En 2010 Gao *et al*. ont synthétisé un composite cœur-coquille Au/C avec un cœur composé de carbone et une coquille d'or. Les auteurs ont évalué les propriétés antibactériennes de ce composite sur *E. coli*, *S. aureus et C. albicans*. Les résultats ont montré une zone d'inhibition de croissance pour les 3 microorganismes testés [133]. En 2016 Shamaila *et al.* ont montré que des nanoparticules d'or avaient un effet antibactérien contre *E. coli*, *S. aureus*, *B. subtilis* et *K. pneumonia* [134]. Cui *et al.*, puis Uma Suganya *et al.*, ont respectivement montré des propriétés antibactériennes de nanoparticules d'or sur *E. coli* et sur *S. aureus* et *B. subtilis*. Les auteurs indiquent que les nanoparticules induisent un disfonctionnement des membranes bactériennes, une réduction de la production d'ATP, une modification de leur morphologie et la détérioration de la membrane qui perd donc sa fonction protectrice [135,136].

Enfin il a aussi été montré que les nanoparticules d'or en combinaison avec des antibiotiques avaient des propriétés antibactériennes. Fayaz *et al.* ont montré que des nanoparticules d'or liées à de la vancomycine avaient un effet antibactérien supérieur contre *E. coli, S. aureus* et *S. aureus* résistant à la vancomycine, comparé à l'antibiotique utilisé seul [137]. En 2019 Lee *et al.* ont montré que des nanoparticules d'or avaient une activité antibactérienne comparable à celle des antibiotiques céfotaxime et ciprofloxacine sur 3 souches de *Salmonella* : *S. typhimurium*, *S. typhi* et *S. enteriditis*. Les auteurs ont aussi montré que ces nanoparticules couplées au céfotaxime et à la ciprofloxacine avaient un effet synergique sur l'activité antibactérienne. Ils concluent que l'effet antibactérien est plus important quand les nanoparticules d'or sont utilisées en combinaison avec ces 2 antibiotiques. Ils montrent également que les nanoparticules agissent en perturbant l'homéostasie intracellulaire et que les antibiotiques créent des ROS, ce qui conduit à la mort des bactéries [138].

4.4.3. Propriétés ostéogéniques de l'or

L'or est beaucoup moins utilisé comme dopants dans les biomatériaux que le cuivre et l'argent. Cependant il peut être intéressant puisque des études ont montré que des nanoparticules d'or avaient des effets sur l'ostéogénèse.

En 2010 Yi *et al.* ont étudié les effets de nanoparticules d'or sur des cellules souches mésenchymateuses de souris. Les résultats ont indiqué une augmentation de la différenciation cellulaire des cellules souches en ostéoblastes et une diminution de leur différenciation en adipocytes. Aussi les auteurs ont montré une meilleure minéralisation des cellules, une augmentation de l'expression des gènes marqueurs de l'ostéogénèse (ALP, Runx2, OCN, ColI, et BMP2). Plus précisément les auteurs ont suggéré que les nanoparticules d'or sont internalisées au contact de la membrane cellulaire ce qui induit un stimulus qui active une protéine kinase MAPK p38 (Mitogen-Activated Protein Kinase) qui favorise la différenciation

ostéoblastique [139]. En 2015 Choi *et al.* ont étudié l'effet de nanoparticules d'or conjuguées à du chitosan, les résultats ont montré une augmentation de l'ostéogénèse de cellules souches humaines dérivées d'adipocytes. Les auteurs suggèrent que la voie de signalisation Wnt/β-caténine est utilisée pour orienter la différenciation cellulaire des cellules souches adipogéniques vers l'ostéogénèse et non vers l'adipogénèse [140].

Yao *et al.* ont démontré que des nanoparticules d'or de 30 nm à une concentration de 10-11 ppm augmentaient l'expression de gènes marqueurs de l'ostéogénèse (ALP, Runx2, OCN, OPN) chez des pré-ostéoblastes murins ainsi que leur prolifération et leur différenciation en ostéoblastes [141].

En 2014 Heo *et al.* ont synthétisé un hydrogel chargé avec des nanoparticules d'or et les résultats *in vitro* ont indiqué une augmentation de la prolifération et de la différenciation de cellules souches humaines dérivées d'adipocytes en ostéoblastes. De plus, les expérimentations *in vivo* sur des défauts osseux chez des lapins ont montré une formation de nouveau tissu osseux plus importante en présence d'hydrogel chargé avec des nanoparticules d'or [142].

Récemment Xia *et al.* ont incorporé des nanoparticules d'or dans un ciment phosphocalcique et étudié ses propriétés sur l'ostéogénèse de cellules souches de pulpe dentaire humaine. Les résultats ont montré que les cellules cultivées sur les matériaux contenant Au avaient une meilleure adhésion et prolifération par rapport au contrôle sans nanoparticules d'or. D'autre part ces cellules exprimaient à un plus fort niveau les gènes marqueurs de l'ostéogénèse comme l'ALP, Runx2, ColI et OCN ainsi qu'une meilleure synthèse minérale indiquant la formation de matrice osseuse. Les auteurs ont aussi démontré que les nanoparticules étaient internalisées dans les cellules souches utilisées et que c'est bien ces nanoparticules d'or qui apportent ces propriétés ostéogéniques [143].

Il apparaît donc que l'utilisation d'or dans les biomatériaux pourrait permettre de répondre aux besoins biologiques des implants osseux en apportant des propriétés antibactériennes et ostéogéniques.

5. Objectifs de la thèse

La régénération osseuse est un processus physiologique complexe qui nécessite la mise en place de conditions biologiques strictes et coordonnées. Dans certains cas il est nécessaire d'apporter une aide à l'organisme pour reconstruire un stock osseux déficient. Les biomatériaux osseux synthétiques apparaissent comme des substituts très intéressants pour

le comblement ou le revêtement osseux. Ils doivent cependant posséder des caractéristiques essentielles pour permettre une régénération osseuse complète. Les biocéramiques de phosphates de calcium biphasiques apparaissent comme des candidats idéaux par leur très forte similarité chimique avec la partie minérale de l'os, leur biocompatibilité et leur biodégradabilité modulable. Cependant le risque d'infection lors de l'implantation d'un substitut et l'augmentation croissante des bactéries résistantes aux antibiotiques sont des facteurs non négligeables qu'il faut prendre en compte lors de la synthèse de ces biomatériaux osseux.

Ce travail porte donc sur l'étude du dopage chimique de biocéramiques de phosphates de calcium biphasiques avec des ions métalliques et l'étude de leurs propriétés biologiques dans l'objectif d'apporter une réponse antibactérienne locale lors d'actes chirurgicaux orthopédiques. Plus précisément ici, les mécanismes structuraux des dopages avec les ions de métaux nobles cuivre, argent et or ont été réalisés : les compositions chimiques des matériaux obtenus ont été analysées et la localisation – à l'échelle atomique (cristallographique) – des éléments dopant a été élucidée. Ensuite les propriétés biologiques et antibactériennes des substituts dopés au cuivre sous formes de pastilles et de poudres ont été étudiées en détail.

CHAPITRE 2 : SYNTHÈSES ET MISE EN FORME DES MATÉRIAUX

1. Techniques expérimentales utilisées pour la caractérisation des matériaux

Cette première partie a pour objectif de décrire les techniques expérimentales qui ont été employées dans la suite de ce chapitre pour décrire et caractériser les matériaux synthétisés.

1.1. Diffraction des Rayons X et affinements Rietveld

Les échantillons obtenus ont été caractérisé par diffraction des rayons X (DRX) à l'aide d'un diffractomètre Philips X'Pert Pro PANalytical (Almelo, Pays-Bas). Les analyses ont été réalisées à température ambiante, avec l'intervalle $3° < 2\theta < 120°$, un pas de $\Delta 2\theta = 0{,}0167°$ et un temps de comptage de 200s pour chaque valeur (soit un temps de mesure d'environ 3 heures par échantillon).

Les affinements Rietveld ont été réalisés avec le logiciel FullProf.2k [144]afin d'extraire les analyses minéralogiques quantitatives et de localiser les positions cristallographiques des dopants. Les paramètres cristallographiques initiaux de l'hydroxyapatite, $Ca_{10}(PO_4)_6(OH)_2$, ont été pris du travail de Rodriguez-Lorenzo *et al.* [145] : groupe d'espace $P6_3/m$, Z = 1, a = 9.4218 Å et c = 6.8813 Å, 7 positions atomiques indépendantes : deux positions Ca sur les sites 4*f* (z = 0.0007) et 6*h* (x = 0.2465, y = 0.9933), une position P sur le site 6*h* (x = 0.3968, y = 0.3693), et quatre positions O sur les sites 6*h* (x = 0.331, y = 0.480 et x = 0.579, y = 0.455), 12*i* (x = 0.3394, y = 0.2569, z = 0.0694) et 4*e* (z = 0.192 avec un taux d'occupation de ½). Les paramètres cristallographiques initiaux de β-TCP, $Ca_3(PO_4)_2$, ont été pris du travail de Yashima *et al.* [146] : groupe d'espace *R*3*c*, Z = 21, a = 10.4352 Å et c = 37.4029 Å, 18 positions atomiques indépendantes : cinq positions Ca (trois en site 18*b* et deux en site 6*a* dont un avec un taux d'occupation de ½), trois positions P (deux en site site18*b* et un en site 6*a*), et dix positions O (neuf en site 18*b* et un en site 6*a*). Le principe général d'un affinement Rietveld consiste à simuler les données de diffraction expérimentales par un modèle cristallographique très détaillé du matériau, et est réalisé par un affinement par moindres carrés de l'ensembles des paramètres cristallographiques : paramètres de maille, quantités relatives des phases, coordonnées atomiques et contenu des sites cristallographiques. A ces paramètres cristallographiques (propres au matériau) s'ajoutent des paramètres expérimentaux (décalage du zéro, largeur instrumentale, asymétrie).

1.2. MP-AES

Les mesures de concentrations des ions cuivre en solution ont été réalisées par spectroscopie d'émission atomique avec l'appareil Agilent 4200 MP-AES. Une gamme étalon a été réalisée à partir d'une solution normadose d'ions cuivre à 1000 µg/mL (Agilent Technologies) diluée dans le solvant correspondant à celui des échantillons mesurés. Avant les mesures, les échantillons ont été dilués au 1/10 dans une solution d'HNO_3 à 2%. Les deux longueurs d'onde d'émission les plus intenses de Cu (324,754 nm et 327,395 nm) ont été sélectionnées pour réaliser les mesures.

2. Synthèses sol-gel et caractérisations des matériaux dopés au cuivre, à l'argent et à l'or

Dans cette étude le dopage de biocéramiques de phosphates de calcium de type BCP a été étudié. Plus précisément 3 éléments chimiques ont été utilisés en tant que dopant : le cuivre (Cu), l'argent (Ag) et l'or (Au) (**Figure 2.1**). Ces éléments groupe 11 (ou IB) sont considérés comme nobles (Au et Ag) ou semi-noble (Cu) ; indiquant une bonne résistance à la corrosion. D'autre part ces 3 éléments sont reconnus pour leurs propriétés antibactériennes.

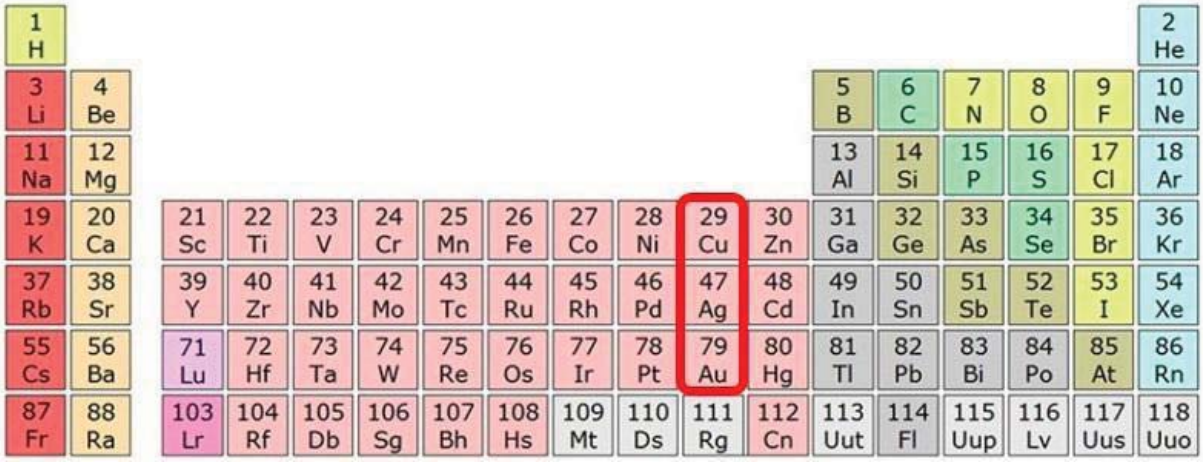

Figure 2.1 : Tableau périodique des éléments. Les 3 éléments chimiques utilisés en tant que dopant sont entourés en rouge : le cuivre Cu, l'argent Ag et l'or Au.

2.1. Synthèse par voie sol-gel

Les poudres de phosphates de calcium biphasiques (BCP) ont été synthétisées par chimie douce. Un procédé sol-gel a été utilisé (afin d'avoir une répartition la plus homogène possible du dopant amené en faible quantité) suivi de calcinations à hautes températures permettant la cristallisation des phases recherchées (**Figure 2.2**). Tous les produits chimiques utilisés proviennent de chez Sigma Aldrich et sont de grade analytique. Le protocole de synthèse pour obtenir environ 4g de poudres non dopées est le suivant :

- Dans un ballon dissoudre avec précaution 1,7 g de P_2O_5 (CAS No : 1314-56-3, pureté ≥ 99,99 %) dans de l'éthanol absolu (CAS No : 64-17-5, pureté ≥ 99,8%), sous agitation magnétique à 200 rpm (tours par minute).
- Dans un autre ballon dissoudre 9,4 g de $Ca(NO_3)_2{\cdot}4H_20$ (CAS No : 13477-34-4, pureté ≥ 99%) dans de l'éthanol absolu, sous agitation magnétique à 200 rpm.
- Après dissolution, mélanger dans un ballon les 2 solutions précédentes et porter à reflux (85°C) sous agitation magnétique pendant 24h à 200 rpm.
- Placer la solution obtenue dans une étuve à 55°C pendant 24h.
- Placer le gel résultant dans une étuve à 80°C pendant 10h.
- Broyer la poudre obtenue dans un mortier et la placer dans une étuve à 130°C pendant 4h pour éliminer toutes traces de solvant.
- Broyer une nouvelle fois la poudre puis la calciner dans un four à moufle à 500°C pendant 15h avec une montée en température de 4°C/min (Nabertherm LH 30/13) afin d'éliminer les nitrates.
- Faire un recuit à la température voulue (de 500°C à 1200°C) pendant 15h.

Il est important que la verrerie utilisée soit parfaitement sèche et que les pesées soient réalisées très rapidement afin de s'assurer d'un rapport molaire Ca/P de 1,67 (du fait du caractère fortement hygroscopique de P_2O_5).

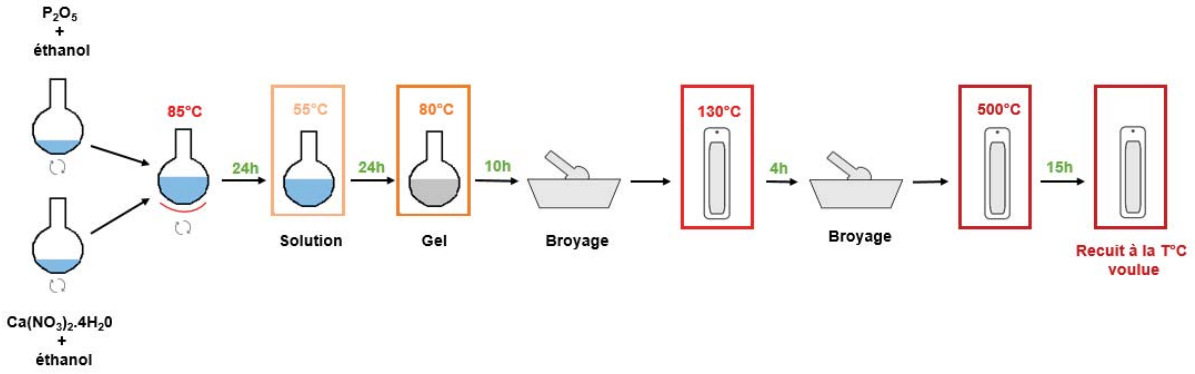

Figure 2.2 : Protocole de synthèse des BCP non dopées.

2.2. Dopage au cuivre

Des BCP dopées au cuivre ont été synthétisés en visant la composition d'une hydroxyapatite dopée en Cu par un mécanisme interstitiel $Ca_{10}Cu_x(PO_4)_6(OH)_{2-2x}O_{2x}$; par suite des résultats précédents de l'équipe sur l'étude du dopage au zinc [65,99,147] et d'autres éléments de la 1ère série de transition [99,147]. Pour cela le protocole décrit précédemment a été utilisé et complété. Une étape supplémentaire consiste à dissoudre également du $Cu(NO_3)_2{\cdot}3H_2O$ en quantité appropriée suivant le taux de dopage souhaité.

Les échantillons synthétisés sont référencés sous la nomenclature " *X*Cu-*T*" où *X* fait référence à la proportion de cuivre et *T* correspond à la température de recuit. Les matériaux synthétisés ont les taux de dopage suivant : *x* = 0 (00Cu-*T*), 0,05 (05Cu-*T*), 0,1 (10Cu-*T*), 0,15 (15Cu-*T*), 0,2 (20Cu-*T*), 0,25 (25Cu-*T*), 0,50 (50Cu-*T*) et 0,75 (75Cu-*T*) et les températures de recuits sont : 500°C, 600°C, 700°C, 800°C, 900°C, 1000°C, 1100°C, 1150°C et 1200°C.

Afin de connaître la composition précise des différentes poudres de BCP dopées et non dopées, des mesures par diffraction des rayons X ont été réalisées. Ensuite une analyse fine de la composition et de la structure cristalline des échantillons a été effectuée par une modélisation des diffractogrammes par la méthode Rietveld. Le but étant d'identifier, de quantifier et de caractériser finement chacune les phases en présence pour chaque échantillon afin de comprendre les mécanismes d'incorporation des ions cuivre dans les matériaux ; c'est-à-dire localiser le plus précisément possible l'élément dopant apporté en faible quantité.

En résumé, les mécanismes d'incorporation du cuivre sont dépendant de la température de recuit et diffèrent selon les phases. Pour la phase HAp un mécanisme d'insertion en site interstitiel permet d'incorporer le cuivre et pour la phase ß-TCP il s'agit d'un mécanisme de substitution.

A 500°C il se forme de l'HAp faiblement dopée, selon la formule suivante : $Ca_{10}Cu_x(PO_4)_6(OH)_{2-2x}O_{2x}$ avec $x < 0.1$. Entre 700°C et 1000°C il se forme une phase ß-TCP dopée comme suit : $Ca_{3-x}Cu_x(PO_4)_2$, avec également la phase HAp faiblement dopée. Enfin à partir de 1100°C les échantillons sont majoritairement composés d'une phase HAp très riche en ions cuivre, selon la formule suivante : $Ca_{10}Cu^{2+}_xCu^{+}_y(PO_4)_6(OH)_{2-2x-y}O_{2x+y}$ avec $x+y \sim 0.5$.

Une première évaluation de la cytotoxicité de ces matériaux a montré de bons résultats sur des CSM humaines après une étape de pré-immersion des matériaux dans de l'eau et/ou du milieu de culture. Ces résultats préliminaires ont été approfondis et font l'objet du chapitre 3.

L'intégralité des résultats obtenus décrivant les mécanismes de dopage par le cuivre et les résultats préliminaires de l'évaluation de la cytotoxicité des matériaux sont présentés dans l'article suivant :

Sandrine Gomes, Charlotte Vichery, Stéphane Descamps, Hervé Martinez, Amandeep Kaur, Aurélie Jacobs, Jean-Marie Nedelec and Guillaume Renaudin, **Cu-doping of calcium phosphate bioceramics: From mechanism to the control of cytotoxicity,** *Acta Biomaterialia*, 2018, 65:462–474. https://doi.org/10.1016/j.actbio.2017.10.028

Acta Biomaterialia 65 (2018) 462–474

Contents lists available at ScienceDirect

Acta Biomaterialia

journal homepage: www.elsevier.com/locate/actabiomat

Full length article

Cu-doping of calcium phosphate bioceramics: From mechanism to the control of cytotoxicity

Sandrine Gomes [a], Charlotte Vichery [a], Stéphane Descamps [a], Hervé Martinez [b], Amandeep Kaur [a,1], Aurélie Jacobs [a], Jean-Marie Nedelec [a], Guillaume Renaudin [a,*]

[a] Université Clermont Auvergne, CNRS, SIGMA Clermont, ICCF, F-63000 Clermont-Ferrand, France
[b] Université de Pau et des Pays de l'Adour, IPREM CNRS UMR 5254, Helioparc Pau Pyrénées, 2 Avenue de Président Angot, F-64053 Pau Cedex 9, France

ARTICLE INFO

Article history:
Received 25 July 2017
Received in revised form 9 October 2017
Accepted 17 October 2017
Available online 21 October 2017

Keywords:
Copper-doping
Hydroxyapatite
X-ray diffraction
X-ray absorption spectroscopy
X-ray photoelectron spectroscopy
Cytotoxicity

ABSTRACT

In this study, the Cu-doping mechanism of Biphasic Calcium Phosphate (BCP) was thoroughly investigated, as was its ionic release behavior, in order to elucidate cytotoxicity features of these bioceramics. BCP are composed of hydroxyapatite ($Ca_{10}(PO_4)_6(OH)_2$) and β-TCP ($Ca_3(PO_4)_2$). The two phases present two different doping mechanisms. Incorporation into the β-TCP structure is achieved at around 700 °C thanks to a substitution mechanism leading to the Cu-doped $Ca_{3-x}Cu_x(PO_4)_2$ compound. Incorporation into the HAp structure is achieved thanks to an interstitial mechanism that is limited to a Cu-poor HAp phase for temperatures below 1100 °C ($Ca_{10}Cu_x(PO_4)_6(OH)_{2-2x}O_{2x}$ with $x < 0.1$). Above 1100 °C, the same interstitial mechanism leads to the formation of a Cu-rich HAp mixed-valence phase ($Ca_{10}Cu^{2+}_xCu^{+}_y(PO_4)_6(OH)_{2-2x-y}O_{2x+y}$ with $x + y \sim 0.5$). The formation of both high-temperature Cu-doped α-TCP and $Cu_3(PO_4)_2$ phases above 1100 °C induces a transformation into the Cu-rich HAp phase on cooling. The linear O—Cu—O oxocuprate entity was confirmed by EXAFS spectroscopy, and the mixed Cu^+/Cu^{2+} valence was evidenced by XPS analyses. Ionic releases (Cu^+/Cu^{2+}, Ca^{2+}, PO_4^{2-} and OH^-) in water and in simulated body media were investigated on as-synthesized ceramics to establish a pretreatment before biological applications. Finally the cytotoxicity of pretreated disks was evaluated, and results confirm that Cu-doped BCP samples are promising bioceramics for bone substitutes and/or prosthesis coatings.

Statement of Significance

Biphasic Calcium Phosphates (BCP) are bioceramics composed of hydroxyapatite (HAp, $Ca_{10}(PO_4)_6(OH)_2$) and beta-Tricalium Phosphate (β-TCP, $Ca_3(PO_4)_2$). Because their chemical and mineral composition closely resembles that of the mineral component of bone, they are potentially interesting candidates for bone repair surgery. Doping can advantageously be used to improve their biological behaviors; however, it is important to describe the doping mechanism of BCP thoroughly in order to fully appraise the benefit of the doping process.
The present paper scrutinizes in detail the incorporation of copper cation in order to correctly interpret the behavior of the Cu-doped bioceramic in biological fluid. The understanding of the copper doping mechanism, related to doping mechanism of others 3d-metal cations, makes it possible to explain the rates and kinetic of release of the dopant in biological medium. Finally, the knowledge of the behavior of the copper doped ceramic in biological environment allowed the tuning of its cytotoxicity properties. The present study resulted on pre-treated ceramic disks which have been evaluated as promising biocompatible ceramic for bone substitute and/or prosthesis coating: good adherence of bone marrow cells with good cell viability.

1. Introduction

The utilization of synthetic materials for bone reconstructive surgery is generally necessary, because autograft and allograft

* Corresponding author.
E-mail address: guillaume.renaudin@sigma-clermont.fr (G. Renaudin).
[1] Present address: VIT University, Vellore, Tamil Nadu 632014, India.

https://doi.org/10.1016/j.actbio.2017.10.028
1742-7061/

practice is limited by the quantity of available material and entails a second surgical procedure in the first case [1]. Among the numerous synthetic materials investigated for bone replacement and/or prosthesis coating, hydroxyapatite (HAp, $Ca_{10}(PO_4)_6(OH)_2$) is the most often-used material due to its chemical and structural similarities with the bone mineral constituent [2–5]. Biological apatite refers to the main constituent of bone and hard tissue in mammals: a poorly crystallized non-stoichiometric carbonate-containing HAp that composes about 65 weight percent (wt%) of bone and about 90 wt% of dental enamel [6]. Apatite is a complex and diverse class of materials, with a flexible structure that accepts many substitutions; either cationic or anionic [7]. Because biological apatites are formed in biological conditions, they usually contain a large variety of trace elements (F, Si, Sr, Mg, etc.) that can have specific biological properties. The incorporation of selected doping elements can be used advantageously to tune the bioactivity of the implant: antibacterial, anti-inflammatory, anti-osteoporotic or angiogenic properties, for instance. Biphasic Calcium Phosphates (BCP) are composed of a mixture of HAp with tricalcium phosphate (β-TCP, $Ca_3(PO_4)_2$). BCP are interesting bioceramics because of the difference in the solubility of the two compounds, which allows the kinetic release of the doping elements to be regulated. A fast release occurs with β-TCP immediately after a surgical operation, whereas a continuous effect is then ensured with HAp. Our previous studies have described in detail the temperature-dependent mechanism of Zn^{2+} insertion in BCP bioceramics [8–10]. Contrary to previous reports in the literature, Zn^{2+} incorporates the HAp structure into an interstitial crystallographic site (Wyckoff site 2*b*) leading to an insertion solid solution of general composition $Ca_{10}Zn_x(PO_4)_6(OH)_{2-2x}O_{2x}$ with a constant Ca/P ratio of 1.67. The insertion of Zn^{2+} is performed for temperatures above 900°C. For lower temperatures, Zn-doping is mainly efficient for the β-TCP phase, evincing a calcium substitution mechanism $Ca_{3-x}Zn_x(PO_4)_2$. Recent works on Fe-doping have confirmed this temperature-dependent process leading to a HAp interstitial mechanism for temperatures above 900 °C [11]. A complete study of 3d-metal cation (from Mn to Zn) incorporation in BCP has confirmed a global equivalent doping mechanism with interesting characteristics [12]. In order to perfectly interpret the biological behavior of doped bioceramics, it is of great importance to correctly characterize the structural location of the doping elements. Metal ions such as Zn^{2+}, Cu^{2+} and Ag^{+} are known not to be cytotoxic at low concentrations, and to exhibit antimicrobial/bactericidal activity at the site of the implantation materials [13–19]. However, the biological responses of the dopant strongly depend on its release amount and kinetic [20]. Jin et al. published last year a review of the development of bio-functional Cu containing biomaterials (including copper-doped HAp), illustrating the renewed interest in copper bioactivity [21].

The present study aims to fully investigate the Cu-doped BCP system. Besides its antimicrobial activity, copper is an essential trace element, necessary for mammalian life [22] and it plays a role in the cross-linking of collagen and bone elastin [23–25]. Cu^{2+} ions have been reported to enhance angiogenesis potential, osteostimulation and antibacterial properties [26–28], to stimulate the proliferation of endothelial cells [29], to promote wound healing in rats [30,31], and to enhance cell activity and the proliferation of osteoblastic cells [32]. A recent study on copper containing glass-ceramic has shown the interesting potential of Cu^{2+} doping for bioactivity and biocompatibility, with the necessity to control the CuO content, i.e. to manage Cu^{2+} release, in order to tune activity and viability [20,33]. Several hydroxyapatite copper doping mechanisms have so far been described in the literature. Whereas some authors have presented a substitution mechanism [34–36], others have described an insertion mechanism with the formation of linear O—Cu—O entities [12,37–39] and the possible presence of mixed Cu^{+}/Cu^{2+} valence. It is necessary to investigate in detail and correctly describe the mechanism of incorporating copper into BCP in order to 1/adequately prepared the doped ceramic, and 2/ understand and tune the biological behavior of Cu-doped BCP bioceramics. Our prepared Cu-doped disks were evaluated with respect to ionic release in simulated biological media (DMEM), and in terms of cytotoxicity using human mesenchymal cells in order to be close to clinical conditions.

2. Materials and methods

2.1. Sol-gel elaboration of Cu-doped BCP samples

The sol-gel route previously proposed by the authors was used to synthesize both undoped and Cu-doped series of BCP samples [8]. Briefly, to produce 2 g of undoped BCP powder, 4.7 g of $Ca(NO_3)_2{\cdot}4H_2O$ (Aldrich) and 0.84 g of P_2O_5 (Avocado Research chemicals) were dissolved in ethanol under stirring and refluxed at 85 °C for 24 h. The solution was then maintained at 55 °C for 24 h to obtain a white consistent gel, and further heated at 80 °C for 10 h to obtain a white powder. Finally, the powder was heat-treated for 15 h. This heat treatment was performed at 500 °C, 600 °C, 700 °C, 800 °C, 900 °C, 1000 °C, 1100 °C, 1150 °C and 1200 °C. Required amounts of $Cu(NO_3)_2{\cdot}3H_2O$ (Sigma-Aldrich) were added to the solution simultaneously with $Ca(NO_3)_2{\cdot}4H_2O$ (Sigma-Aldrich) in order to synthesize the Cu-doped series. To obtain a series of nine samples with the same copper-containing amount, a single batch was prepared for each series and used for all the subsequent heat treatments. Nominal compositions were calculated, assuming the insertion of Cu^{2+} cations in the interstitial crystallographic site (i.e. Ca/P = 1.67), similarly to previous results for the Zn^{2+} insertion mechanism [8–10]. In the following, the samples are labelled '*x*Cu-*T*' with *x* = 00, 10, 15, 25, 50 and 75 for samples with respectively the targeted nominal $Ca_{10}(PO_4)_6(OH)_2$ (i.e. undoped), $Ca_{10}Cu_{0.10}(PO_4)_6(OH)_{1.80}O_{0.20}$, $Ca_{10}Cu_{0.15}(PO_4)_6(OH)_{1.70}O_{0.30}$, $Ca_{10}Cu_{0.25}(PO_4)_6(OH)_{1.50}O_{0.50}$, $Ca_{10}Cu_{0.50}(PO_4)_6(OH)_{1.00}O_{1.00}$ and $Ca_{10}Cu_{0.75}(PO_4)_6(OH)_{0.50}O_{1.50}$ compositions. In this label, *T* indicates the sintering temperature. More than 50 samples were prepared and characterized. A low-doped 10Cu-*T* series was used for dopant release and cell viability studies. Elemental analyses of the samples by ICP-AES confirmed the targeted nominal compositions. Sample color is sintering-temperature dependent. As-prepared powders obtained after the sol-gel process were blue. Heat treatments at 500 °C produced grey samples: from light grey to dark grey as the amount of copper increased. Samples still had a grey color up to 1000 °C, and became purple from 1100 °C. Finally, heat treatments at 1200 °C resulted in dark purple powders.

2.2. X-ray powder diffraction (XRPD) and Rietveld analyses

XRPD patterns were recorded on a Philips X'Pert Pro PANalytical diffractometer (Almelo, Netherlands), with θ-θ geometry, reflection mode, equipped with a solid detector X-Celerator and using Cu Kα radiation (λ = 1.54184 Å). XRPD patterns were recorded at room temperature in the interval $3° < 2\theta < 120°$, with a step size of $\Delta 2\theta = 0.0167°$ and a counting time of 200s for each data value. The 45 synthesized samples from series 00Cu-*T*, 15Cu-*T*, 25Cu-*T* and 75Cu-*T* series were systematically analyzed by XRPD in reflection mode.

Two supplementary measurements were collected for samples 75Cu-1100 and 75Cu-1200 using Debye-Scherrer geometry (transmission mode) to improve diffraction peak resolution (2 theta resolution). Transmission measurements were recorded using a Philips X'Pert Pro diffractometer equipped with a Ge hybrid monochromator (Cu $K\alpha_1$ = 1.54056 Å). A total counting time of

40 h was used in the range $3° < 2\theta < 120°$, with a step size of $\Delta 2\theta = 0.0167°$, using a 0.3 mm diameter filled glass capillary.

In-situ temperature-dependent XRPD patterns were recorded for the 75Cu-*T* series. XRPD patterns were collected on a Philips X'Pert Pro diffractometer equipped with a high-temperature HTK chamber (Anton Paar, Graz, Austria) with the following measurement conditions: two theta range $8° < 2\theta < 100°$, step size $\Delta 2\theta = 0.0167°$, time per step = 165 s. A series of diffraction patterns was recorded, from 500 °C up to 1200 °C (using the starting 75Cu-500 sample). Data were collected at 500 °C, 600 °C, 700 °C, 800 °C, 900 °C, 1000 °C, 1100 °C, 1150 °C and 1200 °C. Then data measurements were performed during the cooling from 1200 °C to room temperature: 1150 °C, 1100 °C, steps of 100 °C down to 100 °C and finally 25 °C.

Rietveld refinements were systematically performed for each measurement using the program FullProf.2k [40]. The Rietveld strategy was detailed in a previous related work [8].

2.3. X-ray absorption spectroscopy (XAS)

Cu K-edge Extended X-ray Absorption Fine Structure (EXAFS) spectra, simultaneously with the X-ray Absorption Near Edge Structure (XANES) part of the spectra, were collected on the Cu-doped samples from the 15Cu-*T* series and one reference compound (CuO) at the SuperXAS beam line at the SLS synchrotron (Villigen, Switzerland) in order to determine the electronic state, as well as to describe accurately the coordination spheres of the Cu atoms. Samples from the 15Cu-*T* series were chosen because other series present higher amounts of CuO impurities. The SLS synchrotron was running at 4.5–35 keV with an average current of 400 mA. The X-ray beam was obtained with a two-crystal Si(1 1 1) monochromator, which features an energy resolution of $\Delta E/E = 2.0 \times 10^{-4}$, necessary to resolve the XANES structure. The experiments were calibrated using a Cu metallic reference foil (K-edge 8981 eV). Experiments were performed at room temperature and atmospheric pressure. Spectra were collected in an energy range of between 8500 and 9500 eV, with energy steps varying from 0.5 eV (XANES part) to 2.0 eV (end of the EXAFS part) and a 1s dwell time per point. XAS spectra were obtained in fluorescence mode using Ge-solid-state detectors (13-element detector). The size of the beam was determined by a set of slits (200 μm × 500 μm). Data was processed using the Athena and Artemis programs from the IFFEFIT software package [41] by merging 4 successively-recorded absorption spectra. Single scattering theory was used here. Following Lengeler-Eisenberg normalization, EXAFS oscillations were Fourier Transformed (FT) using a Hanning window between 3.0 and 9.0 $Å^{-1}$. The $\chi(k)$ function was Fourier transformed using k^3 weighting, and all shell-by-shell fitting was done in *R*-space. Theoretical backscattering paths were calculated using successively ATOMS [42] and FEFF6 [43].

2.4. X-ray photoelectron spectroscopy (XPS)

XPS measurements were carried out to determine the mean oxidation state of Cu with a Thermo Scientific K-Alpha X-ray photoelectron spectrometer using focused monochromatized Al Kα radiation (hν = 1486.6 eV). The XPS spectrometer was directly connected through a glove box under argon atmosphere in order to avoid exposing the samples to moisture or air. For the Ag 3d5/2 line the full width at half-maximum (FWHM) was 0.50 eV under the recording conditions. The X-ray spot size was 400 μm. Peaks were recorded with a constant pass energy of 20 eV. The pressure in the analysis chamber was less than 1×10^{-8} Pa. Short acquisition time spectra were recorded at the beginning and at the end of each experiment to check that the samples did not suffer from degradation during the measurements. Peak assignments were made with respect to reference compounds analyzed in the same conditions. The binding energy scale was calibrated from the hydrocarbon contamination using the C 1s peak at 285.0 eV. Core peaks were analyzed using a nonlinear Shirley-type background [44]. The peak positions and areas were optimized by a weighted least-square fitting method using 70% Gaussian and 30% Lorentzian line shapes. Quantification was performed on the basis of Scofield's relative sensitivity factors [45]. For each sample, several XPS analyses were performed at different positions to ensure that the results were statistically reliable.

2.5. MP-AES measurements

Ionic releases in both water and a culture medium used to simulate body fluid (DMEM; Dulbecco Modified Eagle Medium) were measured by Microwave Plasma - Atomic Emission Spectroscopy (4200 MP-AES from Agilent) in order to evaluate the behavior of the Cu-doped bioceramic in solution, and to determine the pretreatment of Cu-doped BCP disks intended for biological applications. A series of calibration samples was prepared using a 1000 μg/mL Cu ion normadose (diluted in 5% HNO_3 solutions, distributed by Agilent Technologies), diluted in a solvent similar to those of the solutions measured, which is to say 1/1 ratio for DMEM/HNO_3 2% and ultra-pure water/HNO_3 2% solutions.

2.6. Cytotoxicity evaluation

Following the BCP structural characterization, the 10Cu-*T* (*T* = 600, 900 and 1200 °C) samples were prepared for cytotoxicity assessment and undoped copper-free samples were used as reference. The 10Cu-*T* series was chosen because of the absence of copper oxide impurities (see Table 1). Cell viability was assessed through a cell count after a period of cell culture on the studied material (using flat pressed disks). All conditions were tested in triplicate.

2.6.1. Bone marrow cell (BMC) preparation: human normal bone marrow cell source, isolation and in vitro expansion of BM mesenchymal cells before use

Human BMC were obtained from metaphysal cancellous bone collected during hip arthroplasty. Pieces of femoral metaphysis cancellous bone were gathered during surgical procedures in patients who had signed an authorization for the use of their bone for research purposes. All donors had normal hematopoietic function. The samples were collected in a sterile culture medium (αMEM) and transported immediately to the culture lab. After washing once in phosphate-buffered saline (PBS) 4% fetal calf serum (FCS), the BMC were re-suspended in a standard marrow cell culture medium consisting of αMEM 10% FCS, 100 U penicillin, 100 μg/mL streptomycin, 2 mM L-Glutamine and plated at 1.5×10^5 cells/cm^2 in 25 cm^2 tissue culture flasks at 37 °C with 5% of humidified CO_2 for two days. The non-adherent BMC were harvested in two gentle rinses and removed. Adherent cells were fed by a weekly change of medium. Mesenchymal cells were expanded through one of three passages (re-plated between 5×10^2 and 1×10^3 cells/cm^2) before being collected by trypsinization.

2.6.2. Assessment of mesenchymal cell proliferation on samples disks

Sterilization of each disk was completed with a sequence of ethanol (95%) for 30 min followed by PBS for 30 min; this was performed twice. The disks were placed in 24-well cell culture trays, with 8×10^3 cells/well seeded in each well. One disk per well was plated in triplicate in 24-well plates to produce a representative series. Each disk was sowed with the same number of expanded mesenchymal cells (8×10^4 cells) in a standard medium with 700 μL of medium in each, which was changed twice weekly.

Table 1
Results of quantitative analyses (wt%) extracted from Rietveld refinements for the undoped BCP series and the Cu-doped BCP series. Standard deviations are indicated in parentheses.

Samples	Mineralogical composition (wt%)						
	HAp1	HAp2	β-TCP	α-CDP	$CaCO_3$	CaO	CuO
00Cu-500	91.2 (9)	–	–	4.4 (3)	3.7 (2)	0.8 (1)	–
00Cu-600	88.1 (9)	–	2.9 (3)	7.2 (3)	0.9 (1)	1.0 (1)	–
00Cu-700	87.1 (9)	–	7.9 (3)	3.9 (3)	0.5 (1)	0.6 (1)	–
00Cu-800	88.4 (9)	–	11.1 (3)	–	–	0.5 (1)	–
00Cu-900	96.6 (6)	–	3.2 (3)	–	–	0.2 (1)	–
00Cu-1000	98.4 (9)	–	1.5 (3)	–	–	0.1 (1)	–
00Cu-1100	100 (-)	–	–	–	–	–	–
00Cu-1150	100 (-)	–	–	–	–	–	–
00Cu-1200	100 (-)	–	–	–	–	–	–
10Cu-600	88.5 (9)	–	2.4 (4)	6.2 (4)	1.1 (1)	1.8 (1)	–
10Cu-900	94.2 (8)	–	5.8 (4)	–	–	–	–
10Cu-1200	98.6 (5)	–	1.4 (3)	–	–	–	–
15Cu-500	92.9 (4)	–	–	2.9 (1)	3.1 (1)	0.5 (1)	0.6 (1)
15Cu-600	80.4 (4)	–	7.1 (2)	9.2 (2)	1.3 (2)	1.0 (1)	1.0 (1)
15Cu-700	76.8 (3)	–	17.7 (2)	3.4 (1)	0.8 (1)	0.9 (1)	0.3 (1)
15Cu-800	86.4 (3)	–	12.8 (1)	–	–	–	0.9 (1)
15Cu-900	91.9 (3)	–	7.2 (1)	–	–	–	0.9 (1)
15Cu-1000	90.2 (3)	–	8.9 (9)	–	–	–	0.9 (1)
15Cu-1100	88.3 (3)	–	10.9 (1)	–	–	–	0.8 (1)
15Cu-1150	88.0 (3)	–	12.0 (1)	–	–	–	–
15Cu-1200	88.6 (3)	–	11.4 (1)	–	–	–	–
25Cu-500	92.8 (4)	–	–	2.4 (1)	2.5 (1)	1.3 (1)	1.0 (1)
25Cu-600	83.9 (4)	–	4.7 (1)	8.5 (2)	0.3 (1)	1.5 (1)	1.0 (1)
25Cu-700	77.6 (3)	–	17.1 (2)	2.4 (1)	–	1.7 (1)	1.0 (1)
25Cu-800	86.7 (3)	–	11.0 (1)	–	–	0.5 (1)	1.8 (1)
25Cu-900	96.6 (3)	–	1.4 (7)	–	–	–	2.0 (1)
25Cu-1000	97.8 (3)	–	–	–	–	–	2.2 (1)
25Cu-1100	98.1 (4)	–	–	–	–	–	1.9 (1)
25Cu-1150	98.7 (4)	–	–	–	–	–	1.3 (1)
25Cu-1200	98.9 (4)	–	–	–	–	–	1.1 (1)
50Cu-500	90.8 (4)	–	–	2.3 (1)	2.5 (1)	0.8 (1)	2.9 (1)
50Cu-600	83.0 (4)	–	6.0 (2)	6.9 (1)	–	1.4 (1)	2.7 (1)
50Zn-700	78.4 (3)	–	17.6 (2)	–	–	1.2 (1)	2.8 (1)
50Cu-800	88.7 (3)	–	7.4 (2)	–	–	0.4 (1)	3.5 (1)
50Cu-900	96.4 (3)	–	–	–	–	–	3.6 (1)
50Cu-1000	96.2 (3)	–	–	–	–	–	3.8 (1)
50Cu-1100	96.6 (3)	–	–	–	–	–	3.4 (1)
50Cu1150	67.8 (4)	29.1 (3)	–	–	–	–	2.8 (1)
50Cu1200	66.5 (4)	30.6 (3)	–	–	–	–	2.7 (1)
75Cu-500	91.7 (4)	–	–	1.9 (1)	1.7 (1)	0.3 (1)	4.3 (1)
75Cu-600	83.3 (4)	–	5.3 (2)	6.3 (2)	–	0.8 (1)	4.3 (1)
75Zn-700	80.9 (3)	–	14.0 (2)	–	–	0.7 (1)	4.4 (1)
75Cu-800	86.3 (3)	–	8.0 (1)	–	–	0.2 (1)	5.4 (1)
75Cu-900	91.7 (3)	–	2.6 (2)	–	–	–	5.7 (1)
75Cu-1000	94.4 (3)	–	–	–	–	–	5.6 (1)
75Cu-1100	94.8 (4)	–	–	–	–	–	5.2 (1)
75Cu-1100*	81 (1)*	13.5 (6)*	–	–	–	–	5.1 (1)*
75Cu-1150	75.5 (5)	20.6 (3)	–	–	–	–	3.9 (1)
75Cu-1200	62.6 (4)	34.1 (3)	–	–	–	–	3.3 (1)
75Cu-1200*	58.9 (8)*	37.6 (7)*	–	–	–	–	3.5 (1)*

* Rietveld refinement results from XRPD in transmission mode measured with capillaries.

All disks were colonized by cells coming from the same patient during the same expansion process.

To evaluate cell viability, the wells were sacrificed to collect cells after one week of culture. Cells were harvested after detachment by trypsin/EDTA 0.25% and counted in Malassez. For each arm, we evaluated in parallel the viability of cell proliferation on equivalent uncoated plastic wells in the absence of a disk as a control, in order to estimate the effect of ceramic disks only. One extra disk was seeded in the same way and sacrificed at day 6 to study cell morphology using SEM.

2.6.3. Statistical analysis

Results were expressed as means ± standard error of mean, considering triplicate samples. Limiting Dilution Analysis (LDA) was performed according to the Poisson statistical model using L-Calc™ software (StemCell Technologies, Vancouver, Canada). Statistical analysis used the bilateral paired Student's test with a significant p value < 0.05.

3. Results: materials characterization

3.1. Temperature-dependent phase composition of the samples

To correctly interpret the behavior of our samples, their mineral compositions were extracted from Rietveld analyses (selected XRPD patterns are shown in Fig. SEI1). Mineral compositions of the undoped BCP series and of the four Cu-doped BCP series (x = 15, 25, 50 and 75) of samples are indicated in Table 1. Results

are extracted from XRPD measurements performed with the θ-θ geometry except when indicated by an asterisk (transmission mode on capillary) in Table 1 and Table SEI1. Fig. 1 represents the thermal composition variation for the two main phases: HAp and β-TCP. Other minor phases were observed. α-CDP (diCalcium DiPhosphate with composition $Ca_2P_2O_7$) was observed up to 700 °C, with a maximum amount – around 6–9 wt% – at 600 °C. Calcite $CaCO_3$ was present in samples which were heat treated at 500 °C, and decarbonation mainly occurred at 600 °C. CuO was generally observed in samples from the Cu-doped series – except for 15Cu-1150 and 15Cu-1200 (which are composed of HAp and β-TCP only) – indicating that part of the incorporated copper amount is not inserted in the two main phases. β-TCP was stabilized for intermediate temperatures and the presence of copper increased the β-TCP amount at 700 °C. Samples became almost exclusively composed of HAp phases for the higher temperatures, except for the 15Cu-*T* series with about 10 wt% of β-TCP remaining above 1000 °C.

Thermal variations in the HAp lattice parameters (Fig. 2 and Table SEI1) showed only minor variations between undoped and Cu-doped series from 500 °C up to 1100 °C (the maximum heat treatment usually used in our previous studies on BCP doping [8–12,46–48]). Weak copper insertion into the interstitial 2*b* Wyckoff site was observed up to 1100 °C from Rietveld refinements on samples belonging to the four Cu-doped series: between 1 and 5% occupancies leading to a maximum inserted copper composition $Ca_{10}Cu_{0.1}(PO_4)_6(OH)_{1.8}O_{0.2}$ for the 50Cu-1100 sample (Table SEI1). The *a* lattice parameter of Cu-doped samples heat treated at temperatures between 500 °C and 700 °C shows a decrease compared to the undoped series (Fig. 2). Attempts to substitute calcium atoms during the Rietveld procedure (considering both the Ca1 and Ca2 crystallographic sites in the HAp structure [49]) failed, whatever the amount of copper and the sintering temperature. Higher-temperature treatments were performed (1150 °C and 1200 °C) in order to pursue the temperature-dependent study on copper insertion. For temperatures above 1100 °C, lattice parameters sharply increased. These variations in the HAp unit cell were accompanied by a large increase in copper occupancy at the interstitial 2*b* Wyckoff site (Fig. 2 and Table SEI1). More surprisingly, samples heat treated at 1150 °C and 1200 °C from the 50Cu-*T* and 75Cu-*T* series showed systematic shoulders for almost all diffraction peaks related to the HAp structure. Such behavior can be explained by the presence of two HAp phases with slightly different lattice parameters. Rietveld refinements were then performed on XRPD patterns recorded in transmission mode on capillaries filled with the two 75Cu-1100 and 75Cu-1200 samples in order to improve the diffraction peak resolution (Fig. 3). The presence of two HAp phases was clearly evidenced. Results indicated that one phase (HAp1 in Fig. 3) corresponding to the HAp phase observed in samples heat treated below 1100 °C relates to the previously indicated composition $Ca_{10}Cu_{0.1}(PO_4)_6(OH)_{1.8}O_{0.2}$; called Cu-poor HAp phase hereafter. The second, and new, HAp phase (HAp2 in Fig. 3) presents larger lattice parameters and a larger quantity of copper cations at the interstitial site, leading to the refined $Ca_{10}Cu_{0.6}(PO_4)_6(OH)_{0.8}O_{1.2}$ composition, called Cu-rich HAp phase hereafter. Fig. 2 and Table SEI1 take into consideration the characteristics of these two HAp phases for the 50Cu-*T* and 75Cu-*T* series. Structural parameters of both Cu-poor and Cu-rich HAp phases from sample 75Cu-1200 are gathered in Table 2.The main structural parameters of the β-TCP phase in samples from each series – containing the largest amount of β-TCP phase (800 °C for the undoped series and 700 °C for the Cu-doped series; see Table 1) – can be seen in Table SEI2. The substitution mechanism was evidenced by the decrease in the lattice parameters of its rhombohedral structure [50]. Refinement of the atomic occupancy factors showed that the substitution mechanism occurs in the low-density column [48] at both the Ca4 and Ca5 crystallographic sites – in agreement with previous observations on the transition metal insertion mechanism [8–12]. Maximum refined substitution led to the $Ca_{2.72(3)}Cu_{0.28(3)}(PO_4)_2$ composition for 75Cu-700 (Table SEI2). The literature already indicates the existence of $Ca_{19}Cu_2(PO_4)_{14}$ – polymorphic to β-TCP with the same rhombohedral *R3c* structure – very close to our refined composition [51]. Higher amounts of copper substitution lead to structure modifications: monoclinic $P2_1/c$ $Ca_{1.5}Cu_{1.5}(PO_4)_2$ [52] and triclinic $P\bar{1}$ calcium-free $Cu_3(PO_4)_2$ [53].

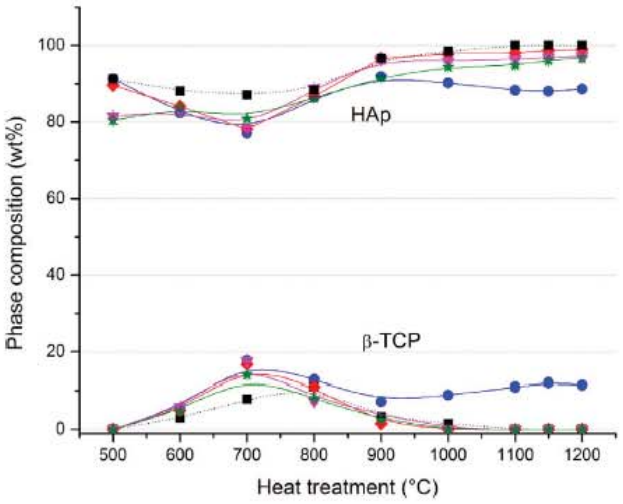

Fig. 1. Mineral composition of the two main phases (HAp and β-TCP) as a function of sintering temperature for the five series: undoped (black squares, dotted lines), 15Cu-T (blue circles, solid lines), 25Cu-T (red diamonds, solid lines), 50Cu-T (pink triangles, solid lines) and 75Cu-T (green stars, solid lines). (For interpretation of the references to colour in this figure legend, the reader is referred to the web version of this article.)

3.2. Formation of the second, copper-rich, HAp phase

In order to understand the formation mechanism of the two HAp phases for high sintering temperatures – the Cu-poor and the Cu-rich HAp phases – in-situ high-temperature XRPD measurements were performed on the 75Cu-*T* series. Rietveld refinements enabled the temperature-dependent quantitative phase analysis and the corresponding assemblage variation to be identified (Fig. 4). The 75Cu-500 sample was introduced into the high-temperature HTK chamber, and XRPD patterns were recorded during heating from 500 °C up to 1200 °C and then during cooling down to room temperature. From 500 °C to 1000 °C, phase mixtures were coherent with those previously observed from measurements performed at room temperature on cooled samples: namely the stabilization of β-TCP observed around 700 °C. Nevertheless, above 700 °C the amount of β-TCP remained almost unchanged, and the amount of HAp increased, together with the consumption of copper oxide CuO. This last point was not evidenced from measurements carried out at room temperature on cooled samples, where the CuO amount remained constant at around 5 wt% (Table SEI1). Between 1000 °C and 1100 °C the β-TCP transformed into the α-TCP polymorph and the tri-copper phosphate, triclinic $Cu_3(PO_4)_2$, appeared [53]. Between 1100 °C and 1200 °C the β-TCP phase completely disappeared and the HAp phase was considerably destabilized (about 20 wt% only at 1200 °C) to the benefit of α-TCP and $Cu_3(PO_4)_2$. Minor changes were observed during cooling from 1200 °C and 1100 °C. At 1000 °C, both α-TCP and $Cu_3(PO_4)_2$ phases disappeared, concomitantly with a large increase in the HAp phase and the formation of about

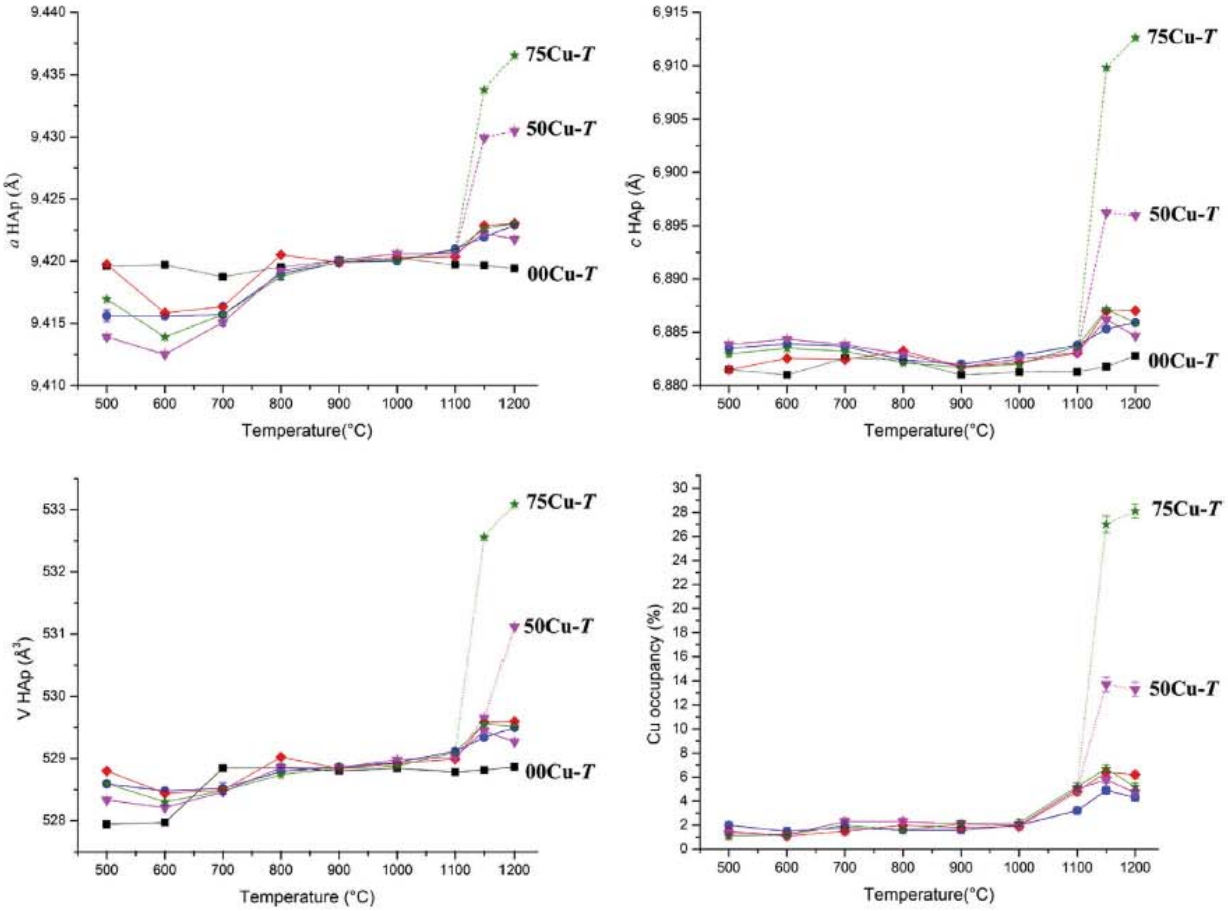

Fig. 2. Thermal variations in HAp lattice parameters: (a) lattice parameters a, (b) lattice parameter c, (c) unit cell volume, and (d) the Cu occupancy factor attributed to the 2b Wyckoff site (0,0,0). The undoped series 00Cu-T (black squares), and the Cu-doped series 15Cu-T (blue circles), 25Cu-T (red diamonds), 50Cu-T (pink triangles and 75Cu-T (green stars) are represented. Solid lines correspond to variation in the undoped and Cu-poor HAp (i.e. HAp1 in Tables 1 and 2) phases, whereas dotted lines correspond to the Cu-rich HAp (i.e. HAp2 in Tables 1 and 2) phase resolved in the two 50Cu-T and 75Cu-T series. (For interpretation of the references to colour in this figure legend, the reader is referred to the web version of this article.)

10 wt% of the β-TCP polymorph. Because of the relatively low 2-theta resolution of the XRPD patterns recorded using the HTK chamber, Rietveld refinements did not enable us to discriminate clearly the presence of two HAp phases. Cooling from 1000 °C to room temperature did not show a significant evolution. Nevertheless, information provided by these HTK measurements indicated that the Cu-rich HAp phase came from the transformation of both α-TCP (certainly copper substituted) and $Cu_3(PO_4)_2$ phases between 1200 °C and 1100 °C. This transformation, performed above 1100 °C, explained the absence of the Cu-rich HAp phase for heat treatments up to 1100 °C (Fig. 2). The presence of both HAp1 and HAp2 phases in Fig. 4 during cooling was extrapolated from previous transmission results.

3.3. Copper location in the HAp structure

During Rietveld refinements the occupancy factors of all calcium and phosphorus crystallographic sites were systematically tested, as well as the eventual copper substitutions at calcium sites (two crystallographic sites for HAp and five crystallographic sites for β-TCP) and copper insertion at the interstitial 2*b* Wyckoff site. Results indicated, as already thoroughly described for Zn^{2+} doping, that the mechanism is temperature-dependent with a first step around 700 °C corresponding to a substitution mechanism in the β-TCP phase, followed by an insertion mechanism in the HAp phase. The latter is fully accomplished for sintering temperatures higher than 1100 °C to obtain the Cu-rich HAp phase with the Ca_{10}-$Cu_{0.6}(PO_4)_6(OH)_{0.8}O_{1.2}$ composition. In order to confirm this insertion mechanism, XAS analyses were performed on five samples from the 15Cu-*T* series (15Cu-500, 15Cu600, 15Cu-800, 15Cu-1100, 15Cu-1200 samples: Fig. SEI2) at the SuperXAS beam line at the SLS synchrotron (Villigen, Switzerland). Samples from the 15Cu-*T* series were chosen because of the lower amounts of CuO impurity for all samples of the series (less than 1 wt% and total absence for 15Cu-1200; see Table1). EXAFS spectra were expected to enable us to evidence the formation of linear O—Cu—O entities with short Cu—O interatomic distances. Previous Rietveld refinements did not allow this short Cu—O interatomic distance to be determined because of statistical disorder around the oxygen atoms in the HAp hexagonal channel: the O4 crystallographic site corresponds either to oxygen from isolated hydroxyl groups or to oxygen from linear O—Cu—O entities. Rietveld analyses indicated only the wide 1.40–2.05 Å range for the Cu—O interatomic distance. Fourier-transformed amplitudes (not corrected for phase shift) are shown in Fig. 5b in *R*-space. Radial distributions for the different samples did not show great variations, and were relatively similar to that of the CuO reference compound in the 1 Å–3 Å *R* range. It should be remembered that samples were not single-phase, and several phases contribute to the spectra: copper

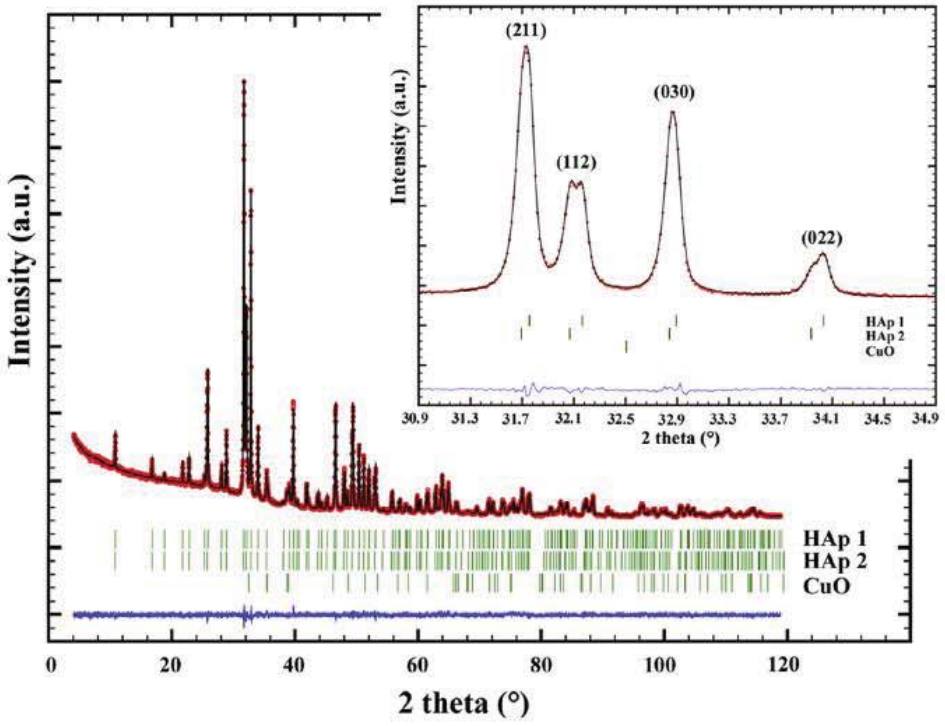

Fig. 3. Rietveld refinement performed on 75Cu-1200 pattern recorded in transmission mode, showing the presence of two HAp phases: HAp1 for the Cu-poor HAp phase and HAp2 for the Cu-rich HAp phase. Inset shows the 2-theta resolution conveyed by transmission geometry.

Table 2
Rietveld refinement results from XRPD patterns recorded in transmission mode on capillaries (lattice parameters a and c, unit cell volume V, atomic coordinates x, y and z, temperature factors B_{iso} and occupancies) for the two HAp phases from the 75Cu-1200 samples. Standard deviations are indicated in parentheses. $R_p = 0.11$ and $R_{wp} = .10$ represent conventional Rietveld agreement factors.

HAp	Atom	Site	*x*	*y*	*z*	B_{iso} (Å^2)	Occ.*
HAp1: Cu-poor HAp phase; $Ca_{10}Cu_{0.10(1)}(PO_4)_6(OH)_{1.80(2)}O_{0.20(2)}$							
$P6_3/m$	Ca1	4*f*	⅓	⅔	0.0023(4)	0.5(1)	1(–)
a = 9.42492(8) Å	Ca2	6*h*	0.2468(3)	0.9933(3)	¼	= B_{Ca1}	1(–)
c = 6.88839(6) Å	P1	6*h*	0.3992(3)	0.3684(3)	¼	0.3(1)	1(–)
V = 529.912(8) Å^3	O1	6*h*	0.3264(7)	0.4819(7)	¼	0.5(1)	1(–)
	O2	6*h*	0.5853(7)	0.4658(7)	¼	= B_{O1}	1(–)
	O3	12*i*	0.3406(4)	0.2549(5)	0.0705(5)	= B_{O1}	1(–)
	O4	4*e*	0	0	0.203(2)	= B_{O1}	½(–)
	Cu1	2*b*	0	0	0	= B_{Ca1}	0.048(6)
HAp2: Cu-rich HAp phase; $Ca_{10}Cu_{0.61(1)}(PO_4)_6(OH)_{0.78(2)}O_{1.22(2)}$							
$P6_3/m$	Ca1	4*f*	⅓	⅔	0.0018(7)	0.5(1)	1(–)
a = 9.43954(9) Å	Ca2	6*h*	0.2488(4)	0.9933(4)	¼	= B_{Ca1}	1(–)
c = 6.91356(7) Å	P1	6*h*	0.3981(4)	0.3677(4)	¼	0.3(1)	1(–)
V = 533.500(9) Å^3	O1	6*h*	0.330(1)	0.486(1)	¼	0.5(1)	1(–)
	O2	6*h*	0.587(1)	0.465(1)	¼	= B_{O1}	1(–)
	O3	12*i*	0.3426(7)	0.2591(7)	0.0696(7)	= B_{O1}	1(–)
	O4	4*e*	0	0	0.209(3)	= B_{O1}	½(–)
	Cu1	2*b*	0	0	0	= B_{Ca1}	0.307(6)

* Occupancy parameters.

from CuO impurity, substituted copper in *β*-TCP and inserted copper in HAp. Nevertheless, careful analysis of the radial distribution showed that the first peak is slightly displaced toward the small *R* values for the 15Cu-1200 sample: 1.48 Å against 1.51 Å for other 15Cu-*T* samples and for the CuO reference compound. 15Cu-1200 is the only sample without any CuO impurity. Fitting the k^3-weighted EXAFS raw data of 15Cu-1200 (Fig. SEI3) confirmed the two oxygen neighbors and indicated a refined Cu—O interatomic distance of 1.91 (1) Å. This relatively short interatomic distance (compared to $d_{Cu-O} = 1.96$ Å in CuO) agrees with the insertion mechanism of copper cations at the 2*b* interstitial Wyckoff site, leading to linear O—Cu—O oxocuprate. The XANES part of the spectra (Fig. 5a) showed the appearance of a pre-edge peak at 8983 eV from a sintering temperature of 1100 °C: a shoulder for the 15Cu-1100 sample and a sharp pre-edge signal for the 15Cu-1200 sample. Analysis of the EXAFS data is a direct method that probes the electronic and structural nature of the metal site [54–56]. Empirical correlations of the energies of copper X-ray absorption edge features were used to detect the presence of Cu^+. It was recognized that the pre-edge feature at 8983 eV is present in the absorption edge spectra of Cu^+ complexes but not in those of Cu^{2+}. Kau et al. have shown that samples containing Cu^+ exhibit

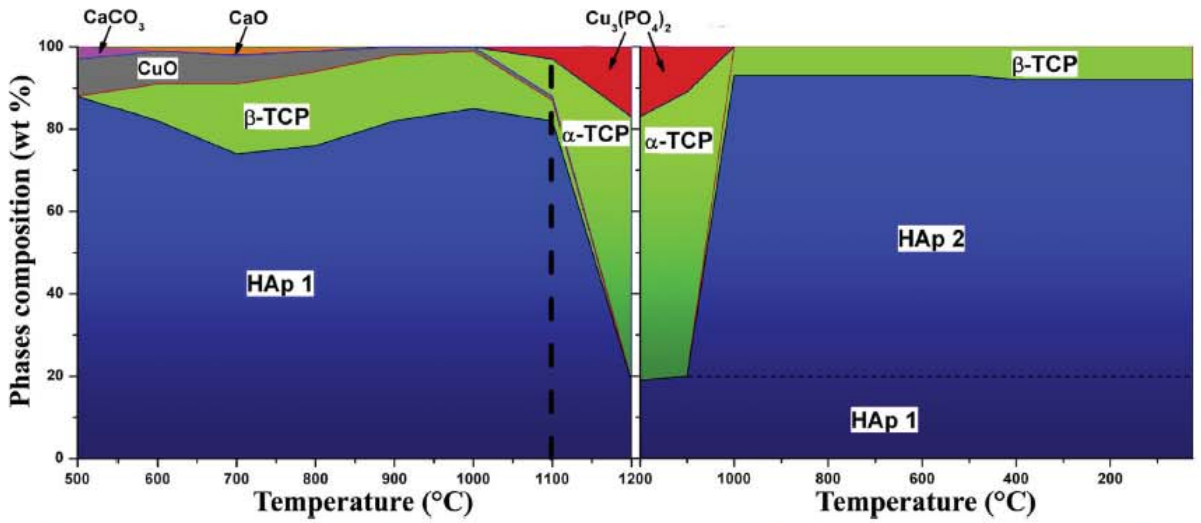

Fig. 4. Temperature phase evolution extracted from Rietveld refinements performed on in-situ XRPD measurements using a HTK chamber on the 75Cu-*T* series.

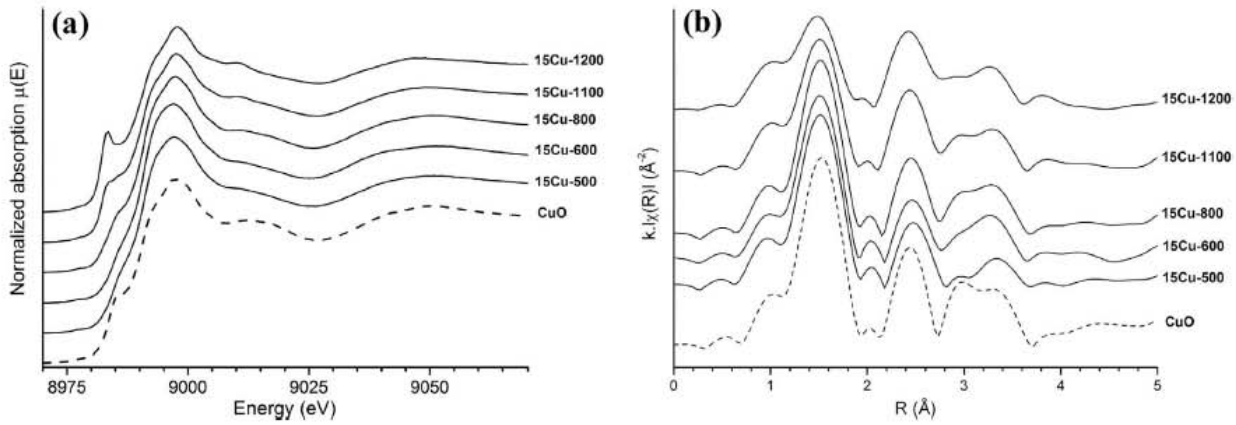

Fig. 5. (a) XANES part of the XAS spectra, and (b) k-weighted amplitudes of the Fourier transform, uncorrected for phase shift, for the 15Cu-T series samples (solid lines) and the reference compound (CuO, dashed lines).

a near-edge absorption feature at 8983.5(3) eV, consistent with the 1s–4p transition of a Cu^{+} center, whereas Cu^{2+} entities do not exhibit a peak below 8985 eV [57]. Cu^{2+} cations are characterized by a broader signal [58]: the shoulder of the Cu Kα edge observed in Fig. 5a for the CuO reference compound and for samples 15Cu-500, 15Cu-600 and 15Cu-800.

3.4. Cu^{+}/Cu^{2+} mixed valence in HAp above 1100 °C

Samples from the 75Cu-T series were analyzed by XPS spectroscopy in order to confirm the presence of Cu^{+} cations for heat treatments above 1100 °C. XPS spectra ($2p_{3/2}$) from samples 75Cu-1000 to 75Cu-1200, presented in Fig. 6, have been interpreted according to literature peak assignments described in Comment SEI1 from supplementary information section [59–62]. The Cu^{+}/Cu^{2+} ratio was estimated for the three samples considering the following conditions (based on the spectral analyses of the reference compounds): the binding energy for Cu^{+} is positioned at 932.7 eV and the associated component presents a constant full width at half maximum (FWHM) of 1.3 eV for the three samples. Furthermore, the relative proportion of Cu^{2+} for the 75Cu-1000, 75Cu-1100 and 75Cu-1200 samples could be also estimated by taking into account the ratio between the main Cu $2p_{3/2}$ peak and the corresponding satellite peaks located in the range 940–945 eV. The Cu^{+} amount is weak for 75Cu-1000 (Fig. 6) with an experimental Cu^{+}/Cu^{2+} ratio of 0.03. This ratio increases to 0.10 for 75Cu-1100 and to 0.24 for 75Cu-1200. Note that for the last compound (75Cu-1200), the experimental envelope of the $2p_{3/2}$ component presents a shoulder at low binding energy. Furthermore, the ratio between the Cu^{2+} $2p_{3/2}$ contribution and the associated satellite peaks is lower than for 75Cu-1000 and 75Cu-1100, which is in agreement with a higher proportion of Cu^{+} in the 75Cu-1200 sample.

Thus XPS reveals the partial Cu^{2+} reduction for temperatures above 1100 °C, and indicates that Cu^{+} is inserted in the Cu-rich HAp phase. Only about 16 atomic % of copper is in the Cu^{+} oxidation state in 75Cu-1200, indicating that the Cu-rich HAp phase did not contain exclusively Cu^{+}. The Cu-rich $Ca_{10}Cu_{0.6}(PO_4)_6(OH)_{0.8}O_{1.2}$ is a mixed-valence Cu^{+}/Cu^{2+}-doped HAp. It should be borne in mind that XPS is a surface analysis (depth analysis about 5 nm) and that results are not necessarily bulk representative. The main and significant XPS result here is the confirmation of the Cu^{+} electronic state, in agreement with XANES observation and the evidence of sintering temperature-dependence.

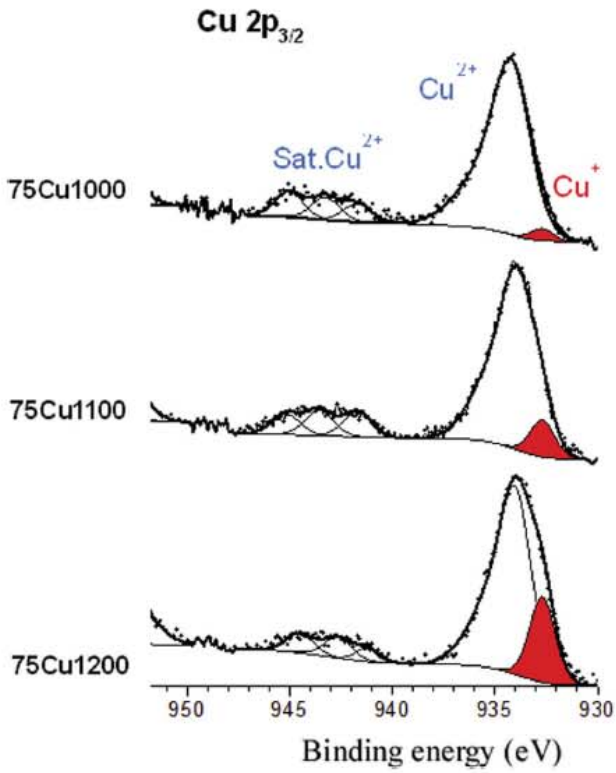

Fig. 6. Cu $2p_{3/2}$ XPS core peak of three samples from the 75Cu-T series (from 1000 °C to 1200 °C).

4. Results: material behavior in a biological medium

4.1. Ionic release

The impact of the release of copper ions on cytotoxicity was studied for the 10Cu-*T* series, with *T* = 600, 900, and 1200 °C. For comparison, measurements were also performed with the undoped series. Samples with a nominal composition of $Ca_{10}Cu_{0.10}(PO_4)_6(OH)_{1.80}O_{0.20}$ were selected because of the absence of copper oxide impurities previously observed in the 15Cu-*T* series, and because too high a quantity of copper ions released could indeed increase cytotoxicity. In addition, samples heat-treated at the three temperatures (600 °C, 900 °C and 1200 °C) were chosen in order to vary the disk composition, the copper location and the degree of oxidation of the copper ions. As shown, a higher annealing temperature induces a higher HAp/β-TCP ratio, which could give rise to different copper ion release kinetics, the β-TCP phase being dissolved much faster than the HAp one.

To be close to cytotoxicity test experimental conditions, in a first experiment, each disk was immersed in 20 mL of a solution of simulated body fluid (DMEM – Dulbecco's Modified Eagle Medium, without D-Glucose and L-Glutamine). The closed bottles were maintained at 37 °C in an oven, with 5% of humidified CO_2, for several days. As can be seen in Fig. 7, after one day the concentration of copper ions in the solution was already high, and even reached 50 ppm after 21 days for the 900 °C annealed sample. It is interesting to note that the Cu-doped BCP sample heat-treated at 1200 °C shows a much lower copper ion release, which is directly correlated with its composition (no β-TCP phase and copper completely inserted in the weakly soluble HAp phase). The concentrations obtained, from 0.02 to 0.28 ppm for the undoped samples, confirm the non-contamination of these samples as well as the sensitivity

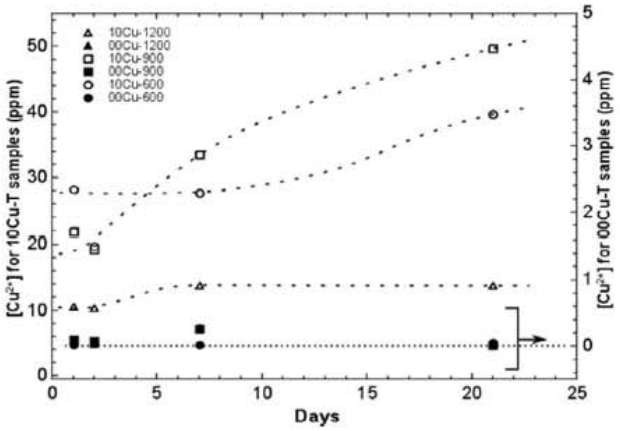

Fig. 7. Copper ion concentration in DMEM versus disk immersion time at 37 °C for undoped and 10Cu-T samples annealed at 600, 900 and 1200 °C.

of the measurements. During this experiment it was noticed that the pH of all the solutions significantly increased, probably due to the dissolution of the small amount of CaO in the samples. As such a pH increase could be harmful for the cell's viability in biological conditions, a post-synthesis treatment of the disks was performed in order to remove free CaO before carrying out cytotoxicity measurements. In addition, it could be interesting to reduce the quantity of copper ions released, as a high concentration could also damage the cells.

In a second experiment, in order to dissolve CaO and prevent a rise in pH during the cytotoxicity tests, each disk was immersed in 20 mL of ultra-pure water, in a closed bottle placed in an oven at 37 °C (5% of humidified CO_2). For the 6 samples (from both undoped and 10Cu-*T* series) the pH increased, reaching about 11.7 after 24 h, proof of CaO dissolution. Surprisingly, almost no Cu ions were released, their concentration in water being less than the detection limit of the MP-AES (~0.01 ppm). The disks were then dried and immersed again for 24 h at 37 °C in ultra-pure water to ensure the complete dissolution of CaO. Then the disks were immersed in DMEM for 24 h at 37 °C, following the same protocol. The pH was measured and shown to be equal to that of pure DMEM after 24 h at 37 °C. Contrary to the treatment in water, copper ions were released in DMEM, their concentration reaching 16.7, 17.2 and 3.0 ppm respectively for 10Cu-600, 10Cu-900 and 10Cu-1200 samples. Copper ion concentration was finally measured after a second treatment of 24 h in DMEM, and showed a release of 3.0, 6.6 and 0.4 ppm for 10Cu-600, 10Cu-900 and 10Cu-1200 samples respectively, far less than the concentration obtained from the first experiment, with no post-treatment of the samples. Fig. SEI4 illustrates these two experiments, and the corresponding disk preparations for the three cytotoxicity evaluation campaigns (0, A and B).

4.2. Cytotoxicity evaluation

Three cytotoxicity (i.e. cell viability) evaluation campaigns were conducted: first, experiments with disks from as-synthesized pressed powder (campaign 0; 13 mm diameter disks obtained with 0.25 g of powder pressed under 1 ton using three *x*Cu-*T* series with x = 00, 10 and 25); and second, experiments with disks post-treated by two water immersions (campaign A) and with a third DMEM immersion (campaign B). Thus, for both campaigns, the pH should not rise during the cytotoxicity tests and different copper ion concentrations can be tested, campaign A showing a higher Cu ion release compared to campaign B. In addition to the 10Cu-600, 10Cu-900 and 10Cu-1200 samples, post-synthesis treatments

were performed on the 00Cu-600, 00Cu-900 and 00Cu-1200 samples, in order to have copper-free reference samples for the cytotoxicity interpretation. Results from the three evaluation sets (described in Fig. SEI4) are shown in Fig. 8. For each campaign, one 24-well plate was used with all the composition/sintering temperatures in triplicate, including controls corresponding to disk-free wells. We did not note any bacterial contamination during the culture period. Control measurements were 24-well plate-dependent with viable cell count values from 7.6×10^3 to 2.5×10^4 cells/well. In order to easily compare measurements from different campaigns, control results were normalized to 100 (then applying the same scale factor for all the measurements from the same 24-well plate; cytotoxicity values should be understood as a percentage of cell viability).

Campaign 0 with as-prepared disks evidences the dramatic impact of pH increase due to small amounts of free CaO in the sample (Fig. 8a). In the presence of disks, undoped or Cu-doped, cell viability was continuously below the control with five samples around or (largely) below 20% cell viability. Nevertheless it is complicated to advance general observations from campaign 0. For a sintering temperature of 600 °C, copper incorporation dramatically reduces cytotoxicity from about 50% (00Cu-600) to about 5% (25Cu-600). A similar trend was observed for a sintering temperature of 900 °C, with slightly improved values (from about 65% for the 00Cu-900 sample to about 20% for the 25Cu-900 sample). For a sintering temperature of 1200 °C, the case was completely different, with an improvement in cell viability in the presence of copper (from about 20% for undoped 00Cu-1200 sample to 50% for Cu-doped samples). This toxic behavior of the disks cannot be attributed solely to the presence of lime. The amount of CaO increases with copper insertion for heat treatment at 600 °C (1.0 wt% of CaO for 00Cu-600 against 1.5 wt% for 25Cu-600; Table 1). Nevertheless, CaO was negligible with copper insertion at 900 °C (0.2 wt% for 00Cu-900 and 0 wt% for (25Cu-900), and had completely disappeared from the samples at 1200 °C. Certainly the CaO and CuO combination should be considered to explain the toxicity of the disks prepared with as-synthesized powders. In fact, the first experiments on copper releases showed rapid and large copper concentrations in DMEM (more than 50 ppm, Fig. 7).

Campaigns A and B still showed complex behaviors, although with better results in terms of cell viability (Fig. 8b), indicating the beneficial effect of the disk post-treatments. In general, measurements from these two campaigns showed good cell viability at one week with respect to the control wells. For two samples only, the benefit of post-treatment was not observed: cell proliferation dropped for 00Cu-600 and there was no effect for 00Cu-900. Moreover, cell proliferation was clearly improved for the Cu-containing samples (10Cu-600, 10Cu-900 and 10Cu-1200). Again, the comparison between campaigns A and B does not enable obvious general guidelines to be drawn up. Campaign A seems favorable for samples 10Cu-600 and 10Cu-1200, whereas campaign B seems favorable for sample 10Cu-900. Fig. 8b also highlights the favored proliferation for cells in contact with ceramics sintered at 1200 °C. It is clear from these three cytotoxicity evaluation campaigns that controlling the preparation conditions (composition, temperature and post-treatment) makes it possible to increase cell viability in the vicinity of the ceramic. As an example, cell viability doubled with the 00Cu-1200 ceramic post-treated by water immersion.

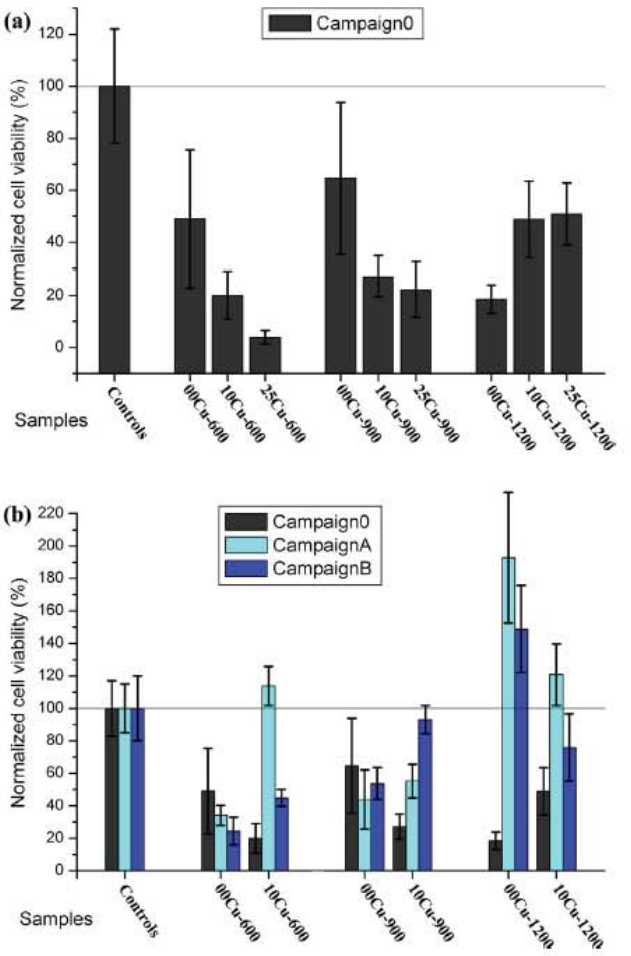

Fig. 8. Cell viability evaluation for a) Series 0 for xCu-T samples with x = 00, 10 and 20; and b) with Series A and B for xCu-T samples with x = 00 and 10. Error bars represent the standard error of mean from triplicate samples.

5. Discussion

The copper incorporation mechanism in BCP samples presents similarities with the temperature-dependent mechanism previously described in the case of Zn-doping [8–10] and Fe-doping [11]. The main outlines of the temperature variations of the two HAp and β-TCP phases are extremely similar for the first row transition metal series from Mn to Zn [12]. Whatever the sintering temperature or the amount of incorporated copper, Rietveld refinement did not show copper to calcium substitution in the HAp structure. Both Ca1 and Ca2 crystallographic sites of the HAp structure were tested: no copper substitution and no calcium deficiency were evidenced. This interstitial mechanism contradicts two earlier studies considering a substitution mechanism, carried out in 1989 on copper and zinc co-doped hydroxyapatite dried at 110 °C only [35] and on copper-doped strontium substituted hydroxyapatite, heat-treated at 950 °C [34]. The substitution mechanism was also mentioned in a recent study performed on copper-doped hydroxyapatite and fluorapatite, heat-treated at 700 °C [36], although the indicated lattice parameters did not convincingly evince Vegard's law. On the other hand, the location of copper cations at the interstitial 2*b* Wyckoff site, along the HAp hexagonal channel, has already been reported. Crystallographic studies based on single crystal data indicated Cu atoms at the 2*b* site (0,0,0) with the formation of linear oxocuprate entities O—Cu—O in the belovite structure [63] and also in the hydroxyapatite structure [37]. EXAFS analysis of our samples confirmed the twofold coordination for copper cations, with the d_{Cu-O} interatomic distance refined at 1.91 (1) Å. This value, greater than the previously determined d_{Zn-O} = 1.72 Å [10] and d_{Fe-O} = 1.84 Å [11], is certainly overesti-

mated because of the presence of about 10 wt% of Cu-substituted β-TCP in the analyzed sample (15Cu-1200). For the lower sintering temperatures investigated in this study (below 1000 °C), Cu-incorporation in the HAp phase is limited to the $Ca_{10}Cu_{0.05}(PO_4)_6(OH)_{1.90}O_{0.10}$ composition (Table SEI1). Heat treatment at 1100 °C led to the refined $Ca_{10}Cu_{0.10(1)}(PO_4)_6(OH)_{1.80(2)}O_{0.20(2)}$ composition for the 50Cu-1100 sample (Table SEI1). The inserted metal cation amount at 1100 °C is lower than that observed, in the same experimental conditions, for the Zn-doped series ($Ca_{10}Zn_{0.25}(PO_4)_6(OH)_{1.50}O_{0.50}$ [9]) or the Fe-doped series ($Ca_{9.75}Fe_{0.50}(PO_4)_6(OH)_1O_1$ [11]). An increase in sintering temperature, up to 1200 °C, enables the $Ca_{10}Cu_{0.61(1)}(PO_4)_6(OH)_{0.78(2)}O_{1.22(2)}$ composition to be obtained (Table SEI1). Such a large amount of inserted copper is coherent with previous indications in the literature: $Ca_{10}Cu_{0.54}(PO_4)_6O_{1.72}H_y$ for a single crystal grown at 1300 °C and slowly cooled to room temperature [37], and $Ca_{10}Cu_{0.72}(PO_4)_6(OH)_{0.56}O_{1.44}$ for a powder sintered at 1100 °C and air quenched [38]. To increase the copper occupancy factor from about 5% (corresponding to $Ca_{10}Cu_{0.10}(PO_4)_6(OH)_{1.80}O_{0.20}$: the Cu-poor HAp phase) to about 30% (corresponding to $Ca_{10}Cu_{0.60}(PO_4)_6(OH)_{0.80}O_{1.20}$: the Cu-rich HAp phase), it is necessary to apply temperatures greater than 1100 °C. Above this temperature, the β-TCP phase and a large part of the hydroxyapatite are transformed into the α-TCP polymorph and tricopper phosphate $Cu_3(PO_4)_2$. We have shown that the copper-rich HAp phase, with composition $Ca_{10}Cu_{0.60}(PO_4)_6(OH)_{0.80}O_{1.20}$, is obtained during cooling by the transformation of both α-TCP polymorph and $Cu_3(PO_4)_2$ into a new copper-rich HAp phase (Fig. 4). Contrary to the case of Zn^{2+}, oxocuprate insertion into the hexagonal channel led to an isotropic increase in the HAp unit cell volume (Fig. 2). The insertion of linear O—Zn—O entities, at the same crystallographic site, induced an increase in the hexagonal c lattice parameter, concomitant with a decrease in the basal a lattice parameter [8–10], whereas we observe here a simultaneous increase in both the a and c lattice parameters of HAp. The comparison of Zn-doping and Cu-doping with equivalent doping levels shows relatively equivalent c values and very different a values: $a = 9.4305$ Å and $c = 6.8959$ Å ($V = 531.12$ Å^3) for $Ca_{10}Cu_{0.27(1)}(PO_4)_6(OH)_{1.46(2)}O_{0.54(2)}$ (Table SEI1) against $a = 9.4077$ Å and $c = 6.9077$ Å ($V = 529.46$ Å^3) for $Ca_{10}Zn_{0.26(1)}(PO_4)_6(OH)_{1.48(2)}O_{0.52(2)}$ [8]. The a lattice parameter of undoped HAp is intermediate, about 9.420 Å (Table SEI1). It indicates that O—Zn—O attracts adjacent phosphate groups, and this is not the case with the oxocuprate entity. Phosphate anions are localized at 2.96 Å from the inserted copper cations (through the O3 crystallographic site) while this distance is reduced to 2.92 Å in the case of zinc cations. In a manner similar to the Zn-doping case, β-TCP was stabilized for heat treatments at around 700 °C. About 17 wt % of β-TCP is observed at 700 °C (Table 1) with the formation of a Cu-substituted β-TCP phase with an average $Ca_{2.75}Cu_{0.25}(PO_4)_2$ composition (Table SEI2). The substitution occurs without structural modification, in agreement with literature. A change in symmetry is reported for larger amounts of copper: a monoclinic $P2_1/c$ structure for the $Ca_{1.5}Cu_{1.5}(PO_4)_2$ compound [52]. The high-temperature tri-copper phosphate $Cu_3(PO_4)_2$ formed at 1100 °C and above – which corresponds to a complete copper substitution of β-TCP, chemically speaking – has its own triclinic $P\bar{1}$ structure [53]. The Cu-rich HAp phase is formed during cooling by the transformation of both α-TCP and $Cu_3(PO_4)_2$ phases. XANES observations, confirmed by XPS analyses, showed the presence of mixed Cu^+/Cu^{2+} valence in samples heat-treated at 1100 °C and above (Fig. 6). The Cu-rich HAp phase contains both Cu^{2+} and Cu^+ cations, and the $Ca_{10}Cu_x(PO_4)_6(OH)_{2-2x}O_{2x}$ general formula used does not reflect the real copper electronic state; to be exact, it should be written $Ca_{10}Cu^{2+}{}_xCu^+{}_y(PO_4)_6(OH)_{2-2x-y}O_{2x+y}$. The refined compositions indicated in Table SEI1 consider only the presence of Cu^{2+} cation. XPS analyses determined a y/x ratio of 0.2 for the Cu-rich HAp phase in the 75Cu-1200 sample, leading to the composition $Ca_{10}Cu^{2+}_{0.51}Cu^{+}_{0.10}(PO_4)_6(OH)_{0.88}O_{1.12}$. Nevertheless we should remember that XPS is strictly a surface technique, with the possibility that the bulk y/x ratio can differ from the experimental 0.2 value. The mixed valence in Cu-doped HAp was already brought to light in a previous study thanks to magnetic susceptibility measurements without the quantification of the Cu^+/Cu^{2+} ratio [37]. In the case of Cu-doped belovite, larger quantities of copper cations are inserted in the apatite hexagonal channel $Sr_{10}Cu_{1.70}(PO_4)_6O_2H_y$ with exclusively the Cu^+ electronic state for a sample annealed in argon atmosphere [39,63]. The authors attributed the presence of Cu^+ to its preference for the linear coordination compared to Cu^{2+}.

As clearly reported in the review of Jin et al. [21], the benefits of using Cu-doping in the development of biomaterial applications have attracted more and more attention in recent years, despite the fact that Cu has long been considered as toxic (when its amount exceeds certain limitations). Copper is not only an essential trace element required for human body health but it presents interesting antibacterial performances, stimulates angiogenesis, and promotes osteogenesis and the inhibition of in-stent restenosis [20,21,33,64,65]. The development of Cu-containing biomaterials with better bio-adaptation must now involve a better understanding of the cytotoxicity caused by the release of copper ions in physiological fluid: the dose-dependent cytotoxicity of copper [20]. We had in this study a complete set of materials to evaluate the cytotoxicity of the copper dopant with variations in 1) the HAp/β-TCP ratio, which impacts the copper release kinetic due to the difference in solubility between the two phases, 2) the amount of incorporated copper, which impacts the level of copper release, and 3) the copper valence (Cu^+ and Cu^{2+}), which should impact biological behavior. First, it is essential to carry out a post-treatment on BCP sintered disks in order to suppress the high toxicity of the as-prepared samples (Fig. 8a). Post-treatment is simply a washing of the disks with water, which can be combined with DMEM washing. The efficiency of these post-treatments is easily explained by the mineralogical characterization and copper location in the ceramic. The combination of the presence of free CaO (basic oxide, Table 1) and readily-available Cu^{2+} cations (either from the CuO phase for sintering at 600 °C, or substituted in the soluble β-TCP for sintering at 900 °C) explains the poor results in terms of cytotoxicity for disks pressed from as-synthesized BCP powder. The washing post-treatments enable the free basic CaO phase to be removed (by aqueous solubilisation) and also limit the level of copper physiological release (by a previous release in DMEM). Fig. 7 evidences an almost instantaneous copper release that exceeds 10 ppm for the copper-doped samples and reaches up to 50 ppm in three weeks. Wang et al. [20] determined a critical biological level of Cu^{2+} at 10 ppm. The disk washing post-treatment enables the release level to be reduced to below 10 ppm: about 3 ppm for 600 °C sintering, about 7 ppm for 900 °C sintering and below 1 ppm for 1200 °C sintering. These results highlight the difference in phase solubility between the known soluble β-TCP (which is mainly present in the case of 900 °C sintering) and the known low-solubility HAp (single doped-HAp phase samples obtained with 1200 °C sintering). On the other hand, the presence of mixed valence Cu^+/Cu^{2+} in the low soluble HAp phase does not penalize cell viability. As shown in Fig. 8b, the best cell viabilities (above or close to the expected 100%) have been measured for the 1200 °C sintering temperature; i.e. when the mixed valence is formed (Fig. 6). Finally, our MEB observations showed the biocompatibility with bone marrow cells; good adherence was highlighted with Cu-doped BCP samples (Fig. 9).

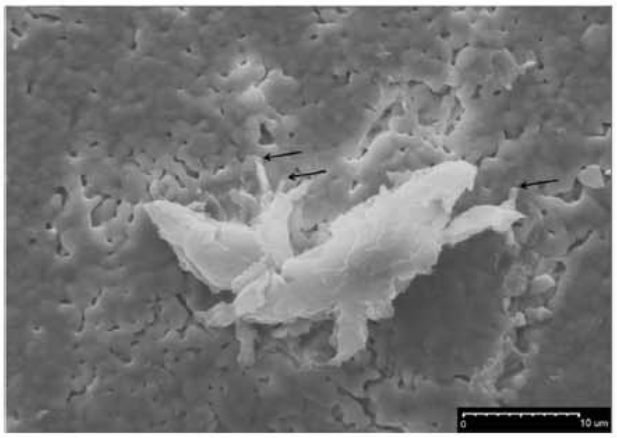

Fig. 9. Bone marrow adherent cell after 8 days of culture on a 10Cu-600 ceramic disk. These cells develop a strong attachment to the material surface through cellular expansion (black arrows).

6. Conclusion

The present study detailed the phase composition, the copper location and the copper electronic state of a total of 36 Cu-doped BCP samples. The temperature-dependent copper incorporation mechanism was thoroughly described. The first step (at 500 °C) lead to CuO mixed with weakly-doped HAp (Cu-poor HAp). The second step, between 700 °C and 1000 °C, corresponds to the formation of a Cu-doped β-TCP phase mixed with the Cu-poor HAp. Finally, at 1100 °C and above, samples are mainly composed of the Cu-doped HAp phase $Ca_{10}Cu_{0.6}(PO_4)_6(OH)_{0.8}O_{1.2}$ (the Cu-rich HAp). The main features of the HAp copper doping are: 1) a low amount of metal insertion for temperatures below 1100 °C in Cu-poor HAP $Ca_{10}Cu_{0.1}(PO_4)_6(OH)_{1.8}O_{0.2}$, and a higher amount for temperatures above 1100 °C in Cu-rich HAP $Ca_{10}Cu_{0.6}(PO_4)_6(OH)_{0.8}O_{1.2}$; 2) the necessity to decompose high-temperature Cu-doped α-TCP polymorph and $Cu_3(PO_4)_2$ to form the Cu-rich HAp phase; and 3) the presence of the mixed Cu^+/Cu^{2+} valence. Amongst our set of copper-doped BCP samples, we have several promising bioceramics for bone substitution and/or prosthesis coating. A mixture of HAp and β-TCP phases is interesting because of their difference in solubility; mixing Cu-doped HAp and β-TCP phases enables the copper releasing kinetics to be regulated. And the presence of Cu^+ cations in samples heat-treated at 1100 °C and above is potentially interesting for biomaterial applications. The ionic releases from sintered disks obtained from pressed BCP powder were observed, in order to establish a post-treatment to obtain acceptable or even very good cytotoxicity values. An understanding of the biological behavior (here in terms of cytotoxicity) and the mastery of BCP bioceramic preparation are only possible because the BCP doping mechanism has been clearly identified beforehand.

Acknowledgements

This work was supported by ANR under project NANOSHAP (ANR-09-BLAN-0120-03) and the CNRS 2015 PEPS project. We gratefully acknowledge SLS for the provision of synchrotron radiation facilities and we would like to thank Maarten Nachtegaal for his assistance in using the SuperXAS beamline.

Appendix A. Supplementary data

Supplementary data associated with this article can be found, in the online version, at https://doi.org/10.1016/j.actbio.2017.10.028.

References

[1] S.V. Dorozhkin, Biocomposites and hybrid biomaterials based on calcium orthophosphates, Biomatter 1 (2011) 3–56.
[2] S.G. Dahl, P. Allain, P.J. Marie, Y. Mauras, G. Boivin, P. Ammann, Y. Tsouderos, P. D. Delmas, C. Christiansen, Incorporation and distribution of strontium in bone, Bone 28 (2001) 446–453.
[3] R. Lagier, C.A. Baud, Magnesium whitlockite, a calcium phosphate crystal of special interest in pathology, Pathol. Res. Pract. 199 (2003) 329–335.
[4] R.S. Lee, M.V. Kayser, S.Y. Ali, Calcium phosphate microcrystal deposition in the human intervertebral disc, J. Anat. 208 (2006) 13–19.
[5] C. Rey, C. Combes, C. Drouet, M.J. Glimcher, Bone mineral: update on chemical composition and structure, Osteoporos. Int. 20 (2009) 1013–1021.
[6] S. Cazalbou, C. Combes, D. Eichert, C. Rey, Adaptative physico-chemistry of bio-related calcium phosphates, J. Mater. Chem. 14 (2004) 2148–2153.
[7] J.C. Elliot, Structure and Chemistry of the Apatite and Other Calcium Orthophosphates, Elsevier, Amsterdam, 1994.
[8] S. Gomes, J.-M. Nedelec, E. Jallot, D. Sheptyakov, G. Renaudin, Structural characterization and biological fluid interaction of solgel-derived Mg-substituted biphasic calcium phosphate ceramics, Chem. Mater. 23 (2011) 3072–3085.
[9] S. Gomes, J.-M. Nedelec, G. Renaudin, On the effect of temperature on the insertion of zinc into hydroxyapatite, Acta Biomater. 8 (2012) 1180–1189.
[10] S. Gomes, A. Kaur, J.-M. Nedelec, G. Renaudin, X-ray Absorption Spectroscopy shining (synchrotron) light onto the insertion of Zn^{2+} in calcium phosphate ceramics and its influence on their behaviour in biological conditions, J. Mater. Chem. B 2 (2014) 536–545.
[11] S. Gomes, A. Kaur, J.-M. Grenèche, J.-M. Nedelec, G. Renaudin, Atomic scale modeling of iron-doped biphasic calcium phosphate bioceramics, Acta Biomater. 50 (2017) 78–88.
[12] G. Renaudin, S. Gomes, J.-M. Nedelec, First-row transition metal doping in calcium phosphate bioceramics: a detailed crystallographic study, Materials 10 (2017) 92–113.
[13] Z. Radovanovic, B. Jokic, D. Veljovic, S. Dimitrijevic, V. Kojic, R. Petrovic, D. Janackovic, Antimicrobial activity and biocompatibility of Ag^+- and Cu^{2+}-doped biphasic hydroxyapatite/α-tricalcium phosphate obtained from hydrothermally synthesized Ag^+- and Cu^{2+}-doped hydroxyapatite, Appl. Surf. Sci. 307 (2014) 513–519.
[14] D.H. Nies, Microbial heavy-metal resistance, Appl. Microbiol. Biotechnol. 51 (1999) 730–750.
[15] H.G. Petering, Pharmacology and toxicology of heavy metals: silver, Pharmacol. Ther. A 1 (1976) 127–130.
[16] W.J. Schreurs, H. Rosenberg, Effect of silver ions on transport and retention of phosphate by Escherichia coli, J. Bacteriol. 152 (1982) 7–13.
[17] R.O. Darouiche, Anti-infective efficacy of silver-coated medical prostheses, Clin. Infect. Dis. 29 (1999) 1371–1377.
[18] G. Borkow, J. Gabbay, Copper as a biocidal tool, Curr. Med. Chem. 12 (2005) 2163–2175.
[19] Q.L. Feng, J. Wu, G.Q. Chen, F.Z. Cui, T.N. Kim, J.O. Kim, A mechanistic study of the antibacterial effect of silver ions on Escherichia coli and Staphylococcus aureus, J. Biomed. Mater. Res. 52 (2000) 662–668.
[20] X. Wang, F. Cheng, J. Liu, J.-H. Smatt, D. Gepperth, M. Lastusaari, C. Xu, L. Hupa, Biocomposites of copper-containing mesoporous bioactive glass and nanofibrillated cellulose: Biocompatibility and angiogenic promotion in chronic wound healing application, Acta Biomater. 46 (2016) 286–298.
[21] S. Jin, L. Ren, K. Yang, Bio-functional Cu containing biomaterials: a new way to enhance bio-adaption of biomaterials, J. Mater. Sci. Technol. 32 (2016) 835–839.
[22] B.R. Stern, Essentiality and toxicity in copper health risk assessment: overview, update and regulatory considerations, J. Toxicol. Environ. Health Part A 73 (2010) 114–127.
[23] M. Hunt, Copper and boron as examples of dietary trace elements important in bone development and disease, Curr. Opin. Orthop. 9 (1998) 28–36.
[24] H. Opsahl, Zeroniam, M. Ellison, D. Lewis, R.B. Rucker, R.S. Riggins, Role of copper in collagen cross-linking and its influence on selected mechanical properties of chick bone and tendon, J. Nutr. 112 (1982) 708–716.
[25] N.M. Lowe, W.D. Fraser, M.J. Jackson, Is there a potential therapeutic value of copper and zinc for osteoporosis?, Proc Nutr. Soc. 61 (2002) 181–185.
[26] C. Wu, Y. Zhou, M. Xu, P. Han, L. Chen, J. Chang, Y. Xiao, Copper-containing mesoporous bioactive glass scaffolds with multifunctional properties of angiogenesis capacity, osteostimulation and antibacterial activity, Biomaterials 34 (2013) 422–433.
[27] E.A. Neel, I. Ahmed, J. Prattern, S.N. Nazhat, J.C. Knowles, Characterisation of antibacterial copper releasing degradable phosphate glass fibres, Biomaterials 26 (2005) 2247–2254.
[28] S. Jaiswal, P. McHale, P. Duffy, Preparation and rapid analysis of antibacterial silver, copper and zinc doped sol–gel surfaces, Colloids Surf., B 94 (2012) 170–176.
[29] G.F. Hu, Copper stimulates proliferation of human endothelial cells under culture, J. Cell. Biochem. 69 (1998) 326–335.
[30] C.K. Sen, S. Khanna, M. Venojarvi, P. Trikha, E.C. Ellison, T.K. Hunt, Copper-induced vascular endothelial growth factor expression and wound healing, Am. J. Physiol Heart Circ. Physiol. 282 (2002) H1821–1827.
[31] M. Frangoulis, P. Georgiou, C. Chrisostomidis, D. Perrea, I. Dontas, N. Kavantzas, Rat epigastric flap survival and VEGF expression after local copper application, Plast. Reconstr. Surg. 119 (2007) 837–843.

[32] A. Ewald, C. Kappel, E. Vorndran, C. Moseke, M. Gelinsky, U. Gbureck, The effect of Cu(II)-loaded brushite scaffolds on growth and activity of osteoblastic cells, J. Biomed. Mater. Res. Part A 100 (2012) 2392–2400.
[33] R.A. Popescu, K. Magyari, A. Vulpoi, D.L. Trandafir, E. Licarete, M. Todea, R. Stefan, C. Voica, D.C. Vodnar, S. Simon, I. Papuc, L. Baia, Bioactive and biocompatible copper containing glass-ceramics with remarkable antibacterial properties and high cell viability designed for future in vivo trials, Biomater. Sci. 4 (2016) 1252–1265.
[34] M. Pujari, P.N. Patel, Strontium-copper-calcium hydroxyapatite solid solutions: Preparation, infrared, and lattice constant measurements, J. Solid State Chem. 83 (1989) 100–104.
[35] N.K. Triphathy, P.N. Patel, A. Panda, Preparation, IR, and lattice constant measurements of mixed (Ca + Cu + Zn) hydroxylapatites, J. Solid State Chem. 80 (1989) 1–5.
[36] S. Shanmugam, B. Gopal, Copper substituted hydroxyapatite and fluorapatite: Synthesis, characterization and antimicrobial properties, Ceram. Int. 40 (2014) 15655–15662.
[37] A.S. Karpov, J. Nuss, M. Jansen, P.E. Kazin, Y.D. Tretyakov, Synthesis, crystal structure and properties of calcium and barium hydroxyapatites containing copper ions in hexagonal channels, Solid State Sci. 5 (2003) 1277–1283.
[38] T. Baikie, G.M.H. Ng, S. Madhavi, S.P. Pramana, K. Blake, M. Elcombe, T.J. White, The crystal chemistry of the alkaline-earth apatites $A_{10}(PO_4)_6Cu_xO_y(H)_z$ (A = Ca, Sr and Ba), Dalton Trans. 34 (2009) 6722–6726.
[39] F.E. Imrie, J.M.S. Skakle, I.R. Gibson, Preparation of copper-doped hydroxyapatite with varying x in the composition $Ca_{10}(PO_4)_6Cu_xO_yH_z$, Bioceram. Dev. Appl. S1 (2013) 005, https://doi.org/10.4172/2090-5025.S1-005.
[40] J. Rodriguez-Carvajal, PROGRAM FullProf.2k – version 3.20; Laboratoire Léon Brillouin (CEA-CNRS): Saclay, France, 2005; FullProf.2k manual available on http://www-llb.cea.fr/fullweb/fp2k/fp2k_divers.htm. See also J. Rodriguez-Carvajal, T. Roisnel, EPDIC-8; May 23-26, 2002; Trans. Tech. Publication: Uppsala, Sweden; Mater. Sci. Forum 2004; 123:443.
[41] N. Newville, IFEFFIT : interactive XAFS analysis and FEFF fitting, J. Synchrotron Rad. 8 (2001) 322–324.
[42] B. Ravel, ATOMS: crystallography for the X-ray absorption spectroscopist, J. Synchrotron Rad. 8 (2001) 314–316.
[43] J.J. Rehr, J. Mustre de Leon, S.I. Zabinsky, R.C. Albers, Theoretical x-ray absorption fine structure standards, J. Am. Chem. Soc. 113 (1991) 5135–5145.
[44] D. Shirley, High-resolution X-ray photoemission spectrum of the valence bands of gold, Phys. Rev. B 5 (1972) 4709–4714.
[45] J. Scofield, Hartree-Slater subshell photoionization cross-sections at 1254 and 1487 eV, J. Electron. Spectrosc. Relat. Phenom. 8 (1976) 129–137.
[46] G. Renaudin, P. Laquerrière, Y. Filinchuk, E. Jallot, J.-M. Nedelec, Structural characterization of sol–gel derived Sr-substituted calcium phosphates with anti-osteoporotic and anti-inflammatory properties, J. Mater. Chem. 18 (2008) 3593–3600.
[47] G. Renaudin, E. Jallot, J.-M. Nedelec, Effect of strontium substitution on the composition and microstructure of sol-gel derived calcium phosphate, J. Sol-Gel Sci. Technol. 51 (2009) 287–294.
[48] S. Gomes, G. Renaudin, E. Jallot, J.-M. Nedelec, Structural characterization and biological fluid interaction of sol-gel derived Mg-substituted biphasic calcium phosphate ceramics, Appl. Mater. Interfaces 1 (2009) 505–513.
[49] L.M. Rodriguez-Lorenzo, J.N. Hart, A. Gross, Structural and chemical analysis of well-crystallized hydroxyfluorapatites, J. Phys. Chem. B 107 (2003) 8316–8320.
[50] M. Yashima, A. Sakai, T. Kamiyama, A. Hoshikawa, Crystal structure analysis of β-tricalcium phosphate $Ca_3(PO_4)_2$ by neutron powder diffraction, J. Solid State Chem. 175 (2003) 272–277.
[51] B.I. Lazoryak, N. Khan, V.A. Morozov, A.A. Belik, S.S. Khasanov, Preparation, structure determination, and redox characteristics of new calcium copper phosphates, J. Solid State Chem. 145 (1999) 345–355.
[52] V.Yu. Pomjakushin, A. Furrer, D.V. Sheptyakov, E.V. Pomjakushina, K. Conder, Crystal and magnetic structures of the spin-trimer compounds $Ca_3Cu_{3-x}Ni_x(PO_4)_4$ (x = 0,1,2), Phys. Rev. B 76 (2007) 174433–174439.
[53] G.L. Shoemaker, J.B. Anderson, E. Kostiner, Copper(II) phosphate, Acta Crystallogr. Sect. B: Sturct. Sci. 33 (1977) 2969–2972.
[54] S.P. Cramer, K.O. Hodgson, X-ray absorption spectroscopy: a new structural method and its applications to bioinorganic chemistry, Prog. Inorg. Chem. 25 (1979) 1–39.
[55] P.A. Lee, P.H. Citrin, P. Eisenberger, B.M. Kincaid, Extended x-ray absorption fine structure—its strengths and limitations as a structural tool, Rev. Mod. Phys. 53 (1981) 769–806.
[56] Comments of Inorganic Chemistry vol. 3 (1984) 225–320.
[57] L.S. Kau, D.J. Spria-Solomon, J.E. Penner-Hahn, K.O. Hodgson, E.I. Solomon, X-ray absorption edge determination of the oxidation state and coordination number of copper. Application to the type 3 site in Rhus vernicifera laccase and its reaction with oxygen, J. Am. Chem. Soc. 109 (1987) 6433–6442.
[58] A. Gaur, B.D. Shrivastava, S.K. Joshi, 14th International Conference on X-Ray Absorption Fine Structure (XAF14), J. Phys. Conf. Ser. 190 (2009) 012084.
[59] L. Martin, H. Martinez, D. Poinot, B. Pecquenard, F. Le Cras, Comprehensive X-ray photoelectron spectroscopy study of the conversion reaction mechanism of CuO in lithiated thin film electrodes, J. Phys. Chem. C 117 (2013) 4421–4430.
[60] S. Harmer, W. Skinner, A. Buckley, L.-J. Fan, Species formed at cuprite fracture surfaces; observation of O 1s surface core level shift, Surf. Sci. 603 (2009) 537–545.
[61] F. Parmigiani, L. Depero, T. Minerva, J. Torrance, The fine structure of the Cu 2p3/2 X-ray photoelectron spectra of copper oxide based compounds, J. Electron Spectrosc. Relat. Phenom. 58 (1992) 315–323.
[62] F. Parmigiani, G. Pacchioni, F. Illas, P. Bagus, Studies of the Cu-O bond in cupric oxide by X-ray photoelectron spectroscopy and ab initio electronic structure models, J. Electron Spectrosc. Relat. Phenom. 59 (1992) 255–269.
[63] P.E. Kazin, A.S. Karpov, J. Martin, J. Nuss, Y.D. Tretyakov, Crystal structure and properties of strontium phosphate apatite with oxocuprate ions in hexagonal channels, Z. Anorg. Allg. Chem. 629 (2003) 344–3520.
[64] V. Stanic, S. Dimitrijevic, J.A. Stankovic, M. Mitric, B. Jokic, I.B. Plecas, S. Raicevic, Synthesis, characterization and antimicrobial activity of copper and zinc-doped hydroxyapatite nanopowders, Appl. Surf. Sci. 256 (2010) 6083–6089.
[65] N. Matsumoto, K. Sato, K. Yoshida, K. Hashimoto, Y. Toda, Preparation and characterization of β-tricalcium phosphate co-doped with monovalent and divalent antibacterial metal ions, Acta Biomater. 5 (2009) 3157–3164.

Dans le cadre de cette thèse des BCP avec différents taux de dopage au cuivre et différentes températures de recuits ont été synthétisés selon le protocole décrit précédemment et le **tableau 2.1** résume les échantillons obtenus. Comme dans l'étude précédente, les échantillons synthétisés sont référencés sous la forme "*X*Cu-*T*" où *X* représente la proportion de cuivre et *T* correspond à la température de recuit.

Tableau 2.1 : Différents échantillons de BCP dopés au cuivre obtenus.

Echantillons	Taux de dopage *x*	T°C de recuit
00Cu-600	0	600°C
00Cu-900	0	900°C
00Cu-1200	0	1200°C
05Cu-600	0,05	600°C
05Cu-900	0,05	900°C
05Cu-1200	0,05	1200°C
10Cu-600	0,10	600°C
10Cu-900	0,10	900°C
10Cu-1200	0,10	1200°C
20Cu-600	0,20	600°C
20Cu-900	0,20	900°C
20Cu-1200	0,20	1200°C

2.3. Dopage à l'argent

Des BCP dopées à l'argent ont été synthétisées en suivant le même protocole que celui cité précédemment en utilisant cette fois-ci de l'$AgNO_3$ en quantité appropriée suivant le taux de dopage souhaité.

Lors de cette étude 2 taux de dopage ont été réalisés en considérant un mécanisme de substitution des ions calcium par les ions argent, du fait des tailles relativement proches des

cations Ca^{2+} et Ag^{+}. Un premier avec 2,5% de substitution en calcium, correspondant à la composition $Ca_{9.75}Ag_{0.25}(PO_4)_6(OH)_{1.75}$ appelé 25Ag-*T*. Et un second avec 10% de substitution : $Ca_9Ag_1(PO_4)_6(OH)$ appelé 100Ag-*T*. Des échantillons non dopés ont aussi été synthétisés et nommés 0Ag-*T*. Les matériaux ont subi des recuits allant de 400°C à 1200°C avec un pas de 100°C. Pour connaître la composition des matériaux obtenus et quantifier les phases en présence, le même protocole que précédemment a été utilisé.

En résumé, 2 types d'incorporation du cuivre ont été observé : une substitution des ions Ca^{2+} par les ions Ag^{+} dans les phases HAp et ß-TCP et la formation de nanoparticules d'argent métallique Ag°. Les matériaux obtenus aux températures de recuit comprises entre 400°C et 1000°C sont des nanocomposites nommés Ag°/BCP comprenant des nanoparticules d'Ag° et des BCP dopés par Ag^{+}. Entre 400°C et 700°C les ions Ag^{+} sont localisés principalement dans la phase HAp dont la composition est $Ca_{10-x}Ag_x(PO_4)_6(OH)_{2-x}$. A partir de 600°C les ions Ag^{+} migrent également dans la phase ß-TCP pour former un composé défini de formule chimique $Ca_{10}Ag(PO_4)_7$. A 1000°C et au-dessus il n'y a plus d'argent dans les échantillons puisque le point de fusion d'Ag° est de 961,8°C. A 400°C les nanoparticules ont une taille d'environ 100 nm de diamètre puis elles coalescent avec la montée en température pour atteindre à 700°C environ 300 nm pour les échantillons les moins dopés (25Ag-700) et entre 500 et 1000 nm pour les échantillons plus dopés (100Ag-700).

L'analyse précise de la composition de ces BCP dopées à l'argent est un travail très important puisque comme démontré dans cette étude les 2 formes Ag^{+} et Ag° sont retrouvées dans les matériaux, ce qui peut largement influencer les propriétés de relargage des ions et donc sur les propriétés biologiques des matériaux, notamment du fait que l'argent métal est reconnu pour ses propriétés antibactériennes.

L'intégralité des résultats obtenus décrivant le mécanisme d'incorporation de l'argent dans les phosphates de calcium biphasiques sont présentés dans l'article suivant :

Aurélie Jacobs, Morgane Gaulier, Alexis Duval and Guillaume Renaudin, **Silver Doping Mechanism in Bioceramics — From Ag^{+}:Doped HAp to Ag°/BCP Nanocomposite,** *Crystals,* 2019, *9*, 326. https://doi.org/10.3390/cryst9070326

crystals

MDPI

Article

Silver Doping Mechanism in Bioceramics—From Ag^+: Doped HAp to Ag°/BCP Nanocomposite

Aurélie Jacobs, Morgane Gaulier, Alexis Duval and Guillaume Renaudin *

Université Clermont Auvergne, CNRS, SIGMA Clermont, ICCF, F-63000 Clermont-Ferrand, France; aurel.jacobs@gmail.com (A.J.); morgane.gaulier@etu.uca.fr (M.G.); alexis.duval@etu.uca.fr (A.D.)

* Correspondence: guillaume.renaudin@sigma-clermont.fr; Tel.: 00-334-7340-7336, Fax.: 00-334-7340-7095

Received: 24 May 2019; Accepted: 23 June 2019; Published: 26 June 2019

Abstract: The results presented in this paper, based on the powder X-ray diffraction technique followed by Rietveld analyses, are devoted to the mechanism of silver incorporation in biphasic calcium phosphates. Results were confirmed by SEM observation. Samples were synthesized via the sol-gel route, followed by heat treatments. Two incorporation sites were highlighted: Ca^{2+} replacement by Ag^+ into the calcium phosphates (HAp: hydroxyapatite and β-TCP: tricalcium phosphate), and the other as metallic silver Ag° nanoparticles (formed by autogenous reduction). The samples obtained were thus nanocomposites, written Ag°/BCP, composed of closely-mixed Ag° particles of about 100 nm at 400 °C (which became micrometric upon heating) and calcium phosphates, themselves substituted by Ag^+ cations. Between 400 °C and 700 °C the cationic silver part was mainly located in the HAp phase of the composition $Ca_{10-x}Ag_x(PO_4)_6(OH)_{2-x}$ (written Ag^+: HAp). From 600 °C silver cations migrated to β-TCP to form the definite compound $Ca_{10}Ag(PO_4)_7$ (written Ag^+: TCP). Due to the melting point of Ag°, the doping element completely left our sample at temperatures above 1000 °C. In order to correctly understand the biological behavior of such material, which is potentially interesting for biomaterial applications, its complex doping mechanism should be taken into consideration for subsequent cytotoxic and bacteriologic studies.

Keywords: biomaterial; silver-doping; silver nanocomposite; hydroxyapatite; powder X-ray diffraction

1. Introduction

The utilization of synthetic materials for bone reconstructive surgery is generally necessary, because autograft and allograft practices are limited by the quantity of available material, and in the first case entails a second surgical procedure [1]. Among the numerous synthetic materials investigated for bone replacement and/or prosthesis coating, hydroxyapatite (HAp, $Ca_{10}(PO_4)_6(OH)_2$) is the most often-used material due to its chemical and structural similarities with the bone mineral constituent [2–5]. Biological apatite refers to the main constituent of bone and hard tissue in mammals: a poorly crystallized non-stoichiometric carbonate-containing HAp that composes about 65 weight percent (wt %) of bone and about 90 wt % of dental enamel [6]. Apatite is a complex and diverse class of materials, with a flexible structure that accepts many substitutions, either cationic or anionic [7]. Hydroxyapatite is therefore an interesting biocompatible and osteoconductive material, but it has limited antibacterial properties [8], even though bacterial infections are the main cause of postoperative problems [9]. Bacterial overgrowth on the surface of orthopaedic implants-that is, biofilm formation-potentially leads to serious complications during reconstructive surgery, with severe physiological damage, significant patient discomfort, and additional costly surgical procedures [10–12]. About 1% of total joint hip arthroplasties, and about 3% in the case of knees, require a second (or multiple) surgical intervention(s) because of bone healing process complications,

which makes it a real societal problem on a global scale [13–17]. Nowadays, an antibacterial effect at the surgical site is ensured by systematic antibiotic administration via the blood, which potentially generates toxicity, poor penetration into the surgical site, and also the problem of bacterial resistance. The delivery, or the presence, of a bactericidal agent directly at the surgical site would ensure a really promising alternative [18,19]. Among the various possibilities, the use of silver—well known in medicine since ancient times in the treatment of bacterial infection—seems very promising by combining broad spectrum and long term antimicrobial activity with the absence of microorganisms developing resistance [20–25]. A particularity of the antiseptic properties of silver is the possibility of using it in metallic or ionic form, without a loss of efficiency [26–41]. For these reasons, research on silver incorporation into hydroxyapatite has developed in recent years, and has shown the high potential of the synthesized materials [17,22,29–35]. Although the results agree regarding the beneficial biological effects, the literature on the topic does not address the fine description of the synthesized materials and the mechanisms of silver incorporation. Many synthesis methods have been described (co-precipitation [29,35,42] potentially followed by a thermal [8,22,33,36,38] or reducing treatment [34,41], sol-gel [17,30,40,43], electrochemical [31,37], hydrothermal [32], microwave [26,39], sonochemical [44], plasma-spraying [42,45], and also impregnation [46,47] methods), with the formation of two different kinds of material: either an Ag^{+}:doped HAp compound or an Ag°/HAp nanocomposite material. The difference is—of course—fundamental, since in the first case the single-phase material contains Ag^{+} cations that substitute Ca^{2+} from the HAp crystal structure, while in the second case metallic silver particles are intimately mixed in a multi-phase composite. Although these two alternatives are listed and described in the literature [44] there is a lack of understanding the mechanisms that lead to one or the other.

The purpose of this paper is to fully characterize the silver–HAp doping mechanism in the case of sol-gel synthesis followed by gradual thermal treatment leading to silver auto-reduction. The study is a continuation of our previous work on the BCP (biphasic calcium phosphate) doping mechanism with cations from the first-row transition metals [48]. The case of zinc doping, with an interstitial mode of incorporation into the HAp crystal structure, was first fully characterized [49–51], then investigated for iron [52]. In the case of copper, it transpired that control of the doping mechanism allowed an insight into behavior in a biological environment [53]. For a complete understanding of the present paper it is very important to note the difference between the notations used: Ag^{+}: HAp and Ag°/HAp. Ag^{+}: HAp corresponds to the incorporation of Ag^{+} cations within the crystal structure of hydroxyapatite (which is expected in the case of conventional cationic doping), whereas Ag°/HAp means the formation of a composite containing two distinct phases, the hydroxyapatite trapping nanoparticles of Ag° metallic silver.

2. Materials and Methods

2.1. Sol-Gel Elaboration of Silver Containing BCP Samples

The sol-gel route previously proposed by the authors was used to synthesize both undoped and Ag-doped series of BCP samples [51]. Briefly, to produce 2 g of undoped BCP powder, 4.7 g of $Ca(NO_3)_2{\cdot}4H_2O$ (Sigma–Aldrich, Saint Quentin Fallavier, France), and 0.84 g of P_2O_5 (Sigma–Aldrich, Saint Quentin Fallavier, France) were dissolved in ethanol under stirring and refluxed at 85 °C for 24 hours. The solution was then maintained at 55 °C for 24 hours to obtain a white consistent gel, and further heated at 80 °C for 10 hours to obtain a white powder. Finally, the powder was heat-treated for 15 hours. This thermal treatment was performed between 100 °C and 1200 °C. Samples from the undoped series were named the 0Ag-*T* series with *T* indicating the temperature (from 400 °C to 1200 °C) of the following thermal treatment. Required amounts of $AgNO_3$ (Sigma–Aldrich, Saint Quentin Fallavier, France) were added to the solution simultaneously with $Ca(NO_3)_2{\cdot}4H_2O$ (Sigma–Aldrich, Saint Quentin Fallavier, France) in order to synthesize the Ag-doped series. Nominal compositions were calculated, assuming Ag^{+} calcium substitution (i.e., assuming a (Ca+Ag)/P = 1.67 constant ratio) with two doping levels: a 2.5% calcium substitution (Ag/(Ca+Ag) = 0.025 corresponding to the nominal composition $Ca_{9.75}Ag_{0.25}(PO_4)_6(OH)_{1.75}$; named the 25Ag-*T* series) and a 10% calcium

substitution (Ag/(Ca+Ag) = 0.1 corresponding to the nominal composition $Ca_9Ag_1(PO_4)_6(OH)$; named the 100Ag-*T* series). As-synthesized Ag-doped powders were pale yellow; heat treatments turn the color to light grey, and then to white above 1000 °C.

2.2. Powder X-Ray Diffraction (PXRD) and Rietveld Analyses

Powder X-ray diffraction (PXRD) patterns were recorded on a Philips X'Pert Pro PANalytical diffractometer (Almelo, Netherlands), with θ-θ geometry, reflection mode, equipped with a solid-state X-Celerator detector (PANalytical, Almelo, Netherlands), and using Cu Kα radiation (λ = 1.54184 Å). PXRD patterns were recorded at room temperature in the interval $3° < 2\theta < 120°$, with a step size of $\Delta 2\theta = 0.0167°$ and a counting time of 200 s for each data value.

Rietveld refinements were systematically performed for each measurement (13 temperatures for the 3 series) using the FullProf.2k program [54]. The Rietveld strategy was detailed in previous related works [48-53]. A new additional phosphate compound was considered here: $AgCa_{10}(PO_4)_7$, which crystallizes in the trigonal *R*3*c* space group with a = 10.4372 Å and c = 37.3379 Å [55]. It is isotopic with members of the $MCa_{10}(PO_4)_7$ (M = Li, Na, K, and Cs) series, and is closely related to the structure of β-TCP (β-$Ca_3(PO_4)_2$, *R*3*c* symmetry with a = 10.4352 Å and c = 37.4029 Å [56]). The half-occupied Ca4 site of β-TCP [56] becomes fully occupied by silver cations in $AgCa_{10}(PO_4)_7$ [55], explaining the charge compensation between Ca^{2+} and Ag^{+}. The metal Ag° phase was also considered in several samples; it is a compact cubic structure $Fm\overline{3}m$ with a = 4.085 Å [57]. An example of a Rietveld plot is shown in Figure S1 (Supplementary Materials).

2.3. Scanning Electron Microscopy (SEM)

Electronic microscopy observations used a ZEISS SUPRA 55VP (Carl Zeiss Microscopy Ltd, Cambridge, UK) with GEMINI Field Emission-Scanning Electron Microscope (Carl Zeiss Microscopy Ltd, Cambridge, UK) and were carried out on pressed pellets after gold metallization. No polishing was carried out to avoid the leaching of the silver cations and to avoid the deformation of the ductile metallic silver particles. The main object of this analysis is not the quantification, but the localization, of the silver element. Quantitative analyses were performed using an EDS (OXFORD XMAX 80 N+ 80 mm^2 Si-detector (Oxford Instruments, High Wycombe, UK) combined with OXFORD AZtec Advanced V3.3 software (Oxford Instruments, High Wycombe, UK) on Ca, P, and Ag elements. Measurements were made using an acceleration voltage of 20 kV and 30 seconds of acquisition on three wide areas (magnification ×100) before averaging. Some specific isolated measurements were performed using ×5000 magnification. A 4QBSD detector (Carl Zeiss Microscopy Ltd, Cambridge, UK) was used to acquire chemical contrast images to highlight silver particles.

The following nine samples were characterized by SEM: 0Ag-400, 0Ag-700, 0Ag-1200, 25Ag-400, 25Ag-700, 25Ag-1200, 100Ag-400, 100Ag-700, and 100Ag-1200.

3. Results: Materials Characterization

3.1. Quantitative Phase Analysis

To correctly interpret the behavior of our samples, their phase compositions were extracted from Rietveld analyses (PXRD patterns from the 25Ag-*T* series are shown in Figure 1). Figure 1 evidences the gradual increase in crystallinity of HAp with respect to temperature by the decrease in the diffraction peak width. Phase compositions of the undoped BCP series and of the two Ag-doped BCP series (x = 25 and 100) are presented in Table 1, and Figure 2a represents the thermal composition variation for the two main phases: HAp and β-TCP. Supplementary minor phases were observed. α-CDP (dicalcium diphosphate with composition $Ca_2P_2O_7$) was observed up to 700 °C, with a maximum amount of 4 wt % at 500–600 °C. CaO and $CaCO_3$ (calcite) were present in the samples. They are indicated in CaO equivalent content in Table 1, as calcite decarbonation leads to CaO formation at about 800 °C. The amount of CaO equivalent becomes negligible at high temperatures, where the BCP were mainly composed of HAp (corresponding to the nominal composition). All these

observations—on main and minor phases—were similar to those of our previous studies on first-row transition metal doping [48–53]. The β-TCP phase is stabilized for intermediate temperatures, with a maximum amount close to 20 wt % around 900 °C for the undoped series and around 700 °C for the two silver-doped series. The main difference compared to our previous works concerns the formation of metallic silver, Ag°, already at 400 °C in the Ag-doped series (contrary to metal oxide formation for the first-row transition metals, including ZnO and CuO). The amount of metallic silver reached 1 wt % for the 25Ag-*T* series and 6 wt % for the 100Ag-*T* series (Table 1 and Figure 2b). These values are to be compared to the quantities introduced during the syntheses: 2.65 wt % for the nominal $Ca_{9.75}Ag_{0.25}(PO_4)_6(OH)_{1.75}$ composition and 10.22 wt % for the nominal $Ca_9Ag_1(PO_4)_6(OH)$ composition (respectively the 25Ag-*T* and the 100Ag-*T* series). Figure 2b highlights the fact that the entirety of the dopant introduced was not found exclusively in metallic form, but rather of the order of half of this quantity. The reduction of the incorporated Ag^+ silver cation to Ag° silver metal was autogenous, and monitored by the thermal treatment only, without any reducing agent.

The formation of Ag°/HAp nanocomposite by heating Ag^+-incorporated hydroxyapatite has already been mentioned in the literature, either using a reducing agent ($NaBH_4$ [34,58], hydrazine [41]) or not [17,22,26,38,44]. However, the nanocomposite formation mechanism, the main subject of this paper, has never been studied and detailed. It may first be pointed out that a thermal study on silver nitrate ($AgNO_3$; not shown here) showed decomposition accompanied by reduction at 300 °C, which leads to the production of metallic silver (Ag°). To complete this information, the color changes of our samples are also interesting. The undoped series remained constantly white, while the doped series were yellow at 400 °C (pale yellow for the 25Ag-*T* series and yellow-brown for the 100Ag-*T* series), then turned grey up to 1000 °C before bleaching above 1100 °C. The grey color can be attributed to the silver nanoparticles present in the Ag°/HAp composite. It is therefore normal to lose the grey color above 1000 °C, since silver has a melting point of 962 °C. Thus it is difficult to design Ag°/HAp composites which could be obtained following heat treatments at more than 1000 °C [8,36,39,59]. Our white 25Ag-1100, 25Ag-1200, and 100Ag-1200 samples were then exempt of silver particles, and certainly just composed of undoped HAp counterbalanced by a few wt % of β-TCP due to the introduced Ca/P ratio (1.625 for the 25Ag-*T* series and 1.5 for the 100Ag-*T* series instead of the 1.67 value for HAp). By wetting calcium phosphate particles, metallic silver was still present in the 25Ag-1000 sample (in very little amount) and in 100Ag-1100 sample (although the Ag° amount decrease is very clear at above 900 °C).

Table 1. Quantitative phase analysis (wt %) of the 27 samples; standard deviations are indicated in brackets (CDP: $Ca_2P_2O_7$ and 'Eq. CaO' considers both the CaO and $CaCO_3$ amounts).

Sample	Phase Composition (wt %)				
	HAp	TCP	CDP	Eq. CaO	Ag°
0Ag-400	97.1 (2.0)	2.9 (1.0)	/	/	/
0Ag-500	94.8 (2.0)	1.5 (0.5)	2.1 (0.5)	1.6 (0.5)	/
0Ag-600	91.8 (2.0)	3.3 (1.0)	3.8 (1.0)	1.2 (0.5)	/
0Ag-700	85.8 (2.0)	9.3 (1.0)	3.1 (1.0)	1.9 (0.5)	/
0Ag-800	81.9 (2.0)	16.0 (1.0)	/	2.1 (0.5)	/
0Ag-900	81.4 (2.0)	16.7 (1.0)	/	1.9 (0.5)	/
0Ag-1000	85.8 (2.0)	13.6 (1.0)	/	0.6 (0.5)	/
0Ag-1100	92.5 (2.0)	7.1 (1.0)	/	0.4 (0.2)	/
0Ag-1200	96.0 (2.0)	3.8 (1.0)	/	0.2 (0.2)	/
25Ag-400	92.7 (2.0)	2.5 (0.5)	3.1 (1.0)	1.2 (0.5)	0.3 (0.2)
25Ag-500	88.5 (2.0)	3.6 (1.0)	4.1 (1.0)	2.6 (0.5)	1.1 (0.5)
25Ag-600	81.9 (2.0)	11.3 (1.0)	3.5 (1.0)	2.4 (0.5)	0.8 (0.5)
25Ag-700	80.4 (2.0)	15.8 (1.0)	1.1 (0.5)	2.2 (0.5)	0.7 (0.5)
25Ag-800	82.9 (2.0)	14.0 (1.0)	/	2.2 (0.5)	0.9 (0.5)
25Ag-900	87.1 (2.0)	19.9 (1.0)	/	2.0 (0.5)	1.0 (0.5)
25Ag-1000	93.1 (2.0)	5.3 (1.0)	/	1.5 (0.5)	0.1 (0.2)
25Ag-1100	96.8 (2.0)	2.0 (0.5)	/	1.2 (0.5)	/

25Ag-1200	99.0 (2.0)	0.5 (0.2)	/	0.5 (0.2)	/
100Ag-400	92.3 (2.0)	/	/	2.4 (0.5)	5.3 (1.0)
100Ag-500	81.4 (2.0)	7.4 (1.0)	2.3 (0.5)	3.4 (1.0)	5.5 (1.0)
100Ag-600	76.8 (2.0)	12.5 (1.0)	1.8 (0.5)	3.0 (1.0)	5.9 (1.0)
100Ag-700	73.8 (2.0)	16.1 (1.0)	1.0 (0.5)	3.2 (1.0)	6.0 (1.0)
100Ag-800	77.3 (2.0)	13.9 (1.0)	/	2.9 (0.5)	5.9 (1.0)
100Ag-900	79.4 (2.0)	13.5 (1.0)	/	1.4 (0.5)	5.6 (1.0)
100Ag-1000	85.5 (2.0)	8.7 (1.0)	/	1.1 (0.5)	4.8 (1.0)
100Ag-1100	92.2 (2.0)	4.7 (1.0)	/	0.4 (0.2)	2.8 (0.5)
100Ag-1200	96.8 (2.0)	3.0 (1.0)	/	0.1 (0.2)	/

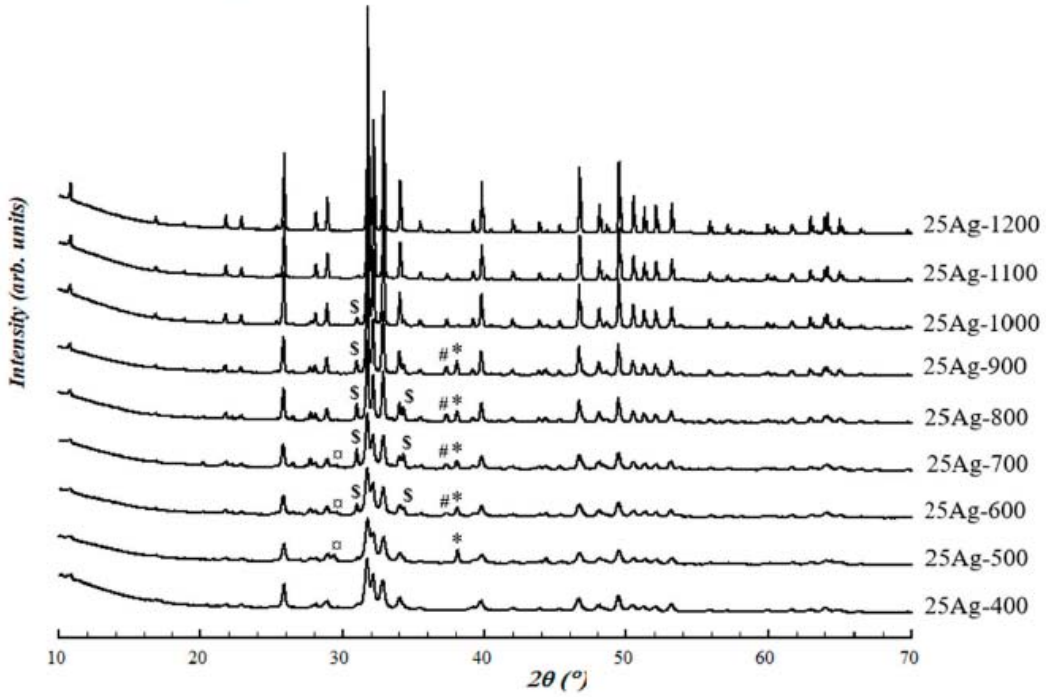

Figure 1. Powder X-ray diffraction (PXRD) patterns from the 25Ag-*T* series. Scattering signals are mainly those from the hydroxyapatite (HAp) phase, and other phases are identified thanks to their intense diffraction peaks (*: Ag°, #: CaO, ¤: $CaCO_3$, and $: tricalcium phosphate (β-TCP)).

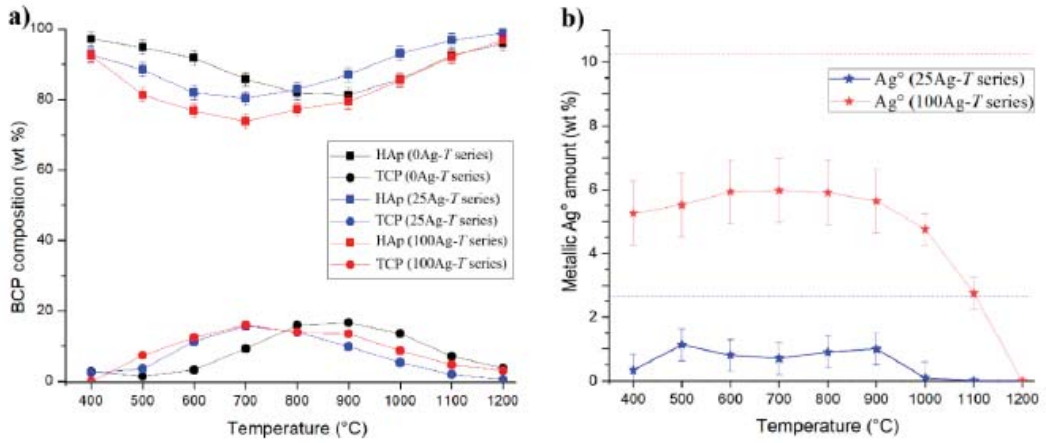

Figure 2. Thermal variation in a) the two main phase contents (squares: HAp; circles: TCP) from the biphasic calcium phosphates (BCP) samples and b) the metallic silver amount (stars) for the undoped 0Ag-*T* series (black symbols), the 25Ag-*T* series (blue symbols), and 100Ag-*T* series (red symbols). Dotted lines indicate the nominal silver amounts, and lines are only guides for the eyes.

3.2. Thermal Variation in the HAp Structural Parameters

Thermal variations in the HAp lattice parameters are shown in Figure 3 and collated in Table S1 (Supplementary Materials). Figure 3 clearly shows that the parameters of the HAp network evolved for the lowest temperatures and then showed no more variations. The undoped series presents a relatively weak contraction between 400 °C and 500 °C for both *a* and *c* lattice parameters (and consequently for the unit cell volume). This contraction is also observed between 400 °C and 500 °C on the basal *a* lattice parameter for the two silver-doped series, but much more markedly. Concerning the hexagonal *c* lattice parameter, the difference between the undoped and the two-doped series extends up to 700 °C, which of course also affects the unit cell volume difference up to 700 °C. For the lowest temperatures, an enlargement of the HAp network is in favor of a calcium-to-silver substitution, explained by the larger cationic radius of the Ag^+ cation: 1.28 Å for Ag^+ against 1.12 Å for Ca^{2+} in eightfold coordination [60]. This indication of a silver substitution mechanism to form Ag^+: HAp with larger lattice parameters is consistent with previous literature results [32,33,38], but more marked in our study. Indeed, the large values found here (a = 9.488 Å and c = 6.901 Å for the 100Ag-400 sample) have never been evinced before. Despite the electronic contrast between Ag^+ and Ca^{2+} cations, the last Rietveld refinement cycles failed to clearly locate the silver atoms in the hydroxyapatite structure. Nevertheless, the indications obtained support the notion of a substitution mechanism at the Ca1 and Ca2 sites; the results indicate substitution rates which are too weak, but which are present (silver occupancies about 3% and 5%-instead of the expected 10 %—for the Ca1 and Ca2 sites respectively), and show the absence of chemical elements at the interstitial site within the hexagonal channel (i.e., the 2*b* Wyckoff site). This leads us to privilege the $Ca_{10-x}Ag_x(PO_4)_6(OH)_{2-x}$ stoichiometry for the doped Ag^+: HAp phase, and not that proposed by Geng et.al., $Ca_{10-x}Ag_{2x}(PO_4)_6(OH)_2$ [32], which implies a double mechanism by substitution and insertion. Our work on the structural parameters of hydroxyapatite enables us to conclude that the HAp silver-doped phase is present in our samples from 400 °C to 600 °C. This is correlated with the refined isotropic thermal parameters (see B_{iso} in Table S1, Supplementary Materials) of hydroxyl anions, which are exaggerated in these samples: 25Ag-400, 25Ag-500, 25Ag-600, 100Ag-400, 100Ag-500, and 100Ag-600. We will consider below for these temperatures that the Ag^+: HAp phase presents the nominal stoichiometry, that is to say $Ca_{9.75}Ag_{0.25}(PO_4)_6(OH)_{1.75}$ for the 25Ag-*T* series and $Ca_9Ag_1(PO_4)_6(OH)$ for the 100Ag-*T* series, although there is no definitive experimental proof for these compositions.

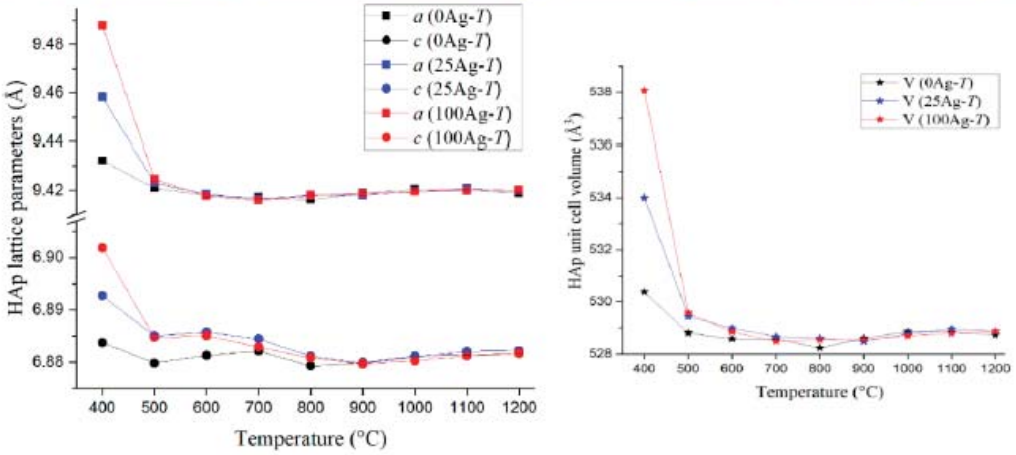

Figure 3. Thermal variation in the HAp lattice parameters for the three series of samples. **Left:** *a* (squares) and *c* (circles) hexagonal lattice parameters; **right:** unit cell volume (stars). Lines are guides for the eyes only.

3.3. .Thermal Variation in the β-TCP Structural Parameters

Thermal variations in the TCP lattice parameters, shown in Figure 4 and collated in Table S2 (Supplementary Materials), are very different from those presented above for HAp. The basal *a* lattice parameter remained constant whatever the synthesis series and heat treatment temperature. On the

other hand, variations in the axial *c* lattice parameter provide interesting information. The *c* lattice parameter—and consequently the unit cell volume-for the two silver-doped series is below the value refined for the undoped series, except for the temperature of TCP appearance (400 °C for the 25Ag-*T* series and 500 °C for the 100Ag-T series) and for the higher temperatures (1100 °C and 1200 °C). It corresponds to the formation of the ordered calcium-to-silver substitution in β-TCP that leads to the $AgCa_{10}(PO_4)_7$ compound. This compound is isotypic to β-TCP (trigonal *R*3*c* space group, 18 independent atomic positions) with its half-occupied Ca4 site (at the special 6*a* Wyckoff site [56]) fully filled by Ag^+ cations [55]. The content of the unit cell is then $Ag_6Ca_{60}(PO_4)_{42}$; i.e., $AgCa_{10}(PO_4)_7$ corresponding to $Ca_{3-x}Ag_{2x}(PO_4)_2$ with $x = 0.143$. This ordered substitution mechanism, leading to a definite compound, is accompanied by a decrease in the axial *c* lattice parameter despite the larger size of Ag^+: 37.403 Å for β-TCP [56] against 37.338 Å for $AgCa_{10}(PO_4)_7$ [55]. Thus, the value of the *c* axial lattice parameter allows us to determine whether the present TCP phase corresponds to the undoped β-TCP phase or the silver-containing $AgCa_{10}(PO_4)_7$ phase. Table S2 (Supplementary Materials) indicates the TCP phase attribution for each sample; either β-TCP (implied undoped $Ca_3(PO_4)_2$) or $AgCa_{10}(PO_4)_7$ (called Ag^+: TCP here).

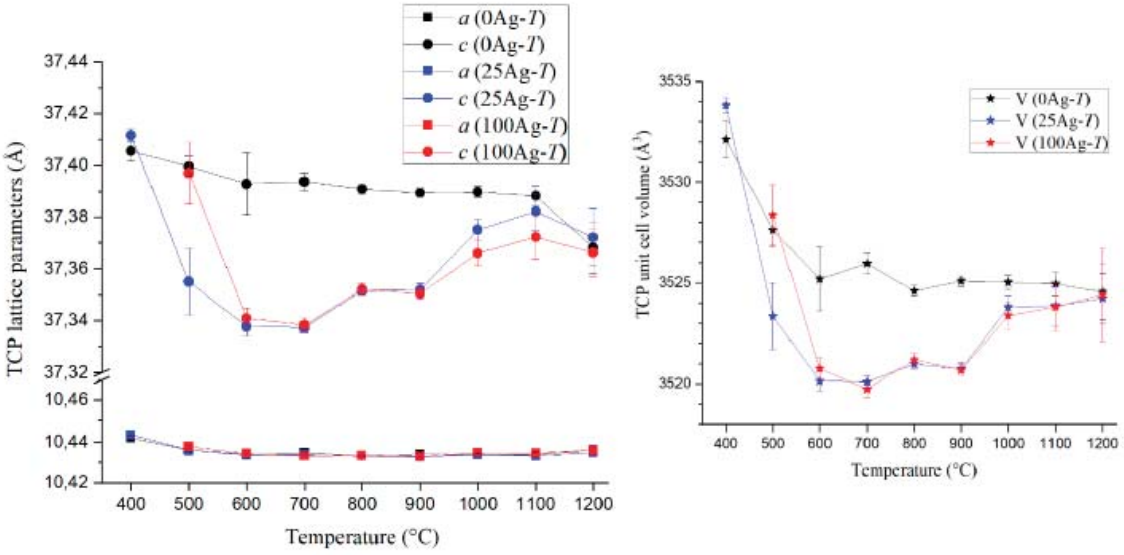

Figure 4. Thermal variation in TCP lattice parameters for the three series of samples. **Left:** *a* (squares) and *c* (circles) trigonal lattice parameters; **right:** unit cell volume (stars). Lines are guides for the eyes only.

3.4. Ag Location Studied by SEM Analyses

SEM analyses were used to evaluate the silver amount and location in selected samples from the doped series. Results from elemental quantifications made with EDS spectroscopy are summarized in Table 2. The calculated Ca/P ratio indicates that results should be considered as semi-quantitative only because of large deviations from the expected values as well as large variations within a single series. This must be connected to the unpolished surface state of the pellets and the use of internal calibration lines in the software. However, interesting additional information is provided by these analyses.

Table 2. Quantitative elemental analyses performed by EDS/SEM.

Sample	Analysis	Atomic Composition (%)			Calculated Ratio		Expected Ratio	
		Ca	Ag	P	Ag/Ca	Ca/P	Ag/Ca	Ca/P
0Ag-400	global	65.63	0.00	34.37	0.00	1.91		
0Ag-700	global	59.80	0.00	40.20	0.00	1.49	0.00	1.67
0Ag-1200	global	68.02	0.00	31.98	0.00	2.13		
25Ag-400	global	66.47	2.17	31.37	0.03	2.12	0.03	1.62

25Ag-700	global	60.14	1.43	38.43	0.02	1.56		
25Ag-1200	global	65.48	0.00	34.52	0.00	1.90		
100Ag-400	global	62.39	3.94	33.68	0.06	1.85		
100Ag-700	global	62.35	3.03	34.61	0.05	1.80	0.11	1.50
100Ag-1200	global	60.59	0.00	39.41	0.00	1.54		
25Ag-400 (*)	local_1	65.21	1.24	33.55	0.019	1.94		
	local_2	40.26	24.64	35.11	n.c. (**)	n.c.		
	local_3	7.40	89.95	2.65	n.c.	n.c.	0.03	1.62
	local_4	64.25	1.39	34.36	0.022	1.87		
25Ag-700 (*)	local_5	63.88	0.00	36.12	0.00	1.77		

(*) corresponding images are shown in Figure 6. (**) non-calculated ratio because the analyzed area did not correspond to a calcium phosphate.

First, results from Table 2 confirm the complete disappearance of silver in doped series after heat treatment at 1200 °C. We can conclude that above the melting point of silver, not only did the metallic Ag° particles leave the sample, but the calcium phosphate phases were also completely free of Ag^+ cations. The chemical contrast imaging performed with the backscattered electron detector makes it possible to highlight the notion of Ag° particles (Figure 5). The use of low magnifications shows the presence of large, micrometric particles (already present in the 25Ag-400 sample, and in large quantities in the 100Ag-700 sample). Then, thanks to higher magnifications, it is possible to visualize nanometric particles of small size. Figure 5a3 evidences the presence of silver particles of less than 100 nm diameter in 25Ag-400. These particles merged on heating to reach diameters of 200–400 nm in the 25Ag-700 sample (Figure 5b3) and 500–1000 nm in the 100Ag-700 sample (Figure 5c3). Images from Figure 5 clarify the composite feature of the samples.

Finally, local elemental analyses were performed to conclude the SEM characterization (see selected zones in Figure 6). Results from selected areas (EDS shown in Figure 7) are presented in Table 2 for the 25Ag-*T* series. These results confirm that nanoparticles were exclusively composed of silver: metallic Ag° as shown in area 3 (and also area 2) in the 25Ag-400 sample. Indeed, the results from the local zone '3' are in favor of particles containing only the silver element (the minor Ca and P contents come from the not really punctual electron beam), and therefore of a metallic nature (i.e., Ag° particles). These results also confirm the presence of silver in the phosphate calcium phases for the lowest heat treatment temperatures. Areas 1 and 4 indicate the presence of small amounts of silver, in combination with large amounts of calcium and phosphor at 400 °C, corresponding to an Ag^+:doped HAp phase. This is no longer true at 700 °C, where the calcium and phosphorus elements are completely separated from the silver element; area 5 in sample 25Ag-700 is only composed of Ca and P corresponding to undoped calcium phosphate compounds (Figure 7 and Table 2).

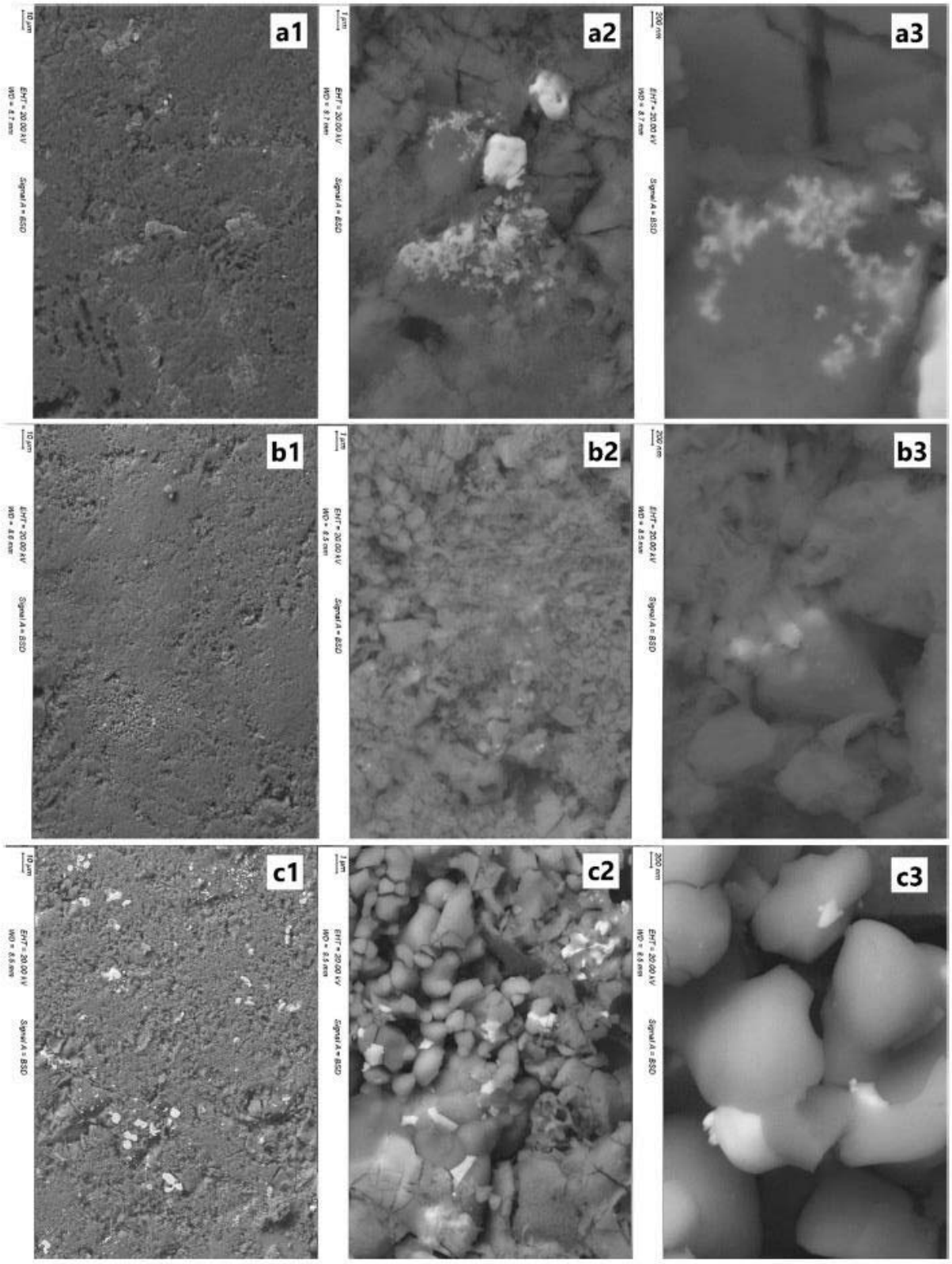

Figure 5. Electron backscattered SEM images showing the metallic silver particles in the samples. a) 25Ag-400; b) 25Ag-700, and c) 100Ag-700 samples using 1: ×500, 2: ×5000, and 3: ×20000 magnifications.

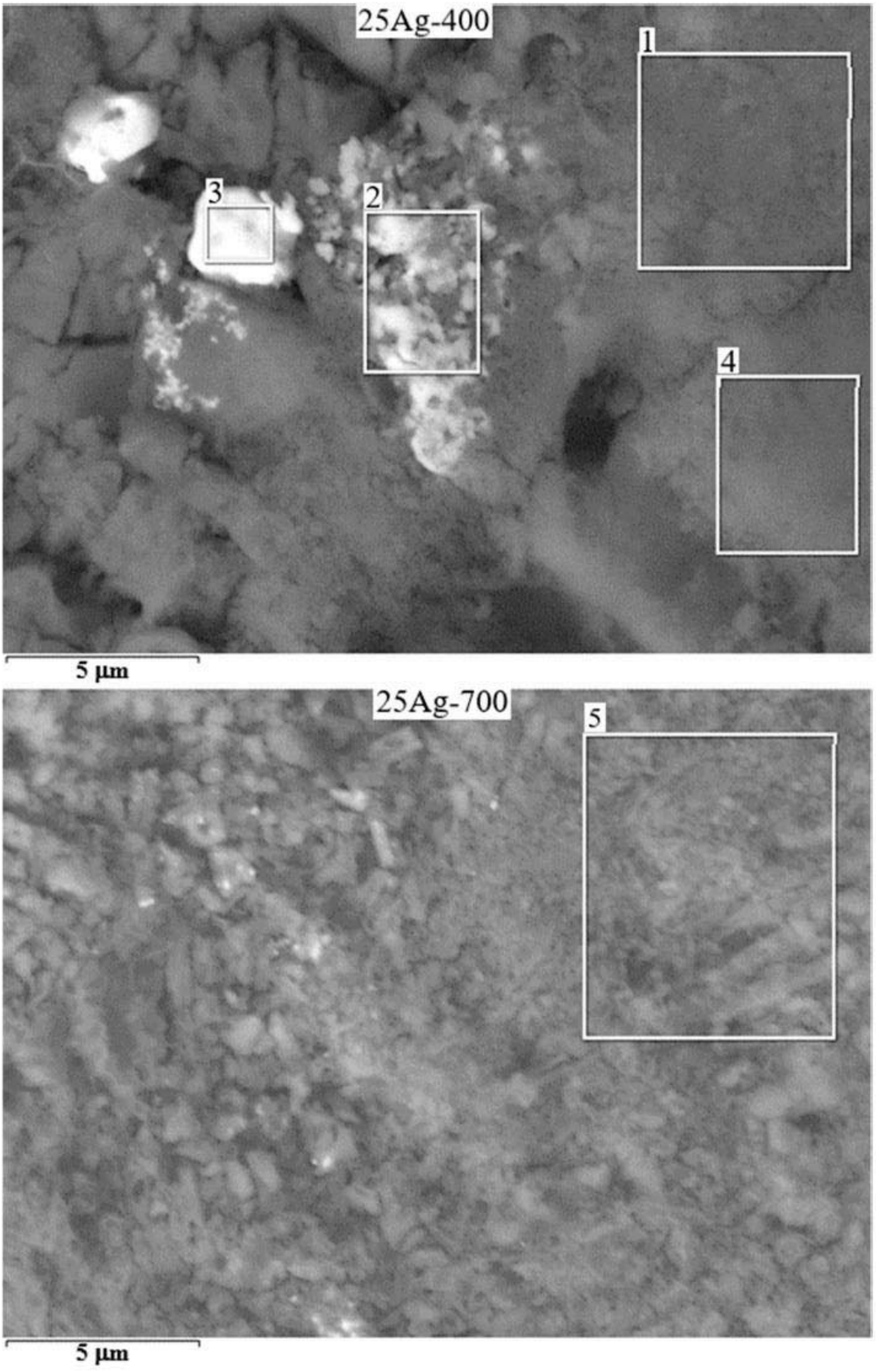

Figure 6. Electron backscattered SEM photographs used for local elemental analyses (presented in Table 2) of the 25Ag-400 and 25Ag-700 samples.

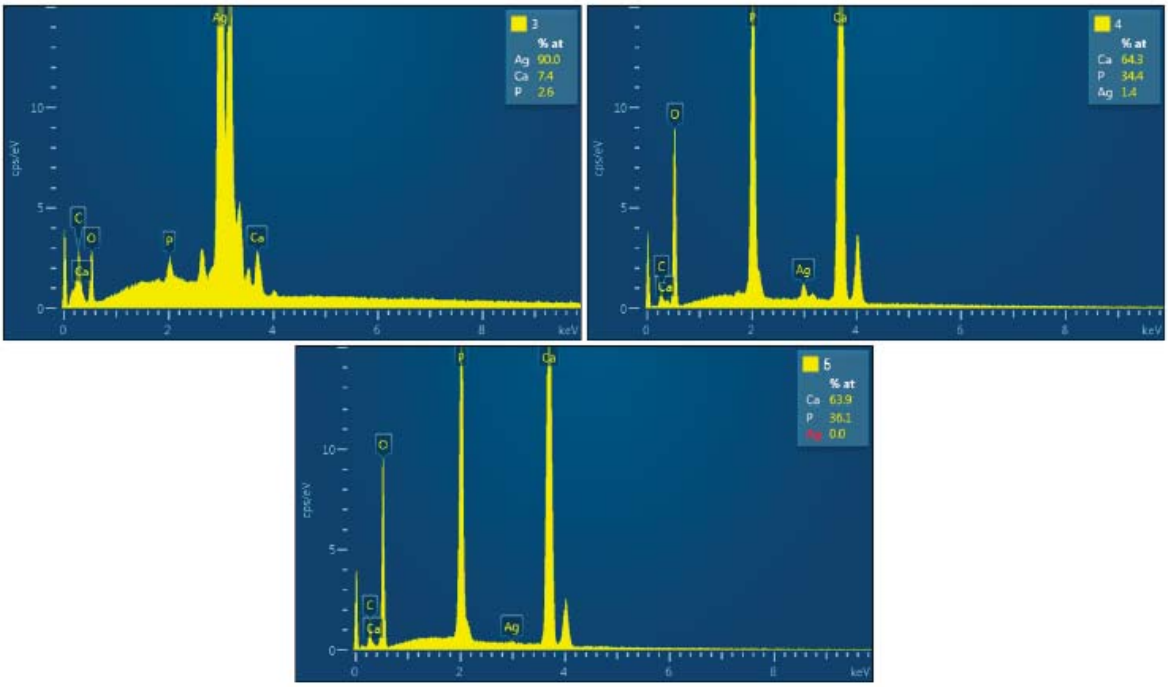

Figure 7. Selected local EDS analyses (presented in Table 2) from zones '3' and '4' of the 25Ag-400 sample and from zone '5' of the 25Ag-700 sample (shown in Figure 6).

4. Discussion

The results presented above evidence three distinct locations for silver atoms in the synthesized BCP samples, including two distinct chemical states (metallic and ionic). A part of the introduced silver cations is found in the metallic state, in the form of nanoparticles, already present at 400 °C. The remainder is in the cationic form in substitution for calcium cations, either in the HAp phase (at low temperatures: from 400 °C to 600 °C) or in the TCP phase (at the following temperatures and up to 1000 °C). From 1000 °C silver leaves the samples, especially because of the melting point of Ag° (962 °C). The cumulative amounts of located silver atoms are shown in Figure 8 for both the 25Ag-*T* and 100Ag-*T* doped series. It appears that calculations for the lowest (400 °C) temperature are in good agreement with the nominal introduced amounts (i.e., 2.67 wt % for the 25Ag-*T* series and 10.22 wt % for the 100Ag-*T* series). We then observe an overestimation of the silver content up to 600 °C, before seeing it start to plummet at 700 °C. These fluctuations around the expected values indicate that the amount of silver in the HAp phase is overestimated above 500 °C, and conversely the amount of silver in substitution in β-TCP is certainly underestimated from 800 °C upwards.

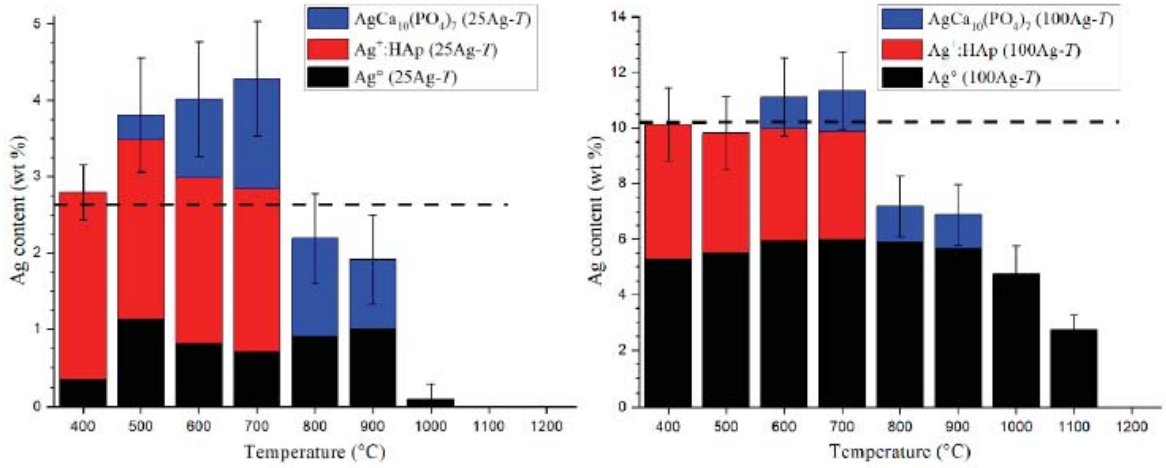

Figure 8. Cumulative silver amount taken from metallic Ag° (black), substituted HAp (red), and $AgCa_{10}(PO_4)_7$ (or substituted TCP, blue) for the 25Ag-*T* series (left) and the 100Ag-*T* series (right). Dotted lines indicate the nominal silver amounts, and error bars correspond to cumulative standard deviation considering the three phases.

Nanoparticles of metallic silver therefore formed very quickly in our samples by the autogenous reduction of silver nitrate. The set of samples can thus be considered as an Ag°/BCP composite. However, at low temperatures, we also observe the formation of a silver-doped Ag^+: HAp phase whose composition is close to the nominal composition (i.e., $Ca_{9.75}Ag_{0.25}(PO_4)_6(OH)_{1.75}$ for the 25Ag-*T* series and $Ca_9Ag_1(PO_4)_6(OH)$ for the 100Ag-*T* series). Beyond 400 °C, this doped Ag^+: HAp phase persists while gradually lowering its doping element content. The drop in the doping rate was notably predictable by observing the variations in the HAp lattice parameters between 400 °C and 700 °C (Figure 3). Both *a* and *c* lattice parameters of the Ag^+: HAp phase are vastly superior to those from the undoped series at 400 °C. This difference fades at 500 °C and disappears at 700 °C. SEM analyses confirmed the presence of dopant in the calcium phosphate phase at 400 °C, followed by its exclusion at 700°C. Concomitantly, cationic Ag^+ substitutes calcium cations into the β-TCP phase, which stabilizes around 700 °C. First, the $AgCa_{10}(PO_4)_7$ definite compound is formed; it is distinguishable from the undoped β-TCP phase thanks to the smaller *c* lattice parameter (Figure 4). The underestimation of silver content from 800 °C upwards suggests that the Ag^+ amount in the TCP phase continues to increase; however, no experimental proof has been brought to support this.

The characterization of the doped Ag^+: HAp phase with increased lattice parameters, by comparison with an undoped HAp lattice, has already been reported in the literature. This is notably the case in the study of Geng et al. [32], where the $Ca_{10-x}Ag_{2x}(PO_4)_6(OH)_2$ doped composition was considered. This nominal composition suggests two kinds of doping mechanisms: only half of the silver cations (*x* value) can substitute calcium cations into the Ca1 or Ca2 crystallographic sites of the HAp crystal structure. The second half of silver cations (to reach the 2*x* doping level) must be located at interstitial sites. Our crystallographic study, based on Rietveld refinement, did not enable us to highlight the presence of silver cations at interstitial crystallographic sites, not to mention that this situation is not preponderant for large cations like Ag^+. For these reasons we preferred to note the chemical composition of the doped Ag^+: HAp phase as follows: $Ca_{10-x}Ag_x(PO_4)_6(OH)_{2-x}$, in which only the substitution mechanism was considered in agreement with the paper by Badrour et al. [61]. However, we must admit that our Rietveld refinements did not make it possible to clearly quantify the silver substitution rates at both the Ca1 and Ca2 crystallographic sites in the HAp structure.

5. Conclusion

During the past decade, several studies have been devoted to silver incorporation in HAp (or BCP) samples due to their high potential for biomaterial applications, namely because of the well-known bactericide properties of silver. Unanimously, the results have shown a very interesting bactericidal effect following the doping of calcium phosphates with silver. However, the material aspect of the samples studied in the literature showed some disparities, in particular due to a lack of understanding of the doping mechanism. Some works mention metallic silver nanoparticles; others focus on cationic substitution in phosphate phases. The results presented in the present paper are especially devoted to the description of the mechanism by which silver is incorporated into BCP samples. This work follows the experience previously acquired on the BCP doping mechanism of the first-row transition elements. It appears that both electronic states are simultaneously present in the silver-doped samples: metallic Ag° and cationic Ag^+. Synthesized samples are composites comprising closely-mixed Ag° nanoparticles and Ag^+: doped calcium phosphate phases. At the lowest temperature (400 °C), it is the HAp phase which presents a silver-to-calcium substitution leading to the doped $Ca_{10-x}Ag_x(PO_4)_6(OH)_{2-x}$ compounds. Then, by increasing the temperature (above 600 °C) the Ag^+ cations migrate to the β-TCP phase to form the definite $Ca_{10}Ag(PO_4)_7$ compound corresponding to $Ca_{3-x}Ag_{2x}(PO_4)_2$ with $x = 0.143$ (i.e., $Ca_{2.857}Ag_{0.286}(PO_4)_2$). Finally, the composite aspect of the prepared samples disappears above 1000 °C because of the relatively low melting point of silver (962 °C). In

the light of these results, it appears important for the study of biological properties to distinguish the behavior in biological conditions of metallic silver nanoparticles from that of substituted cationic Ag^{+}, particularly in terms of bactericidal power and release rate/kinetics in the human body.

Supplementary Materials: The following are available online at www.mdpi.com/xxx/s1, Figure S1: Rietveld plot (conventional Rietveld agreement factors: Rp = 0.048, Rwp = 0.053, χ^2 = 2.26) of the powder pattern of the 25Ag-600 sample with experimental data (red circles), simulated pattern (black line), difference curve (blue line) and Bragg peak position for the six phases present: HAp, Ag^{0}, β-TCP, CDP, CaO and $CaCO_3$. Table S1: HAp structural parameters refined by Rietveld analyses on the 27 samples; standard deviations are indicated in brackets. Table S2: TCP lattice parameters refined by Rietveld analyses on the 27 samples; standard deviations are indicated in brackets.

Author Contributions: conceptualization, G.R. and A.J.; methodology, G.R. and A.J.; software, G.R. and A.J.; validation, G.R. and A.J.; formal analysis, G.R., A.J., M.G. and A.D.; investigation, G.R., A.J., M.G. and A.D.; resources, G.R., A.J., M.G. and A.D.; data curation, G.R., A.J., M.G. and A.D.; writing-original draft preparation, G.R.; writing—review and editing, G.R.; visualization, G.R.; supervision, G.R.; project administration, G.R.", please turn to the CRediT taxonomy for the term explanation.

Acknowledgments: The authors warmly thank Anne-Marie Gelineau for the electron microscopy performed at 2MATech–Clermont-Ferrand, a few days before her retirement. Reviewers and guest editor, Francesco Capitelli, are also grateful for their questions and comments that have improved the content and understanding if this paper.

Conflicts of Interest: The authors declare no conflict of interest.

References

1. Dorozhkin, S.V. Biocomposites and hybrid biomaterials based on calcium orthophosphates. *Biomaterials* **2011**, *1*, 3–56.
2. Dahl, S.G.; Allain, P.; Marie, P.J.; Mauras, Y.; Boivin, G.; Ammann, P.; Tsouderos, Y.; Delmas, P.D.; Christiansen, C. Incorporation and distribution of strontium in bone. *Bone* **2001**, *8*, 446–453.
3. Lagier, R.; Baud, C.A. Magnesium whitlockite, a calcium phosphate crystal of special interest in pathology. *Pathol. Res. Pract.* **2003**, *199*, 329–335.
4. Lee, R.S.; Kayser, M.V.; Ali, S.Y. Calcium phosphate microcrystal deposition in the human intervertebral disc. *J. Anat.* **2006**, *208*, 13–19.
5. Rey, C.; Combes, C.; Drouet, C.; Glimcher, M.J. Bone mineral: Update on chemical composition and structure. *Osteoporos. Int.* **2009**, *20*, 1013–1021.
6. Cazalbou, S.; Combes, C.; Eichert, D.; Rey, C. Adaptative physico-*chemistry* of bio-related calcium phosphates. *J. Mater. Chem.* **2004**, *14*, 2148–2153.
7. Elliot, J.C. *Structure and Chemistry of the Apatite and Other Calcium Orthophosphates*; Elsevier: Amsterdam, The Netherlands, 1994.
8. Turkoz, M.; Atilla, A.O.; Evis, Z. Silver and fluoride doped hydroxyapatite: Investigation by microstructure, mechanical and antibacterial properties. *Ceram. Int.* **2013**, *39*, 8925–8931.
9. Diaz, M.; Zia, R.; Sameemi, F.; Ikram, H.; Bashir, F. In vitro antimicrobial activity of ZnO based glass-ceramics against pathogenic bacteria. *J. Mater. Sci. Mater. Med.* **2015**, *26*, 268.
10. Khan, M.S.; ur Rehman, S.; Ali, M.A.; Sultan, B.; Sultan, S. Infection in orthopedic implant surgery, its risk factors and outcome. *J. Ayub Med. Coll. Abbottabad* **2008**, *20*, 23–25.
11. Cremet, L.; Corvec, S.; Bemer, P.; Bret, L.; Lebrun, C.; Lesimple, B.; Miegeville, A.F.; Reynaud, A.; Lepelletier, D.; Caroff, N. Orthopaedic-implant infection by Escherichia coli: Molecular and phenotypic analysis of the causative strains. *J. Infect.* **2012**, *64*, 169–175.
12. Salwiczek, M.; Qu, Y.; Gardiner, J.; Strugnell, R.A.; Lithgow, T.; McLean, K.M.; Thissen, H. Emerging rules for effective antimicrobial coatings. *Trends Biotechnol.* **2014**, *32*, 82–90.
13. Nasser, S. Prevention and treatment of sepsis in total hip replacement surgery. *Orthop. Clin. N. Am.* **1992**, *23*, 265–277.
14. Li, P.L.; Zamora, J.; Bentley, G. The results at ten years of the Insall-Burstein II total knee replacement: Clinical, radiological and survivorship studies. *J. Bone Joint Surg. Br.* **1999**, *81*, 647–653.

15. Hendriks, J.G.E.; van Horn, J.R.; van der Mei, H.C.; Busscher, H.J. Background of antibiotic-loaded bone cement and prosthesis-related infection. *Biomaterials* **2004**, *25*, 545–556.
16. Fan, J.C.H.; Hung, H.H.; Fung, K.Y. Infection in primary total knee replacement. *Hong Kong Med. J.* **2008**, *14*, 40–45.
17. Sygnatowicz, M.; Keyshar, K.; Tiwari, A. Antimicrobial properties of silver-doped hydroxyapatite nano-powders and thin films. *Biol. Biomed. Mater.* **2010**, *62*, 65–70.
18. Rauschmann, M.A.; Wichelhaus, T.A.; Stirnal, V.; Dingeldein, E.; Zichner, L.; Schnettler, R.; Alt, V. Nanocrystalline hydroxyapatite and calcium sulphate as biodegradable composite carrier material for local delivery of antibiotic in bone infections. *Biomaterials* **2005**, *26*, 2677–2684.
19. Baradari, H.; Damia, C.; Dutreih-Colas, M.; Laborde, E.; Pecout, N.; Champion, E.; Chulia, D.; Viana, M. Calcium phosphate porous pellets as drug delivery systems: Effect of drug carrier composition on drug loading and in vitro release. *J. Eur. Ceram. Soc.* **2012**, *32*, 2679–2690.
20. Clement, J.L.; Jarrett, P.S. Antibacterial silver. *Metal. Based Drugs* **1994**, *1*, 467–482.
21. Marambio-Jones, C.; Hoek, E.M.V. A review of the antibacterial effects of silver nanomaterials and potential implications for human health and the environment. *J. Nano Res.* **2010**, *12*, 1531–1551.
22. Iqbal, N.; Kadir, A.R.M.; Malek, N.N.A.N.; Mahmood, H.N.; Murali, R.M.; Kamarul, T. Rapid microwave assisted synthesis and characterization of nanosized silver-doped hydroxyapatite with antibacterial properties. *Mater. Lett.* **2012**, *89*, 118–122.
23. Ning, C.; Wang, X.; Li, L.; Zhu, Y.; Li, M.; Yu, P.; Zhou, L.; Zhou, Z.; Chen, J.; Tan, G.; et al. Concentration ranges of antibacterial cations for showing the highest antibacterial efficacy but the least cytotoxicity against mammalian cells: Implications for a new antibacterial mechanism. *Chem. Res. Toxicol.* **2015**, *28*, 1815–1822.
24. Kim, T.N.; Feng, Q.L.; Kim, J.O.; Wu, J.; Wang, H.; Chen, G.C.; Cui, F.Z. Antimicrobial effects of metal ions (Ag^{+}, Cu^{2+}, Zn^{2+}) in hydroxyapatite. *J. Mater. Sci. Mater. Med.* **1998**, *8*, 129–134.
25. Feng, Q.L.; Wu, J.; Chen, G.Q.; Cui, F.Z.; Kim, T.N. A mechanistic study of the antibacterial effect of silver ions on Escherichia coli and staphylococcus aureus. *J. Biomed. Mater. Res.* **2000**, *52*, 662–668.
26. Rameshbabu, N.; Sampath Kumar, T.S.; Prabhakar, T.G.; Sastry, V.S.; Murty, K.V.G.K.; Prasad Rao, K. Antibacterial nanosized silver substituted hydroxyapatite: Synthesis and characterization. *J. Biomed. Mater. Res. A* **2007**, *80*, 581–591.
27. Klasen, H.J. Historical review of the use of silver in the treatment of burns: I. Early uses. *Burns* **2000**, *26*, 117–130.
28. Gosheger, G.; Hardes, J.; Ahrens, H.; Streitburger, A.; Buerger, H.; Erren, M.; Gunsel, A.; Kemper, F.H.; Winkelmann, W.; von Eiff, C. Silver-coated megaendoprostheses in a rabbit model—an analysis of the infection rate and toxicological side effects. *Biomaterials* **2004**, *25*, 5547–5556.
29. Ciobanu, C.S.; Iconaru, S.L.; Pasuk, I.; Vasile, B.S.; Lupu, A.R.; Hermenean, A.; Dinischiotu, A.; Predoi, D. Structural properties of silver doped hydroxyapatite and their biocompatibility. *Mater. Sci. Eng. C* **2013**, *33*, 1395–1402.
30. Jadalannagari, S.; Deshmukh, K.; Ramanan, S.R.; Kowshik, M. Antimicrobial activity of hemocompatible silver doped hydroxyapatite nanoparticles synthesized by modified sol-gel technique. *Appl. Nanosci.* **2014**, *4*, 133–141.
31. Fu, C.; Zhang, X.; Savino, K.; Gabrys, P.; Gao, Y.; Chaimayo, W.; Miller, B.L.; Yates, M.Z. Antimicrobial silver-hydroxyapatite composite coating through two-stage electrochemical synthesis. *Surf. Coat. Technol.* **2016**, *301*, 13–19.
32. Geng, Z.; Cui, Z.; Li, Z.; Zhu, S.; Liang, Y.; Liu, Y.; He, X.; Yu, X.; Wang, R.; Yang, W. Strontium incorporation to optimize the antibacterial and biological characteristics of silver-substituted hydroxyapatite coating. *Mater. Sci. Eng. C* **2016**, *58*, 467–477.
33. Gokcekaya, O.; Webster, T.J.; Ueda, K.; Narushima, T.; Ergun, C. In vitro performance of Ag-incorporated hydroxyapatite and its adhesive porous coating deposited by electrostatic spaying. *Mater. Sci. Eng. C* **2017**, *77*, 556–564.
34. Wang, J.; Gong, X.; Hai, J.; Li, T. Synthesis of silver-hydroxyapatite composite with improved antibacterial properties. *Vacuum* **2018**, *152*, 132–137.
35. Riaz, M.; Zia, R.; Ijaz, A.; Hussain, T.; Mohsin, M.; Malik, A. Synthesis of monophasic Ag doped hydroxyapatite and evaluation of antibacterial activity. *Mater. Sci. Eng. C* **2018**, *90*, 308–313.

36. Dubnika, A.; Loca, D.; Rudovica, V.; Parekh, M.B.; Berzina-Cimdina, L. Functionalized silver-doped hydroxyapatite scaffolds for controlled simultaneous silver ion and drug delivery. *Ceram. Int.* **2017**, *43*, 3698–3705.
37. Zhang, X.; Chaimayo, W.; Yang, C.; Yao, J.; Miller, B.L.; Yates, M.Z. Silver-hydroxyapatite composite coatings with enhances antimicrobial activities through heat treatment. *Surf. Coat. Technol.* **2017**, *325*, 39–45.
38. Gokcekaya, O.; Ueda, K.; Narushima, T.; Ergun, C. Synthesis and characterization of Ag-containing calcium phosphates with various Ca/P ratios. *Mater. Sci. Eng. C* **2015**, *53*, 111–119.
39. Iqbal, N.; Kadir, M.R.A.; Mahmood, N.H.; Salim, N.; Froemming, G.R.A.; Balaji, H.R.; Kamarul, T. Characterization, antibacterial and in-vitro compatibility of zinc-silver doped hydroxyapatite nanoparticles prepared through microwave synthesis. *Ceram. Int.* **2014**, *40*, 4507–4513.
40. Kaygili, O.; Keser, S.; Dorozhkin, S.V.; Yakuphanoglu, F.; al-Ghamdi, A.A.; Kirbag, S.; Sertkaya, D.; Ates, T.; Gursoy, N.C. Structural and dielectrical properties of Ag- and Ba-substituted hydroxyapatites. *J. Inorg. Organomet. Polym.* **2014**, *24*, 1001–1008.
41. Liu, X.; Mou, Y.; Wu, S.; Man, H.C. Synthesis of silver-incorporated hydroxyapatite nanocomposites for antimicrobial implant coatings. *Appl. Surf. Sci.* **2013**, *273*, 748–757.
42. Chen, Y.; Zheng, X.; Xie, Y.; Ji, H.; Ding, C.; Li, H.; Dai, K. Silver release from silver-containing hydroxyapatite coatings. *Surf. Coat. Technol.* **2010**, *205*, 1892–1896.
43. Chen, W.; Oh, S.; Ong, A.P.; Oh, N.; Liu, Y.; Courtney, H.S.; Appleford, M.; Ong, J.L. Antibacterial and osteogenic properties of silver-containing hydroxyapatite coatings produced using sol-gel process. *J. Biomed. Mater. Res. A* **2007**, *82*, 899–906.
44. Vukomanovic, M.; Bracko, I.; Poljansek, I.; Uskokovic, D.; Skapin, S.D.; Suvorov, D. The growth of silver nanoparticles and their combination with hydroxyapatite to form composites via a sonochemical approach. *Cryst. Growth Des.* **2011**, *11*, 3802–3812.
45. Chen, W.; Liu, Y.; Courtney, H.S.; Bettenga, M.; Agrawal, C.M.; Bumgardner, J.D.; Ong, J.L. In vitro anti-bacterial and biological properties of magnetron co-sputtered silver-containing hydroxyapatite coating. *Biomaterials* **2006**, *27*, 5512–5517.
46. Feng, Q.L.; Kim, T.N.; Wu, J.; Park, E.S.; Kim, J.O.; Lim, D.Y.; Cui, F.Z. Antibacterial effects of Ag-HAp thin films on alumina substrates. *Thin Solid Films* **1998**, *335*, 214–219.
47. Shirkhanzadeh, M.; Azadegan, M.; Liu, G.Q. Bioactive delivery systems for the slow release of antibiotics: Incorporation of Ag^{+} ions into micro-porous hydroxyapatite coatings. *Mater. Lett.* **1995**, *24*, 7–12.
48. Renaudin, G.; Gomes, S.; Nedelec, J.-M. First-row transition metal doping in calcium phosphate bioceramics: A detailed crystallographic study. *Materials* **2017**, *10*, 92–113.
49. Gomes, S.; Nedelec, J.-M.; Renaudin, G. On the effect of temperature on the insertion of zinc into hydroxyapatite. *Acta Biomater.* **2012**, *8*, 1180–1189.
50. Gomes, S.; Kaur, A.; Nedelec, J.-M.; Renaudin, G. X-ray Absorption Spectroscopy shining (synchrotron) light onto the insertion of Zn^{2+} in calcium phosphate ceramics and its influence on their behaviour in biological conditions. *J. Mater. Chem. B* **2014**, *2*, 536–545.
51. Gomes, S.; Nedelec, J.-M.; Jallot, E.; Sheptyakov, D.; Renaudin, G. Unexpected mechanism of Zn^{2+} insertion in calcium phosphate bioceramics. *Chem. Mat.* **2011**, *23*, 3072–3085.
52. Gomes, S.; Kaur, A.; Grenèche, J.-M.; Nedelec, J.-M.; Renaudin, G. Atomic scale modeling of iron-doped biphasic calcium phosphate bioceramics. *Acta Biomater.* **2017**, *50*, 78–88.
53. Gomes, S.; Vichery, C.; Descamps, S.; Martinez, H.; Kaur, A.; Jacobs, A.; Nedelec, J.-M.; Renaudin, G. Cu-doping of calcium phosphate bioceramics: From mechanism to the control of cytotoxicity. *Acta Biomater.* **2018**, *65*, 462–474.

54. Rodriguez-Carvajal, J. *PROGRAM FullProf.2k—Version 3.20*; Laboratoire Léon Brillouin (CEA-CNRS): Saclay, France, 2005; FullProf.2k Manual. Available online http://www-llb.cea.fr/fullweb/fp2k/fp2k_divers.htm (accessed on 24 June 2019).
55. Strutynska, N.Y.; Zatovsky, I.V.; Ogorodnyk, I.V.; Slobodyanik, N.S. Rietveld refinement of $AgCa_{10}(PO_4)_7$ from X-ray powder data. *Acta Cryst. E* **2013**, *69*, i23.
56. Yashima, M.; Sakai, A.; Kamiyama, T.; Hoshikawa, A. Crystal structure analysis of beta-tricalcium phosphate $Ca_3(PO_4)_2$ by neutron powder diffraction. *J. Sol. State Chem.* **2003**, *175*, 272–277.
57. Owen, E.A.; Yates, E.L. Precision measurement of crystal parameters. *Philos. Mag.* **1933**, *15*, 472–488.
58. Mocanu, A.; Furtos, G.; Rapuntean, S.; Horovitz, O.; Flore, C.; Garbo, C.; Danisteanu, A.; Rapuntean, G.; Prejmerean, C.; Tomoaia-Cotisel, M. Synthesis; characterization and antimicrobial effects of composites based on multi-substituted hydroxyapatite and silver nanoparticles. *Appl. Surf. Sci.* **2014**, *298*, 225–235.
59. Singh, B.; Dubey, A.K.; Kumar, S.; Saha, N.; Basu, B.; Gupta, R. In vitro biocompatibility and antimicrobial activity of wet chemically prepared $Ca_{10-x}Ag_x(PO_4)_6(OH)_2$ ($0.0 \leq x \leq 0.5$) hydroxyapatites. *Mater. Sci. Eng. C* **2011**, *31*, 1320–1329.
60. Shannon, R.D. Revised effective ionic radii and systematic studies of interatomic distances in halides and chalcogenides. *Acta Cryst. A* **1976**, *32*, 751–767.
61. Badrour, L.; Sadel, A.; Zahir, M.; Kimakh, L.; el Hajbi, A. Synthesis and physical and chemical characterization of Ca10-xAgx(PO4)6(OH)2-x□x apatites. *Ann. Chim. Sci. Mat.* **1998**, *23*, 61–64.

2.4. Dopage à l'or

2.4.1. Synthèse

Des BCP dopés à l'or ont été synthétisés en suivant le même protocole que celui cité précédemment en utilisant cette fois-ci de l'hydroxyde d'or $Au(OH)_3$ (Sigma Aldrich) en quantité appropriée suivant le taux de dopage souhaité. Un mécanisme de substitution a été envisagé comme pour l'argent, soit $Ca_{10-x}Au_x(PO_4)_6(OH)_{2-x}O_x$. Pour cela un taux de dopage de x = 0,25 a été utilisé lors de la synthèse donc avec des matériaux dont la composition visée était : $Ca_{9,75}Au_{0,25}(PO_4)_6(OH)_{1,75}O_{0.25}$.

Au cours de la synthèse des difficultés ont été rencontrées lors de la dissolution de la poudre d'$Au(OH)_3$ dans l'éthanol absolu. Il a été difficile de mettre en solution toute la poudre pesée et des résidus (provenant de la réduction de Au^{3+} en Au° en milieu alcoolique) n'ont pas pu être ajoutés pour la suite de la synthèse (**Figure 2.3**), faussant fortement la stœchiométrie visée.

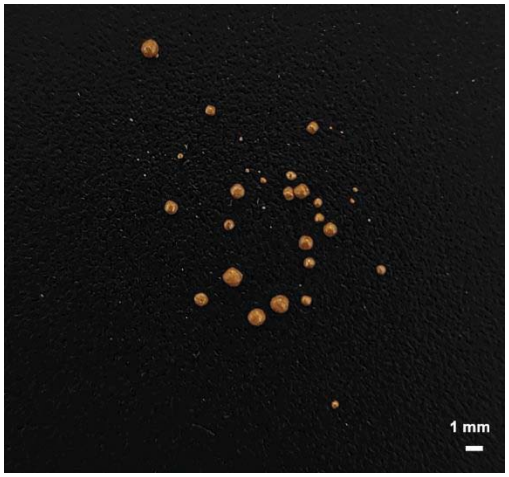

Figure 2.3 : Résidus d'Au° précipité dans l'éthanol absolu.

Concernant les traitements thermiques réalisés, les poudres dopées à l'or obtenues ont subi différents recuits : 400°C, 600°C, 800°C, 1000°C et 1200°C, pouvant être comparés à l'étude précédente (**Figure 2.4**).

Figure 2.4 : Poudres de phosphates de calcium dopées à l'or et les différents traitements thermiques ; 25Au-*T*.

2.4.2. Caractérisation

Les diffractogrammes obtenus sont présentés **Figure 2.5**. Les matériaux sont cristallisés dès le recuit à 400°C et la cristallinité augmente avec la température de recuit. Les échantillons sont principalement composés d'HAp et ne sont jamais monophasés. Les **figure 2.5** et **2.6** permettent d'observer les phases cristallines présentent dans les échantillons aux différentes températures de recuit. L'HAp est toujours majoritaire (#). Les particules d'or métallique (*) sont présentes pour les températures de recuits allant jusqu'à 1000°C. La calcite ($) est présente à 400°C et se décarbonate progressivement en CaO (°) avec la montée en température. Les phosphates tricalciques sont également observés à partir de 600°C sous la forme β-TCP (%), puis sous la forme α-TCP (£) à 1200°C.

Les résultats de l'analyse quantitative sont présentés dans le **tableau 2.2** et sur la **figure 2.7**. La phase HAp est très majoritaire pour tous les échantillons avec un % massique >90%, sauf pour la température intermédiaire de 800°C où elle est légèrement inférieure (85%). La phase β-TCP est retrouvée jusqu'à 600°C, puis se transforme en α-TCP aux températures supérieures. Il faut noter en plus des phases classiques retrouvées, la présence relativement importante de calcite puis de CaO, qui mettent en évidence un excès de calcium et donc un ratio Ca/P trop élevé. Cela peut être expliqué par les difficultés de mises en solution de $Au(OH)_3$ et donc les modifications des rapports molaires initialement calculés.

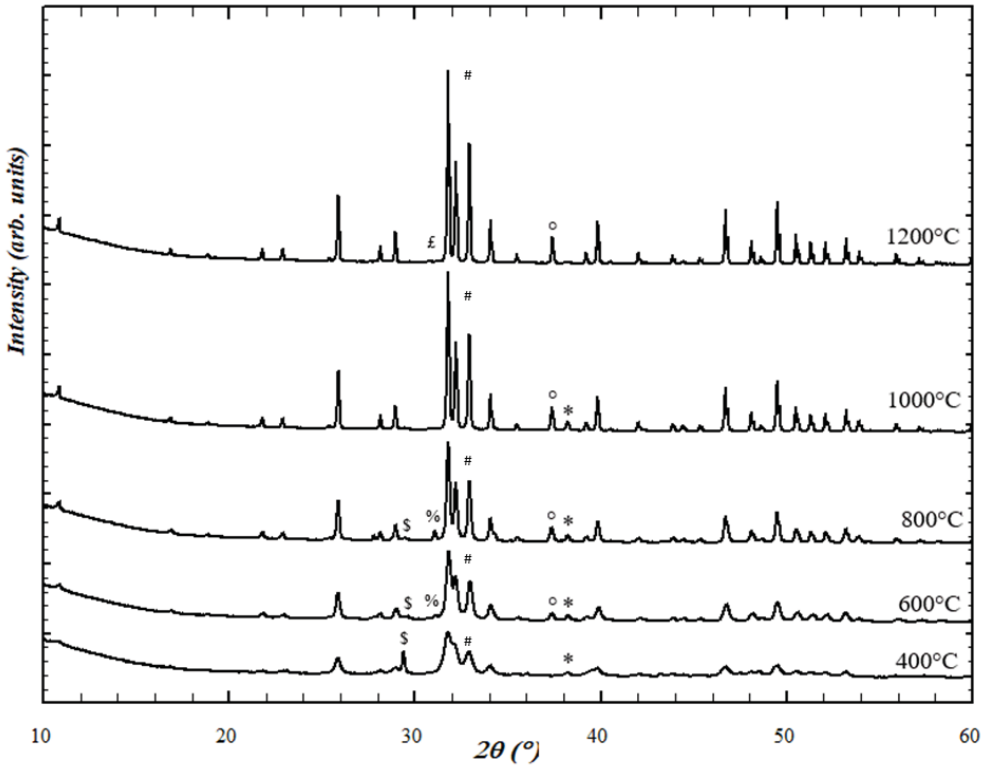

Figure 2.5 : Diffractogrammes des échantillons de BCP dopés à l'or aux différentes températures de recuit et identification des phases cristallines présentes. Les phases retrouvées sont : HAp (#), or métallique (*), calcite ($), CaO (°), β-TCP (%) et α-TCP (£).

Tableau 2.2 : Analyse quantitative des phases présentes dans les BCP dopés à l'or aux différentes températures de recuit (% massique arrondi à l'unité).

Température (°C)	HAp	Au°	$CaCO_3$	CaO	β-TCP	α-TCP
400	91	<1	9	-	-	-
600	91	<1	3	3	3	-
800	85	<1	2	4	8	-
1000	93	<1	-	5	1	<1
1200	93	<1	-	5	-	2

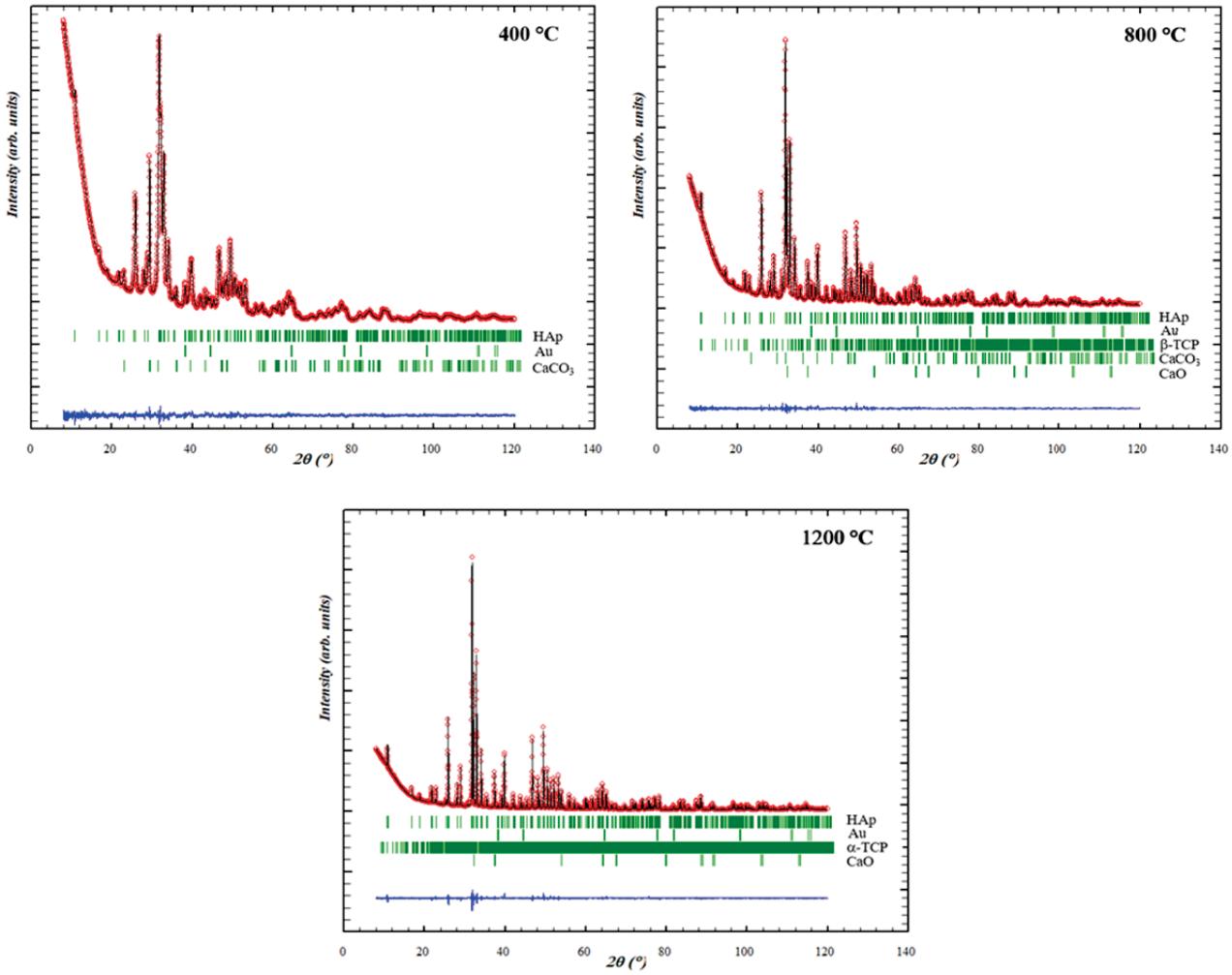

Figure 2.6 : Tracés Rietveld des matériaux recuits à 400°C, 800°C et 1200°C et identifications des phases. Les points rouges représentent les données expérimentales, les lignes noires correspondent aux diffractogrammes simulés, les lignes bleues traduisent la courbe de différence entre expérimentation et modélisation et les traits verts indiquent les positions des pics de diffraction des différentes phases présentes.

L'or métallique est clairement observable sur les diffractogrammes **Figures 2.5** et **2.6**, cependant les quantités calculées sont très faibles : de l'ordre de 0,5 % massique. Cela peut s'expliquer, à nouveau, par les difficultés pour passer en solution l'hydroxyde d'or en début de synthèse, ainsi les quantités d'or introduites dans le matériau sont largement inférieures à celles souhaitées initialement. A 1200°C seulement 0,1% massique d'or sont retrouvées, cette diminution est à relier avec la température de fusion de l'or de 1064°C.

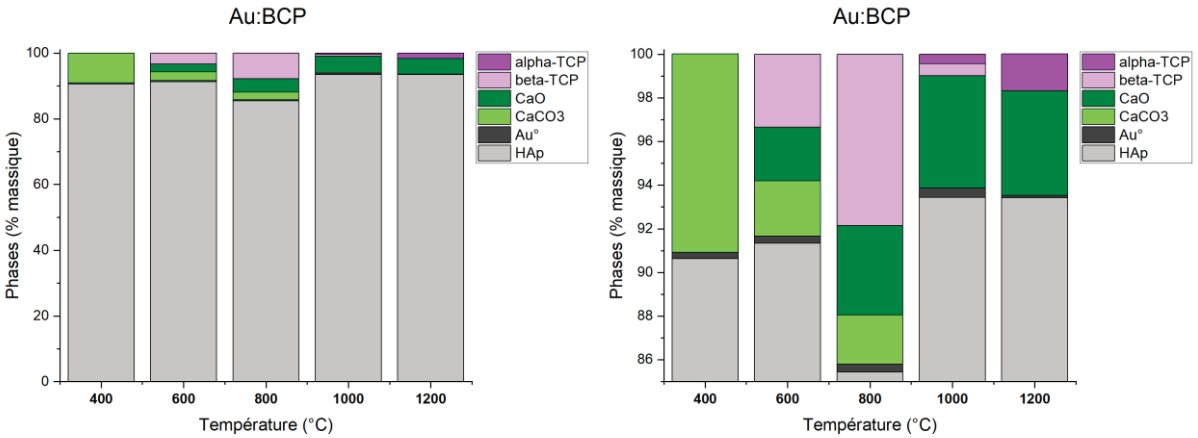

Figure 2.7 : Représentation quantitative des phases présentes dans les BCP dopés à l'or aux différentes températures de recuit (% massique). La Figure de droite est un zoom de la Figure de gauche sur les phases mineures.

2.4.3. Localisation de l'or dans les matériaux

Les quantités d'or métalliques observées dans les échantillons ne correspondent pas à la quantité introduite lors de la synthèse ; à savoir 4.72% massique (**Figure 2.8**). Bien que l'intégralité de l'hydroxyde d'or n'ait pas été introduite pendant la synthèse il est nécessaire d'estimer si de l'or cationique est localisé dans les phases HAp et/ou β-TCP.

Lors des affinements Rietveld, aucun atome d'or en substitution n'a pu être mis en évidence sur les sites de calcium Ca1 et Ca2 de l'HAp. Dans le cas du dopage à l'Ag une augmentation des paramètres de maille de l'HAp aux basses températures indiquait très certainement une incorporation de cations Ag^{+} en substitution de cations Ca^{2+} (en accord avec les rayons ioniques respectifs). Dans le cas du dopage à l'or, cette augmentation n'est pas mise en évidence puisque les paramètres de maille de l'HAp restent très proches de ceux retrouvés sans dopage (**Figure 2.9**). La phase Au:HAp (HAp dopée à l'or) ne semble pas être présente.

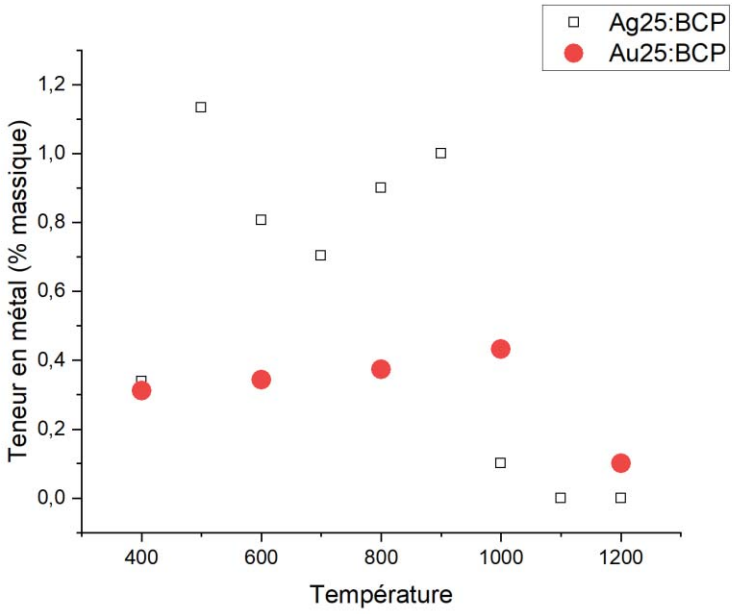

Figure 2.8 : Quantité d'or métallique retrouvée dans les BCP dopés aux différentes températures (% massique) ; comparaison avec les quantités d'argent métallique d'une des séries précédente (25Ag-*T*).

A) B)

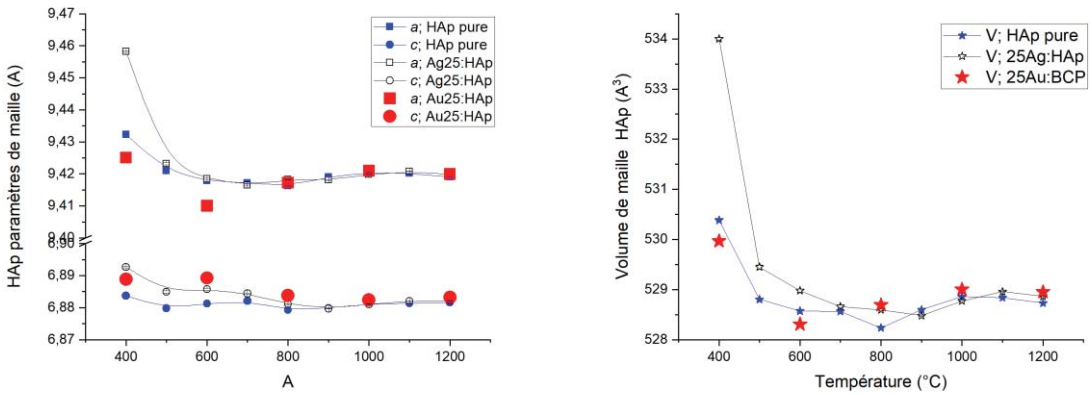

Figure 2.9 : Evolutions des paramètres de maille de l'HAp aux différentes températures de recuit (25Au-*T*, 25Ag-*T* et non dopés) : A) Evolutions des paramètres *a* et *c*. B) Evolution du volume de maille.

Concernant la phase β-TCP, une contraction marquée du paramètre de maille *c* est observée et est encore plus marquée que celle retrouvée pour le dopage à l'argent. Une légère augmentation du paramètre de maille *a* est aussi observée (**Figure 2.10**). Ces 2 évolutions en sens inverses font qu'aucun effet n'est alors visible sur le volume de maille *V*, contrairement au cas du dopage à l'Ag. Cependant, l'échantillon traité à 800°C contenant de l'ordre de 8% massique de β-TCP permet d'avoir une précision largement suffisante pour confirmer les effets antagonistes décrit précédemment sur les paramètres de maille *a* et *c* (**Figure 2.11**). Par conséquent, ces analyses permettent de conclure sur la très probable incorporation d'atome d'Au en substitution sur des sites de calcium de la phase β-TCP : $Ca_{3-3x}Au_{2x}(PO_4)_2$, en considérant la substitution des cations Ca^{2+} par des cations Au^{3+} correspondant au degré d'oxydation de l'ion aurique utilisé lors de la synthèse. Dans la littérature aucun composé correspondant à une phase β-TCP dopée à l'Au n'a été décrite jusqu'à présent.

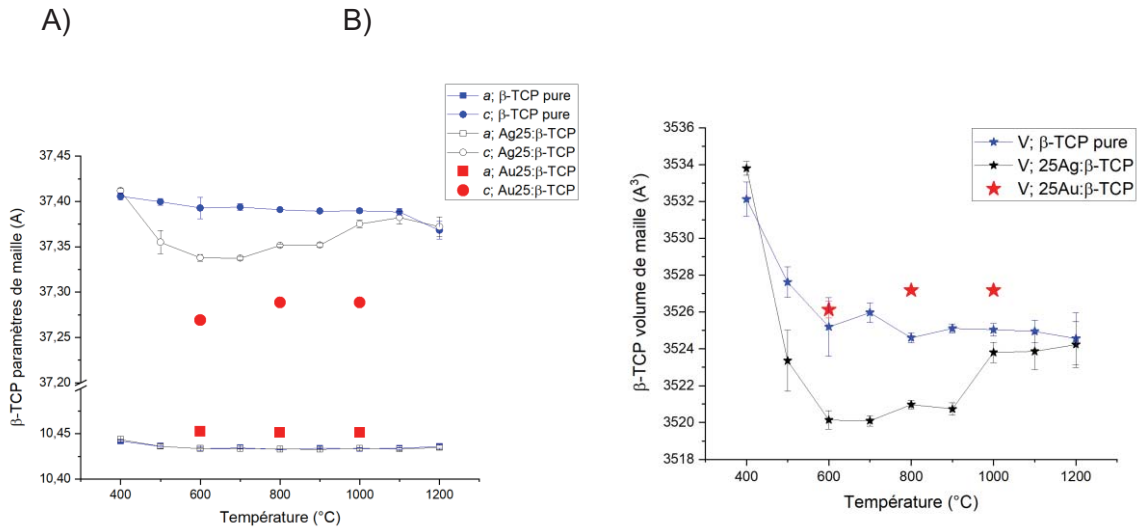

Figure 2.10 : Evolutions des paramètres de maille de la phase β-TCP aux différentes températures de recuit (25Au-*T*, 25Ag-*T* et non dopés) : A) Evolutions des paramètres *a* et *c*. B) Evolution du volume de maille.

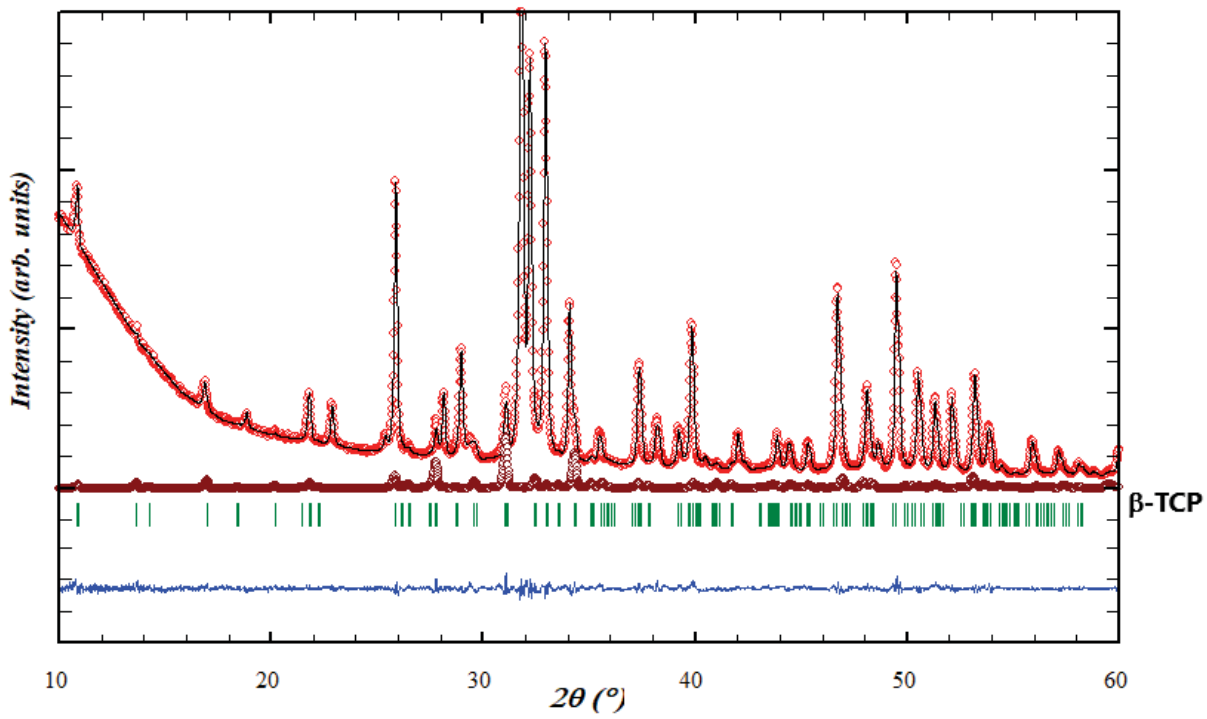

Figure 2.11 : Affinements Rietveld de l'échantillon recuit à 800°C et identification du profil de diffraction de la phase β-TCP.

En conclusion, les mécanismes d'incorporation des ions cuivre, argent et or dans les matériaux apatitiques sont très différents. Pour le cuivre un mécanisme d'insertion en site interstitiel dans la phase HAp est observé et pour la phase ß-TCP il s'agit d'un mécanisme de substitution ; mécanisme commun pour les cations de la 1ère série de transition. Pour l'argent une substitution des ions Ca^{2+} par les ions Ag^{+} dans les phases HAp et ß-TCP est observée ainsi que la formation de nanoparticules d'argent métallique Ag°. Enfin pour l'or uniquement une phase β-TCP dopée est observée avec incorporation d'atome d'or en substitution des cations Ca^{2+}, à nouveau en présence de nanoparticules métalliques d'or.

3. Synthèses par précipitation en voie aqueuse des matériaux dopes au cuivre

Les synthèses par précipitation en voie aqueuse ont été réalisées par l'équipe Ingénierie des Biomatériaux et des Particules Inhalées (BioPI) du Centre Ingénierie et Santé (CIS) de l'Ecole des Mines de Saint-Etienne. Ce travail a été réalisé plus particulièrement lors des stages de Master de Lorélène Gasnier et Mathilde Prudent, avec l'aide de Coralie Laurent et sous la direction de David Marchat. L'intérêt principal de ces synthèses était la possibilité de préparation de poudre en grande quantité, puis la maîtrise du procédé de frittage pour la réalisation de pastilles denses.

3.1. Synthèse des matériaux non dopés Cu0-1050

Les poudres non dopées ont été synthétisées par précipitation en voie aqueuse. Pour cela, une solution de phosphate d'ammonium $(NH_4)_2HPO_4$ est mélangée à une solution de nitrate de calcium tétra-hydraté $Ca(NO_3)_2{\cdot}4H_2O$ à une vitesse de 350 mL/min. La réaction est maintenue sous agitation (600 rpm) à 35°C et est balayée par un flux d'argon afin d'éviter la carbonatation de la phase apatitique. Le pH est maintenu à 7,0 par l'addition d'une solution d'ammoniaque à 28%. Après maturation pendant 19h la suspension d'HAp obtenue est centrifugée à 4000 rpm pendant 5 min. L'équation de réaction correspondante à cette synthèse est la suivante :

$$(10\text{-}x)\ Ca^{2+} + 6\ HPO_4^{2-} + (8\text{-}2x)\ OH^- \leftrightarrows Ca_{10-x}(PO_4)_{6-x}(HPO_4)_x(OH)_{2-x} + (6\text{-}x)\ H_20 \qquad \text{Eq.1}$$

3.2. Synthèse des matériaux dopés Cu10-1050

Les synthèses de poudres dopées Cu10-1050 ont été réalisées par deux réactions successives : la précipitation puis l'hydrolyse d'une brushite dopée au cuivre. Le taux de dopage x a été fixé à x = 0,1 selon un mécanisme d'insertion du cuivre du type : $Ca_{10}Cu_x(PO_4)_6(OH)_{2-2x}O_{2x}$. Cette synthèse passe par 2 réactions successives qui sont la formation d'un phosphate dicalcique hydraté (brushite, $CaHPO_4{\cdot}2H_2O$) (1) et hydrolyse de la brushite en HAp déficiente en calcium.

La synthèse de la brushite est réalisée à partir d'une solution de nitrate d'ammonium $(NH_4)_2HPO_4$ mélangée dans un réacteur maintenu sous agitation (400 rpm) avec une solution de nitrate de calcium tétra-hydraté $Ca(NO_3)_2{\cdot}4H_2O$ et de nitrate de cuivre tri-hydraté $Cu(NO_3)_2{\cdot}3H_2O$ à une vitesse de 100 mL/min. Le mélange est maintenu sous agitation (550

rpm) pendant 3h à 40°C. Un flux d'argon balaye le réacteur afin d'éviter la carbonatation du précipité. La formation de la brushite dopée au cuivre suit la réaction suivante :

$(1\text{-}z)\ Ca^{2+} + z\ Cu^{2+} + H_2PO_4^{2-} \leftrightarrows Ca_{(1-z)}Cu_{(z)}HPO_4,\ 2H_2O + H_30^+$ Eq.2

avec $z_1 < 0.25$. [148]

La conversion de la brushite dopée en hydroxyapatite dopée est réalisée en ajustant le à 7,0 avec l'ajout d'une solution d'ammoniaque NH_3+H_20 à 28% et suit la réaction suivante en considérant l'insertion des ions cuivre en site interstitiel [4] :

$(4\text{-}x+6z_1)\ Ca^{2+} + z_2\ Cu^{2+} + 6\ Ca_{(1-z1)}Cu_{(z1)}HPO_4,2H_2O + (8\text{-}2x+2z)\ OH^- \leftrightarrows Ca_{10-x}Cu_z(PO_4)_{6-x}(HPO_4)_x(OH)_{2-2z-x}(O)_{2z} + (6\text{-}x+2z)\ H_20$ Eq.3

avec $z = 6z_1 + z_2$, $0 \leq x \leq 1$ et $z \leq 0.1$ [4]

Ensuite la suspension est maintenue sous agitation pendant 24h à 40 °C. Finalement, afin de séparer la phase liquide du précipité la suspension est centrifugée 5 min à 4000 rpm.

Les précipité obtenus (Cu0-1050 et Cu10-1050) sont congelés à -80°C puis lyophilisés (lyophilisateur Pilote Compact de Crytec France) pour éliminer l'eau contenue dans les poudres.

4. Mise en forme et caractérisations des matériaux à partir des poudres synthétisées

4.1. Pastillage

Les mises en forme par pastillage ont été réalisées par l'équipe Ingénierie des Biomatériaux et des Particules Inhalées (BioPI) du Centre Ingénierie et Santé (CIS) de l'Ecole des Mines de Saint-Etienne. Ce travail a été réalisé plus particulièrement par David Marchat et Coralie Laurent.

Les poudres obtenues après lyophilisation sont pré-calcinées à 700°C pendant 2h (4°C/min) sous atmosphère N_2 à une pression de 93kPa et H_2O à une pression de 7kPa.

Pour former des pastilles, 500 mg de chaque poudre sont introduits dans une matrice de 12.7 mm de diamètre en acier inoxydable. Un pressage uniaxial avec une charge de 50 MPa est effectué suivi par un pressage isostatique à 300 MPa (Nova swiss, Suisse).

Les pastilles sont frittées à 1050°C dans un four tubulaire (Nabertherm, Allemagne) pendant 3h sous air à une pression partielle de 7 kPa puis à 1050°C pendant 5h sous atmosphère sous atmosphère N_2 à une pression de 93kPa et H_2O à une pression de 7kPa.

Durant ces traitements thermiques les poudres composées d'hydroxyapatite non dopée et dopée se décomposent en BCP non dopés et dopés selon l'équation suivante :

$$Ca_{10-x}Cu_z(PO_4)_{6-x}(HPO_4)_x(OH)_{2-2z-x}(O)_{2z} \xrightarrow{\Delta} \left(\frac{1-x+z}{1+z}\right) Ca_{10}Cu_z(PO_4)_6(OH)_{2-2z}(O)_{2z} + \left(\frac{3x}{1+z}\right) Ca_{3-\frac{z}{3}}Cu_{\frac{z}{3}}(PO_4)_2 + \left(\frac{x\,(1-z)}{1+z}\right) H_2O \quad \text{Eq.4}$$

avec $0 \leq x \leq 1$ et $z \leq 0.1$.

Les pastilles sont ensuite polies sur une face jusqu'au grade de 1 µm à l'aide d'une pâte diamantée. Les pastilles obtenues sont représentées en **Figure 2.12**.

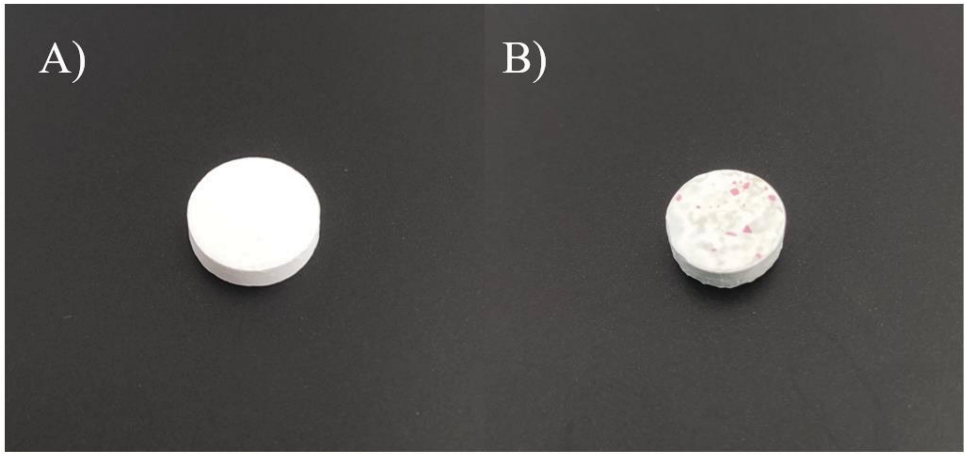

Figure 2.12 : A) pastille Cu0-1050 et B) pastille Cu10-1050.

Les caractéristiques des pastilles Cu0-1050 et Cu10-1050 obtenues après frittage et polissage sont présentées dans le **tableau 2.3**.

Tableau 2.3 : caractéristiques des pastilles Cu0-1050 frittées et polies, moyennes obtenues sur des lots d'environ 35 échantillons.

Pastilles	Masse (g)	Diamètre (mm)	Epaisseur (mm)	Volume (mm^3)	Masse volumique ($g.cm^{-3}$)	% densité
Cu0-1050	0,495	9,69	2,584	190,6	2,60	82,7
	± 0,003	± 0,06	± 0,045	± 4,9	± 0,07	± 2,1
Cu10-1050	0,486	8,86	3,10	190,8	2,55	81.0
	±	±	±	±	±	±
	0,006	0,06	0,06	3,4	0,04	1,3

4.2. Caractérisation minéralogique des pastilles frittées et polies Cu0-1050

Les échantillons obtenus ont été caractérisés par DRX (directement sur pastille) suivis d'affinements Rietveld. Pour les pastilles non dopées le résultat de l'affinement est présenté **figure 2.13**. Les pastilles Cu0-1050 sont composées des 2 phases mélangées : HAp et β-TCP. D'après la quantification des phases présentes, les pastilles Cu0-1050 sont constituées d'HAp à 60,0% massique et de B-TCP à 40,0% massique.

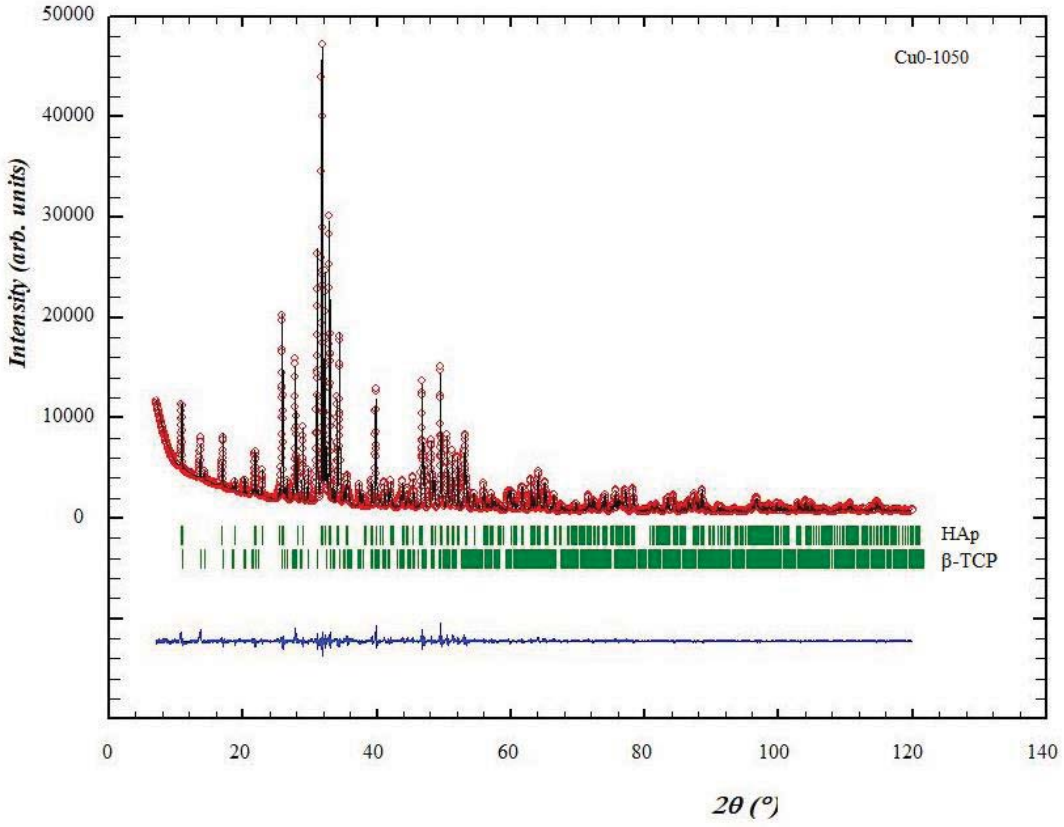

Figure 2.13 : Affinements Rietveld des pastilles Cu0-1050 frittées à 1050°C et identification des phases HAp et β-TCP.

4.3. Caractérisation des pastilles frittées et polies Cu10-1050

Pour les pastilles dopées le résultat de l'affinement est présenté **figure 2.14**. Les pastilles Cu10-1050 sont également composées des 2 phases HAp et β-TCP en proportion équivalentes aux pastilles non-dopées (60,4% HAp et 39,6% β-TCP).

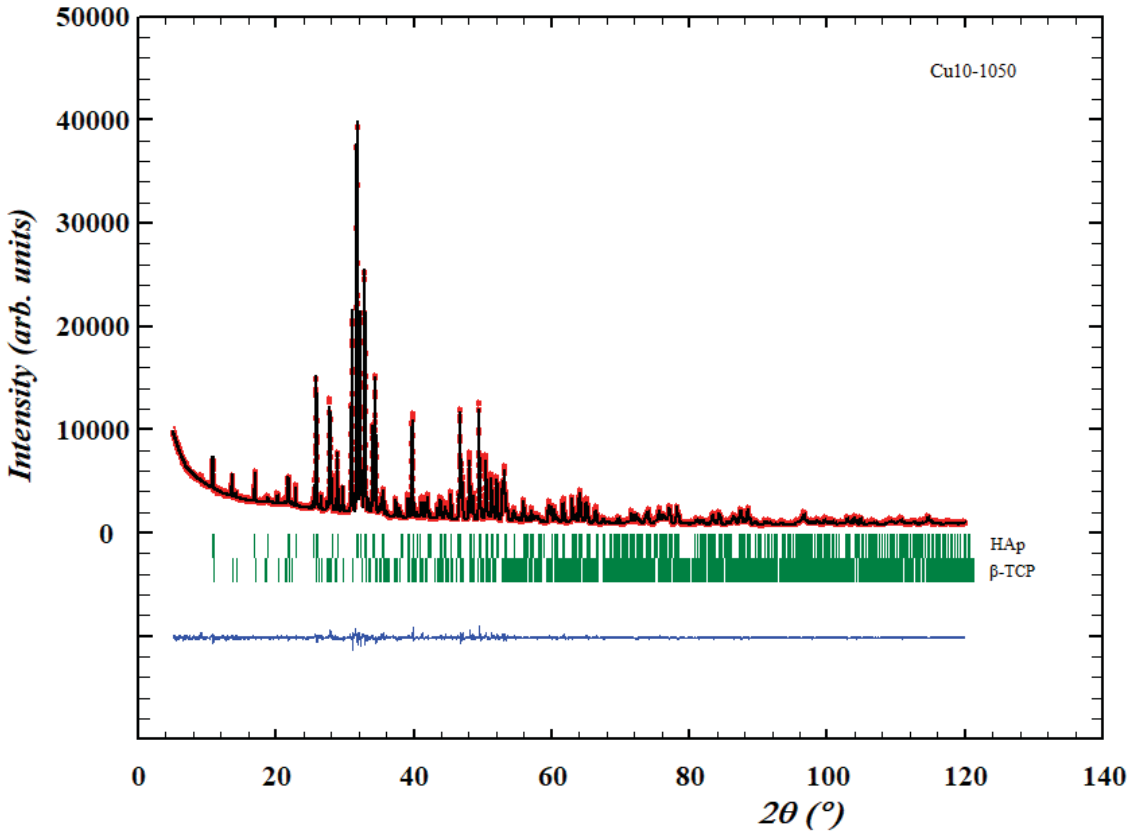

Figure 2.14 : Affinements Rietveld des pastilles Cu10-1050 frittées à 1050°C et identification des phases HAp et β-TCP.

Les 2 types de pastilles (non dopées et dopées) ont donc une composition identique, de l'ordre de 60% d'HAp et 40% de β-TCP (**Tableau 2.4**). La présence ou non de cuivre étant la seule différence entre ces matériaux, ils peuvent donc parfaitement être utilisés pour évaluer les effets biologiques du dopage au cuivre, en utilisant Cu0-1050 comme référence.

Tableau 2.4 : Composition minéralogique des pastilles Cu0-1050 et Cu10-1050.

Echantillon	HAp (%)	β-TCP (%)
Cu0-1050	60.0	40.0
Cu10-1050	60,4	39,6

4.4. Mécanisme d'incorporation du cuivre

Afin d'étudier les mécanismes d'incorporation du cuivre dans ces matériaux synthétisés par voie aqueuse, les paramètres de mailles des 2 phases présentes ont été comparées à ceux trouvés dans les matériaux synthétisés par voir sol-gel et décrit dans l'article de Gomes *et al.* 2018 [4].

Les paramètres de mailles des phases HAp et β-TCP des matériaux Cu0-1050 et Cu10-1050 sont présentés dans le **tableau 2.5**. Le **tableau 2.6** donne, pour comparaison, ces mêmes paramètres extraits de la publication [4], sur des préparations par voie sol-gel.

Tableau 2.5 : Evolutions des paramètres de mailles des phases HAp et β-TCP des matériaux non dopés Cu0-1050 et dopés Cu10-1050 synthétisés par voie aqueuse.

	HAp		β-TCP	
	Cu0-1050	**Cu10-1050**	**Cu0-1050**	**Cu10-1050**
***a* (Å)**	9,42004	9,41976	10,42065	10,41117
***c* (Å)**	6,88099	6,87881	37,36754	37,42646
V (Å^3)	528,795	528,596	3514,103	3513,244

Tableau 2.6 : Evolutions des paramètres de mailles des phases HAp et β-TCP des matériaux non dopés et dopés synthétisés par voie sol-gel ([4]).

	HAp				β-TCP	
	00Cu-1000	**00Cu-1100**	**15Cu-1000**	**15-Cu1100**	**00Cu-800**	**15Cu-700**
***a* (Å)**	9,42025	9,41972	9,41886	9,41749	10,4260	10,3925
***c* (Å)**	6,88127	6,88129	6,88282	6,88378	37,3689	37,3302
V (Å^3)	528,840	528,782	528,933	529,117	3517,85	3491,68

Les paramètres de maille des 2 phases des pastilles non dopées (Cu0-1050) sont en très bon accord avec ceux trouvés dans l'étude de Gomes *et al.* 2018 [4] (00Cu-1000, 00Cu-1100 et 00Cu-800). Les deux modes de synthèse (voies sol-gel et aqueuse) aboutissent à des matériaux équivalents. Cette équivalence se retrouve également sur la phase HAp des pastilles dopées (Cu10-1050) : une légère diminution des paramètres de mailles de l'HAp est observée, et la localisation des cation Cu^{2+} indique l'absence de substitution sur les sites de calcium (Ca1 et Ca2), et la présence en site interstitiel comme décrit dans l'étude Gomes *et al.* 2018 [4].

Concernant la phase β-TCP des matériaux dopés, une diminution du paramètre de maille *a* est observée ainsi qu'une forte augmentation du paramètre *c* pour les pastilles Cu10-1050 en comparaison avec Cu0-1050. La diminution du paramètre de maille *a* est en accord avec les poudres 00Cu-800 et 15Cu-700 présentées dans le tableau 9 (voie sol-gel). En revanche, l'augmentation du paramètre de maille *c* diffère des échantillons 00Cu-800 et 15Cu-700. Les températures de recuit utilisées entre les 2 modes de synthèse sont assez éloignées, et pourraient expliquer cette différence sur le paramètre *c*. D'autre part, les affinements Rietveld ont mis en évidence la présence d'atomes de cuivre en substitution sur le site de calcium Ca4 ; de façon similaire au phénomène de substitution décrit dans l'article de Gomes *et al.* 2018 [4] (sur les sites de calcium Ca4 et Ca5).

En conclusion, les mécanismes d'incorporation des ions cuivre dans les matériaux synthétisés par précipitation en voie aqueuse sont similaires à ceux observés dans les matériaux synthétisés par voir sol-gel, avec une insertion dans la phase HAp et une substitution dans la phase β-TCP. La principale différence entre les pastilles préparées en voie aqueuse et poudre synthétisée par voie sol-gel réside dans le ratio massique entre les 2 phases HAp/β-TCP : 60/40 en voie aqueuse et ~90/10 en voie sol-gel.

5. Prétraitements des matériaux avant leurs évaluations biologiques

5.1. Poudres issues de la synthèse sol-gel

Des premiers essais du comportement des matériaux en milieux biologiques ont été réalisés avant de les mettre au contact de cellules. Les deux principaux tests ont consisté à évaluer le pH des milieux après immersion des échantillons et à mesurer les concentrations de cuivre relargué.

Ces travaux ont montré qu'il était nécessaire de prétraiter les poudres avant leur utilisation pour éliminer les traces de CaO présentes qui induisent une forte augmentation du pH pouvant entrainer une cytotoxicité cellulaire. De plus, il a été montré que le cuivre n'était pas relargué dans l'eau distillée [4].

C'est pourquoi dans ce travail, les poudres ont été pré-incubées dans de l'eau distillée avant leur utilisation afin d'éliminer toutes traces de CaO tout en conservant les ions cuivre dans leur composition. Afin de valider le protocole de pré-incubation, des mesures de pH d'eau distillée et de milieu de culture cellulaire ont été réalisés afin de s'assurer qu'il n'y ait plus d'augmentation.

Les conditions de pré-incubation suivantes ont été réalisées : 250 mg de poudres ont été incubés dans 1L d'eau distillée pendant 48 h à 37°C. Les mesures de pH qui ont suivis n'ont pas montré d'augmentation et ont donc permis de valider ce protocole de pré-incubation. Ainsi toutes les poudres utilisées pour la suite de ce travail ont été préalablement incubées 48h à 37°C dans de l'eau distillée à une concentration de 250 mg/L.

5.2. Détermination de la quantité de poudres à utiliser pour les évaluations biologiques

D'après une étude de Wang *et al.*, une concentration d'ions cuivre Cu^{2+} supérieure à 10 ppm induit des effets cytotoxiques sur des fibroblastes murins [149]. A partir de cette information, les concentrations de cuivre relargué par les poudres ont été mesurées par spectroscopie d'absorption atomique afin de déterminer une quantité de poudre pour laquelle le taux de cuivre relargué est inférieur à 10 ppm.

En se basant sur les précédents travaux de l'équipe les tests de relargage ont été effectué dans les conditions suivantes : 16 mg de poudres dans 24 mL de milieu de culture, soit une concentration de 0,67 mg/mL [150]. Les mesures ont été prises à J1, J2, J7 et J15. Les résultats sont présentés **Figure 2.15**.

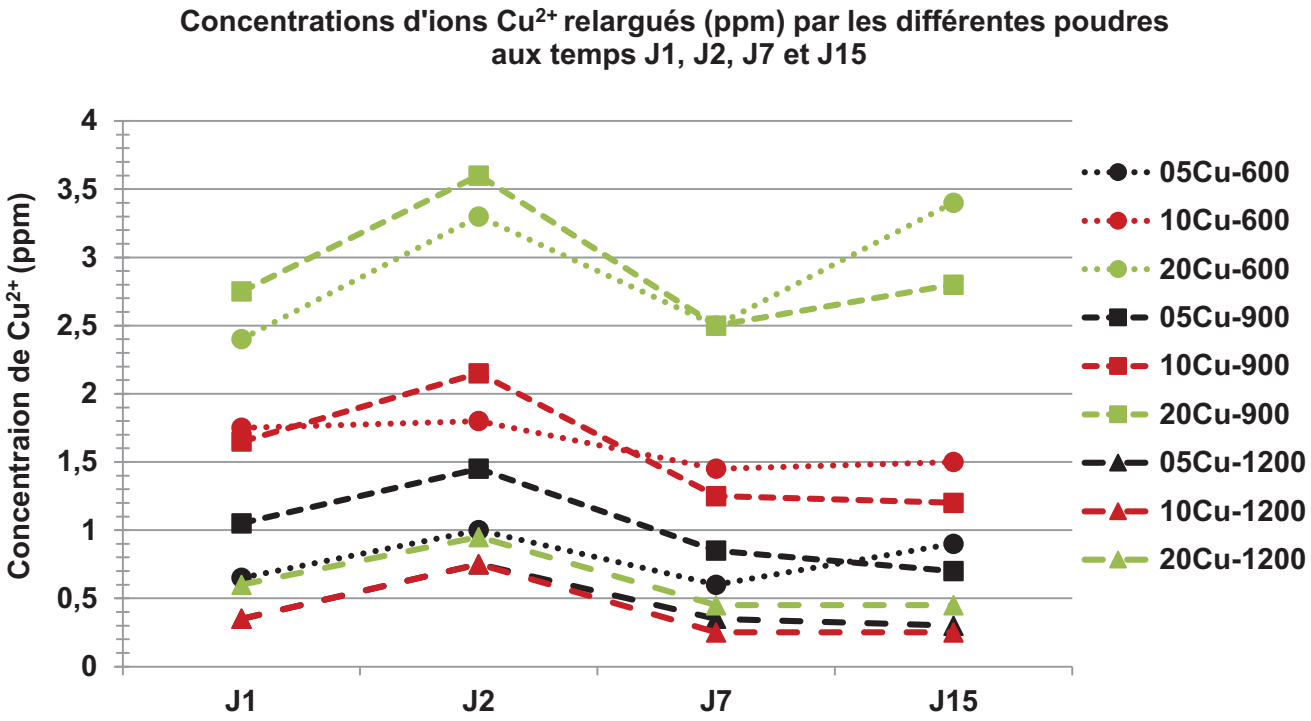

Figure 2.15 : Mesures des concentrations d'ions cuivre Cu^{2+} relargués (ppm) par les différentes poudres synthétisées par voir sol-gel aux temps J1, J2, J7 et J15.

D'après les résultats obtenus, pour une concentration de poudre de 0,67 mg/mL de milieu de culture, la concentration de cuivre relargué est maximale à J2 pour les poudres 20Cu-600 et 20Cu-900 avec respectivement 3,3 et 3,6 ppm. Il a donc été décidé de travailler pour la suite des expérimentations avec une concentration de poudre de 1.7 mg/mL de milieu de culture afin de relarguer des concentrations de cuivre plus importantes tout en restant inférieures à 10 ppm.

5.3. Pastilles issues de la synthèse par précipitation en voie aqueuse

Comme précédemment les concentrations de cuivre relargué par les pastilles Cu10-1050 en milieu de culture ont été mesurées par MP-AES, avant d'utiliser les pastilles pour les évaluations biologiques.

Le test a consisté à incuber 1 pastille dans 1mL de milieu de culture et de mesurer le cuivre relargué après 1 jour et après 3 jours. Après 1 jour d'incubation la concentration en ions Cu^{2+} était de 16,6 ppm et après 3 jours de 41,6 ppm. Ces concentrations étant très élevées, notamment après 3 jours, un protocole de pré-incubation a été mis en place avant de pouvoir utiliser ces matériaux pour les évaluations biologiques. Celui-ci a consisté à incuber 1 pastille dans 1 mL de milieu de culture pendant 24h afin de relarguer une première fois du cuivre et

de diminuer la quantité restante dans le matériau dans le but de diminuer les concentrations retrouvées ensuite en solution lors des tests biologiques.

6. Choix des matériaux utilisés pour leurs évaluations biologiques

6.1. Choix du dopant

Trois dopants ont été utilisés lors des synthèses : Cu, Ag et Au. Deux familles différentes de matériaux ont été obtenues :

- pour le dopage au cuivre des BCP dopés en cation Cu^{2+} (Cu:BCP) ont été obtenus
- et pour les dopages à l'argent et à l'or des nano-composites composés de BCP dopées en cation métalliques et des nanoparticules métalliques (Ag°/Ag:BCP et Au°/Au:BCP) ont été obtenues.

Malgré le fort potentiel d'un matériau de type nano-composite, notamment dans le cas de l'argent, et afin de rester fixer sur les objectifs initiaux de ces travaux de thèse (effet d'un dopage des BCP par des cations métalliques d'intérêt), il a été décidé de se focaliser exclusivement sur les matériaux dopés au cuivre (Cu:BCP), sous 2 formes : poudres et pastilles.

6.2. Etude sur poudre

Une première étude sur les poudres dopées au cuivre synthétisées par voie sol-gel a été réalisée pour évaluer leur cytotoxicité et leur propriété antibactérienne. Les poudres utilisées, qui sont présentées dans le **tableau 2.1,** ont 4 taux de dopage et 3 températures de recuits différents ce qui permet de déterminer l'influence de ces 2 paramètres de synthèses (taux de dopage et localisation du dopant) sur les propriétés biologiques observées. Cette étude est présentée dans le chapitre 3 de ce manuscrit.

6.3. Etude sur pastilles

Une seconde étude a consisté à étudier les propriétés biologiques des matériaux sous forme de pastilles. Pour cela les 2 pastilles présentées **Figure 2.12.** (Cu0-1050 et Cu10-1050) ont été utilisées.

L'intérêt de travailler avec des matériaux sous forme de pastille est de s'affranchir des différences de surface spécifiques qui peuvent influer sur les réponses biologiques. Aussi, cela permet d'observer au MEB la morphologie des cellules à la surface des pastilles lors des tests de cytotoxicité, ce qui n'est pas possible avec les poudres. Cette étude est présentée dans le chapitre 4 de ce manuscrit.

CHAPITRE 3 : EVALUATION DE LA CYTOTOXICITE ET DES PROPRIETES ANTIBACTERIENNES DES POUDRES DE PHOSPHATES DE CALCIUM BIPHASIQUES DOPEES AU CUIVRE

La cytotoxicité et l'activité antibactérienne des poudres de BCP présentées dans le **tableau 2.1** du **Chapitre 2** de ce manuscrit ont été évaluées. Les poudres synthétisées ont 3 températures de recuit différentes (600°C, 900°C et 1200°C) et 4 taux de dopage au cuivre différents (x = 0.0, 0.05, 0.10 et 0.20 correspondants à la quantité stœchiométrique de cuivre ; $Ca_{10}Cu_x(PO_4)_6(OH)_{2-2x}O_{2x}$). L'objectif de cette étude est d'évaluer l'impact des caractéristiques chimiques de ces poudres sur le relargage du dopant, ici le cuivre, et donc également sur les réponses biologiques.

Pour évaluer leur cytotoxicité les poudres ont été mises en culture avec des cellules souches mésenchymateuses humaines. Ces cellules ont été récupérées à partir de morceaux de moelle osseuse fémorale prélevés lors de pose de prothèse de hanche sur des patients ayant donnés leur autorisation. Le test colorimétrique MTT a été utilisé, consistant à mesurer par spectroscopie la conversion d'un sel de tétrazolium MTT en formazan par les cellules viables.

L'activité antibactérienne a été évaluée sur 2 souches cliniques Gram positive : *S. aureus* et *S. aureus* résistant à la méticilline, toutes les 2 isolées sur des patients atteints d'infections ostéo-articulaires, et 2 souches de la collection ATCC Gram négative : *E. coli* et *P. aeruginosa*. Cette partie du travail a été réalisée dans les locaux du Laboratoire Microorganismes : Génome et Environnement (LMGE) de l'Université Clermont Auvergne à Clermont-Ferrand et avec la collaboration du Professeur Christiane Forestier.

En parallèle de ces expérimentations, les taux de cuivre relargué pendant ces études biologiques ont été mesurés par spectroscopie d'émission atomique afin d'évaluer les concentrations de dopant impliqués dans les réponses biologiques.

En résumé, cette étude a montré que la composition biphasique des BCP et plus précisément le ratio HAp/β-TCP dépend de la température de recuit. Une augmentation de la phase HAp peu soluble est observée pour les températures de recuit les plus élevées, conduisant à un plus faible relargage d'ions Cu^{2+}. De plus, la concentration de cuivre relargué lors des

expérimentations biologiques est dépendante du taux de dopant ajouté lors de la synthèse des poudres. L'évaluation de la cytotoxicité a montré que les poudres dopées n'induisent aucune cytotoxicité envers les cellules souches mésenchymateuses humaines après 3, 7 et 15 jours de culture ; ceci pour des concentrations de cuivre allant jusqu'à 12 ppm. Les ions cuivre relargués par ces matériaux après 24h, à une concentration d'environ 2,5 ppm, montrent une forte activité antibactérienne envers *S. aureus*, *S. aureus* résistant à la méticilline et *E. coli*. En revanche, il a été montré qu'une dose de cuivre supérieure à celle relarguée par les matériaux, de l'ordre de 10 ppm, est nécessaire pour induire un effet antibactérien envers *P. aeruginosa*. Finalement les résultats ont aussi montré que le milieu de culture utilisé pour les expérimentations a une influence sur l'activité antibactérienne du cuivre puisque dans un milieu TS dilué au 1/500ème 4 ppm de cuivre induisent une diminution totale de la concentration bactérienne de *S. aureus* alors que 20 ppm sont nécessaires pour obtenir le même résultat dans un milieu de culture cellulaire standard non dilué.

L'intégralité des résultats obtenus décrivant la cytotoxicité et l'activité antibactérienne des poudres de BCP dopées au cuivre est présentée dans l'article suivant :

Aurélie Jacobs, Guillaume Renaudin, Nicolas Charbonnel, Jean-Marie Nedelec, Christiane Forestier, Stéphane Descamps, **Copper-doped Biphasic Calcium Phosphate powders: dopant release, cytotoxicity and antibacterial property** (soumis dans cette version, *Biomaterials*)

Copper-doped Biphasic Calcium Phosphate powders: dopant release, cytotoxicity and antibacterial properties

Aurélie JACOBS,[1] Guillaume RENAUDIN,[1]*, Nicolas CHARBONNEL,[2] Jean-Marie NEDELEC,[1] Christiane FORESTIER,[2] Stéphane DESCAMPS[1]

[1] Université Clermont Auvergne, CNRS, SIGMA Clermont, ICCF, F-63000 Clermont-Ferrand, France.

[2] Université Clermont Auvergne, CNRS, Laboratoire Microorganismes : Genome et Environnement, F-63000 Clermont-Ferrand, France.

Abstract

Cytotoxicity and antibacterial properties associated with the dopant release of Cu-doped Biphasic Calcium Phosphate (BCP) powders, mainly composed of hydroxyapatite mixed with β-tricalcium phosphate powders, were investigated. Twelve BCP ceramics were synthesized at 3 different sintering temperatures (600°C, 900°C and 1200°C) and 4 copper doping rates (x = 0.0, 0.05, 0.10 and 0.20, corresponding to the stoichiometric amount of copper in $Ca_{10}Cu_x(PO_4)_6(OH)_{2-2x}O_{2x}$). Cytotoxicity assessments of Cu-doped BCP powders using MTT assay with human-Mesenchymal Stem Cells (h-MSCs) indicated no cytotoxicity and the release of less than 12 ppm of copper into the biological medium. The antibacterial activity of the powders was determined against both Gram-positive (methicillin-sensitive (MS) and methicillin resistant (MR) *Staphylococcus aureus*) and Gram-negative (*Escherichia coli* and *Pseudomonas aeruginosa*) bacteria. The Cu-doped biomaterials exhibited a strong antibacterial activity against MSSA, MRSA and *E. coli*, releasing approximatively 2.5 ppm after 24 hours, whereas 10 ppm were required to induce an antibacterial effect against *P. aeruginosa*. This study also demonstrated that the culture medium used during experiments can directly impact the antibacterial effect observed; only 4 ppm of Cu^{2+} were effective to kill *S. aureus* in a 1:500 diluted TS medium, whereas 20 ppm were necessary to achieve the same result in a rich non-diluted standard marrow cell culture medium.

1. Introduction

Bone substitutes are biomaterials whose aim is to replace the bone and rebuild a deficient bone stock in a completely safe way. They can also act as prosthesis coatings to improve the bond between tissue and material [1]. Ideally, they must be bioactive, osteoconductive, osteoinductive and bioresorbable [2]. In different cases the use of bone substitutes is necessary to fill a damaged area: non-contiguous fractures with a bone defect, bone infection or disease requiring bone tissue removal. Autografts and allografts are conventional substitute techniques which show interesting characteristics. However, they present limits in terms of both quantity and quality, respectively, leading to the development of synthetic bone substitutes [3]. Among these, Biphasic Calcium Phosphates (BCP) are promising candidates for bone repair surgery because their chemical and mineral composition is very similar to that of bone tissues [4]. BCPs are bioceramics composed of a mixture of hydroxyapatite (HAp, $Ca_{10}(PO_4)_6(OH)_2$) and beta-Tricalcium Phosphate (β-TCP, $Ca_3(PO_4)_2$) [5]. An interesting characteristic of the biphasic composition is their solubility complementarity: HAp is poorly resorbable whereas β-TCP is highly degradable, allowing the resorption rate to be adapted to clinical needs [6]. Furthermore, apatitic materials have a flexible structure capable of accepting many ionic substitutions in their composition, enabling adaptable synthesis by doping with an element of biological interest [7]. In addition to these properties, BCPs are interesting materials because it is possible to adjust their composition and therefore to control the kinetic release of the doping element [6].

As well as biocompatibility, another essential factor to control is the risk of infection after the implantation of a bone substitute, especially because infections in bone sites are difficult to treat due to their deep localization in the tissue and poor vascularity. Infections can lead to non-osteointegration and necrosis, and the consequences for patient and society can be devastating [8,9]. With the increase in bacterial resistance to antibiotics [10], research focused on the development of new strategies and the use of metallic ions as antibacterial elements is intensifying.

Copper (Cu) is an essential trace element, involved in several biological processes, which is also known for its antibacterial properties [11,12]. Considering these strong antibacterial properties and its limited cytotoxicity, the Cu^{2+} copper cation appears to be a promising doping candidate to improve the behavior of the bioceramics used in bone repair surgery [13]. In 2014, Radovanovic *et al.*, synthetized Cu-doped BCP powders (HAp/α-TCP), and the results indicated significant antibacterial activity after 24h of incubation for the 4 tested microorganisms, *MSSA*, *E. coli*, *P. aeruginosa* and *C. albicans,* compared to undoped HAp/α-

TCP [14]. Recently, Bhattacharjee *et al.* prepared Cu-doped hydroxyapatite. Results indicated a significant reduction in bacterial viability for *E. coli* and Methicillin-sensitive *Staphylococcus aureus* (MSSA) [15]. All the studies related to the biological behavior of copper-doped materials (antibacterial, angiogenic and osteogenic), in anticipation of orthopedic clinical applications, were presented in a recent review [16]. More than a quarter of the presented papers in this review were published over the past three years, highlighting the interest of the scientific community for the topic.

The purpose of this study was to investigate the cytotoxicity and antibacterial properties of several Cu-doped BCP powders. The influence of the amount of copper and the sintering temperature on biological responses were evaluated. Cytotoxicity assays were performed *in vitro* with human-Mesenchymal Stems Cells (h-MSCs). The antibacterial activity of the powders was investigated against 4 bacterial strains of clinical interest: MSSA, Methicillin-Resistant *Staphylococcus aureus* (MRSA), *Escherichia coli* and *Pseudomonas aeruginosa*. In this study, the bioceramics were tested in the form of uncompacted powder, in order to favor the impact of the copper dopant.

2. Materials and methods

2.1. Sol-gel synthesis of copper-doped BCP samples

Chemical syntheses were performed using the sol-gel route described and used by Gomes *et al.*, 2018 [7]. Briefly, $Ca(NO_3)_2{\cdot}4H_2O$ (Sigma Aldrich) and P_2O_5 (Sigma Aldrich) were separately dissolved in ethanol under stirring and then mixed and refluxed at 85°C for 24 h. The solution obtained was maintained at 55°C for 24 h and the resulting gel was heated at 80°C for 10 h to obtain a white powder. To synthesize Cu-doped samples, the required amounts of $Cu(NO_3)_2{\cdot}3H_2O$ (Sigma Aldrich) were added. Finally, the powder was heat-treated for 15h at 600°C, 900°C and 1200°C, influencing the HAp/β-TCP ratio, and the location and accessibility of the doping element [7]. Four doping rates were synthesized assuming the insertion of Cu^{2+} cations in the interstitial crystallographic sites of the HAp phase, as described in our previous study [7]. The targeted nominal sample compositions were $Ca_{10}(PO_4)_6(OH)_2$ (corresponding to the undoped series), $Ca_{10}Cu_{0.05}(PO_4)_6(OH)_{1.90}O_{0.10}$, $Ca_{10}Cu_{0.10}(PO_4)_6(OH)_{1.80}O_{0.20}$ and $Ca_{10}Cu_{0.20}(PO_4)_6(OH)_{1.60}O_{0.40}$. The materials were mainly composed of the HAp phase, mixed with a small amount of β-TCP. Color samples were dependent on sintering temperature: light grey for the series annealed at 600°C, dark grey for those at 900°C and dark purple for samples treated at 1200°C. In this study, samples are labelled "*X*Cu-*T*" with *X* = 00, 05, 10 and 20 corresponding to the four doping rates (undoped samples with *x* = 0, and *x* = 0.05, 0.10 and

0.20, respectively, for the stoichiometric amount of copper in the doped $Ca_{10}Cu_x(PO_4)_6(OH)_{2-2x}O_{2x}$ samples with *X* = 100*x*) and *T* indicating the sintering temperatures 600°C, 900°C and 1200°C (leading to a total of twelve different powders). Regarding the behavior in solution of these powders, we show that copper is easily accessible for materials treated at 600°C and 900°C, and that this is much less the case for powders treated at 1200°C. Copper ions are located at the HAp crystal surface for the *X*Cu-600 samples, substituted for calcium in the β-TCP structure for the *X*Cu-900 samples, and inserted into the HAp structure for the *X*Cu-1200 samples [7].

Specific surface areas were obtained using MicroActive Software for a TriStar II PLUS Version 2.03 Instrument, and granulometric distributions were obtained with a Malvern Mastersizer 3000 with a Hydro EV automated wet dispersion unit. Phase compositions were determined by X-ray powder diffraction (XRPD) followed by Rietveld treatments to extract the respective amounts of HAp and β-TCP (this procedure was detailed in the related previous work [7]).

After synthesis, Cu-doped BCP powders were pre-treated by incubation in distilled water for 48 h at a concentration of 250 mg/L, in order to remove CaO traces, which were responsible for deleterious pH increases as reported before [7]. Before biological evaluations, Cu-doped BCP samples were sterilized with dry heat in an oven at 180°C for 2 h.

2.2. Cytotoxicity evaluation

2.2.1 Human mesenchymal stem cells (h-MSCs): isolation and culture

H-MSCs were extracted from pieces of metaphysal cancellous bone collected during hip arthroplasty on healthy patients who had signed an authorization for the use of their bone for research purposes. Bone pieces were collected in a solution of sterile phosphate-buffered saline (PBS) supplemented with 2% of heparin and transported directly to the culture lab. Samples were filtrated and washed with PBS. Bones were cut into small pieces and incubated for 15 min at 37°C with 4 mL of minimum essential medium (MEM), 2 mL of PBS and 0.2 mL of collagenase (Stemcell). Samples were filtrated and then washed with PBS again. All the filtrates were mixed and centrifuged, and cell pellets were suspended in a standard marrow cell culture medium (MEM supplemented with gentamycin at 4 µg/mL, sodium pyruvate 1%, vitamins 1%, nonessential amino acids 1%, and fetal bovine serum 10%). Cells were plated in units of 20×10^6 cells in 25 cm^2 tissue culture flasks and incubated at 37°C with 5% humidified CO_2. After 3 days the non-adherent cells were harvested and removed with two gentle rinses with PBS. Adherent h-MSCs were cultured with a weekly change of medium and expanded through one of three passages before being collected by trypsinization.

2.2.2. Cytotoxicity evaluation of Cu-doped powders with MTT assay

H-MSCs were seeded in a 24-well plate (5×10^4 cells/well) with 1.7 mg each of Cu-doped and undoped sterilized powders and 1 mL of standard marrow cell culture medium. Cells cultured without powders were used as a positive control. For negative control 30 µL of cycloheximide (Sigma Aldrich, cycloheximide solution, 100 mg/mL in DMSO) were added 24 h before the MTT assay. After 3, 7 and 15 days the mitochondrial activity of h-MSCs was evaluated with a MTT (3-(4,5-dimethylthiazol-2-yl)-2,5-diphenyl tetrazolium bromide) assay. Concerning assessments of cytotoxicity at day 15, the cell culture medium was refreshed at day 7 so that the cells were properly maintained and in order to avoid a potential cytotoxic effect which would come from the fact that the cell culture medium has not been renewed for 15 days.

For the MTT assay, 100 µL of the MTT reagent (Sigma Aldrich) at a concentration of 5 mg/mL in PBS was added to each well and the plates were then incubated at 37°C with 5% of CO_2. After 3 hours, each well was carefully removed without damaging the cells at the bottom and 500 µL of Dimethyl sulfoxide (DMSO) was added to each well. The plates were incubated in the dark with gentle shaking for 40 minutes to ensure a complete lyse of the cells. Finally, the contents of the wells, except for the powder, were transferred to new wells, and the optical density (OD) was measured at 570 nm and 690 nm with a TEKAN spectrophotometer and Magellan™ software.

2.3. Antibacterial properties

2.3.1. Bacterial strains and growth conditions

Four bacterial strains were used. Two Gram positive clinical strains, a MSSA strain isolated from a patient with osteoarticular infection after total knee replacement [17] and a MRSA isolated from an osteoarticular infection, were collected in Lyon (France) hospital. Two Gram-negative bacilli were also tested: *E. coli* (ATCC® 25922™) and *P. aeruginosa* (ATCC® 27853™).

Precultures were obtained by overnight growth at 37°C in 5 mL of TS medium (Tryptic Soy broth without dextrose). Bacterial concentrations were evaluated by measuring the optical density (OD) at 620 nm.

2.3.2. Antibacterial activity of Cu^{2+} copper ions in 1:500 diluted TS medium

A primary copper solution at 3 mg/mL in a 1:500 diluted TS medium (from the standard JIS Z 2801) was prepared from $Cu(NO_3)_2 \cdot 3H_2O$ (Sigma-Aldrich) and used to test the different concentrations of Cu^{2+} ions. Antibacterial experiments were carried out in 24-well culture plates starting with a bacterial inoculum of 10^3 CFU/mL (Colony-Forming Unit/mL), in a 1:500 diluted TS medium. Copper concentrations ranging from 0 ppm to 5 ppm were tested with MSSA, MRSA, and *E. coli*, and from 0 ppm to 10 ppm with *P. aeruginosa*. Copper was added to each well and mixed with 1 mL of bacterial suspension (10^3 CFU/mL). Control conditions consisted of a bacterial suspension without any added copper. The number of viable bacteria in the inoculum was determined by plating 100 µL of the suspension on TS agar plates and determining the CFUs after 24h of incubation at 37°C. After 24h of incubation in the microtiter plates, 5 min of sonication were performed and repeated twice, and the number of remaining viable bacteria was determined by plating 100 µL of the suspension or serial dilutions of the suspension on TS agar plates, further incubated at 37°C for 24h.

2.3.3. Antibacterial activity of Cu-doped BCP powders

Experiments were performed as described with Cu^{2+} copper ions solutions, *i.e.* 6.8 mg of each powder were mixed with 1 mL of bacterial suspension at 10^3 CFU/mL in each well of the 24-microtiter plate. The number of viable bacteria after 5h and 24h of incubation was measured by plating samples on TS agar plates as described previously.

2.3.4. Antibacterial activity against MSSA of Cu^{2+} copper ions in non-diluted standard marrow cell culture medium

In order to evaluate the influence of the culture medium used on the antibacterial properties of copper, a similar experiment as the one presented in 2.3.2. was performed but with non-diluted standard marrow cell culture medium; that is to say the supplemented medium used during cytotoxicity experiments (2.2.1) without gentamycin, so as to allow bacterial growth. Copper concentrations ranging from 14 ppm to 20 ppm were tested against MSSA.

2.4. Measurement of Cu^{2+} copper ions concentration

Ionic releases during cytotoxicity and antibacterial evaluations were measured by Microwave Plasma - Atomic Emission Spectroscopy (4200 MP-AES from Agilent). Sampling was performed directly during the experiments, so the measurement conditions correspond exactly to those used during the tests. Calibration samples were prepared using a 1000 µg/mL Cu ion

normadose (Agilent Technologies) diluted in the corresponding solvent (cell culture medium or bacterial culture medium). Samples were measured after dilution at 1:10 ratio in HNO_3 2% solution. The two most intense emission wavelengths of Cu (324,754 nm and 327,395 nm) were selected to carry out the measurements.

2.5. Statistical analysis

Results presented in this paper were obtained after 3 technical and 3 biological replicates (n = 9). The antibacterial effects of Cu-doped BCP powders were expressed in the form of a logarithmic difference between the bacterial concentrations obtained with the evaluated powders and the control without powder. The formula used was as follows: Logarithmic difference = log (powder tested) - log (control).

Statistical analyses were performed using the Mann−Whitney non-parametric test followed by the Bonferroni correction with $p < 0.05$ considered as being statistically significant.

3. Results

3.1. Synthesis and characterization of Cu-doped BCP powders

The doping mechanism and chemical compositions of the powders used in this paper were previously described using the Rietveld method in the paper by Gomes *et al.* 2018 [7]. Some of the recorded X-ray powder patterns are shown in **Figure SEI1** (Supplementary Information), and Rietveld analysis results are in agreement with our previous study. The extracted weight amounts of the two HAp and β-TCP phases are reported in **Table 1**, with the corresponding specific surface area for the 3 series of sintering temperatures (600°C, 900°C and 1200°C). With increasing annealing temperature, the specific surface area of the powders decreased (as expected) and the HAp phase, which was already predominant, increased at the expense of the β-TCP phase, with almost only HAp phase for the series at 1200°C. As a reminder, our previous study [7] showed that at 600°C copper is adsorbed on the HAp crystal surface (therefore easily accessible); at 900°C copper substitutes calcium in the soluble β-TCP phase (therefore again easily accessible); and at 1200°C copper is inserted into the less soluble HAp phase (therefore difficult to access). The values in Table 1 indicate that the physico-chemical characteristics of powders are only dependent on the temperature, and not on the amount of Cu doping: the values for the *X*Cu-600 series, then the *X*Cu-900 and *X*Cu-1200 series, are almost invariant for a given *X* value. Thus, the comparison of behaviors in a biological

environment within a series will allow us to highlight the effect of the doping rate, while a comparison between the series will be significant for the localization of the dopant in the material (i.e. dopant release rate associated with copper accessibility).

On the other hand, particle size remains relatively homogenous between powders (see particle size distributions in Supplementary Information **Figure SEI2**): the size of particles was of the order of a few tens of micrometers (up to 100 µm) with the presence of fines (two families centered at 1 µm and 4 µm) due to the grinding effect. The only difference comes from the more brittle nature of the powders with the sintering temperature, resulting in a higher proportion of fines. Since particle sizes were equivalent between powders, the physical particle/cell interactions should not differ between samples, and therefore should not lead to a bias in biological observations.

Table 1. Specific area and mineral composition (weight percent, wt %) of the 3 series of sintering temperatures (*X* = 00, 05, 10 and 20).

Sample series	**Specific surface area (m^2/g)**	**Composition (wt %) ***	
		HAp	**β-TCP**
***X*Cu-600**	**~14.5**	**~88**	**~12**
00Cu-600	15	86	14
05Cu-600	17	88	12
10Cu-600	12	90	10
20Cu-600	14	90	10
***X*Cu-900**	**~3.5**	**~94**	**~6**
00Cu-900	3	96	4
05Cu-900	3	93	7
10Cu-900	4	94	6
20Cu-900	3	93	7
***X*Cu-1200**	**~1.0**	**~98**	**~2**
00Cu-1200	1	99	1
05Cu-1200	0.5	98	2
10Cu-1200	1.	98	2
20Cu-1200	0.5	97	3

* values rounded to the unit, without considering the presence of lime (which never exceeded 1.5 wt %).

3.2. Cytotoxicity measurements

Results obtained from MTT assay are presented in **Fig. 1** and the corresponding values are listed in **Table SEI1**. The positive control corresponds to 100% metabolic activity. At day 3, the metabolic activities of all samples were over 80% except for sample 20Cu-600, with 77.6% (see Supplementary Information **Table SEI1**). However, the statistical analysis, based on 9 replicates, indicated that there was no associated deleterious effect. At day 7, all metabolic activity values were over 90%, and at day 15 all results were over 80% except for 10Cu-600, 20Cu-600 and 10Cu-1200 with 77.9%, 78.4% and 77.8% respectively. No significant difference with the positive control was shown, except for the negative control which was significantly lower compared to all conditions.

The concentrations of Cu^{2+} released by the powders at days 3, 7 and 15, are listed in **Table 2**. These concentrations were obtained directly by sampling the culture media during the cytotoxicity experiments. For measurements at day 15, the cell culture medium had been refreshed at day 7, so the indicated concentrations correspond to the release after the day of refreshment (*i.e.* between day 7 and day 15). At day 7, samples 05Cu-600, 10Cu-600 and 20Cu-600 released 2.8, 4.7 and 12.0 ppm of Cu^{2+}, respectively. Samples 05Cu-900, 10Cu-900 and 20Cu-900 released 2.4, 5.5 and 9.4 ppm, respectively. Samples from the series sintered at 1200°C showed Cu^{2+} concentrations between 0.5 and 1.7 ppm.

Table 2. Cu^{2+} release (ppm) measured by MP-AES during the cytotoxicity evaluation of Cu-doped bioceramics.

Samples	**Cu^{2+} concentration (ppm)**		
	Day 3	Day 7	Day 15*
05Cu-600	2.4	2.8	0.9 (3.7)
10Cu-600	5.1	4.7	2.3 (7.0)
20Cu-600	11.5	12.0	3.5 (15.5)
05Cu-900	2.5	2.4	0.6 (3.0)
10Cu-900	5.2	5.5	1.2 (6.7)
20Cu-900	10.0	9.4	2.4 (11.8)
05Cu-1200	0.5	0.7	0.4 (1.1)
10Cu-1200	0.7	0.8	0.4 (1.2)
20Cu-1200	1.5	1.7	0.6 (2.3)

***** For measurements at day 15, the cell culture medium had been refreshed at day 7, so the concentration indicated corresponds to the release between day 7 and day 15 (the sum with the day 7 measurement is indicated in brackets).

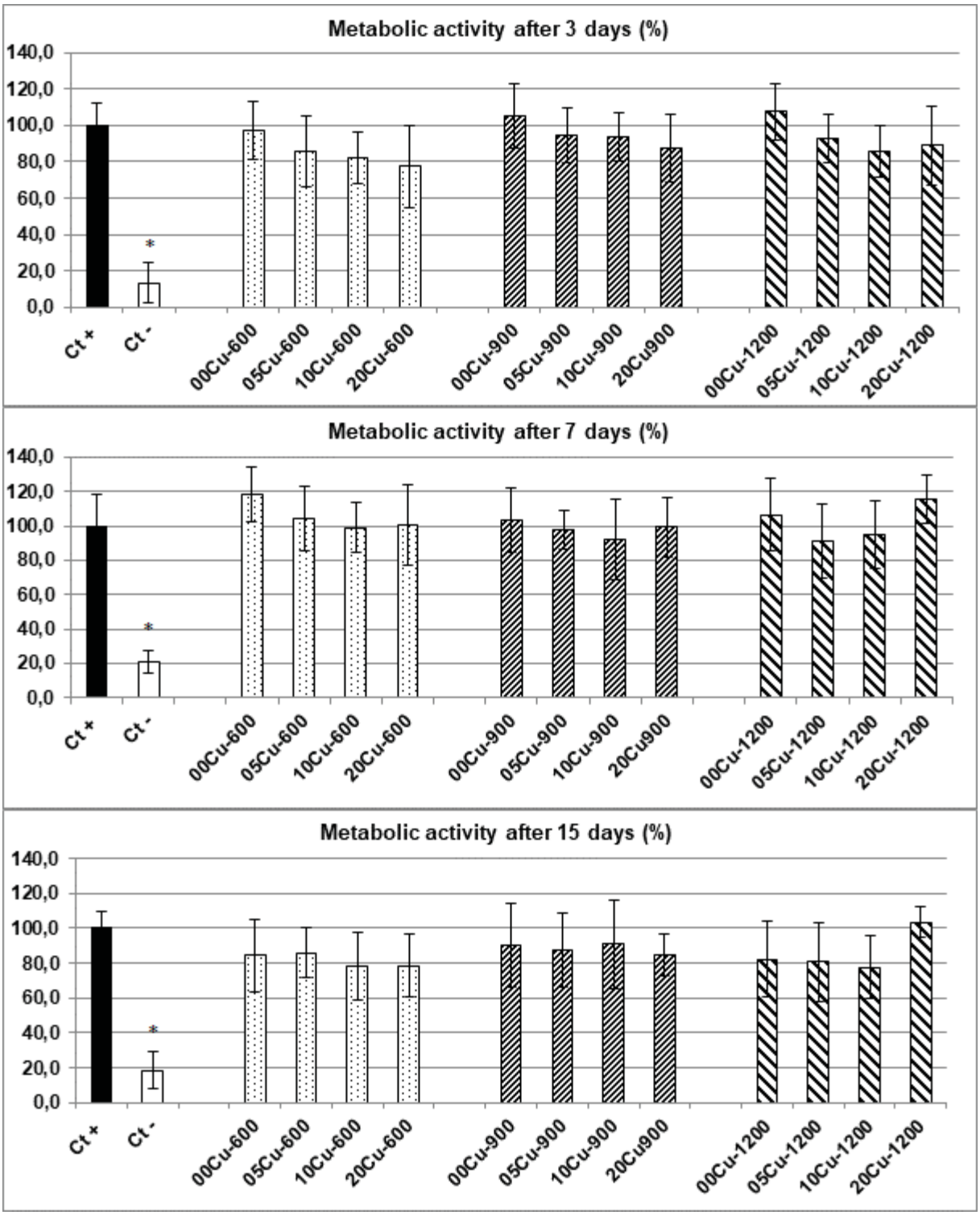

Fig. 1. Metabolic activity (%) of h-MSCs after 3 (top), 7 (middle) and 15 (bottom) days of culture for the different Cu-doped BCP powders. Ct+ corresponds to the positive control and Ct- corresponds to the negative control. Error bars represent the standard mean error from n = 9 replicates. Results which are statistically different compared to the control (with $p < 0.05$) are indicated by "*".

3.3. Antibacterial activity of BCP samples

The antibacterial assessment of Cu-doped powders was first performed for the MSSA strain and the results are presented in **Fig. 2**. After 5 hours of incubation, undoped and Cu-doped samples of the 3 series showed a decrease in bacterial concentration of about one log for both the *X*Cu-600 and *X*Cu-900 series and of about half a log for the xCu-1200 series. After 24 hours of incubation, significant antibacterial activity was observed except for 05Cu-1200. The *X*Cu-1200 series behaved differently from the other two series. For the series sintered at 600°C and 900°C, a reduction in bacterial concentration of more than 5 log was observed in the presence of copper. The decrease even exceeded 8 log compared to the control for samples 10Cu-600, 20Cu-600 and 20Cu-900, reaching the detection threshold. The series sintered at 1200°C showed bactericidal properties but which were less effective: samples 10Cu-1200 and 20Cu-1200 induced a significant decrease in bacterial concentrations, with a logarithmic reduction of -1.0 and -5.8, respectively. After 24 hours of incubation, the three undoped 00Cu-*T* samples did not induce any reduction in the number of CFUs. For the *x*Cu-600 and *x*Cu-900 series, significant bactericidal effects were observed, even for the less doped 05Cu-600 and 05Cu-900 samples, and the effect increased with dopant concentration. Although the antibacterial effects were inferior for the series xCu-1200, the effect also increased with dopant concentration.

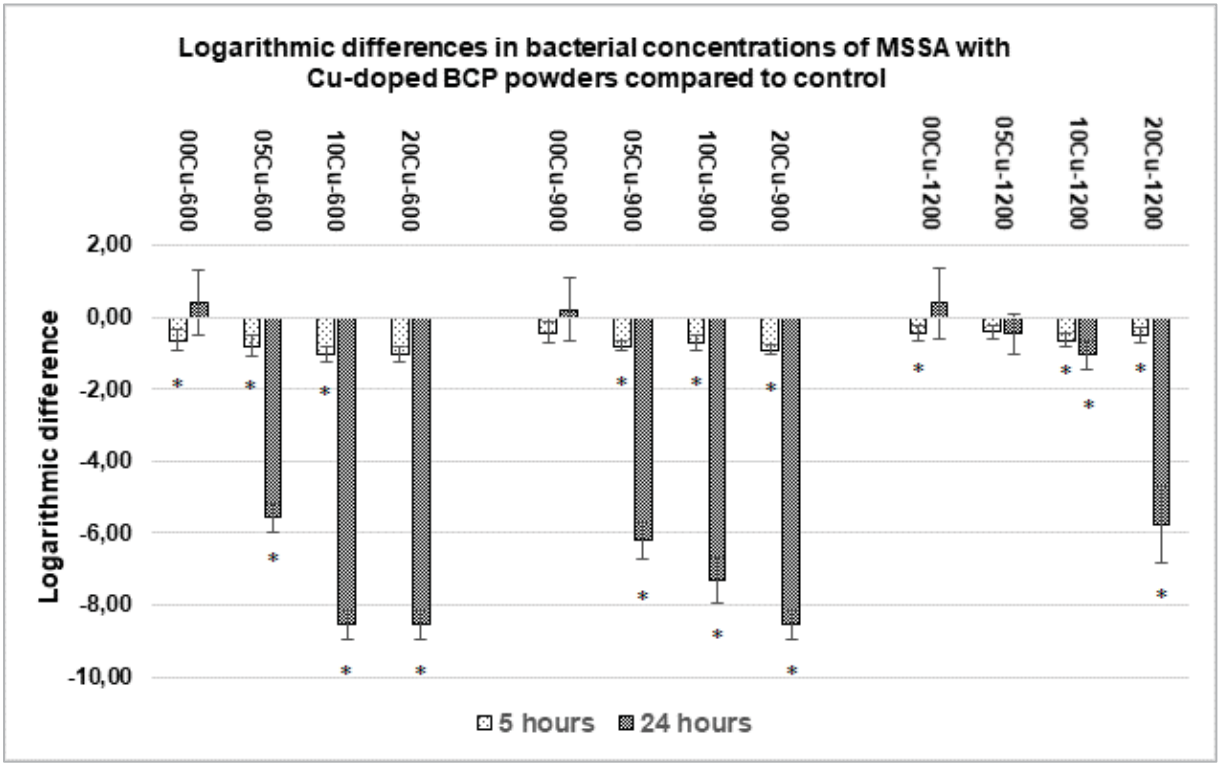

Fig. 2. Concentrations of viable MSSA after incubation with Cu-doped BCP powders compared to the control at 5 hours and 24 hours. Results statistically different compared to the control (with $p < 0.05$) are indicated by "*".

Assays were performed on the three other bacterial strains (MRSA, *E. coli* and *P. aeruginosa*) with 00Cu-*T* undoped powders and 20Cu-*T* doped powders. Results showed an antibacterial activity for 20Cu-600 and 20Cu-900 powders against *E. coli* within 5 hours of incubation, and the number of viable bacteria was reduced by approximatively 8 log after 24 hours (**Fig. 3**). Concerning the series sintered at 1200°C, only a small antibacterial effect was observed after 24 hours with the 20Cu-1200 powder (**Fig. 3**).

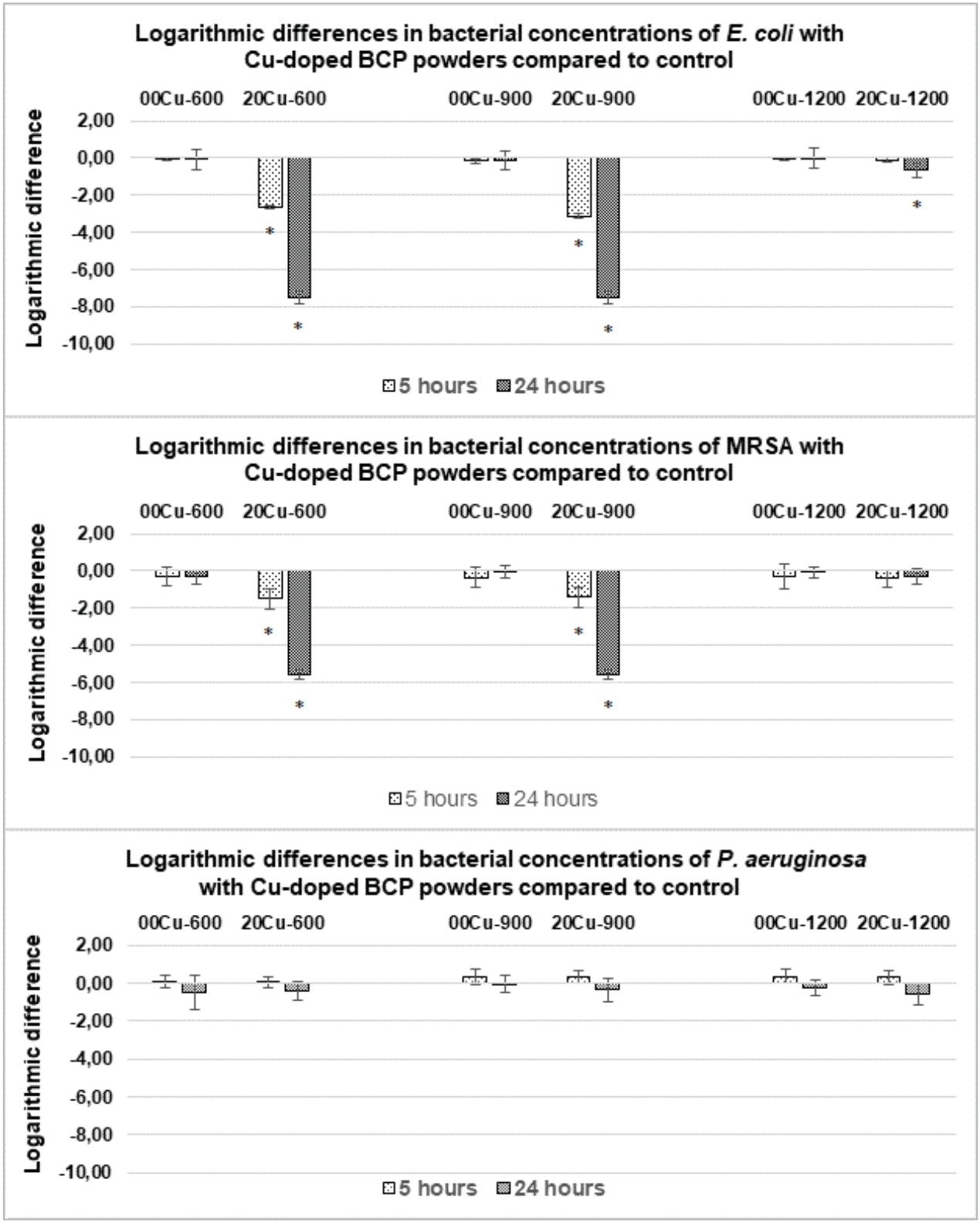

Fig. 3. Logarithmic differences in bacterial concentrations of *E. coli* (top), Methicillin-Resistant *S. aureus* (MRSA) (middle) and *P. aeruginosa* (bottom) with Cu-doped BCP powders compared to the control (undoped powders) after 5 hours and 24 hours. Results statistically different compared to the control (with $p < 0.05$) are indicated by "*".

Concerning the antibacterial activity against the clinical strain of MRSA, after 5 hours of incubation, a reduction of ~1.5 log was observed with 20Cu-600 and 20Cu-900, and after 24 hours no viable bacteria were detected with these 2 powders. The series sintered at 1200°C did not present an antibacterial effect. (**Fig. 3**). No significant antibacterial activity of the Cu-doped powders was observed with *P. aeruginosa,* even after 24 hours (**Fig. 3**).

Sampling was performed during bactericidal assays to measure the concentration of copper released in the culture medium, and the results are listed in **Table 3**. Whatever the strain tested, no variation in the copper release rate was observed. Powders containing higher dopant amounts released higher Cu^{2+} ion concentrations. Medium copper concentrations of the series treated at 600°C were ~2.4 ppm after 5 hours and ~2.6 ppm after 24 hours of incubation. For series treated at 900°C, medium copper concentrations were slightly lower, with ~1.7 ppm after 5 hours and ~2.4 ppm after 24 hours, and powders sintered at 1200°C released lower amounts of copper, with ~0.9 ppm and ~1.3 ppm after 5 hours and 24 hours of incubation, respectively.

Table 3. Average values of Cu^{2+} concentration (ppm) measured my MP-AES during antibacterial assays of the Cu-doped bioceramics.

Samples	Cu^{2+} concentration (ppm)	
	5 hours	24 hours
05Cu-600	2.2	2.2
10Cu-600	2.4	2.7
20Cu-600	2.7	2.8
05Cu-900	1.7	2.1
10Cu-900	1.5	2.2
20Cu-900	1.9	2.8
05Cu-1200	0.7	1.0
10Cu-1200	0.9	1.3
20Cu-1200	1.2	1.7

3.4. Antibacterial activity of Cu^{2+} copper ions in 1:500 diluted TS medium

Bactericidal assays were performed with a copper-containing TS medium (1/500th) over 24 hours. The results are presented in **Fig 4** and **Fig. 5**. Copper ions had an antibacterial activity against MSSA, MRSA and *E. coli* already at 1 ppm concentration (**Fig 4**). These antibacterial activities increased with copper concentration, and above 4 ppm no viable bacteria were detected. Concerning *P. aeruginosa*, no effect was observed with 2, 4, 6 and 8 ppm; 10 ppm was required to induce a reduction in the bacterial concentration (**Fig. 5**).

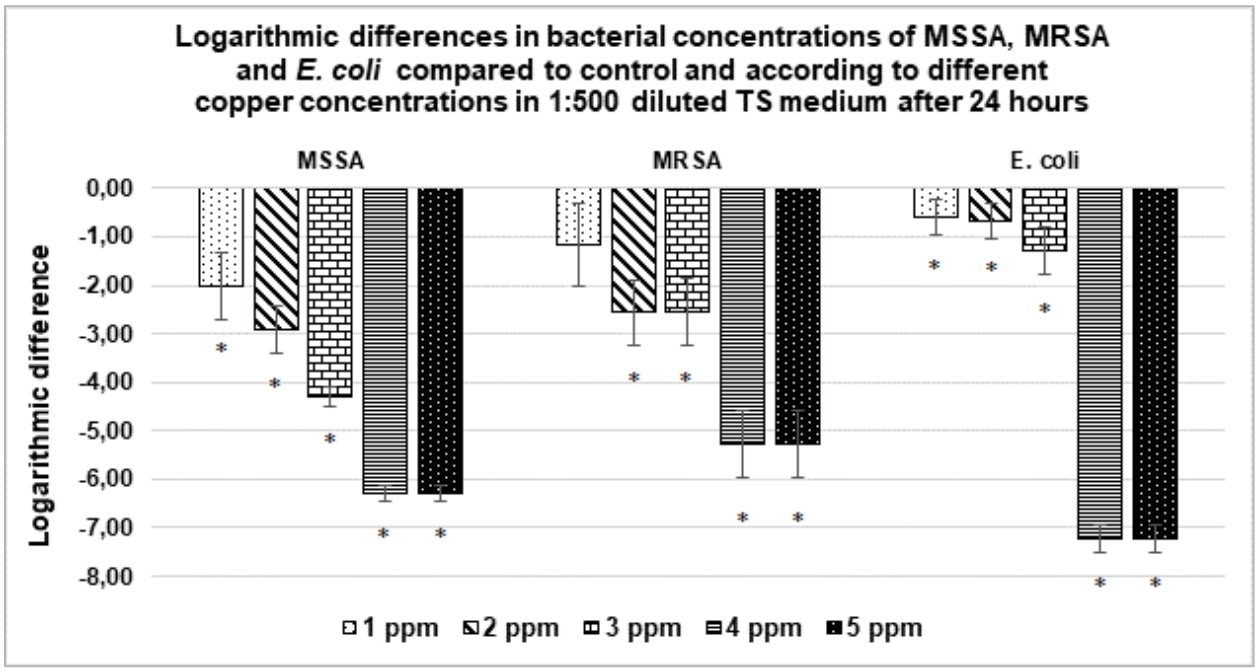

Fig 4. Variation in the bacterial concentration of MSSA, MRSA and *E. coli* with respect to different copper concentrations in 1:500 diluted TS medium after 24 hours. Results statistically different compared to the control (with $p < 0.05$) are indicated by "*".

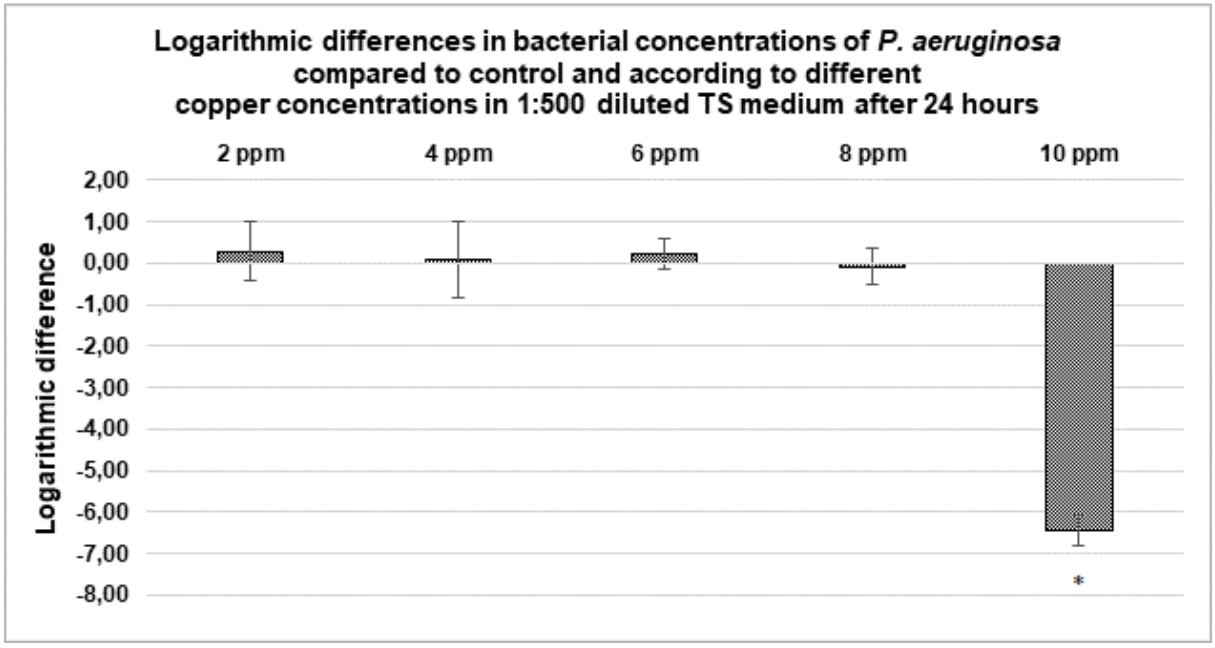

Fig 5. Variation in the bacterial concentration of *P. aeruginosa* with respect to different copper concentrations in 1:500 diluted TS medium after 24 hours. Results statistically different compared to the control (with $p < 0.05$) are indicated by "*".

3.5. Antibacterial activity against MSSA of Cu^{2+} copper ions in a non-diluted standard marrow cell culture medium

The antibacterial properties of copper (from 14 ppm to 20 ppm) were also assessed in a non-diluted standard marrow cell culture medium with the MSSA strain, and results are presented in **Fig. 6.** (copper concentrations below 14 ppm showed results similar to the control (0 ppm); therefore, bacterial concentration values are not presented here). Concentrations of 14, 16 and 18 ppm of Cu^{2+} exhibited antibacterial activity with -3, -4.5 and -5 log reductions, respectively. With 20 ppm no viable bacteria were detected.

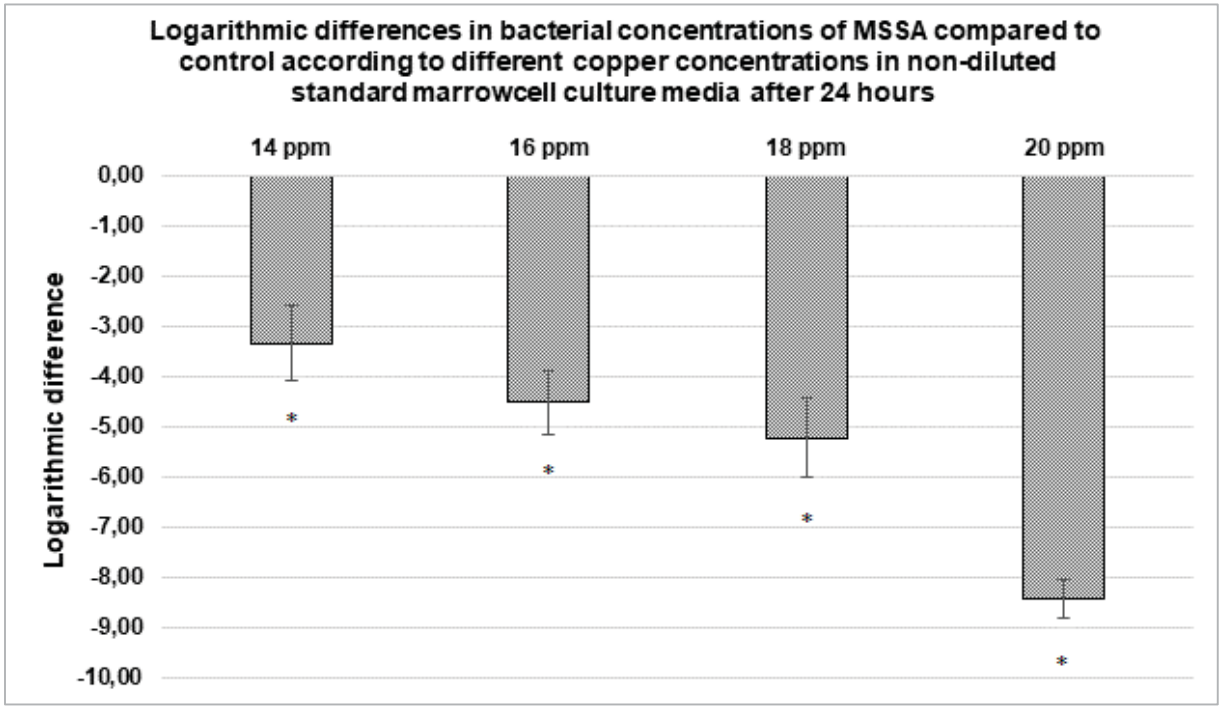

Fig 6. Variation in the bacterial concentration of MSSA with respect to different copper concentrations in a non-diluted standard marrow cell culture medium after 24 hours. Copper concentrations below 14 ppm showed results similar to the control (0 ppm); therefore, bacterial concentrations values are not presented here. Results statistically different compared to the control (with $p<0.05$) are indicated by "*".

4. Discussion

Cu-doped BCP powders are biomaterials capable of releasing Cu^{2+} ions into their environment, inducing biological interactions. This study enabled us to observe the impact of the HAp/β-TCP ratio on the solubility of the material and so on the dopant release rate. In our experiments, samples of the 600°C series containing about 12% of soluble β-TCP phase released the highest amount of copper during biological experiments, compared to the series sintered at 900°C with about 6% of the β-TCP phase (**Tables 1**, **2** and **3**). Series sintered at 1200°C, containing about 98% of poorly soluble HAp phase, presented the lowest copper release rate. Even more important than the HAp/ β-TCP ratio, it is necessary to take into consideration the dopant location at the atomic level in order to predict its rate of release. Our previous study [7] highlighted that thermal treatment at 600°C leads to a location at the crystal surface, at 900°C copper substitutes for calcium into the more soluble β-TCP phase, and at 1200°C copper inserts the less soluble HAp structure. Thus the dopant is easily accessible when sintering at 600°C and 900°C, and less accessible at 1200°C. In addition, results clearly indicate that the

amount of copper incorporated in the material during synthesis impacts the level of copper release (**Tables 2** and **3**).

In this study the cytotoxicity of Cu-doped BCP powders was evaluated with human Mesenchymal Stem Cells (h-MSCs), and none of the different Cu-doped powders tested presented toxicity. Murine/rat cell lines and osteoblastic cells are often used in cytotoxicity assays of bone biomaterials [18–21] and the Cu^{2+} cytotoxicity usually presents dose-dependent responses according to cell types [22]. H-MSCs are more representative of the cell type directly in contact with biomaterials during implantation procedure, so their use represents a suitable model for the development of functional synthetic implants.

Antibacterial assays demonstrated that the Cu-doped BCP powders used in this study had a strong antibacterial effect against clinical bacterial strains, including MRSA and MSSA isolated from osteoarticular infections. The use of clinical isolates is likely to provide a better overview of situations encountered in current medical practice [23,24]. Knowing that the increase in bacterial resistance to antibiotics is a major health issue [10], these results represent a promising solution to counter this issue. However, 10 ppm of Cu^{2+} were necessary to kill *P. aeruginosa*, whereas less than 4 ppm were effective against the other three strains (**Fig. 5** and **Fig. 4**). This opportunistic pathogen is known to be highly resistant, being able to survive drastic osmolarity changes and to develop multiple mechanisms of antimicrobial resistance [25,26]. These discrepancies highlight the importance of measuring the amount of copper released during experiments to determine the potentially dose-dependent effects for each bacterial strain tested.

Regarding the tested bacterial strains, American Type Culture Collection (ATCC) strains are commonly used, and this enables results to be easily compared between studies. Furthermore, the use of clinical strains isolated from patients with bone infections provides a much more realistic view of situations encountered in current medical practice [23,24].

We also showed that the biological environment in which experiments are performed can influence the bactericidal effect of copper. In a diluted and poor medium such as a 1:500 TS medium, 4 ppm of Cu^{2+} were effective to kill all bacteria, whereas in a rich standard marrow cell culture medium 20 ppm were necessary to reach the same effect (**Fig. 4** and **Fig. 6**). The antibacterial properties of copper probably depend on a balance between the amount of copper required for the lysis of bacteria and the division rate of the bacteria, directly related to the richness in nutrients of the environment. To our knowledge, this result has never before been described in the literature.

Copper, besides being an essential trace element required for human body health, is also involved in numerous biological functions and several metabolic processes, such as

angiogenesis and osteogenesis, two essential and related processes of wound-healing after a bone substitute implantation [11,27,28]. In 2009 Barralet *et al.* synthesized a copper-adsorbed macroporous scaffold and showed that low amounts of copper promote micro-vessel formation and the wound-healing process in mice [29]. In 2014 Kong *et al.* demonstrated that Cu ions contained in a calcium silicate bioceramic cause an increase in the vascularization of Human Umbilical Vein Endothelial Cells (HUVEC) and Human Dermal Fibroblasts (HDF) in co-culture and VEGF expression, attesting to a pro-angiogenic effect [30]. Ewald *et al.* observed an enhancement of the expression of bone-specific proteins in osteoblastic cells seeded on a scaffold loaded with Cu ions [31]. Recently, Zhang *et al.* synthesized a Cu-substituted dicalcium silicate cement and showed that the quantitative new bone formation was significantly higher with Cu cement than for undoped cement [32]. Thus the use of materials doped with copper ions, able to both prevent infections and promote wound healing, represents a promising research subject.

5. Conclusion

The aims of this work were to investigate the biological properties of Cu-doped BCP powders and the influence of their chemical characteristics on the results observed. For these purposes, the present study evaluated the cytotoxicity, the antibacterial properties and the release rate of Cu^{2+} ions of a set of twelve Cu-doped BCP powders.

Concerning the chemical characteristics of the powders, this study allowed us to describe the impact of the sintering temperature on the ratio of HAp and β-TCP phases and on the atomic location of the copper, both influencing the accessibility of the doping element during contact with a biological medium. The proportion of the poorly soluble HAp phase increases with the annealing temperature, leading to a lower copper release rate. Furthermore, the amount of copper incorporated in the material during synthesis impacts the level of copper release. These features represent a major factor, which can easily be controlled during synthesis in order to adapt the material to the biological needs. Cytotoxicity evaluation clearly demonstrated that all the Cu-doped BCP powders exhibited no toxicity against h-MSCs, which is an essential step in the implantation of a bone substitute. Copper ions released by the powders exhibit a strong antibacterial activity against 2 clinical strains of *S. aureus*, including one resistant to methicillin, and against *E. coli*. Additional results indicated that a higher Cu^{2+} concentration was required to show an antibacterial effect against *P. aeruginosa*. Newly described results indicated that the antibacterial properties of copper depend on a balance between the copper concentration and the composition of the biological fluids.

In conclusion, this work enabled the development of promising biomaterials, which are biocompatible, with strong antibacterial properties and adjustable synthesis, in order to meet biological needs. A study of complementary biological properties (e.g. angiogenesis and osteogenesis) would further enable the bio-adaptation of bone substitutes and contribute to the development of bone tissue engineering.

References

[1] N. Eliaz, N. Metoki, Calcium phosphate bioceramics: A review of their history, structure, properties, coating technologies and biomedical applications, Materials (Basel). 10 (2017). https://doi.org/10.3390/ma10040334.

[2] S. V Dorozhkin, Bioceramics of calcium orthophosphates, Biomaterials. 31 (2010) 1465–1485. https://doi.org/10.1016/j.biomaterials.2009.11.050.

[3] S. V Dorozhkin, Biocomposites and hybrid biomaterials based on calcium orthophosphates., Biomatter. 1 (2011) 3–56. https://doi.org/10.4161/biom.1.1.16782.

[4] S. V. Dorozhkin, Calcium orthophosphates, J. Mater. Sci. 42 (2007) 1061–1095. https://doi.org/10.1007/s10853-006-1467-8.

[5] G. Daculsi, R.Z. Legeros, E. Nery, K. Lynch, B. Kerebel, Transformation of biphasic calcium phosphate ceramics in vivo: Ultrastructural and physicochemical characterization, J. Biomed. Mater. Res. 23 (1989) 883–894. https://doi.org/10.1002/jbm.820230806.

[6] M. Ebrahimi, M.G. Botelho, S. V. Dorozhkin, Biphasic calcium phosphates bioceramics (HA/TCP): Concept, physicochemical properties and the impact of standardization of study protocols in biomaterials research, Mater. Sci. Eng. C. 71 (2017) 1293–1312. https://doi.org/10.1016/j.msec.2016.11.039.

[7] S. Gomes, C. Vichery, S. Descamps, H. Martinez, A. Kaur, A. Jacobs, J.M. Nedelec, G. Renaudin, Cu-doping of calcium phosphate bioceramics: From mechanism to the control of cytotoxicity, Acta Biomater. 65 (2018) 462–474. https://doi.org/10.1016/j.actbio.2017.10.028.

[8] J. Calhoun, M.M. Manring, M. Shirtliff, Osteomyelitis of the Long Bones, Semin. Plast. Surg. 23 (2009) 059–072. https://doi.org/10.1055/s-0029-1214158.

[9] G.J.A. ter Boo, D.W. Grijpma, T.F. Moriarty, R.G. Richards, D. Eglin, Antimicrobial delivery systems for local infection prophylaxis in orthopedic- and trauma surgery, Biomaterials. 52 (2015) 113–125. https://doi.org/10.1016/j.biomaterials.2015.02.020.

[10] F.C. Tenover, Mechanisms of antimicrobial resistance in bacteria, Am. J. Infect. Control. 34 (2006) S3–S10. https://doi.org/10.1016/j.ajic.2006.05.219.

[11] P. Chellan, P.J. Sadler, The elements of life and medicines, Philos. Trans. R. Soc. A Math. Phys. Eng. Sci. 373 (2015). https://doi.org/10.1098/rsta.2014.0182.

[12] M. Vincent, R.E. Duval, P. Hartemann, M. Engels-Deutsch, Contact killing and antimicrobial properties of copper, J. Appl. Microbiol. 124 (2018) 1032–1046. https://doi.org/10.1111/jam.13681.

[13] F. Heidenau, W. Mittelmeier, R. Detsch, M. Haenle, F. Stenzel, G. Ziegler, H. Gollwitzer, A novel antibacterial titania coating: Metal ion toxicity and in vitro surface colonization, J. Mater. Sci. Mater. Med. 16 (2005) 883–888. https://doi.org/10.1007/s10856-005-4422-3.

[14] Ž. Radovanović, B. Jokić, D. Veljović, S. Dimitrijević, V. Kojić, R. Petrović, D. Janaćković, Antimicrobial activity and biocompatibility of Ag + - and Cu 2+ -doped biphasic hydroxyapatite/α-tricalcium phosphate obtained from hydrothermally synthesized Ag + - and Cu 2+ -doped hydroxyapatite, Appl. Surf. Sci. 307 (2014) 513–519. https://doi.org/10.1016/j.apsusc.2014.04.066.

[15] A. Bhattacharjee, Y. Fang, T.J.N. Hooper, N.L. Kelly, D. Gupta, K. Balani, I. Manna, T. Baikie, P.T. Bishop, T.J. White, J. V. Hanna, Crystal chemistry and antibacterial properties of cupriferous hydroxyapatite, Materials (Basel). 12 (2019). https://doi.org/10.3390/ma12111814.

[16] A. Jacobs, G. Renaudin, C. Forestier, J. Nedelec, S. Descamps, Biological properties of copper-doped biomaterials for orthopedic applications: a review of antibacterial, angiogenic and osteogenic aspects, Acta Biomater. (2020). https://doi.org/10.1016/j.actbio.2020.09.044.

[17] C. Marquès, C. Franceschi, V. Collin, F. Laurent, S. Chatellier, C. Forestier, Genome sequence of a clinical Staphylococcus aureus strain from a prosthetic joint infection, Genome Announc. 4 (2016). https://doi.org/10.1128/genomeA.00198-16.

[18] Y. Li, J. Ho, C.P. Ooi, Antibacterial efficacy and cytotoxicity studies of copper (II) and titanium (IV) substituted hydroxyapatite nanoparticles, Mater. Sci. Eng. C. 30 (2010) 1137–1144. https://doi.org/10.1016/j.msec.2010.06.011.

[19] C.F. Marques, S. Olhero, J.C.C. Abrantes, A. Marote, S. Ferreira, S.I. Vieira, J.M.F. Ferreira, Biocompatibility and antimicrobial activity of biphasic calcium phosphate powders doped with metal ions for regenerative medicine, Ceram. Int. 43 (2017) 15719–15728. https://doi.org/10.1016/j.ceramint.2017.08.133.

[20] K. Sahithi, M. Swetha, M. Prabaharan, A. Moorthi, N. Saranya, K. Ramasamy, N. Srinivasan, N.C. Partridge, N. Selvamurugan, Synthesis and characterization of nanoscale-hydroxyapatite-copper for antimicrobial activity towards bone tissue engineering applications, J. Biomed. Nanotechnol. 6 (2010) 333–339. https://doi.org/10.1166/jbn.2010.1138.

[21] L. Gritsch, C. Lovell, W.H. Goldmann, A.R. Boccaccini, Fabrication and characterization of copper(II)-chitosan complexes as antibiotic-free antibacterial biomaterial, Carbohydr. Polym. 179 (2018) 370–378. https://doi.org/10.1016/j.carbpol.2017.09.095.

[22] K. Li, C. Xia, Y. Qiao, X. Liu, Dose-response relationships between copper and its biocompatibility/antibacterial activities, J. Trace Elem. Med. Biol. 55 (2019) 127–135. https://doi.org/10.1016/j.jtemb.2019.06.015.

[23] A. Gristina, Biomaterial-centered infection: microbial adhesion versus tissue integration, Science (80-.). 237 (1987) 1588–1595. https://doi.org/10.1126/science.3629258.

[24] A. V. Karlov, I.A. Khlusov, V.A. Pontak, V.P. Ignatov, M.A. Ivin, S.Y. Zinatulina, Adhesion of Staphylococcus aureus to implants with different physicochemical characteristics, Bull. Exp. Biol. Med. 134 (2002) 277–280. https://doi.org/10.1023/A:1021567804286.

[25] U. Çetiner, I. Rowe, A. Schams, C. Mayhew, D. Rubin, A. Anishkin, S. Sukharev, Tension-activated channels in the mechanism of osmotic fitness in Pseudomonas Aeruginosa, J. Gen. Physiol. 149 (2017) 595–609. https://doi.org/10.1085/jgp.201611699.

[26] D.M. Livermore, Multiple Mechanisms of Antimicrobial Resistance in Pseudomonas aeruginosa: Our Worst Nightmare?, Clin. Infect. Dis. 34 (2002) 634–640. https://doi.org/10.1086/338782.

[27] N.M. Lowe, W.D. Fraser, M.J. Jackson, Is there a potential therapeutic value of copper and zinc for osteoporosis?, Proc. Nutr. Soc. 61 (2002) 181–185. https://doi.org/10.1079/pns2002154.

[28] W. Opsahl, H. Zeronian, M. Ellison, D. Lewis, R.B. Rucker, R.S. Riggins, Role of copper in collagen cross-linking and its influence on selected mechanical properties of chick bone and tendon, J. Nutr. 112 (1982) 708–716. https://doi.org/10.1093/jn/112.4.708.

[29] J. Barralet, U. Gbureck, P. Habibovic, E. Vorndran, C. Gerard, C.J. Doillon, Angiogenesis in Calcium Phosphate Scaffolds by Inorganic Copper Ion Release, Tissue Eng. Part A. 15 (2009) 1601–1609. https://doi.org/10.1089/ten.tea.2007.0370.

[30] N. Kong, K. Lin, H. Li, J. Chang, Synergy effects of copper and silicon ions on stimulation of vascularization by copper-doped calcium silicate, J. Mater. Chem. B. 2 (2014) 1100–1110. https://doi.org/10.1039/c3tb21529f.

[31] A. Ewald, C. Käppel, E. Vorndran, C. Moseke, M. Gelinsky, U. Gbureck, The effect of Cu(II)-loaded brushite scaffolds on growth and activity of osteoblastic cells, J. Biomed. Mater. Res. - Part A. 100 A (2012) 2392–2400. https://doi.org/10.1002/jbm.a.34184.

[32] F. Zhang, M. Zhou, W. Gu, Z. Shen, X. Ma, F. Lu, X. Yang, Y. Zheng, Z. Gou, Zinc-/Copper-Substituted Dicalcium Silicate Cement: Advanced Biomaterials with Enhanced Osteogenesis and Long-term Antibacterial Properties, J. Mater. Chem. B. (2020) 1–21. https://doi.org/10.1039/c9tb02691f.

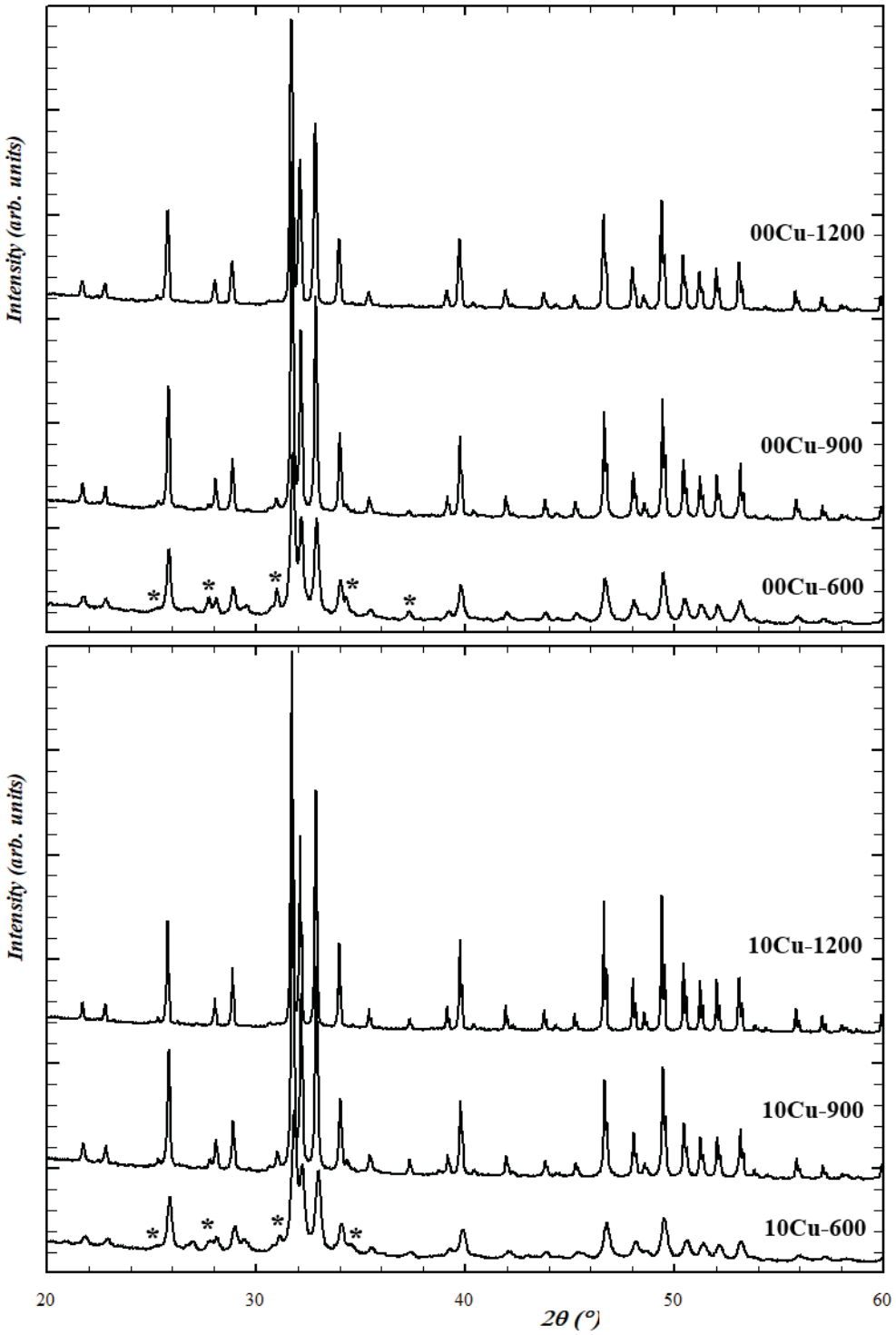

Figure SEI1. Examples of part (20° < 2θ < 60°) of the X-ray powder patterns recorded for the two 00Cu-*T* (top) and 10Cu-*T* series (bottom). Stars locate the main diffraction peaks of β-TCP.

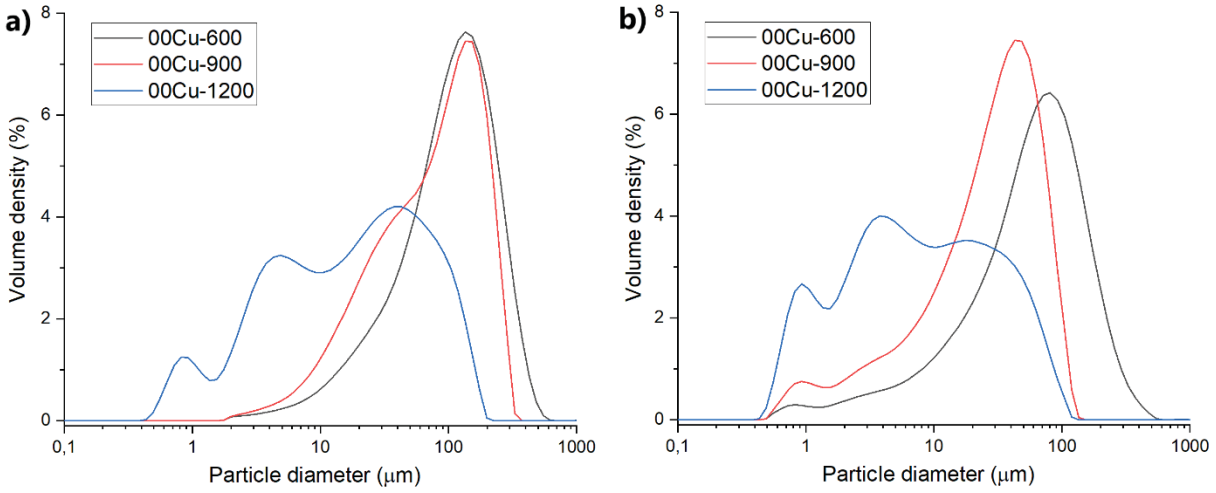

Figure SEI2. Particle size distributions for the undoped 00Cu-*T* series obtained without (a) and with (b) ultrasonic particles separation.

Table SEI1. Values of metabolic activity (%) of h-MSCs obtained after 3, 7 and 15 days of culture with different Cu-doped BCP powders. Ct+ correspond to the positive control and Ct- correspond to the negative control. Data are given as mean ± standard error from n = 9 replicates.

Samples	Metabolic activity (%)		
	Day 3	Day 7	Day 15
Ct+	100 ± 12.3	100 ± 18.1	100 ± 10.1
Ct -	13.3 ± 11.1*	21 ± 6.8*	18.6 ± 10.7*
00Cu-600	97.0 ± 15.9	118.5 ± 16	84.7 ± 20.8
05Cu-600	85.7 ± 19.9	104.6 ± 18.6	85.8 ± 14.3
10Cu-600	82.3 ± 13.8	98.9 ± 14.4	77.9 ± 19.4
20Cu-600	77.6 ± 22.5	100.1 ± 23.5	78.4 ± 18
00Cu-900	105.2 ± 18.1	103.4 ± 18.7	90 ± 24
05Cu-900	94.4 ± 15.2	97.5 ± 11.3	87.4 ± 21
10Cu-900	93.5 ± 13.4	92.1 ± 23.7	90.9 ± 25.5
20Cu-900	87.4 ± 18.8	99.3 ± 17.3	84.6 ± 12.1
00Cu-1200	107.6 ± 15.4	106.6 ± 20.7	82.2 ± 21.7
05Cu-1200	92.7 ± 13.2	90.8 ± 21.6	80.6 ± 22.9
10Cu-1200	85.6 ± 14.2	94.8 ± 19.6	77.8 ± 18
20Cu-1200	88.9 ± 21.5	115.5 ± 13.8	103.6 ± 8.9

* significant decrease

CHAPITRE 4 : EVALUATION DE LA CYTOTOXICITE ET DES PROPRIETES ANTIBACTERIENNES DE PASTILLES DE PHOSPHATES DE CALCIUM BIPHASIQUES DOPEES AU CUIVRE

La cytotoxicité et l'activité antibactérienne des pastilles de BCP (Cu0-1050 et Cu10-1050) présentées **Figure 2.12** et **Tableau 2.3** du **Chapitre 2** de ce manuscrit ont également été évaluées. Les 2 types de pastilles, non dopée et dopée, ont été étudiées dans le but d'évaluer l'impact du dopage au cuivre sur les réponses biologiques observées. Dans ce chapitre une notation différente de celle utilisée dans le Chapitre 2 a été définie, à savoir : « BCP » pour les pastilles non dopées et « Cu:BCP » pour les pastilles dopées, notamment du fait que ces matériaux sont beaucoup plus riches en la phase β-TCP par rapport aux poudres des chapitres précédents. La comparaison de ce chapitre avec le précédent a pour but de regarder l'effet de la mise en forme (poudre versus pastille) sur les réponses en milieu biologique.

Comme précédemment, la cytotoxicité de ces matériaux a été évaluée sur des cellules souches mésenchymateuses humaines ont été mises en culture à la surface des pastilles puis le test colorimétrique MTT a été utilisé pour évaluer l'activité métabolique des cellules après 3 jours, 7 jours et 14 jours de culture.

L'activité antibactérienne a été évaluée sur les mêmes souches que précédemment c'est-à-dire 2 souches cliniques Gram positive : *S. aureus* et *S. aureus* résistant à la méticilline, toutes les 2 isolées sur des patients atteints d'infections ostéo-articulaires, et 2 souches de la collection ATCC Gram négative : *E. coli* et *P. aeruginosa*. Cette partie du travail a été réalisée dans les locaux du Laboratoire Microorganismes : Génome et Environnement (LMGE) de l'Université Clermont Auvergne à Clermont-Ferrand et avec la collaboration du Professeur Christiane Forestier.

En parallèle de ces expérimentations, les taux de cuivre relargué par les pastilles dopées pendant ces études biologiques ont été mesurés par spectroscopie d'émission atomique afin d'évaluer les concentrations de dopant impliqués dans les réponses biologiques observées.

En résumé, cette étude a montré que les pastilles ont une composition biphasique avec 60% d'HAp et 40% de β-TCP. L'évaluation de la cytotoxicité a montré que les pastilles dopées

n'induisent aucune cytotoxicité envers les cellules souches mésenchymateuses humaines après 3, 7 et 15 jours pour des concentrations de cuivre relargué allant jusqu'à 25 ppm. Des images MEB ont montré que les cellules s'étalent largement à la surface des 2 types de pastilles. Concernant l'activité antibactérienne des matériaux dopés, une diminution significative de la concentration bactérienne est observée après 24h pour les 4 souches testées avec en moyenne 1,42 ppm de cuivre relargué.

Il ressort de cette étude que la mise en forme du biomatériau a un impact sur les taux de relargage en cuivre. Ceci n'affecte pas leur biocompatibilité, aucune cytotoxicité n'a été observée. En revanche l'efficacité antibactérienne est impactée : les pastilles présentent une activité antibactérienne sur les 4 souches testées (contre 3 pour les poudres), avec cependant une efficacité moindre pour 3 d'entre elles.

L'intégralité des résultats obtenus décrivant la cytotoxicité et l'activité antibactérienne des pastilles de BCP dopées au cuivre sont présentés dans l'article suivant :

Aurélie Jacobs, Stéphane Descamps, Lorélène Gasnier, Mathilde Prudent, Coralie Laurent, Jean-Marie Nedelec, Christelle Blavignac, Nicolas Charbonnel, Christiane Forestier, David Marchat, Guillaume Renaudin, **Copper-doped Biphasic Calcium Phosphate bioceramic disks: copper release, cytotoxicity and antibacterial property**, (article en préparation pour soumission)

Copper-doped Biphasic Calcium Phosphate bioceramic disks: copper release, cytotoxicity and antibacterial property

Aurélie JACOBS[1], Stéphane DESCAMPS[1], Lorélène Gasnier[3], Mathilde Prudent[3], Coralie LAURENT[3], Jean-Marie NEDELEC[1], Christelle BLAVIGNAC[4], Nicolas CHARBONNEL[2], Christiane FORESTIER[2], David MARCHAT[3], Guillaume RENAUDIN[1*]

[1] Université Clermont Auvergne, CNRS, SIGMA Clermont, ICCF, F-63000 Clermont-Ferrand, France.

[2] Université Clermont Auvergne, CNRS, Laboratoire Microorganismes : Genome et Environnement, F-63000 Clermont-Ferrand, France.

[3] Ecoles des Mines Saint-Etienne, Centre Ingénierie et Santé, F-42000 ; Saint-Etienne, France

[4] Université Clermont Auvergne, Centre Imagerie Cellulaire Santé, F-63000 Clermont-Ferrand, France

Abstract

This study concerns the synthesis of copper-doped biphasic calcium phosphate (BCP) ceramics sintered disks and their chemical and biological characterizations. BCP were synthesized by aqueous precipitation method, including precise control of reaction parameters to obtain copper-doped bioceramics, followed by heat treatment under controlled atmosphere to sinter disks. Materials obtained consist of 60 % of HAp and 40 % of β-TCP (w/w). MTT assays were performed with human-mesenchymal stems cells (h-MSCs) and no cytoxicity was found after two weeks of culture at the surface of copper-doped BCP ceramics disks with concentrations of copper released reaching 25 ppm. Regarding antibacterial properties, our copper doped bioceramic disks induced significant decreases of bacterial concentrations after 24 hours of incubation with the four tested strains: methicillin sensitive *S. aureus* (MSSA), methicillin resistant *S. aureus* (MRSA), *E. coli* and *P. aeruginosa*.

1. *Introduction*

The use of bone substitutes is a common practice since every year bone graft procedures represent 2.2 million surgical acts worldwide [1]. These interventions occur in cases of bone defects or poor filling of the damaged area after a trauma, a non-contiguous fracture or a disease requiring bone tissue removal. Synthetic bone substitutes are in development as conventional solutions (autograft and allograft) are limited in terms of both quantity or quality [2]. Their purpose is to replace bone and rebuild a deficient bone stock in a completely safe way or to act as prosthesis coatings to improve the bond between tissue and material [3].

During biomaterials implantation, the development of infections need to be prevent since infections in bone sites are difficult to treat and consequences for the patient are severe with delayed healing, revision surgery and longer hospitalization times and increased costs [4]. Infections rates vary from 0.7% to 4.2% for elective surgery and reach 30 % in cases of third-degree open fractures [5]. The use of antibiotics in prophylaxis is therefore not always sufficient and the increase of resistance to antibiotics intensifies this problematic [6,7].

Among synthetic bone substitutes, biphasic calcium phosphates (BCP) are widely-studied for bone repair surgery because of their chemical and structural similarities with the mineral part of bones [8]. BCP is by definition composed of hydroxyapatite (HAp, $Ca_{10}(PO_4)_6(OH)_2$) and beta-tricalcium phosphate (β-TCP, $Ca_3(PO_4)_2$) [9]. Contrary to sintered HAp, β-TCP is biodegradable and is readily replaced by new bone [10], allowing to adapt the biodegradation rate and the ion-release kinetics depending on the clinical needs [11]. Furthermore, a striking feature of calcium phosphates (CaP), and particularly of the apatite group, is that the crystal structure can accommodate many different ions [12]. Apatite and β-TCP can incorporate ions of half of the elements in the periodic table into their crystallographic structures, whose some ions of biological interest, especially for bone repair such as zinc, silicate, strontium, carbonate or copper [10,13,14]. In materials chemistry, the addition of chemical elements of interest in small quantities refers to chemical doping [15]. Thus, CaP bioceramics can be used as delivery vehicles for bioinorganics [16], also called by-products, that can affect cell fate decisions [17].

Copper is the third most prevalent mineral present in the body with 100 mg of copper in a 70 kg healthy body [18]. This metallic cation is required by living organisms because it is involved in several biological processes as respiration, production of energy, bone mineralization, osteoblasts functions, maturation and growth of tissues collagens [19–21]. Furthermore, copper is used for centuries for its antibacterial properties with limited cytotoxicity [22]. Cu^{2+} copper cation appears to be a promising doping candidate to improve the behavior of biomaterials used in bone repair surgery. The use of copper with orthopedic biomaterials and

their biological properties (including antibacterial effect) have been widely studied and synthesized in our recent review [23]. For example, in 2010 Li *et al.* evaluated Cu-doped HAp powders against *E. coli* and results indicated a survival rate less than 1% after 24 h [24]. Recently, Bhattacharjee *et al.* synthesized Cu-doped HAp which exhibited antibacterial properties against *E. coli* and *S. aureus* [25]. Conversely, no antibacterial effect of copper-doped BCP ceramics (84% HAp/16% β-TCP w/w) was found by Marques *et al.* with the two same strains but not the same ceramic manufacturing processes [26]. The existence of contradictory results demonstrates the interest of developing this research topic, and the importance of starting these studies with a mastery of the synthetic processes necessary for mastering the chemistry of the materials developed for biological applications.

The purpose of our study was to investigate the cytotoxicity and antibacterial property of undoped and Cu-doped BCP bioceramics. Powders were synthesized by original aqueous precipitation methods, phases composition and incorporation of the dopant within the HAp and β-TCP crystallographic structures were evaluated by X-ray powder diffraction (XRPD) and Rietveld treatments. *In vitro* cytotoxicity assays were performed according to standard procedure with human-Mesenchymal Stems Cells (h-MSCs) collected during hip arthroplasty. The antibacterial activity of copper-doped BCP ceramics was investigated against 4 bacterial strains: Methicillin-sensitive *Staphylococcus aureus* (MSSA), Methicillin-Resistant *S. aureus* (MRSA), *Escherichia coli* and *Pseudomonas aeruginosa*. The biological responses were finally studied as function of the amount of copper released by the ceramics; which was measured alongside with biological responses. The present results from polished ceramic disks complement our previous biological behavior study on related crushed powder bioceramic (Paper submitted to Biomaterials; text available in Chapter III of this manuscript).

2. Materials and methods

2.1. Powders synthesis

Cu-doped (CDCuHA) and undoped (CDHA) calcium deficient hydroxyapatites were synthesized by aqueous precipitation methods using a fully automated apparatus composed of jacketed reactors (20 and 30 L, De Dietrich, France), cryothermostats (Huber, Germany), stirring devices, and peristaltic (Masterflex L/S, U.S.A.) and dosing (ProMinent, U.K.) pumps.
CDHA was obtained by a conventional method where a diammonium hydrogen phosphate aqueous solution ($(NH_4)_2HPO_4$, EMSURE® ACS, Merck, Germany, [P] = 1.43 mol/L) was added at 350 mL/min to calcium nitrate solution ($Ca(NO_3)_2 \cdot 4H_2O$, 99% pure, Merck, Germany, [Ca] = 2.33 mol/L) maintained under stirring (600 rpm). The reaction was performed under an

argon flow (4.8, Air Products, 0.1 mL/min) to prevent the formation of carbonate-containing apatites. The pH of the suspension was adjusted to 7.0 by the addition of 28% ammonia solution (Merck, 28-30% EMSURE® ACS, Germany) using a dosing pump coupled with a pH controller (Mettler Toledo M400, U.S.A.) and a pH electrode (Mettler Toledo Inpro 4800/120/PT100, U.S.A.). The temperature was controlled and regulated automatically at 35 °C with an external T-probe connected to a cryothermostat. After complete introduction of the phosphate solution, the suspension was matured for 19 h and finally centrifuged at 4000 rpm for 5 min (ThermoFisher Scientific, Sorvall Legend XF, France). Based on original unpublished data, and in order to obtain a CDHA powder with a final Ca/P molar ratio of 1.597 (i.e., $Ca_{10-x}(HPO_4)_x(PO_4)_x(OH)_{2-x}$ with $x = 0.42$), the Ca/P molar ratio of the reagents was fixed at 1.624 with these synthesis conditions. The general precipitation reaction in aqueous solution can be written as follows (Eq.1):

$$(10-x)\ Ca^{2+} + 6\ HPO_4^{2-} + (8-2x)\ OH^- \leftrightarrows Ca_{10-x}(PO_4)_{6-x}(HPO_4)_x(OH)_{2-x} + (6-x)\ H_20 \qquad \text{Eq.1}$$

CDCuHA was prepared through two successive reactions: the precipitation then the hydrolysis of a copper-doped brushite. This way was chosen because Cu^{2+} ions is stable below pH 5-6 [27,28], and brushite (dicalcium phosphate dihydrate, DCPD, $CaHPO_4 \cdot 2H_20$) is the most stable phase of calcium-phosphate system in acidic environments [29]. The first stage of the process consisted in adding (100 mL/min) a diammonium hydrogen phosphate aqueous solution (EMSURE® ACS, Merck, Germany, [P] = 0.80 mol/L) to an homogeneous mixture of calcium and copper nitrate solutions ($Ca(NO_3)_2 \cdot 4H_2O$, $Cu(NO_3)_2 \cdot 3H_2O$, EMSURE®, Merck, Germany, [Ca] = 1.08 mol/L, [Cu] = 0.01 mol/L) to form a copper(II)-doped brushite ($Ca_{(1-z)}Cu_{(z)}HPO_4 \cdot 2H_2O$ ([30]) by the following general reaction (3.5<pH<4.5):

$$(1-z)\ Ca^{2+} + z\ Cu^{2+} + H_2PO_4^{2-} \leftrightarrows Ca_{(1-z)}Cu_{(z)}HPO_4 \cdot 2H_2O + H_30^+ \qquad \text{with } z < 0.25\ [30] \qquad \text{Eq.2}$$

This precipitation was performed in an excess of cations with respect to the stoichiometry of the reaction Eq.2 (Ca/P = 1.6667 and (Ca+Cu)/P= 1.6833), and the pH was not adjusted and varied between 3.5 and 4.5. This suspension was maintained under stirring (550 rpm) and argon flow for 3 h at 40 °C.

The conversion of this copper(II)-doped brushite into CDCuHA was made by adjusting the reaction pH at 7.0 with 28% ammonia solution according to the following general reaction (Eq. 3) considering the interstitial insertion of copper (II) ions into the HAp crystal lattice (Wyckoff site 2*b*) [14]:

$$(4-x+6z_1)\ Ca^{2+} + z_2\ Cu^{2+} + 6\ Ca_{(1-z1)}Cu_{(z1)}HPO_4 \cdot 2H_2O + (8-2x+2z)\ OH^- \leftrightarrows Ca_{10-x}Cu_z(PO_4)_{6-x}(HPO_4)_x(OH)_{2-2z-x}(O)_{2z} + (6-x+2z)\ H_20 \qquad \text{with } z = 6z_1 + z_2,\ 0 \le x \le 1 \text{ and } z \le 0.1\ [14] \qquad \text{Eq.3}$$

This reaction was continued for 24 h at 40 °C under stirring (550 rpm) and bubbling nitrogen gas, then stopped by centrifuging the suspension at 4000 rpm for 5 min.
Immediately after centrifugation both CDHA and CDCuHA wet cakes were frozen at - 80 °C, then freeze-dried (Pilote Compact, Cryotec, France) to obtain the raw powders.

2.2. Manufacturing of BCP and Cu:BCP ceramic disks

CDHA and CDCuHA raw powders were heat-treated at 700 °C for 2 h under 93 kPa of N_2 (Azote 5.2, Air products, France) and 7 kPa of H_2O (ramp of 4 °C/min) to remove synthesis residues (e.g., NH_4NO_3) and reduce their specific surface area below 30 m²/g. This heat-treatment was performed in a tube furnace (RS 80/500/13, Nabertherm, Germany) with a gas flow produced by a controlled humidity generator (Wetsys, SETARAM, France; gas temperature = 40 °C with 90% relative humidity and a flow rate of 150 mL/min).

CDHA and CDCuHA disks were formed by pressing 500 mg of each powder at 50 MPa in a 12.7 mm diameter stainless steel die (LR50K, LLOYD Instruments, UK). This uniaxial pressing was followed by a cold isostatic pressing under 300 MPa (Nova Swiss, Switzerland). These pellets were sintered at 1050 °C for 3 h under air (LH15/13, Nabertherm, Germany) and 1050°C for 5 h under 93 kPa of N_2 and 7 kPa of H_2O (ramps of 4 °C/min), respectively. During these heat-treatments, CDHA and CDCuHA decomposed in undoped (BCP) and Cu-doped (Cu:BCP) biphasic calcium phosphates according to the following general reaction occurring between 720°C and 840°C:

$$Ca_{10-x}Cu_z(PO_4)_{6-x}(HPO_4)_x(OH)_{2-2z-x}(O)_{2z} \xrightarrow{\Delta} \left(\frac{1-x+z}{1+z}\right) Ca_{10}Cu_z(PO_4)_6(OH)_{2-2z}(O)_{2z} + \left(\frac{3x}{1+z}\right) Ca_{3-\frac{z}{3}}Cu_{\frac{z}{3}}(PO_4)_2 + \left(\frac{x\,(1-z)}{1+z}\right) H_2O \quad \text{with } 0 \leq x \leq 1 \text{ and } z \leq 0.1 \qquad \text{Eq.4}$$

Finally, ceramic disks were mirror polished with successive diamond pastes to a 1 µm finish (Mecapol P320, PRESI). The ‘BCP’ and ‘Cu:BCP’ labels will be used in the following to indicate respectively the undoped and copper-doped sintered ceramic disks.

2.3. Ceramic disks characterization

2.3.1 Scanning Electronic Microscopy (SEM) coupled with Energy Dispersive X-Ray Spectroscopy (EDS) analyses

Electronic microscopy observations used a ZEISS SUPRA 55VP (Carl Zeiss Microscopy Ltd.,Cambridge, UK) with GEMINI Field Emission-Scanning Electron Microscope (Carl Zeiss MicroscopyLtd., Cambridge, UK) and were carried out on polished surface disks after gold metallization. Quantitative analyses were performed using an EDS (OXFORD XMAX 80N+80 mm2Si-detector (Oxford Instruments, High Wycombe, UK) combined with OXFORD AZtecAdvanced V3.3 software (Oxford Instruments, High Wycombe, UK) on Ca, P, and Cu elements. Measurements were made using an acceleration voltage of 20 kV and 30 seconds of acquisition on two wide areas (magnification ×100 and ×1000).

2.3.2 X-ray Powder Diffraction (XRPD) and Rietveld analyses

XRPD measurements were performed as described in a previous work [14]. Briefly, a Philips X'Pert Pro PANalytical diffractometer (Almelo, Netherlands) equipped with a solid detector X-Celerator was used, with θ-θ geometry, reflection mode, and using Cu K□ radiation (k = 1.54184 Å). XRPD patterns were recorded at room temperature in the interval 3° < 2θ < 120°, with a step size of Δ2θ = 0.0167° and a counting time of 200s for each data value. Rietveld refinements were performed for each samples using the program FullProf.2k and the Rietveld strategy used was detailed in a previous work [31].

2.4. Cytotoxicity evaluation

2.4.1 Human mesenchymal stem cells (h-MSCs) culture

The procedures to collect and to culture these cells are described in our previous work (Paper submitted to Biomaterials; text available in Chapter III of this manuscript). Briefly, h-MSCs were extracted from metaphysal cancellous bone collected during hip arthroplasty on healthy patients who have signed an authorization for the use of their bone for research purposes. Collagenase was used to take off cells from bone pieces. After centrifugation to obtain a cell pellet, all types cells were cultured for 3 days. Finally, rinses allowed to conserve only adherent h-MSCs and cells were cultured with a weekly change of standard marrow cell culture medium (composition available in Chapter III). When cells reach confluence, they are collected by trypsinization for expansion up to have enough cells for cytotoxicity evaluations.

2.4.2. Cytotoxicity evaluation of Cu-doped ceramics with MTT assay

Cu-doped and undoped ceramic discs were sterilized 2h at 180°C, pre-incubated 24h in 1mL of standard marrow cell culture medium and then deposited in 24-well plate and h-MSCs were seeded on the polished side of the ceramic disks at a concentration of 37 000 cells/cm². Wells were then filled with 1mL of standard marrow cell culture medium. Cells cultured in culture well, i.e., without ceramics, were used as positive control. For negative control 30 µL of cycloheximide (Sigma Aldrich, cycloheximide solution, 100 mg/mL in DMSO) were added 24 h before the MTT assay. After 3, 7 and 15 days the mitochondrial activity of h-MSCs was evaluated with MTT (3-(4,5-dimethylthiazol-2-yl)-2,5-diphenyl tetrazolium bromide) assay (Sigma Aldrich). Before adding MTT reagent, the ceramic disks were transferred into new wells with 1 mL of fresh standard marrow cell culture medium. Concerning evaluations of cytotoxicity at day 15, cell culture medium was refresh at day 7 so that the cells were properly maintained and to avoid a potential cytotoxic effect which would come from the fact that the cell culture medium has not been renewed for 15 days. After 3, 7 or 15 days, 100 µL of the MTT reagent (5 mg/mL in PBS) were added to each well and plates were incubated 3 h at 37 °C with 5% of CO_2. Then, the cell culture medium and the MTT reagent were carefully removed without damaging the cells adhered on the ceramic disks and 500 µL of Dimethyl sulfoxide (DMSO) was added to each well. Plates were incubated in the dark with gentle shaking for 40 minutes to ensure the complete dissolution of formazan crystals formed in cells by MTT reagent. Finally, the optical density (OD) was measured at 570 nm and 690 nm with a spectrophotometer TEKAN and Magellan™ software after removing the ceramics.

2.4.3. Scanning Electronic Microscopy (SEM) imaging

SEM imaging was performed on the surface of Cu-doped and undoped ceramic disks to observe the adhesion and spreading of the h-MSCs. Samples were washed in rinsing buffer and fixed for 24 hours at 4 °C in 0.2 mol/L sodium cacodylate buffer, pH 7.4, that contained 1.6% glutaraldehyde. Ceramic disks with adherent h-MSCs were then washed 30 minutes in sodium cacodylate buffer (0.2 mol/L, pH 7.4) and post-fixed 1 hour with 1% osmium tetroxide in same buffer. Samples were washed 20 minutes in distilled water. Dehydration by graded ethanol were performed from 25° to 100° (10 minutes each) to finish in hexamethyldisilazane (HMDS) for 10 minutes. Sample were mounted on stubs using adhesive carbon tabs and sputter-coated with gold-palladium (JFC-1300, JEOL, Japan). Analysis was carried out using a scanning electron microscope (SEM) JSM-6060LV (Jeol, Japan) at 5 kV in high-vacuum mode.

2.5. Antibacterial properties

2.5.1. Bacterial strains and growth conditions

Antibacterial assays were conducted with 4 bacterial strains, 2 Gram positive: MSSA and MRSA derived from clinical bone and joint infections, and 2 Gram negative from the American Type Culture Collection (ATCC): *E. coli* (ATCC® 25922™) and *P. aeruginosa* (ATCC® 27853™). Precultures were obtained by overnight growth at 37 °C in 5 mL of TS medium (Tryptic Soy broth without dextrose). Bacterial concentrations were determined by measurement of the optical density (OD) at 620 nm.

2.5.2. Antibacterial activity of ceramics disks

Experiments were carried out in 24 microtiter plate with a bacterial concentration of 10^3 CFU/mL, contained in 1:500 diluted TS medium (from the standard JIS Z 2801). In each well Cu-doped and undoped ceramic disks were deposited with sterile forceps and 1 mL of bacterial suspension at 10^3 CFU/mL was added. Control condition consisted of bacterial suspension without any ceramics. Concentration of the inoculum was determined by plating 100 µL of suspension on TS agar plates and counting the CFUs after 24 h of incubation at 37 °C. After 5 h and 24 h of incubation with ceramics disks, 5 min of sonication were performed twice and the number of remaining viable bacteria was determined by plating 100 µL of the suspension or serial dilutions of the suspension on TS agar plates further incubated at 37 °C for 24h.

2.6. Measurement of copper ions concentration release

Copper ions released from Cu-doped ceramic disks during cytotoxicity and antibacterial evaluations were measured by Microwave Plasma - Atomic Emission Spectroscopy (4200 MP-AES from Agilent). Sampling was performed directly during experiments, so the measurement conditions correspond exactly to those used during the biological evaluations. Calibration samples were prepared with a 1000 µg/mL Cu ion normadose (Agilent Technologies) diluted in the corresponding solvent (cell culture medium or bacterial culture medium). MP-AES assays were performed on diluted samples stabilized in acidic solution (1/10, v/v, in 0.3 M nitric acid). The two most intense emission wavelengths of Cu (324,754 nm and 327,395 nm) were selected to carry out the measurements.

2.7. Statistical analysis

Biological results presented in this paper were obtained after 3 technical and 3 biological replicates (n = 9). The antibacterial effects of Cu-doped BCP powders were expressed in the form of a logarithmic difference between the bacterial concentrations obtained with the powders evaluated and the control without powder. The formula used is as follows: Logarithmic difference = log (powder tested) - log (control).

Statistical analyses were performed using the Mann−Whitney non-parametric test followed by the Bonferroni correction with $p < 0.05$ considered as being statistically significant.

3. Results

3.1. Synthesis and characterization of ceramics disks

XRPD acquisition, followed by Rietveld refinements, were performed directly on the surface of the polished ceramics; the results are presented in **Fig.1**. BCP and Cu:BCP ceramics are composed of the 2 expected phases (HAp and β-TCP) in the HAp/β-TCP weight ratio of 60.0/40.0 and 60.4/39.6, respectively (**Table 1**). The synthesis conditions were controlled in order to have the same mineralogical composition between the two tested samples; doped versus undoped. Therefore, the effect of the doping element (Cu^{2+}) will be preponderant on the differences observed thereafter.

The lattice parameters, and the associated unit cell volumes, of both phases did not change significantly during doping (the largest variation being +0.16% on the hexagonal parameter of β-TCP, see **Table 1)**. However, significant copper atom occupancies were refined at an interstitial position for HAp (Wyckoff site 2*b*) and in substitution to Ca1 and Ca2 crystallographic positions for β-TCP for the Cu:BCP doped ceramic. Thus, the refined occupancies for copper atoms led to the following chemical formulations: $Ca_{10}Cu_{0.2}(PO_4)_6(OH)_{1.6}O_{0.4}$ for HAp, and $Ca_{2.9}Cu_{0.1}(PO_4)_2$ for β-TCP.

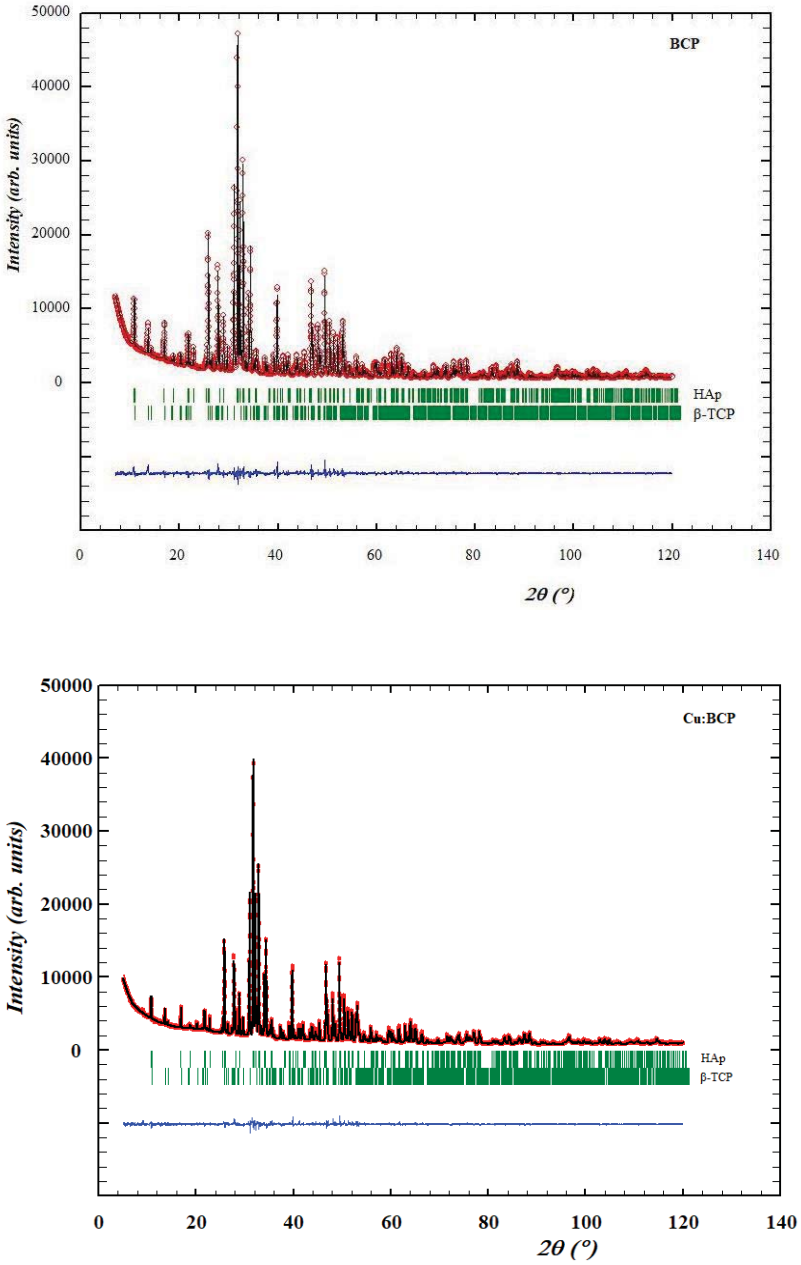

Fig. 1. Rietveld refinements of BCP (top) and Cu:BCP (bottom) pellets sintered at 1050 °C for 3 h under air and 1050°C for 5 h under 93 kPa of N_2 and 7 kPa of H_2O (ramps of 4 °C/min), respectively, and identification of HAp and β-TCP phases.

The global chemical composition of the Cu:BCP has been evaluated by SEM-EDS analyses. Results are shown in Supplementary Information (**Fig SI-1**): both used enlargements (x100 and x1k) gave very similar quantitative results. Values from the largest area (which should be the most representative of the sample) indicated 37.1(2) wt.% for Ca, 18.3(2) wt.% for P and 0.8(2) wt.% for Cu leading to a calculated global composition of $Ca_{9.46}Cu_{0.10}(PO_4)_{5.46}(HPO_4)_{0.54}(OH)_{1.26}O_{0.20}$ (x = 0.54; z = 0.10) using formalism from Eq. 3.

Such a global composition led, after sintering, to the following biphasic composition, according to Eq.4: 0.51 mol of $Ca_{10}Cu_{0.10}(PO_4)_6(OH)_{1.80}O_{0.20}$ + 1.47 mol of $Ca_{2.97}Cu_{0.03}(PO_4)_2$.

Table 1. Crystallographic characterization of the samples extracted from Rietveld refinements. For both the HAp and β-TCP phases: weight amount (wt %), lattice parameters *a* and *c* of the hexagonal lattice (Å), unit cell volume (Å^3) and copper site occupancies for the Cu-doped sample (Cu:BCP).

Sample	**BCP**	**Cu:BCP**
HAp		
Weight amount (wt %)	60.0	60.4
***a* (Å)**	9.4200 (1)	9.4198 (2)
***c* (Å)**	6.8810 (1)	6.8788 (1)
V (Å^3)	528.80 (1)	528.60 (2)
Cu occupancy (% in site 2*b*)	0 (-)	21 (1)
β-TCP		
Weight amount (wt %)	40.0	39.6
***a* (Å)**	10.4207 (2)	10.4112 (2)
***c* (Å)**	37.367 (1)	37.426 (1)
V (Å^3)	3514.1 (1)	3513.2 (2)
Cu occupancy (% in site Ca1)	0 (-)	25 (2)
Cu occupancy (% in site Ca2)	0 (-)	11 (2)

3.2. Cytotoxicity evaluations

MTT assays were performed with h-MSCs cultured on undoped and Cu-doped BCP ceramic disks in order to compare the cytotoxicity of these materials. Results obtained after 3, 7 and 15 days are presented in **Fig. 2**. Positive control, consisting of cells cultured without ceramics, corresponds to 100% of metabolic activity. After 3 days, 92.1% of metabolic activity is found for h-MSCs cultured on undoped BCP and 84.8% for cells cultured on Cu:BCP. No significant difference compare to control was shown, except for negative control which was significantly lower. At day 7 values of metabolic activity are greater than control condition with 130.8% of metabolic activity for both compositions, this increase was significant for Cu:BCP disks only ($p=0.016$). After 15 days, the metabolic activity rates of cells are still higher on BCP and Cu:BCP compare to the control, but difference are not significant (**Fig. 2**).

SEM images of h-MSCs cultured for 3 days on undoped and Cu-doped polished ceramic disks are presented in **Fig. 3**. Cells appear well spread out with elongated filopodia whatever the ceramic composition (doped and undoped).

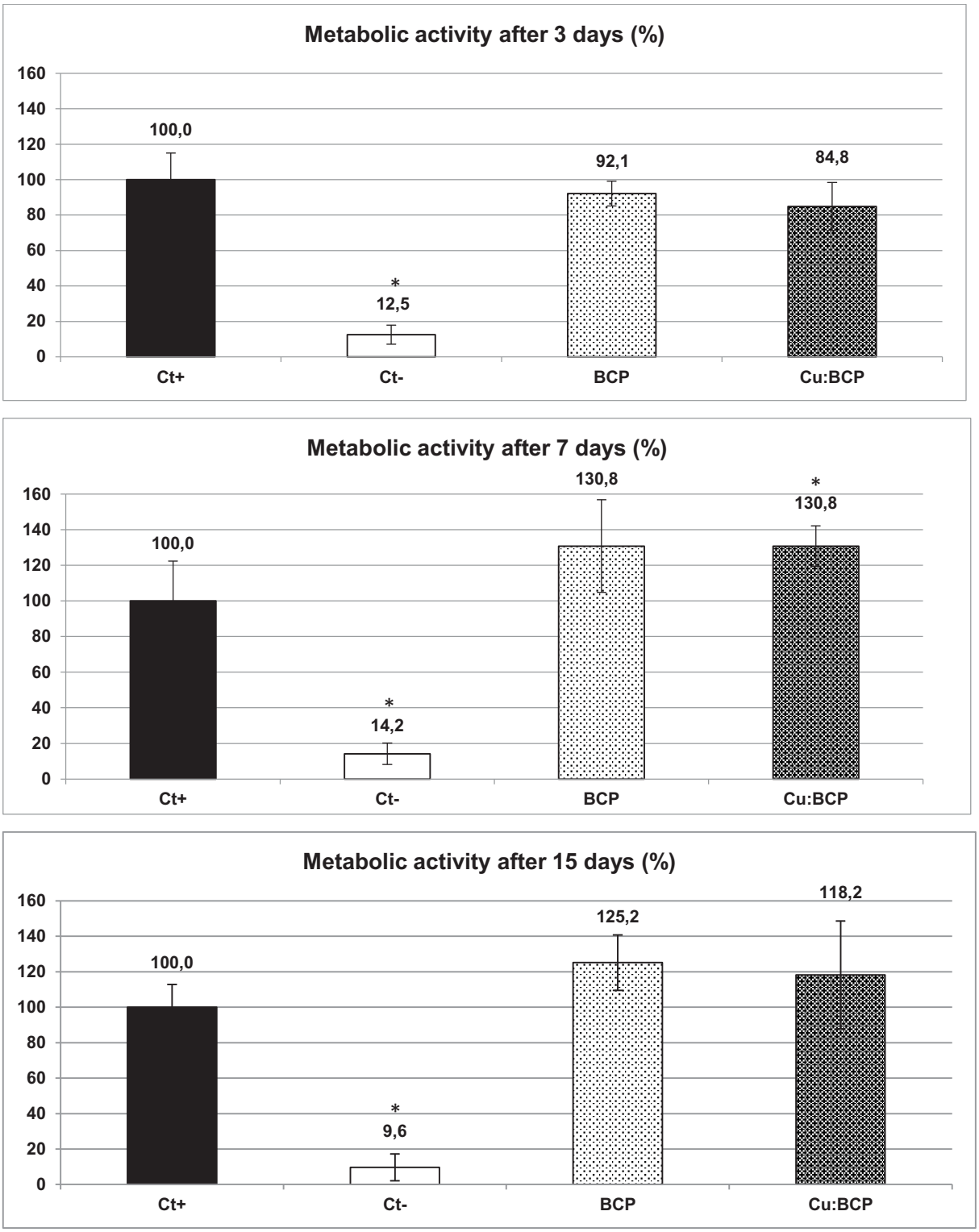

Fig. 2. Metabolic activity (%) of h-MSCs after 3, 7 and 15 days of culture with undoped (BCP) and Cu-doped BCP (Cu:BCP). Ct+ correspond to the positive control, and Ct- correspond to the negative control. Error bars represent the standard error of mean from n=9 samples. Results statistically different compared to control (with $p<0.05$) are indicated with "*".

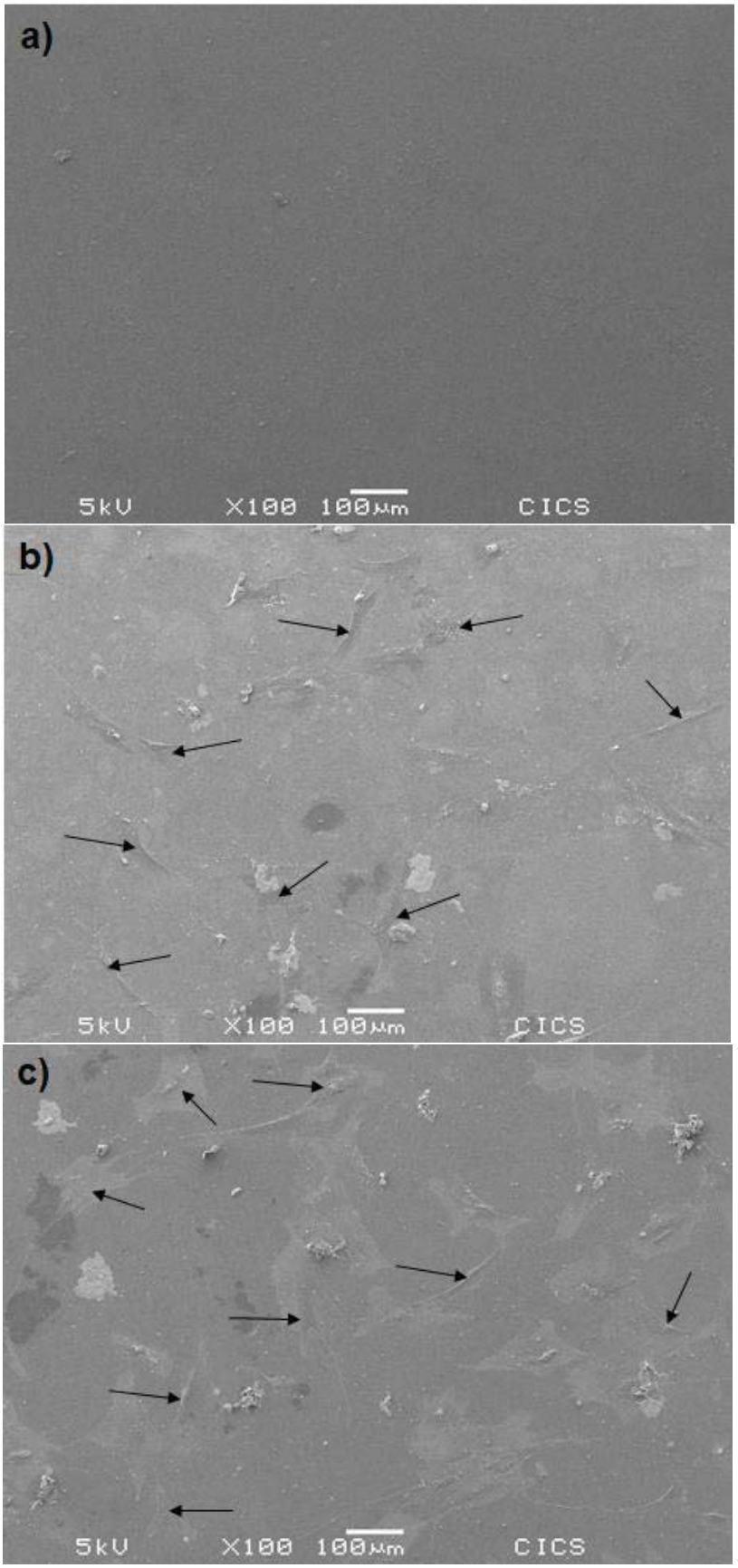

Fig. 3. Scanning Electronic Microscopy (SEM) images of the surface of the disks during cytotoxicity assays at day 3. a) Surface of an undoped BCP polished ceramic without cells. h-MSCs cultured 3 days on b) undoped BCP and c) doped Cu:BCP. Cells are indicated with black arrows.

Table 2 presents the concentrations of Cu^{2+} released by the Cu-doped BCP ceramics in the culture media during the cytotoxicity assays for the same 3, 7 and 15 days' time periods**.** Copper concentration in the culture media increased between day 3 and day 7 ($\Delta[Cu^{2+}]$ = 9.8 ppm). In an equivalent way, the copper concentration released by the ceramic between the day of refresh (i.e., day 7, cf. chapter 2.4.2) and day 15 increased of 22.1 ppm. This series of values indicated that an equilibrium of about 20-25 ppm of Cu^{2+} was reached in culture media within a week, around the copper-doped disk.

Table 2. Cu^{2+} concentration (ppm) measured in culture media by MP-AES during cytotoxicity assays (Cu:BCP).

Material	**Cu^{2+} concentration (ppm)**		
	Day 3	**Day 7**	**Day 15**
Cu:BCP	15.5	25.3	22.1*

***** For measurements at day 15 cell culture medium was refresh before at day 7 so the concentration indicated correspond to the release between the day of refresh at day 7 and day 15.

3.3. Antibacterial activity

Results of antibacterial assays carried out against the four bacterial strains are presented in **Fig. 4**. and are expressed as logarithmic differences in bacterial concentration compared to control consisting of bacteria cultured without biomaterial.

After 5 hours of incubation no logarithmic difference was found with the undoped material. With the copper-doped Cu:BCP sample results showed a slight significant decrease of bacterial concentration with MSSA and *E. coli* (A and B). No significant effect was found with *P. aeruginosa* and MRSA (C and D).

After 24 hours of incubation a significant increase of the bacterial concentration of MSSA compared to control was observed with undoped BCP disks (A). No effect was observed for the 3 other strains.

Concerning the copper-doped Cu:BCP disks, significant decreases of the 4 bacterial strains were observed with log reduction of ~ 1.5 log, 2.8 log, 1 log and 0.6 log for MSSA, *E. coli*, *P. aeruginosa* and MRSA, respectively. The bactericidal effect increased during the first day for the four strains.

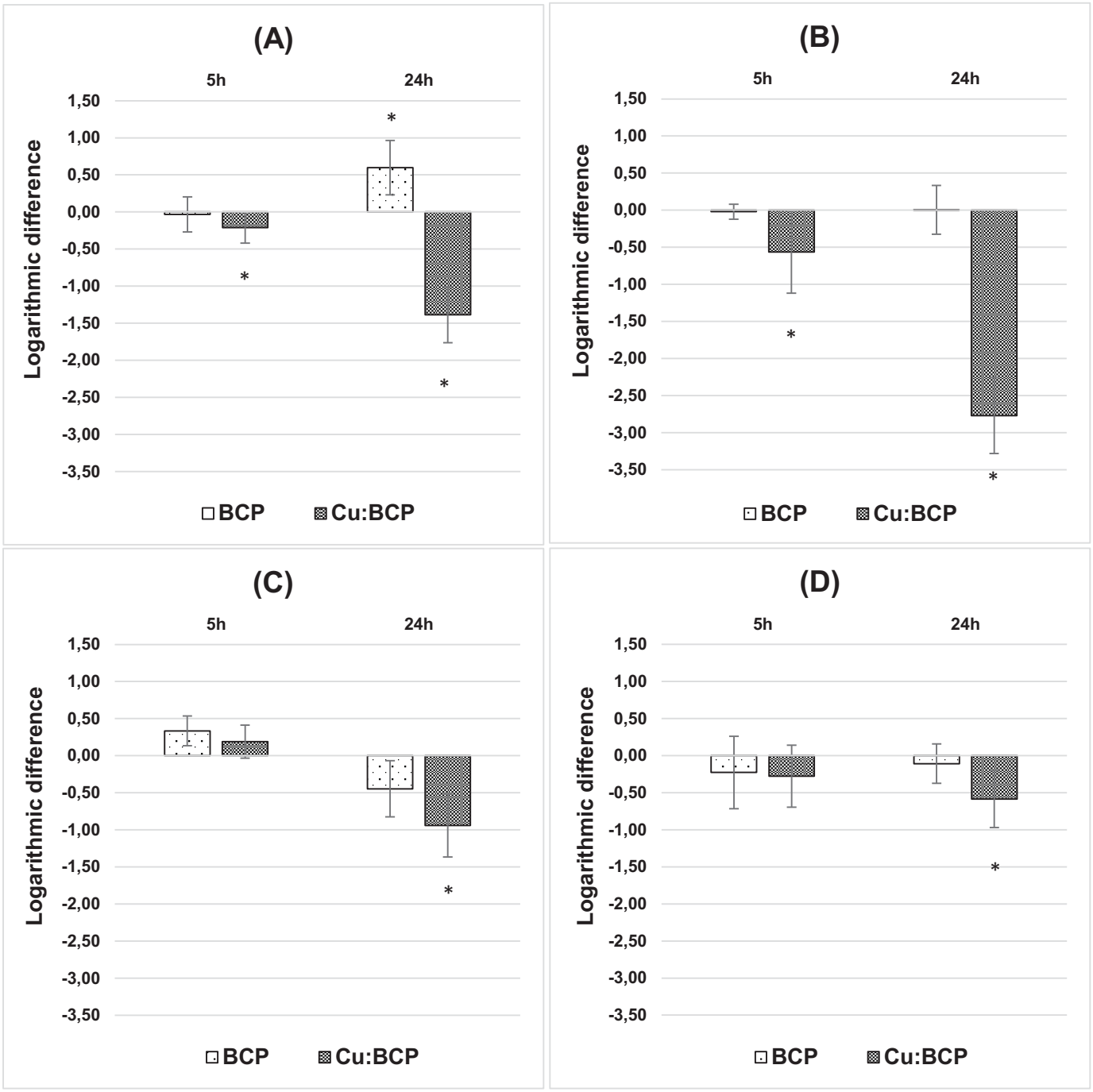

Fig. 4. Logarithmic differences in bacterial concentrations with BCP and Cu:BCP disks compared to control after 5 hours and 24 hours of incubation for (A) MSSA, (B) *E. coli*, (C) *P. aeruginosa* and (D) MRSA. Error bars represent the standard error of mean from n=9 samples. Results statistically different compared to control (with $p<0.05$) are indicated with "*".

In parallel of those experiments, the concentration of copper released by Cu:BCP material during antibacterial assays in the culture medium was measured with MP-AES and results are presented in **Table 3**. After 5 hours Cu:BCP disk released 0.72 ppm of Cu^{2+} and 1.42 ppm after 24 hours in 1:500 diluted TS medium.

Table 3. Cu^{2+} concentration (ppm) measured by MP-AES during antibacterial assays.

Sample	Cu^{2+} concentration (ppm)	
	5 hours	24 hours
Cu:BCP	0.72	1.42

4. Discussion

The chemical composition of the copper-doped ceramic disks was in agreement with the targeted doping level, i.e. a one percent copper replacement of calcium atoms corresponding to global composition of $Ca_{10}Cu_{0.1}(PO_4)_6(OH)_{1.8}O_{0.2}$ if expressed in term of HAp phase exclusively and accordingly to the mechanism of incorporation determined in a previous study [14]. Results from SEM-EDS and XRPD-Rietveld analyses gave relatively equivalent mineral compositions and copper-doping levels. XRPD-Rietveld results indicated 60 wt.% of HAp with $Ca_{10}Cu_{0.2}(PO_4)_6(OH)_{1.6}O_{0.4}$ composition mixed with 40 wt.% of β-TCP with $Ca_{2.9}Cu_{0.1}(PO_4)_2$ composition. Whereas calculation from SEM-EDS analyses indicated 53 wt.% of HAp with $Ca_{10}Cu_{0.1}(PO_4)_6(OH)_{1.8}O_{0.2}$ composition mixed with 47 wt.% of β-TCP with $Ca_{2.97}Cu_{0.03}(PO_4)_2$ composition. Taken into consideration uncertainties relative to each technics, and combined with their respective specificity, the following global compositions could be assumed for the two sintered ceramics disks:

- BCP composed of 60 wt.% of $Ca_{10}(PO_4)_6(OH)_2$ HAp mixed with 40 wt.% of $Ca_3(PO_4)_2$ β-TCP,
- Cu:BCP composed of 60 wt.% of $Ca_{10}Cu_{0.1}(PO_4)_6(OH)_{1.8}O_{0.2}$ HAp mixed with 40 wt.% of $Ca_{2.9}Cu_{0.1}(PO_4)_2$ β-TCP.

It therefore appears that the only difference between the two ceramic disks studied lied in the incorporation of a small quantity of the copper doping element in each phases (present in equivalent proportions). Thus, the effects observed during biological characterizations

(cytotoxicity and bactericidal properties) can be directly attributed to the effect of the copper chemical doping.

Biological evaluations of the two ceramic disks evidenced the absence of cytotoxicity coming either from the BCP material or from copper-doping. Metabolic activity of h-MSCs after one or two weeks was not hampered, quite the contrary, in presence of both the BCP and Cu:BCP disks (**Fig. 2**). Consistent copper release rates, up to 25 ppm in culture medium, were therefore not problematic for cell activity, indicating the biocompatibility of the copper-doped biomaterials. This confirms, and reinforces, the non-cytotoxicity of copper, towards h-MSCs, already noted in our previous study for which BCP powders released up to 12 ppm of Cu^{2+} without harmful effect (Paper submitted to Biomaterials; text available in Chapter III of this manuscript). SEM imaging (**Fig. 3**) demonstrated that h-MSCs are spread out at the surface of the materials. Cell adhesion on a material is a crucial step to successful cell proliferation, differentiation and development of correct cell-cycle progression [32–34]. MSCs are multipotent cells involved in several biological processes of regenerating injured tissues [35,36]. Therefore, evaluate cytotoxicity and adhesion of h-MSCs is relevant and strongly suitable in the case of the characterization of bone substitutes. Although our results do not allow to clearly conclude concerning the attachment of the cells at the surface of bioceramic disks, the SEM imaging did not show modification in cells morphology between BCP and Cu:BCP disks. It would be interesting to explore this point with fluorescence microscope imaging, in order to stain actin and fibronectin which are key markers of cellular adhesion [37,38].

Regarding antibacterial effects, measurements of copper release indicated that Cu:BCP disks releasing 0.72 ppm of Cu^{2+} after 5 hours exhibited a first antibacterial effect against MSSA and *E. coli* (**Fig. 4**). This effect was accentuated after 24 hours with a stronger antibacterial activity observed when a higher concentration of Cu^{2+} was released (1.42 ppm). For *P. aeruginosa* et MRSA strains, 0.72 ppm released after 5 hours were not effective but with 1.42 ppm of Cu^{2+} antibacterial effects were found with significant logarithmic reductions of the bacterial concentrations of the 2 strains. The antibacterial property, effective for the four tested strains after 24 hours, is clearly attributed to the presence of copper in the ceramic disks, and therefore probably to the release of copper cations in the biological medium. Indeed, the undoped BCP disks showed no effect at any time and on any bacterial strains. On the other hand, the bactericidal effect observed for the doped Cu:BCP disks was clearly dependent on the copper release rate since it was time dependent.

It is important to note here the notable difference in the level of copper released in solution between the two types of biological analyzes (cytotoxicity and bacteriology) even if the analysis times were not the same: more than 10 ppm in cytotoxicity assay's culture media versus about 1 ppm in bactericidal assay's culture media (by using the same disk/liquid ratio). The differences in composition and dilution of media between the two experiments are factors that could contribute to the differences observed in copper release. Indeed, cytotoxicity evaluation was performed using non-diluted standard marrow cell culture medium and antibacterial assays were conducted in 1:500 diluted TS medium. The choice of culture medium, or its dilution, will therefore necessarily have an impact on the evaluation results of the invested bactericidal properties. This was noted in the recent review on the biological effect of copper [23]. And it was quantified during our preliminary study on powders of composition close to the present study in which 4 ppm exhibiting antibacterial activity with MSSA in 1:500 diluted TS medium whereas 20 ppm were necessary to reach the same effect in a non-diluted standard bone marrow cell culture medium (Paper submitted to Biomaterials; text available in Chapter III of this manuscript).

The present study is the continuation of our previous biological evaluations of BCP powders (Paper submitted to Biomaterials; text available in Chapter III of this manuscript) and the results complement each other in an informative way. In our previous study, sol-gel route was effective to synthesize materials with biphasic composition. The first part of the present work demonstrates that aqueous precipitation synthesis also provides biphasic calcium phosphate composed of HAp and β-TCP. The two main differences between the disks prepared by aqueous precipitation and powders obtained by sol-gel route are: i/ the ratio between the 2 phases HAp/β-TCP (60/40 for the disks sintered at 1050°C and about 90/10 for powders heated between 600 °C and 1200 °C),and ii/ the sample shaping (polished surface for disks and crushed powder). The copper incorporation mechanisms are similar with an insertion mechanism for the HAp phase and a substitution mechanism for the β-TCP phase, indicating that copper release mechanisms should be identical for both studies.

As previously described, the ratio HAp/β-TCP influence the solubility of the material and the dopant release rate (Paper submitted to Biomaterials; text available in Chapter III of this manuscript). The BCP pellets contain 40 wt.% of the soluble phase β-TCP and therefore should release rapidly large amount of copper compared to BCP powders containing about only 10 wt.% of β-TCP. This has indeed been observed during cytotoxicity evaluation as mentioned above. However, during antibacterial evaluations, the amount of copper released by disk after 24 hours was 1.42 ppm; half of the quantity released by powders in our previous study. This therefore indicates that the shaping of the material also impacts the rate of dopant release, and therefore influences its bacteriological effectiveness. Thus, results showed a bactericidal

effect of the polished doped disk on *P. aeruginosa* with less than 2 ppm released, whereas it had been necessary to rise to 10 ppm during our study based on crushed powder (Paper submitted to Biomaterials; text available in Chapter III of this manuscript). So, it cannot be ruled out that direct contact with the biomaterial surface may have a bactericidal impact.

In the calcium phosphate bioceramic literature, some papers reported that undoped HAp exhibited antibacterial activity which is not the case in our study. Indeed, Stanic *et al*., demonstrated around 60% of bacterial reduction for *S. aureus* and approximatively 70% for *E. coli* with undoped HAp and ~97% of reduction for the two strains with copper-doped HAp [39]. Taking into account the antibacterial effect provided by HAp, the bacterial reduction exhibited by copper-doped HAp is actually around 37% with *S. aureus* and 27% for *E. coli*. Furthermore, the lack of statistical analysis prevents a conclusion on a significant antibacterial effect of copper compared to undoped material. A strong antibacterial activity of undoped HAp was described in the study of Li *et al*., with 73% of bacterial reduction of *E. coli*. However, copper-doped samples were found to exhibit significant antibacterial effect compared to undoped HAp, attesting of the effect of copper doping. However, all the copper-doped samples presented cytotoxicity towards osteoblasts [24]. Radovanovic *et al.* demonstrated a bacterial reduction of 2 log of *S. aureus* and 1 log of *E. coli* with undoped HAp compared to control. The copper doping increased the antibacterial effect with a bacterial reduction of 4 log of *S. aureus* and 3 log of *E. coli* with copper-doped HAp compared to control [40]. In this study the antibacterial effect was less effective against *E. coli* than *S. aureus*, while our results showed opposite effects with a bacterial reduction of *S. aureus* of ~ 1.5 log and approximatively 2.8 log for *E. coli*. Shanmugam *et al.*, synthetized copper substituted hydroxyapatite with a copper rate comparable to our study (i.e. $Ca_{9.9}Cu_{0.1}(PO_4)_6(OH)_2$). Antibacterial essays demonstrated 48.5% and 82.6 % of antibacterial activity of undoped HAp against *S. aureus* and *E. coli* respectively. With copper doping, results showed an increase of the antibacterial effect against *S. aureus* (89.0%) and a decrease on this effect against *E. coli* (28.5%). Authors mentioned that the difference in cell membrane between the two strains could explain this result [41]. In the literature results concerning antibacterial properties of copper-doped calcium phosphate bioceramics are highly heterogeneous since the synthesis method, the doping rate and finally the synthesized biomaterial are different in each study [23].

5. Conclusion

The first objective of this work was to develop a controlled synthesis of copper-doped BCP densified sintered ceramics (i.e. disk) and results shown materials composed of 60 wt % of HAp and 40 wt % of β-TCP; undoped and copper-doped. Copper-doped BCP disks were characterized with the presence of copper in interstitial sites for HAp and in substitution to Ca for β-TCP, as already reported for powdered BCP samples. Afterwards these undoped and copper-doped BCP ceramics disks were evaluated with h-MSCs and no toxicity was observed after 3, 7 and 15 days of culture of the cells at the surface of the materials and with copper released concentrations reaching 25 ppm. To complete these results, evaluation of antibacterial properties of copper-doped BCP ceramics disks showed logarithmic reduction of the four bacterial strains tested: MSSA, MRSA, *E. coli* and *P. aeruginosa*. In comparison with our previous reported results, we were able to establish that the shaping of the bioceramic influences the release rates of the dopant used, but does not affect the investigated biological effects: no cytotoxicity combined with antibacterial capacities.

In conclusion, promising copper-doped BCP ceramics were developed thanks to a precise and controlled synthesis protocol. First biological evaluations demonstrated the biocompatibility and the antibacterial properties of the biomaterials and are encouraging to further improve the biological behaviors of these biomaterials for orthopedic applications.

References

[1] J.T.B. Ratnayake, M. Mucalo, G.J. Dias, Substituted hydroxyapatites for bone regeneration: A review of current trends, J. Biomed. Mater. Res. - Part B Appl. Biomater. 105 (2017). https://doi.org/10.1002/jbm.b.33651.

[2] S. V. Dorozhkin, Biocomposites and hybrid biomaterials based on calcium orthophosphates., Biomatter. 1 (2011) 3–56. https://doi.org/10.4161/biom.1.1.16782.

[3] N. Eliaz, N. Metoki, Calcium phosphate bioceramics: A review of their history, structure, properties, coating technologies and biomedical applications, Materials (Basel). 10 (2017). https://doi.org/10.3390/ma10040334.

[4] J. Calhoun, M.M. Manring, M. Shirtliff, Osteomyelitis of the Long Bones, Semin. Plast. Surg. 23 (2009) 059–072. https://doi.org/10.1055/s-0029-1214158.

[5] M. Clauss, A. Trampuz, O. Borens, M. Bohner, T. Ilchmann, Biofilm formation on bone grafts and bone graft substitutes: Comparison of different materials by a standard in vitro test and microcalorimetry, Acta Biomater. 6 (2010) 3791–3797. https://doi.org/10.1016/j.actbio.2010.03.011.

[6] G.J.A. ter Boo, D.W. Grijpma, T.F. Moriarty, R.G. Richards, D. Eglin, Antimicrobial delivery systems for local infection prophylaxis in orthopedic- and trauma surgery, Biomaterials. 52 (2015) 113–125. https://doi.org/10.1016/j.biomaterials.2015.02.020.

[7] F.C. Tenover, Mechanisms of antimicrobial resistance in bacteria, Am. J. Infect. Control. 34 (2006). https://doi.org/10.1016/j.ajic.2006.05.219.

[8] S. V. Dorozhkin, Calcium orthophosphates, J. Mater. Sci. 42 (2007) 1061–1095. https://doi.org/10.1007/s10853-006-1467-8.

[9] G. Daculsi, R.Z. Legeros, E. Nery, K. Lynch, B. Kerebel, Transformation of biphasic calcium phosphate ceramics in vivo: Ultrastructural and physicochemical characterization, J. Biomed. Mater. Res. 23 (1989) 883–894. https://doi.org/10.1002/jbm.820230806.

[10] M. Bohner, B.L.G. Santoni, N. Döbelin, β-tricalcium phosphate for bone substitution: Synthesis and properties, Acta Biomater. (2020). https://doi.org/10.1016/j.actbio.2020.06.022.

[11] M. Ebrahimi, M.G. Botelho, S. V. Dorozhkin, Biphasic calcium phosphates bioceramics (HA/TCP): Concept, physicochemical properties and the impact of standardization of study protocols in biomaterials research, Mater. Sci. Eng. C. 71 (2017) 1293–1312. https://doi.org/10.1016/j.msec.2016.11.039.

[12] D. Marchat, E. Champion, Ceramic devices for bone regeneration: Mechanical and clinical issues and new perspectives, Elsevier Ltd, 2017. https://doi.org/10.1016/B978-0-08-100881-2.00008-7.

[13] I. Cacciotti, Cationic and Anionic Substitutions in Hydroxyapatite, Handb. Bioceram. Biocomposites. (2016) 145–211. https://doi.org/10.1007/978-3-319-12460-5.

[14] S. Gomes, C. Vichery, S. Descamps, H. Martinez, A. Kaur, A. Jacobs, J.M. Nedelec, G. Renaudin, Cu-doping of calcium phosphate bioceramics: From mechanism to the control of cytotoxicity, Acta Biomater. 65 (2018) 462–474. https://doi.org/10.1016/j.actbio.2017.10.028.

[15] J.M. Nedelec, L. Courtheoux, E. Jallot, C. Kinowski, J. Lao, P. Laquerriere, C. Mansuy, G. Renaudin, S. Turrell, Materials doping through sol-gel chemistry: A little

something can make a big difference, in: J. Sol-Gel Sci. Technol., 2008: pp. 259–271. https://doi.org/10.1007/s10971-007-1665-0.

[16] W. Habraken, P. Habibovic, M. Epple, M. Bohner, Calcium phosphates in biomedical applications: Materials for the future?, Mater. Today. 19 (2016) 69–87. https://doi.org/10.1016/j.mattod.2015.10.008.

[17] W.L. Murphy, T.C. McDevitt, A.J. Engler, Materials as stem cell regulators, Nat. Mater. 13 (2014) 547–557. https://doi.org/10.1038/nmat3937.

[18] A.P. Ingle, P. Paralikar, S. Shende, I. Gupta, J.K. Biswas, L.H. Da Silva Martins, M. Rai, Copper in medicine: Perspectives and toxicity, Biomed. Appl. Met. (2018) 95–112. https://doi.org/10.1007/978-3-319-74814-6_4.

[19] P. Chellan, P.J. Sadler, The elements of life and medicines, Philos. Trans. R. Soc. A Math. Phys. Eng. Sci. 373 (2015). https://doi.org/10.1098/rsta.2014.0182.

[20] N.M. Lowe, W.D. Fraser, M.J. Jackson, Is there a potential therapeutic value of copper and zinc for osteoporosis?, Proc. Nutr. Soc. 61 (2002) 181–185. https://doi.org/10.1079/pns2002154.

[21] W. Opsahl, H. Zeronian, M. Ellison, D. Lewis, R.B. Rucker, R.S. Riggins, Role of copper in collagen cross-linking and its influence on selected mechanical properties of chick bone and tendon, J. Nutr. 112 (1982) 708–716. https://doi.org/10.1093/jn/112.4.708.

[22] G. Grass, C. Rensing, M. Solioz, Metallic copper as an antimicrobial surface, Appl. Environ. Microbiol. 77 (2011) 1541–1547. https://doi.org/10.1128/AEM.02766-10.

[23] A. Jacobs, G. Renaudin, C. Forestier, J. Nedelec, S. Descamps, Biological properties of copper-doped biomaterials for orthopedic applications: a review of antibacterial, angiogenic and osteogenic aspects, Acta Biomater. (2020). https://doi.org/10.1016/j.actbio.2020.09.044.

[24] Y. Li, J. Ho, C.P. Ooi, Antibacterial efficacy and cytotoxicity studies of copper (II) and titanium (IV) substituted hydroxyapatite nanoparticles, Mater. Sci. Eng. C. 30 (2010) 1137–1144. https://doi.org/10.1016/j.msec.2010.06.011.

[25] A. Bhattacharjee, Y. Fang, T.J.N. Hooper, N.L. Kelly, D. Gupta, K. Balani, I. Manna, T. Baikie, P.T. Bishop, T.J. White, J. V. Hanna, Crystal chemistry and antibacterial properties of cupriferous hydroxyapatite, Materials (Basel). 12 (2019). https://doi.org/10.3390/ma12111814.

[26] C.F. Marques, S. Olhero, J.C.C. Abrantes, A. Marote, S. Ferreira, S.I. Vieira, J.M.F. Ferreira, Biocompatibility and antimicrobial activity of biphasic calcium phosphate powders doped with metal ions for regenerative medicine, Ceram. Int. 43 (2017) 15719–15728. https://doi.org/10.1016/j.ceramint.2017.08.133.

[27] M. Tadie, K.C. Corin, J.G. Wiese, C.T. O'Connor, Electrochemical interactions of platinum group minerals with copper sulphate, Miner. Eng. 112 (2017) 43–49. https://doi.org/10.1016/j.mineng.2017.07.004.

[28] T.W.J. Albrecht, J. Addai-Mensah, D. Fornasiero, Effect of pH , Concentration and Temperature on Copper and Zinc Hydroxide Formation / Precipitation in Solution, in: CHEMECA 2011 - "Engineering a Better World" Sydney Hilt. Hotel. NSW, Aust. 18-21 Sept. 2011. Barton, A.C.T. Eng. Aust. 2011 [2100]-[2110]., 2011: pp. 1–10. http://arrow.unisa.edu.au:8081/1959.8/123424.

[29] L. Wang, G.H. Nancollas, Dynamics of Biomineralization and Biodemineralization, Met Ions Life Sci. (2010) 413–456. https://doi.org/10.1038/jid.2014.371.

[30] A. El Hamidi, M. Halim, S. Arsalane, M. Kacimi, M. Ziyad, Synthesis and characterization of new copper(II) substituted dicalcium phosphate dihydrate (CaHPO 4.2H 2O), Asian J. Chem. 24 (2012) 2698–2702.

[31] S. Gomes, J.M. Nedelec, E. Jallot, D. Sheptyakov, G. Renaudin, Unexpected mechanism of Zn2+ insertion in calcium phosphate bioceramics, Chem. Mater. 23 (2011) 3072–3085. https://doi.org/10.1021/cm200537v.

[32] A.A. Khalili, M.R. Ahmad, A Review of cell adhesion studies for biomedical and biological applications, Int. J. Mol. Sci. 16 (2015) 18149–18184. https://doi.org/10.3390/ijms160818149.

[33] S. Huang, D.E. Ingber, The structural and mechanical complexity of cell-growth control, Nat. Cell Biol. 1 (1999) E131–E138. https://doi.org/10.1038/13043.

[34] R.O. Hynes, Integrins: Versatility, modulation, and signaling in cell adhesion, Cell. 69 (1992) 11–25. https://doi.org/10.1016/0092-8674(92)90115-S.

[35] J.S. Park, S. Suryaprakash, Y.H. Lao, K.W. Leong, Engineering mesenchymal stem cells for regenerative medicine and drug delivery, Methods. 84 (2015) 3–16. https://doi.org/10.1016/j.ymeth.2015.03.002.

[36] J. Kobolak, A. Dinnyes, A. Memic, A. Khademhosseini, A. Mobasheri, Mesenchymal stem cells: Identification, phenotypic characterization, biological properties and potential for regenerative medicine through biomaterial micro-engineering of their

niche, Methods. 99 (2016) 62–68. https://doi.org/10.1016/j.ymeth.2015.09.016.

[37] X. Wang, F. Cheng, J. Liu, J.H. Smått, D. Gepperth, M. Lastusaari, C. Xu, L. Hupa, Biocomposites of copper-containing mesoporous bioactive glass and nanofibrillated cellulose: Biocompatibility and angiogenic promotion in chronic wound healing application, Acta Biomater. 46 (2016) 286–298. https://doi.org/10.1016/j.actbio.2016.09.021.

[38] S.A. Hacking, A. Khademhosseini, Cells and Surfaces in vitro, Third Edition, Elsevier, 2013. https://doi.org/10.1016/B978-0-08-087780-8.00037-1.

[39] V. Stanić, S. Dimitrijević, J. Antić-Stanković, M. Mitrić, B. Jokić, I.B. Plećaš, S. Raičević, Synthesis, characterization and antimicrobial activity of copper and zinc-doped hydroxyapatite nanopowders, Appl. Surf. Sci. 256 (2010) 6083–6089. https://doi.org/10.1016/j.apsusc.2010.03.124.

[40] Ž. Radovanović, B. Jokić, D. Veljović, S. Dimitrijević, V. Kojić, R. Petrović, D. Janaćković, Antimicrobial activity and biocompatibility of Ag + - and Cu 2+ -doped biphasic hydroxyapatite/α-tricalcium phosphate obtained from hydrothermally synthesized Ag + - and Cu 2+ -doped hydroxyapatite, Appl. Surf. Sci. 307 (2014) 513–519. https://doi.org/10.1016/j.apsusc.2014.04.066.

[41] S. Shanmugam, B. Gopal, Copper substituted hydroxyapatite and fluorapatite: Synthesis, characterization and antimicrobial properties, Ceram. Int. 40 (2014) 15655–15662. https://doi.org/10.1016/j.ceramint.2014.07.086.

Supplementary Information

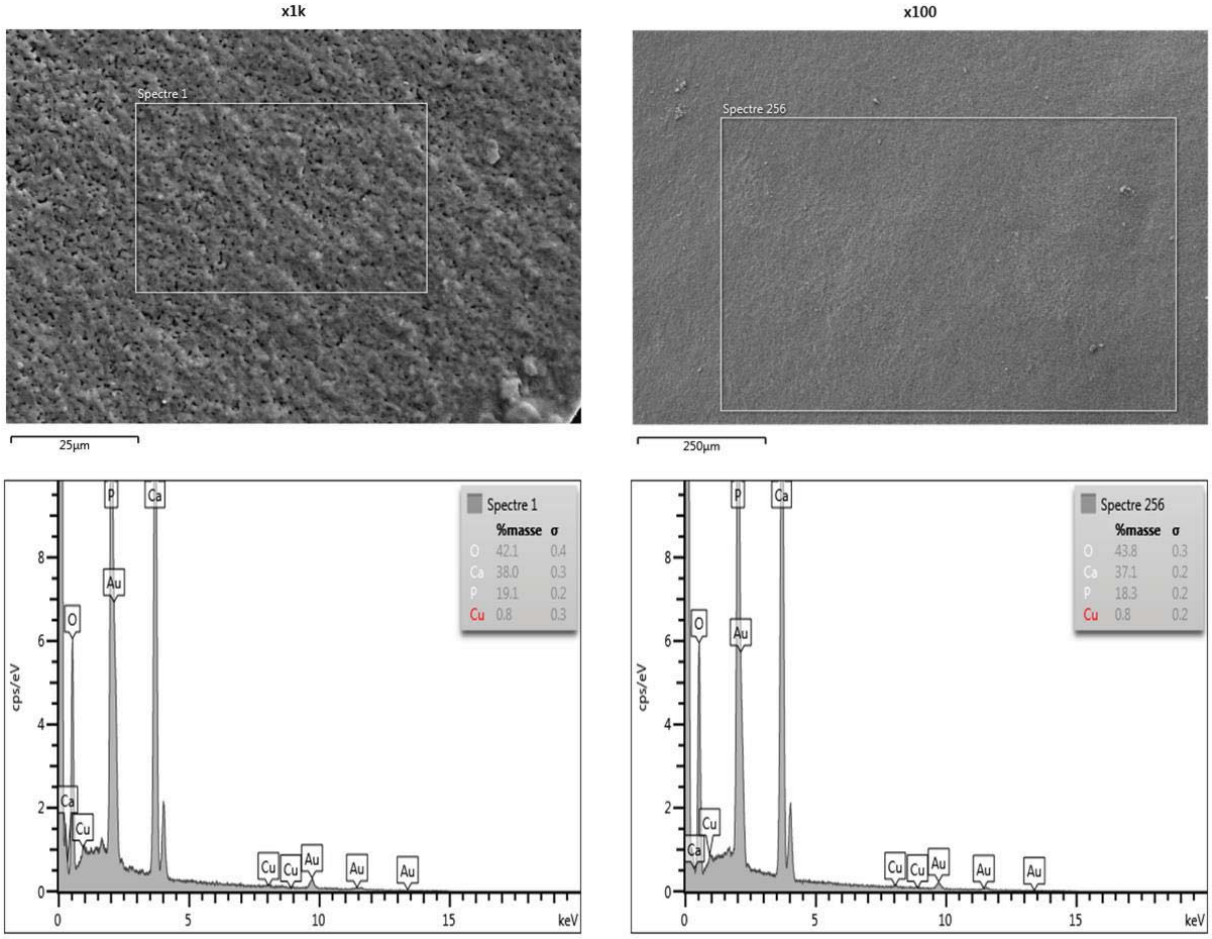

Fig SI-1. SEM-EDS results on the copper doped Cu:BCP sample (polished surface).

CONCLUSION GENERALE ET PERSPECTIVES

Les travaux présentés dans ce manuscrit font suite à plus de dix années de recherche sur les mécanismes de dopage des biocéramiques par l'équipe Matériaux Pour la Santé de l'Institut de Chimie de Clermont-Ferrand (ICCF). Ce travail de recherche pluridisciplinaire permet de faire le lien entre la synthèse et la caractérisation chimique du dopage de biomatériaux apatitiques et l'évaluation de leurs comportements en milieux biologiques ; le lien étant le taux d'élément dopés introduits, puis relargué.

La première partie de cette étude a été consacrée à la synthèse sol-gel de poudres de BCP dopées au cuivre, à l'argent et à l'or et à la caractérisation des mécanismes de dopage impliqués. Ces caractérisations ont permis de montrer que la proportion des 2 phases HAp/ß-TCP est fonction de la température de recuit appliquée en fin de synthèse avec une augmentation progressive de la phase HAp avec l'augmentation de la température. Concernant le dopage au cuivre, un mécanisme d'insertion en site interstitiel des ions Cu^{2+} a été mis en évidence pour la phase HAp et un mécanisme de substitution des ions Ca^{2+} par Cu^{2+} a été retrouvé pour la phase ß-TCP. La localisation du dopant à l'échelle atomique, aura par la suite une influence directe sur sa disponibilité dans le milieu biologique. Pour les matériaux dopés à l'argent une substitution des ions Ca^{2+} par Ag^{+} est retrouvée pour les 2 phases HAp et ß-TCP avec en plus la formation de nanoparticules d'argent métallique Ag°, conduisant à l'obtention de nanocomposites comprenant des nanoparticules d'Ag° et des BCP dopées. Dans le cas du dopage à l'or, aucune phase d'HAp dopée à l'or n'est présente, en revanche une substitution des cations Ca^{2+} par des cations Au^{3+} est retrouvée sur des sites de calcium de la phase ß-TCP ainsi que la présence de nanoparticules métalliques d'or.

Ensuite des synthèses par précipitation en voie aqueuse ont été réalisées par l'équipe Ingénierie des Biomatériaux et des Particules Inhalées (BioPI) du Centre Ingénierie et Santé (CIS) de l'Ecole des Mines de Saint-Etienne dans le but d'obtenir des poudres dopées au cuivre en grande quantité permettant la préparation de pastilles denses par frittage. Les mécanismes d'incorporation du cuivre dans ces matériaux synthétisés par précipitation en voie aqueuse ont été vérifiés, et sont similaires à ceux observés par synthèse sol-gel, à savoir une insertion dans la phase HAp et une substitution dans la phase β-TCP. Les pastilles frittées sont également des BCP, avec un taux de phase β-TCP plus important que ce qu'il y avait dans les poudres.

La seconde partie de ce manuscrit a porté sur les évaluations biologiques des matériaux dopés au cuivre synthétisés et plus précisément l'étude de leur toxicité et de leurs propriétés antibactériennes. L'objectif étant d'observer les impacts potentiels des différentes caractéristiques des matériaux (mise en forme, ratio HAp/ß-TCP, taux de cuivre) sur les réponses biologiques observées.

Les résultats ont montré que les BCP sous forme de poudres, présentant différents taux de dopage et différents ratio HAp/ß-TCP, n'induisent aucune cytotoxicité envers des cellules souches mésenchymateuses humaines après 3, 7 et 15 jours de culture et pour des concentrations de cuivre relargué allant jusque 12 ppm pour les matériaux avec le plus fort taux de dopage. Ces poudres présentent une activité antibactérienne envers 3 souches : *S. aureus*, MRSA, *E. coli* avec un relargage de cuivre de 2 ppm, mais aucun effet n'a été observé envers *P. aeruginosa* en raison d'une concentration de cuivre insuffisante. Ces résultats ont permis de mettre en évidence l'influence du ratio HAp/ß-TCP sur la vitesse de dissolution des matériaux et donc sur le taux de relargage du cuivre, ainsi que l'impact du taux de dopage sur la concentration de cuivre relargué. Derrière le ratio HAp/ß-TCP se retrouve un facteur clé qui est la température de cuisson utilisée qui va impacter la localisation de l'élément dopant à l'échelle atomique, et par conséquent va influer directement sur sa future disponibilité pour le milieu biologique. De plus, ces résultats ont montré que les effets antibactériens du cuivre observés sont dépendants d'une part de la concentration de cuivre présente dans le milieu et d'autre part de la nature du milieu de culture utilisé lors des expérimentations avec une tolérance bactérienne au cuivre supérieure en présence d'un milieu de culture plus riche.

Concernant l'étude des pastilles de BCP dopées au cuivre, une synthèse contrôlée par précipitation en voie aqueuse a été développé et des matériaux composés à 60% d'HAp et 40% de ß-TCP ont été synthétisés. Les mécanismes d'incorporation du cuivre dans les échantillons dopés sont similaires à ceux retrouvés sur les poudres synthétisées par voie sol-gel, à savoir une insertion en site interstitiel pour l'HAp et une substitution du calcium pour la phase ß-TCP. Aucune cytotoxicité n'a été observée après 3, 7 et 15 jours de culture avec des cellules souches mésenchymateuses humaines et pour des concentrations de cuivre allant jusqu'à 25 ppm. Les pastilles dopées présentent une activité antibactérienne après 24h envers les 4 souches bactériennes testées : *S. aureus*, MRSA, *E. coli* et *P. aeruginosa*, avec cependant une efficacité moindre pour 3 d'entre elles en comparaison avec les effets observés avec les poudres.

En conclusion, il a été montré que deux procédés de synthèse différents (sol-gel et précipitation en voie aqueuse) permettent d'obtenir des biocéramiques de phosphates de calcium de composition biphasique (HAp et ß-TCP) mettant en jeu des mécanismes similaires d'incorporation des ions Cu^{2+}. Les matériaux obtenus, sous forme de poudre ou de pastilles sont biocompatibles avec des cellules souches mésenchymateuses humaines et présentent des propriétés antibactériennes envers des souches d'intérêt clinique. Finalement, il a aussi été montré que les caractéristiques chimiques des matériaux et les conditions d'expérimentations influencent les réponses biologiques observées.

A l'issue de ce travail, plusieurs perspectives se dégagent, notamment concernant les caractérisations des propriétés biologiques de ces matériaux. En effet, le cuivre est également connu pour promouvoir l'angiogenèse et l'ostéogénèse qui sont des processus physiologiques clés dans la bio-adaptation d'un substitut osseux après son implantation. Des cellules endothéliales de type HUVECs et l'expression du facteur VEGF sont largement étudiées pour démontrer un effet pro-angiogénique. L'implantation d'un biomatériau dans un défaut de calvaria chez le rat ou l'étude de la membrane chorioallantoïque du poussin sont des modèles d'études *in-vivo* qui permettent aussi d'observer directement la néoformation de vaisseaux sanguins. L'ostéogénèse peut être observée par l'étude de la différenciation et de la prolifération de cellules pré-ostéoblastiques. L'augmentation de l'expression de gènes responsables de l'ostéogénèse comme Col I, OPN et OCN est également un marqueur de stimulation de l'ostéogénèse. La formation d'un nouveau tissu osseux est aussi très souvent étudiée en utilisant un modèle *in-vivo* d'implantation du substitut dans un défaut de calvaria chez le rat. A nouveau, ce qui manque le plus dans la littérature existante sur le sujet est la possibilité de relier propriétés angiogénique et/ou ostéogénique aux quantités de dopant utilisés et/ou relargués.

L'ensemble du travail réalisé au cours de cette thèse a permis de compléter et d'approfondir les connaissances de l'équipe sur le sujet des BCP dopés. Le dopage au cuivre continue d'apparaître comme très prometteur (voire le plus prometteur) du fait des résultats obtenus sur les propriétés biologiques. De plus, la présence préalable de cet élément dans le corps en fait un dopage plus facilement envisageable pour des applications cliniques. Le cas du dopage à l'argent, qui aboutit à un nanocomposite avec présence des deux degrés d'oxydation Ag° et Ag^{+}, devrait conférer au matériau des propriétés antibactériennes exceptionnelles. Cependant l'absence préalable de cet élément dans le corps le rend très certainement plus difficilement concevable en termes d'applications cliniques.

REFERENCES BIBLIOGRAPHIQUES

[1] INVS, Surveillance Des Infections Du Site Opératoire Dans Les Etablissements de Santé Français. Résultats 2015, (2017) 1–214.

[2] D.J. Barillo, M. Pozza, M. Margaret-Brandt, A literature review of the military uses of silver-nylon dressings with emphasis on wartime operations, Burns. 40 (2014) S24–S29. https://doi.org/10.1016/j.burns.2014.09.017.

[3] J.C. Elliott, Structure and Chemistry of the Apatites and Other Calcium Orthophosphates, Elsevier, Amsterdam. 18 (1994) 404.

[4] S. Gomes, C. Vichery, S. Descamps, H. Martinez, A. Kaur, A. Jacobs, J.M. Nedelec, G. Renaudin, Cu-doping of calcium phosphate bioceramics: From mechanism to the control of cytotoxicity, Acta Biomater. 65 (2018) 462–474. https://doi.org/10.1016/j.actbio.2017.10.028.

[5] I. Couret, Biologie du remodelage osseux, Med. Nucl. 28 (2004) 57–65.

[6] N. Loveridge, Bone: more than a stick, J. Anim. Sci. 77 (1999) 190–196. https://doi.org/10.2527/1999.77suppl_2190x.

[7] N. Döbelin, R. Luginbühl, M. Bohner, Synthetic calcium phosphate ceramics for treatment of bone fractures, Chimia (Aarau). 64 (2010) 723–729. https://doi.org/10.2533/chimia.2010.723.

[8] G.S. Travlos, Normal Structure, Function, and Histology of the Bone Marrow, Toxicol. Pathol. 34 (2006) 548–565. https://doi.org/10.1080/01926230600939856.

[9] G.J. Tortora, B. Derrickson, Principes d'anatomie et de physiologie, 4 ème édit, John Wiley & Sons, Inc, 2007.

[10] U. Hansen, S. Masouros, A.A. Amis, (iii) Material properties of biological tissues related to joint surgery, Curr. Orthop. 20 (2006) 16–22. https://doi.org/10.1016/j.cuor.2005.12.001.

[11] R. Legros, N. Balmain, G. Bonel, Age-related changes in mineral of rat and bovine cortical bone, Calcif. Tissue Int. 41 (1987) 137–144. https://doi.org/10.1007/BF02563793.

[12] C.P. Tarnowski, M.A. Ignelzi, M.D. Morris, Mineralization of developing mouse calvaria as revealed by raman microspectroscopy, J. Bone Miner. Res. 17 (2002) 1118–1126.

https://doi.org/10.1359/jbmr.2002.17.6.1118.

[13] T.J. Webster, E.S. Ahn, Nanostructured biomaterials for tissue engineering bone, Adv. Biochem. Eng. Biotechnol. 103 (2006) 275–308. https://doi.org/10.1007/10_021.

[14] M.W. Long, Osteogenesis and bone-marrow-derived cells, Blood Cells, Mol. Dis. 27 (2001) 677–690. https://doi.org/10.1006/bcmd.2001.0431.

[15] A.J. Rosenbaum, D.A. Grande, J.S. Dines, The use of mesenchymal stem cells in tissue engineering: A global assessment, Organogenesis. 4 (2008) 23–27. https://doi.org/10.4161/org.6048.

[16] C. Martinaud, C. Thepenier, M. Trouillas, J. Peltzer, G. Uzan, M.C. Le Bousse Kerdilès, M. Prat, J.J. Lataillade, Les cellules souches mésenchymateuses : Des cellules pour la médecine régénérative du futur ?, Rev. Francoph. Des Lab. 2010 (2010) 47–59. https://doi.org/10.1016/S1773-035X(10)70732-2.

[17] P. Ducy, T. Schinke, G. Karsenty, The osteoblast: A sophisticated fibroblast under central surveillance, Science (80-.). 289 (2000) 1501–1504. https://doi.org/10.1126/science.289.5484.1501.

[18] J. Pratap, M. Galindo, S.K. Zaidi, D. Vradii, B.M. Bhat, J.A. Robinson, J.Y. Choi, T. Komori, J.L. Stein, J.B. Lian, G.S. Stein, A.J. Van Wijnen, Cell growth regulatory role of Runx2 during proliferative expansion of preosteoblasts, Cancer Res. 63 (2003) 5357–5362.

[19] J.E. Aubin, Regulation of Osteoblast Formation and Function, Rev. Endocr. Metab. Disord. 2 (2001) 81–94. https://doi.org/10.1023/A:1010011209064.

[20] P. Marie, Différenciation, fonction et contrôle de l'ostéoblaste, Medecine/Sciences. 17 (2001) 1252–1259. https://doi.org/10.1051/medsci/200117121252.

[21] S.L. Teitelbaum, Bone Resorption by Osteoclasts, Science (80-.). 289 (2000) 1504–1508. https://doi.org/10.1126/science.289.5484.1504.

[22] S.C. Manolagas, Birth and Death of Bone Cells: Basic Regulatory Mechanisms and Implications for the Pathogenesis and Treatment of Osteoporosis, Endocr. Rev. 21 (2000) 115–137.

[23] H. Chen, T. Senda, K. ya Kubo, The osteocyte plays multiple roles in bone remodeling and mineral homeostasis, Med. Mol. Morphol. 48 (2015) 61–68. https://doi.org/10.1007/s00795-015-0099-y.

[24] J.E. Davies, Bone bonding at natural and biomaterial surfaces, Biomaterials. 28 (2007)

5058–5067. https://doi.org/10.1016/j.biomaterials.2007.07.049.

[25] A. Parfitt, Osteonal and Hemi-Osteonal Remodeling: The Spatial and Temporal Framework for Signal Traffic in Adult Human Bone, 1994.

[26] N.A. Sims, T.J. Martin, Coupling the activities of bone formation and resorption: a multitude of signals within the basic multicellular unit, Bonekey Rep. 3 (2014) 1–10. https://doi.org/10.1038/bonekey.2013.215.

[27] B. Langdahl, S. Ferrari, D.W. Dempster, Bone modeling and remodeling: potential as therapeutic targets for the treatment of osteoporosis, Ther. Adv. Musculoskelet. Dis. 8 (2016) 225–235. https://doi.org/10.1177/1759720X16670154.

[28] S. Muruganandan, C.J. Sinal, The impact of bone marrow adipocytes on osteoblast and osteoclast differentiation, IUBMB Life. 66 (2014) 147–155. https://doi.org/10.1002/iub.1254.

[29] W. Liu, X. Zhang, Receptor activator of nuclear factor-κB ligand (RANKL)/RANK/osteoprotegerin system in bone and other tissues (Review), Mol. Med. Rep. 11 (2015) 3212–3218. https://doi.org/10.3892/mmr.2015.3152.

[30] R. Detsch, A.R. Boccaccini, The role of osteoclasts in bone tissue engineering, J. Tissue Eng. Regen. Med. 9 (2014) 1133–1149. https://doi.org/10.1002/term.1851.

[31] F.F. Safadi, M.F. Barbe, S.M. Abdelmagid, M.C. Rico, R.A. Aswad, J. Litvin, S.N. Popoff, Bone Structure, Development and Bone Biology, Bone Pathol. 2 (2009) 1–416. https://doi.org/10.1007/978-1-59745-347-9.

[32] J. Giudicelli, J.C. Souberbielle, Le Remodelage Osseux Et L'Exploration De L' Osteoporose, Rev. l'ACOMEN. 4 (1998) 251–272.

[33] S.C. Manolagas, R.L. Jilka, Bone Marrow, Cytokines, and Bone Remodeling — Emerging Insights into the Pathophysiology of Osteoporosis, N. Engl. J. Med. 332 (1995) 305–311. https://doi.org/10.1056/nejm199502023320506.

[34] J.C. Gallagher, ' D Goldgar, A. Moy', Total Bone Calcium in Normal Women: Effect of Age and Menopause Status, Mary Ann Liebert. Inc., Publishers, 1987.

[35] S. Yamada, D. Heymann, J.-M. Bouler, G. Daculsi, Osteoclastic resort3tion of calcium phosphate ceran&s with different hydroxyapatite@-tricalcium phosphate ratios, 1997.

[36] W.L. Murphy, T.C. McDevitt, A.J. Engler, Materials as stem cell regulators, Nat. Mater. 13 (2014) 547–557. https://doi.org/10.1038/nmat3937.

[37] D.F. Williams, There is no such thing as a biocompatible material, Biomaterials. 35 (2014) 10009–10014. https://doi.org/10.1016/j.biomaterials.2014.08.035.

[38] K. Anselme, Osteoblast adhesion on biomaterials, Biomaterials. 21 (2000) 667–681. https://doi.org/10.1016/S0142-9612(99)00242-2.

[39] J.M. Anderson, A. Rodriguez, D.T. Chang, Foreign body reaction to biomaterials, Semin. Immunol. 20 (2008) 86–100. https://doi.org/10.1016/j.smim.2007.11.004.

[40] R.Z. LeGeros, Properties of osteoconductive biomaterials: Calcium phosphates, Clin. Orthop. Relat. Res. (2002) 81–98. https://doi.org/10.1097/00003086-200202000-00009.

[41] M.R. Urist, Bone: Formation by Autoinduction, Science (80-.). 150 (1965) 893–899. https://doi.org/10.1126/science.150.3698.893.

[42] P. V. Giannoudis, H. Dinopoulos, E. Tsiridis, Bone substitutes: An update, Injury. 36 (2005) S20–S27. https://doi.org/10.1016/j.injury.2005.07.029.

[43] A.J. Salgado, O.P. Coutinho, R.L. Reis, Bone tissue engineering: State of the art and future trends, Macromol. Biosci. 4 (2004) 743–765. https://doi.org/10.1002/mabi.200400026.

[44] D. Le Nihouannen, G. Daculsi, A. Saffarzadeh, O. Gauthier, S. Delplace, P. Pilet, P. Layrolle, Ectopic bone formation by microporous calcium phosphate ceramic particles in sheep muscles, Bone. 36 (2005) 1086–1093. https://doi.org/10.1016/j.bone.2005.02.017.

[45] J.M. Bouler, P. Pilet, O. Gauthier, E. Verron, Biphasic calcium phosphate ceramics for bone reconstruction: A review of biological response, Acta Biomater. 53 (2017) 1–12. https://doi.org/10.1016/j.actbio.2017.01.076.

[46] V. Campana, G. Milano, E. Pagano, M. Barba, C. Cicione, G. Salonna, W. Lattanzi, G. Logroscino, Bone substitutes in orthopaedic surgery: from basic science to clinical practice, J. Mater. Sci. Mater. Med. 25 (2014) 2445–2461. https://doi.org/10.1007/s10856-014-5240-2.

[47] T.T. Roberts, A.J. Rosenbaum, Bone grafts, bone substitutes and orthobiologics, Organogenesis. 8 (2012) 114–124. https://doi.org/10.4161/org.23306.

[48] S. V. Dorozhkin, Bioceramics of calcium orthophosphates, Biomaterials. 31 (2010) 1465–1485. https://doi.org/10.1016/j.biomaterials.2009.11.050.

[49] M. Ebrahimi, M.G. Botelho, S. V. Dorozhkin, Biphasic calcium phosphates bioceramics

(HA/TCP): Concept, physicochemical properties and the impact of standardization of study protocols in biomaterials research, Mater. Sci. Eng. C. 71 (2017) 1293–1312. https://doi.org/10.1016/j.msec.2016.11.039.

[50] M. Vallet-Regí, A.J. Salinas, Ceramics as bone repair materials, in: Bone Repair Biomater., Elsevier Inc., 2009: pp. 194–230. https://doi.org/10.1533/9781845696610.2.194.

[51] D. Puppi, F. Chiellini, A.M. Piras, E. Chiellini, Polymeric materials for bone and cartilage repair, Prog. Polym. Sci. 35 (2010) 403–440. https://doi.org/10.1016/j.progpolymsci.2010.01.006.

[52] J. Zhang, W. Liu, V. Schnitzler, F. Tancret, J.M. Bouler, Calcium phosphate cements for bone substitution: Chemistry, handling and mechanical properties, Acta Biomater. 10 (2014) 1035–1049. https://doi.org/10.1016/j.actbio.2013.11.001.

[53] M.P. Ginebra, T. Traykova, J.A. Planell, Calcium phosphate cements as bone drug delivery systems: A review, J. Control. Release. 113 (2006) 102–110. https://doi.org/10.1016/j.jconrel.2006.04.007.

[54] R. Murugan, S. Ramakrishna, Development of nanocomposites for bone grafting, Compos. Sci. Technol. 65 (2005) 2385–2406. https://doi.org/10.1016/j.compscitech.2005.07.022.

[55] J. Wilson, Metallic biomaterials : State of the art and new challenges, Elsevier Ltd, 2018. https://doi.org/10.1016/B978-0-08-102205-4.00001-5.

[56] A. Bigi, E. Boanini, M. Gazzano, Ion Substitution in Biological and Synthetic Apatites, Elsevier Ltd., 2016. https://doi.org/10.1016/B978-1-78242-338-6.00008-9.

[57] E. Boanini, M. Gazzano, A. Bigi, Ionic substitutions in calcium phosphates synthesized at low temperature, Acta Biomater. 6 (2010) 1882–1894. https://doi.org/10.1016/j.actbio.2009.12.041.

[58] J.F. Osborn, H. Newesely, The material science of calcium phosphate ceramics., Biomaterials. 1 (1980) 108–11. http://www.ncbi.nlm.nih.gov/pubmed/7470556.

[59] W. Cao, L.L. Hench, Bioactive Materials, 1996.

[60] F. Jordana, C. Le Visage, P. Weiss, Substituts osseux, Medecine/Sciences. 33 (2017) 60–65. https://doi.org/10.1051/medsci/20173301010.

[61] S. Gomes, A. Kaur, J.M. Grenèche, J.M. Nedelec, G. Renaudin, Atomic scale modeling of iron-doped biphasic calcium phosphate bioceramics, Acta Biomater. 50

(2017) 78–88. https://doi.org/10.1016/j.actbio.2016.12.011.

[62] G. Daculsi, R.Z. Legeros, E. Nery, K. Lynch, B. Kerebel, Transformation of biphasic calcium phosphate ceramics in vivo: Ultrastructural and physicochemical characterization, J. Biomed. Mater. Res. 23 (1989) 883–894. https://doi.org/10.1002/jbm.820230806.

[63] G. Renaudin, S. Gomes, J.M. Nedelec, First-row transition metal doping in calcium phosphate bioceramics: A detailed crystallographic study, Materials (Basel). 10 (2017) 92. https://doi.org/10.3390/ma10010092.

[64] G. Renaudin, P. Laquerrière, Y. Filinchuk, E. Jallot, J.M. Nedelec, Structural characterization of sol-gel derived Sr-substituted calcium phosphates with anti-osteoporotic and anti-inflammatory properties, J. Mater. Chem. 18 (2008) 3593–3600. https://doi.org/10.1039/b804140g.

[65] S. Gomes, A. Kaur, J.M. Nedelec, G. Renaudin, X-ray absorption spectroscopy shining (synchrotron) light onto the insertion of Zn2+ in calcium phosphate ceramics and its influence on their behaviour under biological conditions, J. Mater. Chem. B. 2 (2014) 536–545. https://doi.org/10.1039/c3tb21397h.

[66] Y. Li, J. Ho, C.P. Ooi, Antibacterial efficacy and cytotoxicity studies of copper (II) and titanium (IV) substituted hydroxyapatite nanoparticles, Mater. Sci. Eng. C. 30 (2010) 1137–1144. https://doi.org/10.1016/j.msec.2010.06.011.

[67] C. Gérard, L.J. Bordeleau, J. Barralet, C.J. Doillon, The stimulation of angiogenesis and collagen deposition by copper, Biomaterials. 31 (2010) 824–831. https://doi.org/10.1016/j.biomaterials.2009.10.009.

[68] S. Kannan, I.A.F. Lemos, J.H.G. Rocha, J.M.F. Ferreira, Synthesis and characterization of magnesium substituted biphasic mixtures of controlled hydroxyapatite/β-tricalcium phosphate ratios, J. Solid State Chem. 178 (2005) 3190–3196. https://doi.org/10.1016/j.jssc.2005.08.003.

[69] J.M. Bouler, M. Trécant, J. Delécrin, J. Royer, N. Passuti, G. Daculsi, Macroporous biphasic calcium phosphate ceramics: Influence of five synthesis parameters on compressive strength, J. Biomed. Mater. Res. 32 (1996) 603–609. https://doi.org/10.1002/(SICI)1097-4636(199612)32:4<603::AID-JBM13>3.0.CO;2-E.

[70] N. Kivrak, A. Cuneyt Tas, Synthesis of Calcium Hydroxyapatite-Tricalcium Phosphate (HA-TCP) Composite Bioceramic Powders and Their Sintering Behavior, ChemInform. 81 (1998) 2245–2252. https://doi.org/10.1002/chin.199849302.

[71] Sunarso, A.F.M. Noor, S.R. Kasim, R. Othman, I.D. Ana, K. Ishikawa, Synthesis of Biphasic Calcium Phosphate by Hydrothermal Route and Conversion to Porous Sintered Scaffold, J. Biomater. Nanobiotechnol. 04 (2013) 273–278. https://doi.org/10.4236/jbnb.2013.43034.

[72] X. Yang, Z. Wang, Synthesis of biphasic ceramics of hydroxyapatite and β-tricalcium phosphate with controlled phase content and porosity, J. Mater. Chem. 8 (1998) 2233–2237. https://doi.org/10.1039/a802067a.

[73] J. Chen, Y. Wang, X. Chen, L. Ren, C. Lai, W. He, Q. Zhang, A simple sol-gel technique for synthesis of nanostructured hydroxyapatite, tricalcium phosphate and biphasic powders, Mater. Lett. 65 (2011) 1923–1926. https://doi.org/10.1016/j.matlet.2011.03.076.

[74] K. Itatani, T. Nishioka, S. Seike, F.S. Howell, A. Kishioka, M. Kinoshita, Sinterability of β-Calcium Orthophosphate Powder Prepared by Spray-Pyrolysis, J. Am. Ceram. Soc. 77 (1994) 801–805. https://doi.org/10.1111/j.1151-2916.1994.tb05368.x.

[75] G. Daculsi, R.Z. LeGeros, M. Heughebaert, I. Barbieux, Formation of carbonate-apatite crystals after implantation of calcium phosphate ceramics, Calcif. Tissue Int. 46 (1990) 20–27. https://doi.org/10.1007/BF02555820.

[76] R.A. Bhatt, T.D. Rozental, Bone Graft Substitutes, Hand Clin. 28 (2012) 457–468. https://doi.org/10.1016/j.hcl.2012.08.001.

[77] INVS, Surveillance des infections du site opératoire, Résultats 2013, 2015.

[78] A. Gristina, Biomaterial-centered infection: microbial adhesion versus tissue integration, Science (80-.). 237 (1987) 1588–1595. https://doi.org/10.1126/science.3629258.

[79] R.M. Donlan, Biofilms and Device-Associated Infections, Emerg. Infect. Dis. 7 (2001) 277–281. https://doi.org/10.3201/eid0702.010226.

[80] Z. Khatoon, C.D. McTiernan, E.J. Suuronen, T.F. Mah, E.I. Alarcon, Bacterial biofilm formation on implantable devices and approaches to its treatment and prevention, Heliyon. 4 (2018). https://doi.org/10.1016/j.heliyon.2018.e01067.

[81] C. Desrousseaux, V. Sautou, S. Descamps, O. Traoré, Modification of the surfaces of medical devices to prevent microbial adhesion and biofilm formation, J. Hosp. Infect. 85 (2013) 87–93. https://doi.org/10.1016/j.jhin.2013.06.015.

[82] M.E. Olson, H. Ceri, D.W. Morck, A.G. Buret, R.R. Read, Biofilm bacteria: Formation

and comparative susceptibility to antibiotics, Can. J. Vet. Res. 66 (2002) 86–92.

[83] T.F.C. Mah, G.A. O'Toole, Mechanisms of biofilm resistance to antimicrobial agents, Trends Microbiol. 9 (2001) 34–39. https://doi.org/10.1016/S0966-842X(00)01913-2.

[84] A. V Karlov, I.A. Khlusov, V.A. Pontak, V.P. Ignatov, M.A. Ivin, S.Y. Zinatulina, Adhesion of Staphylococcus Aureus to Implants with Different Physicochemical Characteristics, 2002.

[85] O. Dumitrescu, O. Dauwalder, S. Boisset, M.E. Reverdy, A. Tristan, F. Vandenesch, Résistance aux antibiotiques chez Staphylococcus aureus: les points-clés en 2010, Medecine/Sciences. 26 (2010) 943–949.

[86] J. Jang, H.G. Hur, M.J. Sadowsky, M.N. Byappanahalli, T. Yan, S. Ishii, Environmental Escherichia coli: ecology and public health implications—a review, J. Appl. Microbiol. 123 (2017) 570–581. https://doi.org/10.1111/jam.13468.

[87] C.Y. Chang, Surface sensing for biofilm formation in Pseudomonas aeruginosa, Front. Microbiol. 8 (2018) 1–8. https://doi.org/10.3389/fmicb.2017.02671.

[88] F.C. Tenover, Mechanisms of antimicrobial resistance in bacteria, Am. J. Infect. Control. 34 (2006) S3–S10. https://doi.org/10.1016/j.ajic.2006.05.219.

[89] EARSS, On-going surveillance of Pneumoniae, S Aureus, S Coli, E Faecium, E Faecalis, E Pneumoniae, K Aeruginosa, P. aeruginosa, 2008. www.rivm.nl/earss,.

[90] S. Leprêtre, F. Chai, J.C. Hornez, G. Vermet, C. Neut, M. Descamps, H.F. Hildebrand, B. Martel, Prolonged local antibiotics delivery from hydroxyapatite functionalised with cyclodextrin polymers, Biomaterials. 30 (2009) 6086–6093. https://doi.org/10.1016/j.biomaterials.2009.07.045.

[91] J.L. Clement, P.S. Jarrett, Antibacterial Silver, Met. Based. Drugs. 1 (1994) 467–482. https://doi.org/10.1155/mbd.1994.467.

[92] G. Borkow, J. Gabbay, Copper as a Biocidal Tool, Curr. Med. Chem. 12 (2005) 2163–2175. https://doi.org/10.2174/0929867054637617.

[93] S. Atmaca, K. Gul, R. Cicek, The Effect of Zinc on Microbial Growth, in: J. Med. Sci., Macmillan Education UK, 1998: pp. 595–597. https://doi.org/10.1007/978-1-349-15747-1_10.

[94] H. qi Sun, X. mei Lu, P. ji Gao, The exploration of the antibacterial mechanism of Fe3+ against bacteria, Brazilian J. Microbiol. 42 (2011) 410–414. https://doi.org/10.1590/S1517-83822011000100050.

[95] S. Kannan, J.M.G. Ventura, J.M.F. Ferreira, Synthesis and thermal stability of potassium substituted hydroxyapatites and hydroxyapatite/β-tricalciumphosphate mixtures, Ceram. Int. 33 (2007) 1489–1494. https://doi.org/10.1016/j.ceramint.2006.05.016.

[96] S. Kannan, J.M.G. Ventura, A.F. Lemos, A. Barba, J.M.F. Ferreira, Effect of sodium addition on the preparation of hydroxyapatites and biphasic ceramics, Ceram. Int. 34 (2008) 7–13. https://doi.org/10.1016/j.ceramint.2006.07.007.

[97] Jacobs, Gaulier, Duval, Renaudin, Silver Doping Mechanism in Bioceramics—From Ag+: Doped HAp to Ag°/BCP Nanocomposite, Crystals. 9 (2019) 326. https://doi.org/10.3390/cryst9070326.

[98] A. Yasukawa, M. Higashijima, K. Kandori, T. Ishikawa, Preparation and characterization of cadmium-calcium hydroxyapatite solid solution particles, Colloids Surfaces A Physicochem. Eng. Asp. 268 (2005) 111–117. https://doi.org/10.1016/j.colsurfa.2005.06.016.

[99] S. Gomes, J.M. Nedelec, G. Renaudin, On the effect of temperature on the insertion of zinc into hydroxyapatite, Acta Biomater. 8 (2012) 1180–1189. https://doi.org/10.1016/j.actbio.2011.12.003.

[100] M. Veiderma, K. Tõnsuaadu, R. Knubovets, M. Peld, Impact of anionic substitutions on apatite structure and properties, J. Organomet. Chem. 690 (2005) 2638–2643. https://doi.org/10.1016/j.jorganchem.2004.11.022.

[101] L.M. Rodríguez-Lorenzo, J.N. Hart, K.A. Gross, Influence of fluorine in the synthesis of apatites. Synthesis of solid solutions of hydroxy-fluorapatite, Biomaterials. 24 (2003) 3777–3785. https://doi.org/10.1016/S0142-9612(03)00259-X.

[102] F. Audubert, J. Carpena, J.L. Lacout, F. Tetard, Elaboration of an iodine-bearing apatite, Solid State Ionics. 95 (1997) 113–119.

[103] S. Kannan, A. Rebelo, A.F. Lemos, A. Barba, J.M.F. Ferreira, Synthesis and mechanical behaviour of chlorapatite and chlorapatite/β-TCP composites, J. Eur. Ceram. Soc. 27 (2007) 2287–2294. https://doi.org/10.1016/j.jeurceramsoc.2006.07.004.

[104] R. Enderle, F. Götz-Neunhoeffer, M. Göbbels, F.A. Müller, P. Greil, Influence of magnesium doping on the phase transformation temperature of β-TCP ceramics examined by Rietveld refinement, Biomaterials. 26 (2005) 3379–3384. https://doi.org/10.1016/j.biomaterials.2004.09.017.

[105] N. Matsumoto, K. Sato, K. Yoshida, K. Hashimoto, Y. Toda, Preparation and characterization of β-tricalcium phosphate co-doped with monovalent and divalent antibacterial metal ions, Acta Biomater. 5 (2009) 3157–3164. https://doi.org/10.1016/j.actbio.2009.04.010.

[106] W. Xue, K. Dahlquist, A. Banerjee, A. Bandyopadhyay, S. Bose, Synthesis and characterization of tricalcium phosphate with Zn and Mg based dopants, J. Mater. Sci. Mater. Med. 19 (2008) 2669–2677. https://doi.org/10.1007/s10856-008-3395-4.

[107] H.J. Klasen, A historical review of the use of silver in the treatment of burns. II. Renewed interest for silver, Burns. 26 (2000) 131–138. https://doi.org/10.1016/S0305-4179(99)00116-3.

[108] S. Silver, L.T. Phung, G. Silver, Silver as biocides in burn and wound dressings and bacterial resistance to silver compounds, J. Ind. Microbiol. Biotechnol. 33 (2006) 627–634. https://doi.org/10.1007/s10295-006-0139-7.

[109] M. Roy, G.A. Fielding, H. Beyenal, A. Bandyopadhyay, S. Bose, Mechanical, in vitro antimicrobial, and biological properties of plasma-sprayed silver-doped hydroxyapatite coating, ACS Appl. Mater. Interfaces. 4 (2012) 1341–1349. https://doi.org/10.1021/am201610q.

[110] D.H. Nies, Microbial heavy-metal resistance, Appl. Microbiol. Biotechnol. 51 (1999) 730–750. https://doi.org/10.1007/s002530051457.

[111] C. Ning, X. Wang, L. Li, Y. Zhu, M. Li, P. Yu, L. Zhou, Z. Zhou, J. Chen, G. Tan, Y. Zhang, Y. Wang, C. Mao, Concentration Ranges of Antibacterial Cations for Showing the Highest Antibacterial Efficacy but the Least Cytotoxicity against Mammalian Cells: Implications for a New Antibacterial Mechanism, Chem Res Toxicol. 28 (2015) 1815–1822. https://doi.org/10.1016/j.physbeh.2017.03.040.

[112] M.L.W. Knetsch, L.H. Koole, New strategies in the development of antimicrobial coatings: The example of increasing usage of silver and silver nanoparticles, Polymers (Basel). 3 (2011) 340–366. https://doi.org/10.3390/polym3010340.

[113] H.J. Park, J.Y. Kim, J. Kim, J.H. Lee, J.S. Hahn, M.B. Gu, J. Yoon, Silver-ion-mediated reactive oxygen species generation affecting bactericidal activity, Water Res. 43 (2009) 1027–1032. https://doi.org/10.1016/j.watres.2008.12.002.

[114] C. Marambio-Jones, E.M.V. Hoek, A review of the antibacterial effects of silver nanomaterials and potential implications for human health and the environment, J. Nanoparticle Res. 12 (2010) 1531–1551. https://doi.org/10.1007/s11051-010-9900-y.

[115] I. Chopra, The increasing use of silver-based products as antimicrobial agents: A useful development or a cause for concern?, J. Antimicrob. Chemother. 59 (2007) 587–590. https://doi.org/10.1093/jac/dkm006.

[116] L.M. Deshpande, B.A. Chopade, Plasmid mediated silver resistance in Acinetobacter baumannii, Biometals. 7 (1994) 49–56. https://doi.org/10.1007/BF00205194.

[117] K.S. Hwang, S. Hwangbo, J.T. Kim, Silver-doped calcium phosphate nanopowders prepared by electrostatic spraying, J. Nanoparticle Res. 10 (2008) 1337–1341. https://doi.org/10.1007/s11051-008-9404-1.

[118] M. Sygnatowicz, K. Keyshar, A. Tiwari, Antimicrobial properties of silver-doped hydroxyapatite nano-powders and thin films, Biol. Biomed. Mater. 62 (2010) 65–70. https://doi.org/10.1007/s11837-010-0111-x.

[119] N. Iqbal, M.R. Abdul Kadir, N.A.N. Nik Malek, N. Humaimi Mahmood, M. Raman Murali, T. Kamarul, Rapid microwave assisted synthesis and characterization of nanosized silver-doped hydroxyapatite with antibacterial properties, Mater. Lett. 89 (2012) 118–122. https://doi.org/10.1016/j.matlet.2012.08.057.

[120] S. Jadalannagari, K. Deshmukh, S.R. Ramanan, M. Kowshik, Antimicrobial activity of hemocompatible silver doped hydroxyapatite nanoparticles synthesized by modified sol–gel technique, Appl. Nanosci. 4 (2014) 133–141. https://doi.org/10.1007/s13204-013-0197-x.

[121] C. Shi, J. Gao, M. Wang, Y. Shao, L. Wang, D. Wang, Y. Zhu, Functional hydroxyapatite bioceramics with excellent osteoconductivity and stern-interface induced antibacterial ability, Biomater. Sci. 4 (2016) 699–710. https://doi.org/10.1039/c6bm00009f.

[122] C. Fu, X. Zhang, K. Savino, P. Gabrys, Y. Gao, W. Chaimayo, B.L. Miller, M.Z. Yates, Antimicrobial silver-hydroxyapatite composite coatings through two-stage electrochemical synthesis, Surf. Coatings Technol. 301 (2016) 13–19. https://doi.org/10.1016/j.surfcoat.2016.03.010.

[123] O. Gokcekaya, K. Ueda, K. Ogasawara, H. Kanetaka, T. Narushima, In vitro evaluation of Ag-containing calcium phosphates: Effectiveness of Ag-incorporated β-tricalcium phosphate, Mater. Sci. Eng. C. 75 (2017) 926–933. https://doi.org/10.1016/j.msec.2017.02.059.

[124] J. Wang, X. Gong, J. Hai, T. Li, Synthesis of silver–hydroxyapatite composite with improved antibacterial properties, Vacuum. 152 (2018).

https://doi.org/10.1016/j.vacuum.2018.03.015.

[125] S.L. Percival, P.G. Bowler, D. Russell, Bacterial resistance to silver in wound care, J. Hosp. Infect. 60 (2005) 1–7. https://doi.org/10.1016/j.jhin.2004.11.014.

[126] N. Turner, M. Armitage, R. Butler, G. Ireland, An in vitro model to evaluate cell adhesion to metals used in implantation shows significant differences between palladium and gold or platinum, Cell Biol. Int. 28 (2004) 541–547. https://doi.org/10.1016/j.cellbi.2004.04.009.

[127] A. Favaretto, USAGE DE L ' OR EN ODONTOLOGIE : ANALYSE CHEZ LES CHIRURGIENS DENTISTES ET LES PROTHESISTES, 2018.

[128] R.A. Sperling, P. Rivera Gil, F. Zhang, M. Zanella, W.J. Parak, Biological applications of gold nanoparticles, Chem. Soc. Rev. 37 (2008) 1896–1908. https://doi.org/10.1039/b712170a.

[129] E. Boisselier, D. Astruc, Gold nanoparticles in nanomedicine: Preparations, imaging, diagnostics, therapies and toxicity, Chem. Soc. Rev. 38 (2009) 1759–1782. https://doi.org/10.1039/b806051g.

[130] D. Giljohann, D. Seferos, W. Daniel, M. Massich, P. Patel, C. Mirkin, Gold Nanoparticles for Biology and Medicine, Angew. Chem. Int. Ed. Engl. 49 (2010) 3280–3294. https://doi.org/10.1002/anie.200904359.Gold.

[131] L. Dykman, N. Khlebtsov, Gold nanoparticles in biomedical applications: Recent advances and perspectives, Chem. Soc. Rev. 41 (2012) 2256–2282. https://doi.org/10.1039/c1cs15166e.

[132] P. Singh, S. Pandit, V.R.S.S. Mokkapati, A. Garg, V. Ravikumar, I. Mijakovic, Gold nanoparticles in diagnostics and therapeutics for human cancer, Int. J. Mol. Sci. 19 (2018). https://doi.org/10.3390/ijms19071979.

[133] Y.H. Gao, N.C. Zhang, Y.W. Zhong, H.H. Cai, Y.L. Liu, Preparation and characterization of antibacterial Au/C core-shell composite, Appl. Surf. Sci. 256 (2010) 6580–6585. https://doi.org/10.1016/j.apsusc.2010.04.051.

[134] S. Shamaila, N. Zafar, S. Riaz, R. Sharif, J. Nazir, S. Naseem, Gold nanoparticles: An efficient antimicrobial agent against enteric bacterial human pathogen, Nanomaterials. 6 (2016) 1–10. https://doi.org/10.3390/nano6040071.

[135] Y. Cui, Y. Zhao, Y. Tian, W. Zhang, X. Lü, X. Jiang, The molecular mechanism of action of bactericidal gold nanoparticles on Escherichia coli, Biomaterials. 33 (2012)

2327–2333. https://doi.org/10.1016/j.biomaterials.2011.11.057.

[136] K.S. Uma Suganya, K. Govindaraju, V. Ganesh Kumar, T. Stalin Dhas, V. Karthick, G. Singaravelu, M. Elanchezhiyan, Blue green alga mediated synthesis of gold nanoparticles and its antibacterial efficacy against Gram positive organisms, Mater. Sci. Eng. C. 47 (2015) 351–356. https://doi.org/10.1016/j.msec.2014.11.043.

[137] A. Mohammed Fayaz, M. Girilal, S.A. Mahdy, S.S. Somsundar, R. Venkatesan, P.T. Kalaichelvan, Vancomycin bound biogenic gold nanoparticles: A different perspective for development of anti VRSA agents, Process Biochem. 46 (2011) 636–641. https://doi.org/10.1016/j.procbio.2010.11.001.

[138] B. Lee, D.G. Lee, Synergistic antibacterial activity of gold nanoparticles caused by apoptosis-like death, J. Appl. Microbiol. 127 (2019) 701–712. https://doi.org/10.1111/jam.14357.

[139] C. Yi, D. Liu, C.-C. Fong, J. Zhang, M. Yang, Gold Nanoparticles Promote Osteogenic, ACS Nano. 4 (2010) 6439–6448.

[140] S.Y. Choi, M.S. Song, P.D. Ryu, A.T.N. Lam, S.W. Joo, S.Y. Lee, Gold nanoparticles promote osteogenic differentiation in human adipose-derived mesenchymal stem cells through the Wnt/β-catenin signaling pathway, Int. J. Nanomedicine. 10 (2015) 4383–4392. https://doi.org/10.2147/IJN.S78775.

[141] Y. Yao, X. Shi, F. Chen, The effect of gold nanoparticles on the proliferation and differentiation of murine osteoblast: A study of MC3T3-E1 cells in vitro, J. Nanosci. Nanotechnol. 14 (2014) 4851–4857. https://doi.org/10.1166/jnn.2014.8717.

[142] D.N. Heo, W.K. Ko, M.S. Bae, J.B. Lee, D.W. Lee, W. Byun, C.H. Lee, E.C. Kim, B.Y. Jung, I.K. Kwon, Enhanced bone regeneration with a gold nanoparticle-hydrogel complex, J. Mater. Chem. B. 2 (2014) 1584–1593. https://doi.org/10.1039/c3tb21246g.

[143] Y. Xia, H. Chen, F. Zhang, C. Bao, M.D. Weir, M.A. Reynolds, J. Ma, N. Gu, H.H.K. Xu, Gold nanoparticles in injectable calcium phosphate cement enhance osteogenic differentiation of human dental pulp stem cells, Nanomedicine Nanotechnology, Biol. Med. 14 (2018) 35–45. https://doi.org/10.1016/j.nano.2017.08.014.

[144] J. Rodriguez-Carvajal, PROGRAM FullProf.2k – version 3.20; Laboratoire Léon Brillouin (CEA-CNRS): Saclay, France, (2005).

[145] L.M. Rodríguez-Lorenzo, J.N. Hart, K.A. Gross, Structural and chemical analysis of well-crystallized hydroxyfluorapatites, J. Phys. Chem. B. 107 (2003) 8316–8320. https://doi.org/10.1021/jp027556o.

[146] M. Yashima, A. Sakai, T. Kamiyama, A. Hoshikawa, Crystal structure analysis of β-tricalcium phosphate Ca 3(PO4)2 by neutron powder diffraction, J. Solid State Chem. 175 (2003) 272–277. https://doi.org/10.1016/S0022-4596(03)00279-2.

[147] G. Renaudin, S. Gomes, J.M. Nedelec, First-row transition metal doping in calcium phosphate bioceramics: A detailed crystallographic study, Materials (Basel). 10 (2017). https://doi.org/10.3390/ma10010092.

[148] A. El Hamidi, M. Halim, S. Arsalane, M. Kacimi, M. Ziyad, Synthesis and characterization of new copper(II) substituted dicalcium phosphate dihydrate (CaHPO 4.2H 2O), Asian J. Chem. 24 (2012) 2698–2702.

[149] X. Wang, F. Cheng, J. Liu, J.H. Smått, D. Gepperth, M. Lastusaari, C. Xu, L. Hupa, Biocomposites of copper-containing mesoporous bioactive glass and nanofibrillated cellulose: Biocompatibility and angiogenic promotion in chronic wound healing application, Acta Biomater. 46 (2016) 286–298. https://doi.org/10.1016/j.actbio.2016.09.021.

[150] S. Gomes, G. Renaudin, E. Jallot, J.M. Nedelec, Structural characterization and biological fluid interaction of sol-gel-derived Mg-substituted biphasic calcium phosphate ceramics, ACS Appl. Mater. Interfaces. 1 (2009) 505–513. https://doi.org/10.1021/am800162a.

LISTE DES PUBLICATIONS SCIENTIFIQUES

Revue bibliographique :

Aurélie Jacobs, Guillaume Renaudin, Christiane Forestier, Jean-Marie Nedelec and Stéphane Descamps**, Biological properties of copper-doped biomaterials for orthopedic applications: a review of antibacterial, angiogenic and osteogenic aspects**, *Acta Biomaterialia*, 2020,

Articles scientifiques :

Sandrine Gomes, Charlotte Vichery, Stéphane Descamps, Hervé Martinez, Amandeep Kaur, Aurélie Jacobs, Jean-Marie Nedelec and Guillaume Renaudin, **Cu-doping of calcium phosphate bioceramics: From mechanism to the control of cytotoxicity.** *Acta Biomaterialia*, 2018, 65:462–474. https://doi.org/10.1016/j.actbio.2017.10.028.

Aurélie Jacobs, Morgane Gaulier, Alexis Duval and Guillaume Renaudin, **Silver Doping Mechanism in Bioceramics — From Ag+:Doped HAp to Ag°/BCP Nanocomposite**. Crystals, 2019, 9, 326.

Aurélie Jacobs, Guillaume Renaudin, Nicolas Charbonnel, Jean-Marie Nedelec, Christiane Forestier and Stéphane Descamps, **Copper-doped Biphasic Calcium Phosphate powders: dopant release, cytotoxicity and antibacterial property**. 1ère version soumise à *Biomaterials*.

Aurélie Jacobs, Stéphane Descamps, Lorélène Gasnier, Mathilde Prudent, Coralie Laurent, Jean-Marie Nedelec, Christelle Blavignac, Nicolas Charbonnel, Christiane Forestier, David Marchat, Guillaume Renaudin, **Copper-doped Biphasic Calcium Phosphate bioceramic disks: copper release, cytotoxicity and antibacterial property**. En cours de préparation pour la soumission.

Xavier Kesse, Charlotte Vichery, Aurelie Jacobs, Stéphane Descamps, and Jean-Marie Nedelec, **Unravelling the Impact of Calcium Content on the Bioactivity of Sol−Gel-Derived Bioactive Glass Nanoparticles**, *ACS Applied Bio Materials*, 2020, 1312-1330.

LISTE DES COMMUNICATIONS SCIENTIFIQUES

Communications orales :

A. Jacobs, G. Renaudin, C. Vichery, J.-M Nedelec, S. Descamps, “Biological interest of cu-doped calcium phosphate bioceramics for bone tissue engineering”, **Congrès de la Société Chimique de France (SCF) 2018**, 30 juin au 4 juillet 2018, Montpellier, France.

A. Jacobs, G. Renaudin, C. Vichery, C. Forestier, N. Charbonnel, S. Descamps, “Biological interest of cu-doped calcium phosphate bioceramics for bone tissue engineering”, **European Orthopaedic Research Society (EORS) 2018**, 25 au 28 septembre 2018, Galway, Irelande.

A. Jacobs, G. Renaudin, C. Vichery, J.-M Nedelec, S. Descamps, “Intérêt biologique de biocéramiques de phosphate de calcium dopées au cuivre”, **Matériaux 2018**, 19 au 23 novembre 2018, Strasbourg, France.

A. Jacobs, G. Renaudin, C. Vichery, J.-M Nedelec, S. Descamps, “Copper-doped calcium phosphate bioceramics: a solution against bone infections?”, **Journées communes LMI/ICCF**, 9 novembre 2018, Clermont-Ferrand, France.

A. Jacobs, G. Renaudin, J.-M Nedelec, S. Descamps, “Cytotoxicity of cu-doped calcium phosphate bioceramics on bone marrow cells”, **3ème Journée scientifique commune TGI-IP/MPS-ICCF/Techmed**, 27 septembre 2019, UFR de Médecine-Pharmacie, Clermont Ferrand, France.

G. Renaudin, S. Gomes, A. Jacobs, S. Descamps, J.-M. Nedelec, “Etude du mécanisme de dopage des biocéramiques apatitiques par les cations des métaux de transition (M^{n+} = Mn^{2+}, Fe^{3+}, Co^{2+}, Ni^{2+}, $Cu^{+/2+}$ et Zn^{2+})”, **Journées Annuelles ‘Matériaux pour la Santé’,** mai 2018, Saint-Etienne, France.

L. Thoraval, C. Guillaume, D. Auzene, C. Demangel, B. Cauwe, M. Lebleu, J.-M Nedelec, G. Renaudin, A. Jacobs, S. Gangloff, F. Velard, “Impact du dopage ionique au cuivre sur la réponse inflammatoire aux biomatériaux céramiques”, **Journée rémoise des jeunes chercheurs en santé**, 2020, Reims, France.

Communication affichée :

A. Jacobs, G. Renaudin, N. Charbonnel, J.-M Nedelec, C. Forestier, S. Descamps, Copper-doped Biphasic Calcium Phosphate powders: dopant release, cytotoxicity and antibacterial property, **Journées de l’Ecole Doctorale 2020**, 14 et 15 octobre 2020, Clermont-Ferrand, France.

RESUME

Les solutions de greffes osseuses actuelles sont limitées en termes de quantité et de qualité c'est pourquoi l'utilisation de substituts osseux synthétiques est en développement. La gestion du risque d'infection lors de l'implantation d'un biomatériau est primordiale, d'autant plus avec la propagation de l'antibiorésistance qui représente un problème majeur de santé publique. C'est dans ce contexte que s'inscrit ce travail. Pour cela des biocéramiques de phosphates de calcium biphasiques (BCP), qui sont des substituts osseux de choix du fait de leur forte similarité chimique avec la partie minérale de l'os et de leur biocompatibilité, ont été synthétisées par voie sol-gel et par précipitation en voie aqueuse. Une de leur particularité est de pouvoir accepter des substitutions ioniques dans leur composition, c'est pourquoi des dopages aux ions cuivre ont été réalisés, ainsi qu'à l'argent et à l'or afin d'étudier les mécanismes d'incorporation de ces ions dans les BCP. Ces 3 éléments métalliques ont été choisis pour leur propriétés antibactériennes très intéressantes dans le contexte de cette étude. Les BCP dopés au cuivre, sous forme de poudres (synthèse sol-gel) et de pastilles (synthèse par précipitation en voie aqueuse), ont été étudiés afin de s'assurer de leur biocompatibilité envers des cellules souches mésenchymateuses humaines. Ensuite les propriétés antibactériennes de ces matériaux ont été évaluées sur des souches d'intérêts cliniques : *S. aureus*, *S. aureus* résistant à la méthicilline, *E. coli* et *P. aeruginosa*.

Ce travail a permis de mettre en évidence différents mécanismes d'incorporation des ions avec notamment la présence de nanoparticules métalliques pour les dopages à l'argent et à l'or. Pour les BCP dopés au cuivre les paramètres de synthèse des matériaux (températures de recuit et taux de dopage) influencent la composition biphasique des matériaux et le taux de relargage du cuivre. Les poudres obtenues par voie sol-gel et les pastilles synthétisées par précipitation en voie aqueuse ne présentent aucune cytotoxicité envers les cellules osseuses humaines après plusieurs jours de culture. Les poudres de BCP dopées au cuivre ont démontré des propriétés antibactériennes après 24h de culture envers *S. aureus*, *S. aureus* résistant à la méthicilline, et *E. coli* et les pastilles de BCP dopées au cuivre ont montré une activité antibactérienne envers les 4 souches testées.

Mots clés :

Substituts osseux ; Biocéramiques ; Dopage ; Cuivre ; Cellules souches mésenchymateuses; Antibactérien.

ABSTRACT

Current bone grafting solutions are limited in terms of quantity and quality, that is why the use of synthetic bone substitutes is on development. Managing the risk of infection during the implantation of a biomaterial is essential, especially with the spread of antibiotic resistance, which represents a major public health problem. It is in this context that this work takes place. For this, bioceramics of biphasic calcium phosphates (BCP), which are bone substitutes of choice because of their strong chemical similarity with the mineral part of the bone and their biocompatibility, were synthesized by the sol-gel route and by aqueous precipitation. One of their particularity is that they can accept ionic substitutions in their composition, which is why doping with copper ions was carried out, as well as with silver and gold in order to study the mechanisms of incorporation of these ions in BCPs. These 3 metallic elements were chosen for their very interesting antibacterial properties in the context of this study. Copper-doped BCPs, in the form of powders (sol-gel synthesis) and disks (synthesis by aqueous precipitation), have been studied to ensure their biocompatibility with human mesenchymal stem cells. Then the antibacterial properties of these materials were evaluated on strains of clinical interest: *S. aureus*, methicillin resistant *S. aureus*, *E. coli* and *P. aeruginosa*.

This work allowed highlighting different mechanisms of ions incorporation, in particular with the presence of metallic nanoparticles for doping with silver and gold. For copper-doped BCPs, the material synthesis parameters (annealing temperatures and doping rate) influence the biphasic composition of the materials and the copper release rate. The powders obtained by the sol-gel route and the disks synthesized by aqueous precipitation do not exhibit any cytotoxicity towards human bone cells after several days of culture. The copper-doped BCP powders demonstrated antibacterial properties after 24 hours of culture against *S. aureus*, *S. aureus* resistant to methicillin, and *E. coli* and the copper-doped BCP disks showed antibacterial activity against the 4 strains tested.

Keywords:

Bone substitutes; Bioceramics; Doping; Copper; Mesenchymal stem cells; Antibacterial.